UNIVERSITY OF NAPLES FEDERICO II

DEPARTMENT OF PHARMACY

Ph.D. THESIS

IN

"PHARMACEUTICAL SCIENCE"

Identification of bioactive natural products from plants and semi-synthetic modifications

Supervisor:
Prof. Orazio Taglialatela-Scafati

Coordinator:
Prof. Maria Valeria D'Auria

Candidate:
Annalisa Lopatriello

XXXII cycle
2017/2020

Abstract

Natural products constitute an outstanding resource of lead compounds in drug discovery, due to their considerable structural diversity and their still not completely unraveled potential. Both marine and terrestrial plants contain an immense reservoir of secondary metabolites which could provide new and unique agents of immense therapeutic potential. Since less than 10% of the world biodiversity has been evaluated for potential biological activity, many more useful natural chemical entities are expected to be discovered. Considering the analysis of Food and Drug Administration (FDA) drug approvals in 2018, new drugs inspired by natural products correspond to approximately one-third compared to the other classes of drugs.

In this context, the study reported in this Ph.D. addressed the research of new natural lead compounds, focusing on two main topics: - the investigation of the antimalarial potential of an African plant, *Lophira lanceolata*; - further exploration of the cannabinoid chemical space, through the isolation and semi-synthetic modifications of the secondary metabolites from a fiber cultivar of *Cannabis sativa*.

A bioassay-guided screening of African plants for the identification of new transmission-blocking antimalarial leads indicated *Lophira lanceolata* (Ochnaceae) as the most promising plant. Specific life stages of the malaria parasite (*Plasmodium* sp.), responsible for the transmission of this desease were analyzed: gametocytes, occurring in the human host, and early sporogonic stages/ookinetes, developing in female mosquitoes of genus *Anopheles* (generally recognized as malaria vector). The phytochemical study of *Lophira lanceolata* led to the isolation of seven biflavonoids, including three previously unreported compounds, along with two known nitrile glycoside esters, lanceolins A and B. Among the isolated compounds, the biflavonoid lophirone E was identified as a potent gametocytocidal agent (IC_{50} = 0.14± 0.04 μM) with negligible cytotoxicity (selectivity index = 570), exhibiting a unique stage-specific activity profile, since it revealed to be about 100 times less active against *P. falciparum* asexual blood stages. Besides, the isolation of structural analogues allowed to draw preliminary structure-activity relationships, identifying the critical positions on the chemical scaffold of lophirone E. On the other hand, lanceolin B was proved to be a potent inhibitor of the development

of the *Plasmodium* early sporogonic stages, indicating that the plant contains two different stage-selective antimalarial agents acting on transmissible stages in the human and mosquito host.

This research work was supported by the Italian MIUR, PRIN2015, project 20154JRJPP "Towards multi-stage drugs to fight poverty related and neglected parasitic diseases: synthetic and natural compounds directed against *Leishmania*, *Plasmodium* and *Schistosoma* life stages and assessment of their mechanisms of action". Parasite's specific life stage assays (gametocytes and asexual stages) were carried out at the University of Milan, while early sporogonic stage and ookinete-stage (Ookinete Development Assay, ODA) at the School of Pharmacy at University of Camerino.

Following a research topic investigated in our group for a long time, in the second part of my PhD, I studied the chemistry of *Cannabis sativa*. Despite the countless studies performed on different *C. sativa* chemotypes, its phytochemical content as well as the pharmacological potential of phytocannabinoids from *C. sativa* appear to be not exhaustively unravelled still today. For this reason, in this thesis the phytochemical content of a fiber hemp variety, as well as the chemistry of some isolated phytocannabinoids were analyzed and reported. The results of this study include the isolation and structure elucidation of a new phytocannabinoid, and the evaluation if its interaction with TRP channels. Besides, the analysis of the reactivity related to other known non-psychotropic phytocannabinoids, especially with iodine-based reagents, expanded the chemical space of cannabinoid chemotype, providing several new chemical entities, which were also pharmacologically evaluated.

This work was financed by Italian MIUR (PRIN2017, Project 2017WN73PL, Bioactivity-directed exploration of the phytocannabinoid chemical space).

The collaboration of the research groups of:

- Prof. A. Habluetzel, School of Pharmacy, University of Camerino (ESS and ODA experiments);
- Prof. D. Taramelli, University of Milan (*Plasmodium* asexual and gametocytes inhibition assays);
- Prof. E. Muñoz, University of Córdoba (PPARs activity evaluation)
- L. De Petrocellis, CNR, Naples (TRPs activity evaluation);

- Prof. A. Kijjoa and Prof. J. A. Pereira, University of Porto (ECD computational calculation)

is gratefully acknowledged.

Publications of the candidate during the PhD period

1. D. Caprioglio, D. Mattoteia, F. Pollastro, A. Lopatriello, G. Chianese, A. Minassi, E. Muñoz, O. Taglialatela-Scafati and G. Appendino. The Oxidation of Phytocannabinoids to Cannabinoquinoids. *Journal of Natural Products*, submitted.

2. H. Soré[#], A. Lopatriello[#], Y. A. Ebstie, A. R. Tenoh Guedoung, A. Hilou, J. A. Pereira, A. Kijjoa, A. Habluetzel, O. Taglialatela-Scafati. Plasmodium stage-selective antimalarials from *Lophira lanceolata* stem bark. *Phytochemistry*, *in press*.
3. A. Lopatriello[#], H. Soré[#], A. Habluetzel, S. Parapini, S. D'Alessandro, D. Taramelli, O. Taglialatela-Scafati. (2019). Identification of a potent and selective gametocytocidal antimalarial agent from the stem barks of *Lophira lanceolata*. *Bioorganic Chemistry*, *93*, 103321.
4. D. Caprioglio, D. Mattoteia, A. Minassi, F. Pollastro, A. Lopatriello, E. Muñoz, O. Taglialatela-Scafati, G. Appendino. (2019). One-pot Total Synthesis of Cannabinol via Iodine-mediated Deconstructive Annulation. *Organic Letters*, *21*, 6122-6125.
5. F. Pollastro, A. Lopatriello, J. F. Vouillamoz, G. Appendino, O. Taglialatela-Scafati, M.Forino. (2019). Non-volatile constituents of the vermouth ingredient *Artemisia vallesiaca*. *Fitoterapia*, *138*, 104312.
6. A. Cuadari, F. Pollastro, J. D. Unciti-Broceta, D. Caprioglio, A. Minassi, A. Lopatriello, E. Muñoz, O. Taglialatela-Scafati, G. Appendino. (2019). The Dimerization of Δ^9-Tetrahydrocannabinolic acid A (THCA-A). *Acta Pharmaceutica Sinica B*, *9*, 1078-1083.
7. D. Caprioglio, G. Allegrone, F. Pollastro, S. Valera, A. Lopatriello, J. A. Collado, E. Muñoz, G. Appendino, O. Taglialatela-Scafati. (2019). O-Methyl Phytocannabinoids: Semi-synthesis, Analysis in Cannabis Flower heads, and Biological Activity. *Planta medica*, *85*, 981-986.
8. C. Formisano, D. Rigano, A. Lopatriello, C. Sirignano, G. Ramaschi, L. Arnoldi, A. Riva, N. Sardone, O. Taglialatela-Scafati. (2019). Detailed Phytochemical Characterization of Bergamot Polyphenolic Fraction (BPF) by UPLC-DAD-MS and LC-NMR. *Journal of Agricultural and Food Chemistry*, *67 (11)*, 3159-3167.

9. A. Habluetzel, B. Pinto, S. Tapanelli, J. Nkouangang, M. Saviozzi, G. Chianese, A. Lopatriello, A. R. Tenoh, R. S. Yerbanga, O. Taglialatela-Scafati, F. Esposito, F. Bruschi. (2019) Effects of *Azadirachta indica* seed kernel extracts on early erythrocytic schizogony of *Plasmodium berghei* and pro-inflammatory response in inbred mice. *Malaria Journal*, *18*, 35.
10. A. Lopatriello, D. Caprioglio, A. Minassi, A. Schiano Moriello, C. Formisano, L. De Petrocellis, G. Appendino, O. Taglialatela-Scafati. (2018). Iodine-mediated cyclization of cannabigerol (CBG) expands the cannabinoid biological and chemical space. *Bioorganic & Medicinal Chemistry*, *26*, 4532–4536.
11. F. Pollastro, M. Talmon, S. Gaeta, S. Rossi, A. Lopatriello, L. G. Fresu. (2018). An *Artemisia*-derived natural product-based fluorescent probe for the bitter taste receptor hTAS2R38. *Fitoterapia*, *127*, 252–256.
12. A. Lopatriello, R. Previtera, S. Pace, M. Werner, L. Rubino, O. Werz, O. Taglialatela-Scafati, M. Forino. (2017). NMR-based identification of the major bioactive molecules from an Italian cultivar of *Lycium barbarum*. *Phytochemistry*, *144*, 52-57.

[#] These Authors contributed equally

Table of contents

List of abbreviations

Abbreviation	Explanation
5-HT	5-hydroxytryptamine
Acetyl-CoA	Acetyl coenzyme A
ACT	Artemisinin-based Combination Therapy
AITC	Allylisothiocyanate
ALU	Arbitrary Luminescent Units
ANOVA	Analysis of Variance
APAD	3-AcetylPyridine Adenine Dinucleotide
BBB	Blood-Brain-Barrier
BCE	Before the Common Era
BHT	Butylated hydroxytoluene
BTIB	bis(trifluoroacetoxy)iodobenzene
calcd	calculated
CBC	Cannabichromene
CBCA	cannabichromenoic acid
CBD	cannabidiol
CBDA	cannabidiolic acid
CBDN	cannabinodiol
CBDV	cannabidivarin
CBDVA	cannabidivarinic acid
CBE	cannabielsoin
CBEA	cannabielsoic acid
CBF	cannabifuran
CBG	cannabigerol
CBGA	cannabigerolic acid
CBM	cannabimovone
CBN	cannabinol
CBV	cannabivarin
CC	column chromatography
CD	circular dichroism
CNR	Italian national research council
CNS	central nervous system
COSY	correlation spectroscopy
CQ	chloroquine
DDQ	2,3-dichloro-5,6-dicyano-1,4-benzoquinone
DFT	density functional theory
DHA	dihydroartemisinin
DMSO	dimethyl sulfoxide
DMP	Dess-Martin periodinane
DNA	deoxyribonucleic acid
DO	developing ookinetes
EC_{50}	half maximal effective concentration
ECD	electronic circular dichroism
ESI	electrospray ionisation
ESIMS	electrospray ionisation mass spectrometry
ESS	early sporogonic stages
EtOAc	ethyl acetate
FAD	flavin adenine dinucleotide
FDA	food and drug administration
FID	free induction decay
FITC	fluorescein isothiocyanate

FT	Fourier transform
FT-ICR	Fourier-transform ion cyclotron resonance
FT-IR	Fourier transform – infrared spectroscopy
FT-MS	Fourier ransform mass spectrometry
G6PD	glucose-6-phosphate dehydrogenase
GCC	gravity column chromatography
GPCR	G protein-coupled receptor
GPP	geranyl pyrophosphate
HD gene	huntingtin gene
HEK293	human embryonic kidney 293
HEPES	hydroxyethylpiperazine ethane sulfonic acid
HIV/AIDS	human immunodeficiency virus/ acquired immune deficiency syndrome
HMBC	heteronuclear multiple bond correlation
HMEC	human dermal microvascular endothelial cells
HPLC	high performance liquid chromatography
HPLC-RI	high performance liquid chromatography - refractive index detectors
HRMS	high-resolution mass spectrometry
HSQC	heteronuclear single quantum correlation
IBX	iodoxybenzoic acid
IC_{50}	half maximal inhibitory concentration
IEFPCM	integral equation formalism polarizable continuum model
IU	international units
LPC	lysophosphatidylcholine
LTQ	linear trap quadrupole
mAbs	monoclonal antibodies
MB	methylene blue
MeOH	methanol
MIUR	Ministero dell'istruzione, dell'università e della ricerca
MM2	molecular mechanics 2
MMFF94	merck molecular force field
MPLC	medium-performance liquid chromatography
MS	Mass Spectrometry
MTT	3-[4,5-dimethylthiazol-2-yl]-2,5-diphenyltetrazoliumbromide
MW	molecular weight
NAG	*N*-acetyl-*D*-glucosamine
NBT	nitroblue tetrazolium chloride
NIS	*N*-iodosuccinimide
NMR	nuclear magnetic resonance
NOESY	nuclear overhauser enhancement spectroscopy
NRs	nuclear receptors
NT	not tested
OD	optical density
ODA	ookinete development assay
PBS	phosphate-buffered saline
PEG-enzymes	polyethylene glycol
PES	phenazine ethosulfate
pLDH	parasite lactate dehydrogenase
PPARs	peroxisome proliferator-activated receptors

PPRE	PPAR responsive element
PRIN	progetti di ricerca di interesse nazionale
PTP	protein tyrosine phosphatase
RBC	red blood cells
ROESY	rotating-frame overhauser spectroscopy
ROS	reactive oxygen species
RP	reverse-phase
RPMI	Roswell park memorial institute
Rt	Retention time
RXR	retinoid X receptor
SD	stardard deviation
SIBX	stabilized 2-iodoxybenzoic acid
T2D	type 2 diabetes
TBHP	tert-butyl hydroperoxide
THC	tetrahydrocannabinol
THCA	tetrahydrocannabinolic acid
TDDFT	time-dependent density functional theory
TLC	thin layer chromatography
™	Trade Mark
TM	*trans*-membrane
TOF	time-of-flight
TRP	transient receptor potential
TRPA	TRP channel of ankyrin
TRPA1	TRP channel of ankyrin type 1
TRPC	TRP canonical channel
TRPM	TRP channel of melastatin
TRPM8	TRP channel of melastatin type-8
TRPML	TRP channel of mucolipin
TRPP	TRP channel of polycystin
TRPV1	TRP channel of vanilloid type-1
TRPV2	TRP channel of vanilloid type-2
TRPV3	TRP channel of vanilloid type-3
TRPV4	TRP channel of vanilloid type-4
TZDs	thiazolidinediones
UV/Vis	ultraviolet-visible
WHO	World Health Organization
WWARN	Worldwide Antimalarial Resistance Network

Chapter 1: Natural products in drug discovery

1.1 Introduction

Throughout the ages, Nature has been considered by humans as the most precious resource able to satisfy their primary needs, including medicines for the treatment of a wide spectrum of diseases. Natural products, produced by natural sources, namely terrestrial or marine organisms, including plants, fungi, marine sponges and so on, are mainly responsible for this huge power of Nature. In particular, natural products are defined as secondary metabolites, which differ from the primary metabolites (nucleic acids, proteins, fats, and carbohydrates), substantially because they are not necessary for survival, but they represent a valid weapon in defending organisms from predators or external threats, and in the interaction between species. Three main biological processes are involved in secondary metabolism: glycolysis, Krebs cycle, and photosynthesis. From these metabolic reactions, different intermediates, namely mevalonic acids, acetyl-CoA and 1-deoxyxylulose-5-phosphate, are synthesized, generating, in the following steps, a countless number of natural compounds. In this regard, it is appropriate to consider that several factors, for example, environmental changes, chemicals, biotic factors, etc., can determine a different profile in terms of secondary metabolites content, depending on the specific organism or species (Croteau, *et al.* 2000).

For this reason, natural products are characterized by a plethora of different structures, which have supported the human being since ancient times in various ways, such as medicinal remedies for the treatment of various troubles. In the past, natural remedies consisted of concoctions, oil or juice mainly of a different part of plants and reported as prescriptions in documents (traditional medicine system), where their preparation along with their applications (e.g. coughs, colds or parasitic infections and inflammation) were described. In the nineteenth century, the era of the ‘modern drugs’ was characterized by a revolution in the medicinal system, moving from ‘traditional prescriptions’ to the use of pharmacologically-active compounds. The first example is represented by morphine, isolated by a young German pharmacist, Friedrich Sertürner, from the opium plant in 1805 (Hamilton *et al.*, 2000). Subsequently, countless active compounds have been identified from natural sources (not only consisted of terrestrial plants, but also fungi, insects, marine organisms, and bacteria). They

were then applied for the treatment of specific diseases, including cancer (Srivastava, *et al.*, 2005; Butler *et al.*, 2004; Mukherjee, *et al.*, 2001), pain (Salim, *et al.*, 2008), malaria (Willcox, *et al.*, 2001), heart disease (Campbell *et al.*, 2000), blood cholesterol control (Steinberg, *et al.*, 1999), and several others human disease treatment.

Moreover, even if the scientific community often criticizes the natural products research as an arduous and slow process, the development of high-throughput synthesis and combinatorial chemistry-based drug development was not able to provide unique chemical structures offered by natural compounds, which results in diversity in their biological activities and drug-like properties (Atanasov, *et al.*, 2015).

As reported, approximately 50% of anticancer drugs approved by the FDA (or similar agencies, responsible for protecting the public health) are derived from natural products, used in their original unmodified form, or with structural modification (Butler, *et al.*, 2014). In the field of anti-cancer agents, the better known examples are paclitaxel and its derivatives obtained from yew (Taxus) species, vincristine and vinblastine from Madagascar periwinkle (*Catharanthus roseus* (L.) G. Don), and camptothecin and its analogues initially discovered in the Chinese tree *Camptotheca acuminata* Decne (Cragg and Newman, 2013).

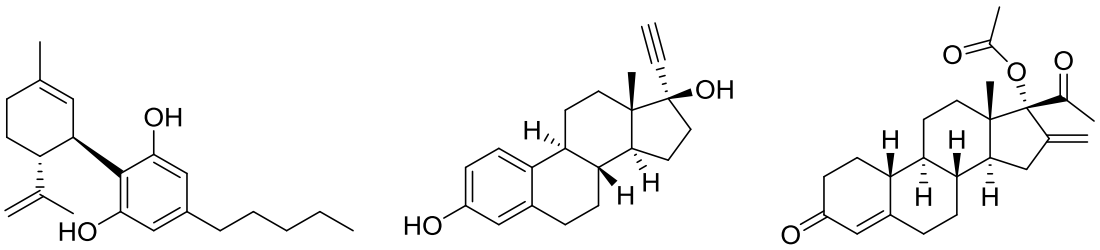

Cannabidiol **Ethinylestradiol** **Segesteron**

Figure 1.1. Structure of cannabidiol (Epidiolex™) and of ethinylestradiol and segesteron (Annovera™)**,** a combined steroid derived drug.

Besides, considering only 2018, the FDA approved 10 new drugs inspired by natural products (de la Torre and Albericio, 2019). Among these, cannabidiol (Epidiolex™) represented the first Cannabis-derived drug approved by the agency; a carbohydrate-inspired drug, namely migalastat (Galafold™), an iminosugar with a stereochemistry similar to D-galactose derived from the natural product nojirimycin; Annovera™, composed of a combination of two steroids, namely the estrogen ethinylestradiol and the progestin segesterone

acetate, belonging to the steroid family. This drug is indicated as a contraceptive vaginal ring (Figure 1.1).

From a quantitative perspective, figure 1.2 shows the relevance of natural products (16%), compared to the other classes of drugs, representing the third category, after mAbs (19%), and fluorinated products (28%).

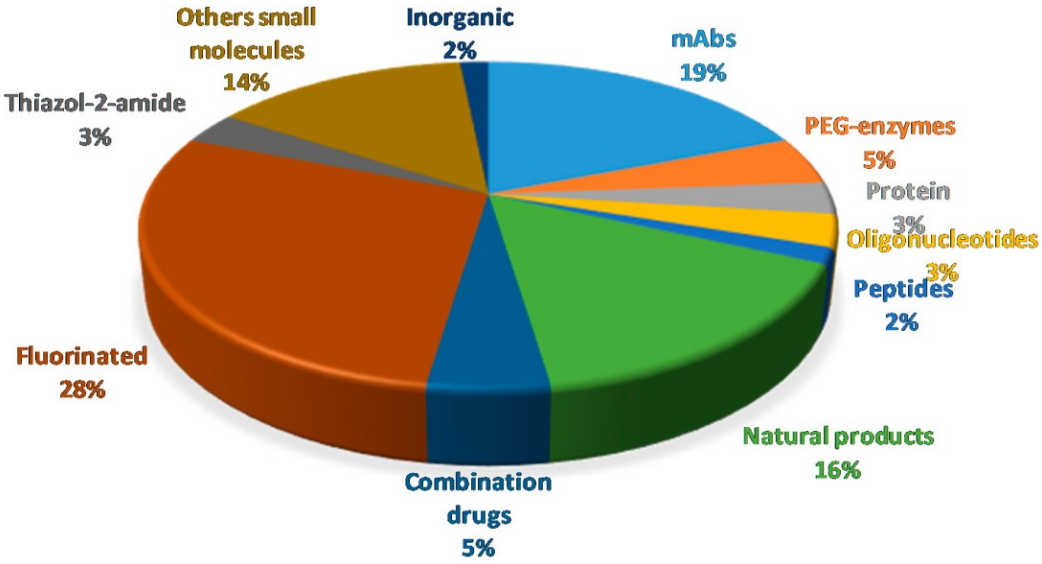

Figure 1.2. Drugs approved by the FDA in 2018 and classified on the basis of their chemical structure (de la Torre and Albericio, 2019).

Furthermore, it is necessary to consider that some fluorinated compounds could derive from nature inspiration, broadening the percentage of the influence of natural products in drug discovery. For example, eravacycline (Xerava™) (Figure 1.3), an antibiotic approved in 2018 by the FDA for severe intra-abdominal infections, is included in the fluorinated drugs, containing one atom of F (fluorine) in its structure. Actually, eravacycline is a synthetic compound (Ronn *et al.*, 2013), that derives from the group of natural tetracyclines, a well-known family of broad-spectrum antibiotics, isolated from *Streptomyces* sp. (Griffin *et al.*, 2010). Their modifications, as well as the synthesis of novel compounds within the tetracycline family have generated many compounds, such as eravacycline.

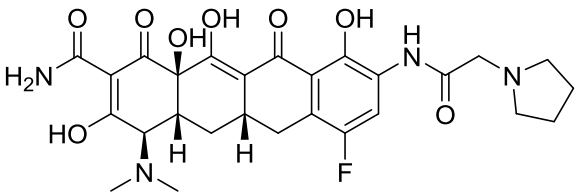

Eravacycline

Figure 1.3. Structure of eravacycline (Xerava™).

All these data highlight the importance of valorizing the role of natural compounds, as a source for new medicines, still today.

There are two main approaches to the discovery of new pharmacologically active plant compounds. The first one is a random screening approach, consisting of plant extracts, enriched fractions, or isolated compounds, randomly selected on the basis of their availability. In that case, it is feasible to identify unexpected bioactivities, which could not have been predicted, based on the existing knowledge. In particular, natural extracts can be screened using functional biological assays and after selecting the most promising fractions, it is possible to purify and identify natural compounds responsible for the activity. A second type is a knowledge-based approach, termed ethnopharmacology, where plants are chosen according to their use in traditional medicine, finding the metabolites acting for the pharmacological effect. Some examples of drugs discovered by the use of ethnopharmacological data are galegine from *Galega officinalis* L., a lead compound for the synthesis of metformin and determined the following development of biguanidine-type antidiabetic drugs or papaverine from *Papaver somniferum* L., the basis for the development of the antihypertensive drug verapamil (Atanasov *et al.*, 2015).

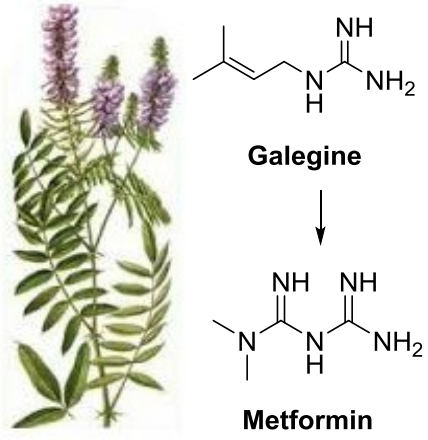

Galegine

Metformin

Figure 1.4. Galegine, natural lead compound isolated from *Galega officinalis* and its synthetic derivative, metformin.

In conclusion, plants elaborate countless chemically diverse secondary metabolites, optimized to exert biological functions. Since these compounds are still far from being exhaustively investigated (Atanasov *et al.*, 2015), the continuing success of plant-derived drug discovery proves that the plant kingdom can still offer new bioactive chemical scaffolds.

1.2 Structural determination methods

The investigation of natural products is carried out by the application of different available techniques, from the isolation to the identification of natural compounds. During my Ph.D. work, the structural elucidation was mostly based on spectroscopic (mainly nuclear magnetic resonance, NMR), and spectrometric (mass spectrometry, MS) techniques In addition, also computational calculations were included in this study, for prediction of configuration. For this reason, short paragraphs containing some related theoretical information are provided in this chapter.

1.2.1 Mass spectrometry

Mass Spectrometry is a powerful analytical technique, principally employed in organic chemistry, which permits to determine the molecular masses of unknown compounds and consequently establish their elementary formula. In contrast to other spectroscopic techniques, mass spectrometry is not based on the interaction between radiations and matter, but involves the destruction of the analyzed material. Pratically, each molecule needs to be ionized and moved to gas phase in the ion source and then it is transferred to the mass analyser where the mass properties are calculated. These three principal procedures take place in three different parts of the mass spectrometer, namely the ionisation source, the analyser, and the detector. The ionisation source generates ions in a gas-phase, thereafter ions are accelerated by an electric field, and when they achieve a specific velocity, are transferred to the mass analyzer. At this point, the analyzer divides different ions on the base of their mass/charge (*m/z*) ratio. The distinc ions are measured on the detector and the results displayed. In this way a mass spectrum is obtained.

Most of compounds described in the following chapters have been analysed by Electrospray Ionisation (ESI) mass spectrometry through an Orbitrap system.

ESI mass spectrometry allows the determination of non-volatile molecules to be analyzed directly from the liquid phase (Fig.1.5). A large number of chemical and physical parameters that together determine the quality of the process governs the electrospray process. An electrical circuit that drives the spray of liquid-charged droplets can define its start and end.

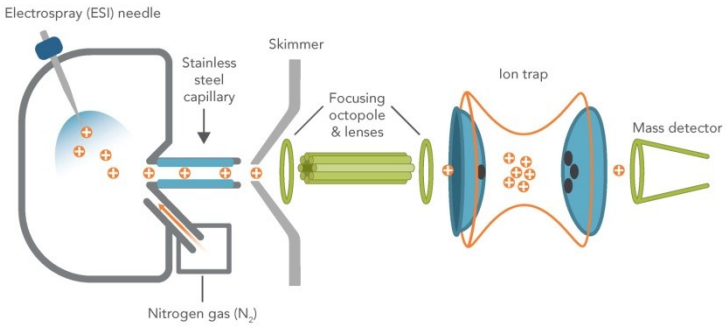

Figure 1.5. General components and mechanism of an ESI-ion trap MS instrument. (https://eu.idtdna.com/pages/education/decoded/article/esi-mass-spectrometry-why-we-use-it-for-oligonucleotide-quality-control)

In this procedure, the biomolecule departs as an entity or aggregate, tipically charged and dissolved in a water-rich medium. At the end of the procedure, the same biomolecule converges around the orifice of a mass analyser as a series of multicharged ions. In a vacuum area, the biomolecular ions are subsequently and selectively examined depending on their mass/charge ratio. As a result of the electric potential of the capillary, each drop of the spray delivers an excess positive or negative charge, and this induces an extensive protonation or deprotonation of the molecules of the sample, which evolve into ions. The ions showed in the mass spectrometry are generated by the addition of a hydrogen cation, and designated as $[M+H]^+$, or of another cation, for example, sodium, $[M+Na]^+$; the expulsion of a hydrogen nucleus, can produce $[M-H]^-$ anion. Multiply charged ions, $[M+nH]^{n+}$ can be also observed.

An uncharged gas such as nitrogen is used as 'vehicle' to facilitate the nebulisation of the liquid and the neutral solvent in the drop and promote the evaporation.

High-resolution mass spectrometry (HRMS) is an excellent approach, which guarantees the calculation of accurate masses of analyzed ions; the

instrumental systems includes Fourier-transform ion cyclotron resonance (FT-ICR), time-of-flight (TOF), and Orbitrap mass spectrometry.

Orbitrap is a type of mass analyser, proposed by Makarov (Hu, *et al.*, 2005). The LTQ-Orbitrap joines the most progressed Ion Trap and Fourier Transform technologies into a one instrument with singular analytical power and flexibility. The instrument offers a high mass resolution, accurate mass, and MS^n for routine high-throughput analysis. In an orbitrap system, ions are infused indirectly into the electric area between the electrodes and captured sincetheir electrostatic attraction to the internal electrode is compensated for centrifugal forces. Thus, ions turn around the central electrode in rings. Then, they return along the axis of the central electrode. For this reason, ions of a specific mass-to-charge ratio travel in rings, which swing along the central spindle (Fig.1.6). The frequency of these harmonious oscillations is not based on the ion velocity and is inversely proportional to the square root of the mass-to-charge ratio (*m/z*).

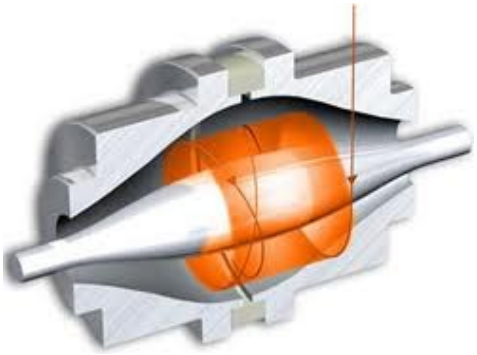

Figure 1.6. Ion trajectories in an Orbitrap mass spectrometer.

Also trap can be employed as a mass analyzer, since it detects the ion oscillation similarly to FT-MS (Fourier transform mass spectrometry).Orbitraps have a high mass accuracy (1-2 ppm), a high resolving power (up to 200,000) (Baneriee and Mazumdar, 2012; Demarque *et al.*, 2016).

1.2.2 Nuclear Magnetic Resonance (Bax *et al.*, 1982; Palmer *et al.*, 1991; Bax *et al.* 1986)

Nuclear Magnetic Resonance spectroscopy is a robust complex analytical tool used for structure elucidation of the isolated secondary metabolites in a non-destructive way. The nuclei of many elemental isotopes are distinguished by a definite number of spin (**I**). A spinning charge can originate a magnetic

field, producing a spin-magnet with a magnetic moment (**μ**) proportional to the spin. Emplying an external magnetic field ($\mathbf{B_0}$), various spin states of a nucleus are obtained, based on the value of I (this number corresponds to 2I+1) with dissimilar energy; this distintion is calculated through the applied magnetic field strength. Nuclei with I=0 are recognized as "NMR inactive", since they do not possess the nuclear spin property, critical to afford an NMR analysis. Hydrogen (^{1}H), carbon (^{13}C), fluorine (^{19}F) and phosphorus (^{31}P) are nuclei with I=1/2, for this reason, they can be examined by NMR. If nuclei with I≠0 are located in a magnetic field, they will acquire several orientations coinciding with specific energy levels; the number is based on the value of I, in particular, it is equal to 2I+1. When an external magnetic field is applied to nuclei with I= ½, they can assume two possible orientations, α parallel (I = ½), corresponding to the lower level of energy, or β antiparallel (I = - ½), corresponding to the higher level. The difference of energy is expressed by the following equation:

$$\Delta E = \gamma B_0$$

In this formula, γ correspond to the gyromagnetic factor, specific for each nucleus. The protons are divided between the two levels (α and β), with an excess of protons population in the α state, possessing a lower energy.

Applying an energy is applied (a radio frequency pulse) to the nuclei, they migrate from lower to higher energy levels; when the radiofrequency finishes the Free Induction Decay (FID) is provided and converted in the frequency domain by the Fourier Transform (FT).

In this study, 1D and 2D NMR experiments have been employed for structural elucidation of compounds. In particular, the COSY (COrrelation SpectroscopY) is a homonuclear chemical shift correlation experiments, that determine protons that are spin-spin coupled.

The HSQC (Heteronuclear Single Quantum Correlation) experiment is 2D NMR heteronuclear correlation experiment, in which only one-bond proton-carbon couplings ($^{1}J_{CH}$) are provided. The HSQC experiment connects the chemical shift of proton with the chemical shift of the directly bonded carbon.

The HMBC (Heteronuclear Multiple Bond Correlation) experiment is a heteronuclear two-and three-bond ^{1}H-^{13}C correlation experiment; cross-peaks evidenced by this experiment reveal the correlations between protons and

carbons distant two, three and, in some cases, four bonds; while correlations between protons and carbons directly bonded are not visible (Palmer *et al.*, 1991).

1.2.3 Stereochemical assignment

In the structure elucidation procedure the determination of the absolute and relative configurations of a previously undescribed natural, synthetic or modified compound is an essential step, since the strict association between the spatial distribution of atoms in a molecule and the biological activity. Nowadays several techniques are applied to determine relative and absolute configurations, and some of them, employed in the work decribed in this thesis, will be briefly discussed in the following paragraphs .

1.2.3.1 Determination of relative configuration

The relative configuration is defined as the organization of atoms or groups in space in relation to something else in the molecule. This feature can be easily defined by the use of NMR experiments. For instance, the proton chemical shifts of the two diastereomers are different since they have diverse chemical surroundings. The Karplus equation explains the relationship between ^{3}J coupling constants and dihedral torsion angles:

$$^3J = A\cos\theta^2 + B\cos\theta + C$$

^{3}J coupling constant expresses the correlation between two vicinal hydrogen atoms, θ is the dihedral angle, and A, B, and C are empiric parameters based on the substituents implicated. Following this equation, when the value of the coupling constant is small, it means that the torsion angle is close to 90°, while when it is large, the angles are between 0° and 180°. In this way, preliminary information about the relative atomic spatial distribution of a molecule is provided (Karplus, 1959).

NOESY (Nuclear Overhauser Enhancement SpectroscopY) is a useful NMR-based method to assign the relative configuration of chiral centers; when a specific NMR signal is irradiated, during the acquisition of the spectra, the NOE effect can be detected. In this way, the relaxation times of all the protons near the irradiated center (distance < 2.5 A°) is altered, along with those protons not

located in the same spin system. The NOE effect is obtained through space, not through chemical bonds; consequently, atoms that are in proximity to each other can produce NOE.

ROESY (Rotating-frame Overhauser SpectroscopY) experiment is similar to the previous method. It is based on a homonuclear correlation that can find ROE (Rotating-frame Overhauser Effect). This method is employed for molecules with a molecular weight around 1000 daltons, for which the NOE is too weak to be observed.

1.2.3.2 Determination of absolute configuration: circular dichroism

Electronic circular dichroism (ECD) is widely applied to identify the absolute configuration of chiral molecules. Circular Dichroism (CD) occurs when a molecule is optically active, it absorbs right-and left-handed circularly polarize light to different extents. Chiral compounds are able to absorb left and right circularly polarized UV/Vis light in different way, that represents the advantage of CD spectroscopy. Plane polarised light is composed by 2 circularly polarised components of equal magnitude, one rotating counter-clockwise (left handed, L) and the other clockwise (right handed, R). Circular dichroism (CD) consists of the differential absorption of these 2 components (Fig. 1.7). When equal intensity of left and right circularly polarized light irradiates a sample simultaneously, symmetrical or racemic sample, in equal amount, absorbs E_L and E_R in equal way. The resulting vector from E_L+E_R appears plane-polarized and non-rotated. As opposite, asymmetrical (chiral) sample absorbs in different way and the resulting electric field E_L+E_R appears elliptically polarized (CD) and rotated (Optical Rotatory Dispersion) as a function of wavelength. The instrument used to record the ECD spectrum of a compound is the spectropolarimeter, which measures ellipticity in terms of angle θ (Kelly and Price, 2000).

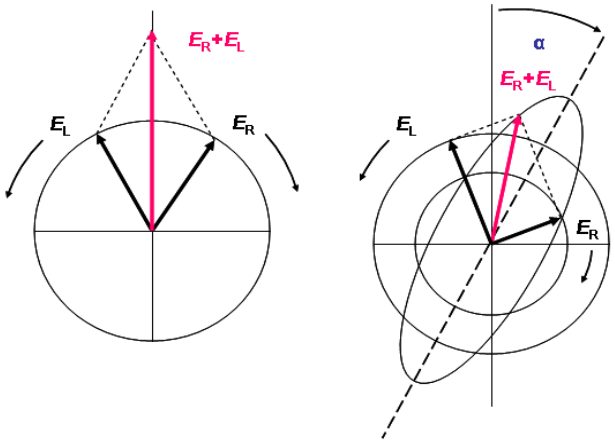

Figure 1.7. Origin of the CD effect. The left (L) and right (R) circularly polarised components of plane polarised radiation: on the left, the two components have the same dimension and when combined the resultant generate plane polarised radiation and non-rotated; on the right the components are of different dimension and the resultant is elliptically polarised.

The interpretation of the obtained results is often obtained by a comparison between the experimental and computationally calculated ECD spectra (Fig. 1.8).

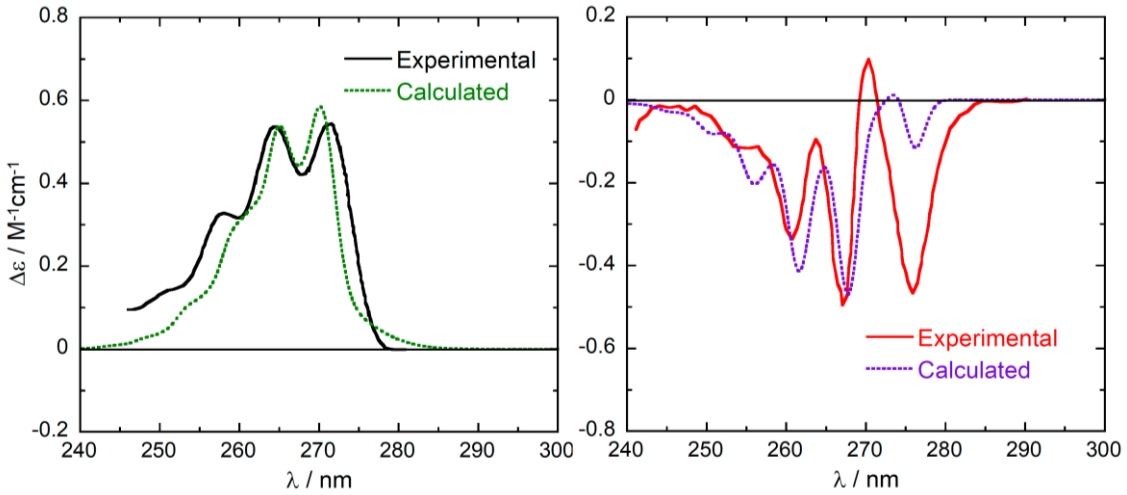

Figure 1.8. Calculated and experimental ECD spectra.

The calculated ECD spectrum is procured through several steps. The first step consists of a conformational analysis of the molecule in order to select all possible conformers based on their relative energy evaluation. This process is defined "minimization", in which the atoms are moved from their positions

measuring the resulting changes of the total energy in the system. Nowadays, several Molecular Mechanics are employed to minimize the energy of each conformer, including MM2, MMFF94 and Extended Hückel. The molecular mechanics is a computational method able to calculate the energy for each specific disposition of atoms, using potential functions known as a force-field. In this way, when the minimum point of this function is found, the conformation and minimum energy are provided. The second step consists of the calculation of Gibbs energy for each conformer, using a faster DFT model (smaller basis set, B3-LYP/6-31G). This step results in the exclusion of conformers with $\Delta\Delta G$ > 2 kcal/mol. At this point the more relevant conformers are considered to perform the UV/ECD TDDFT (time-dependent density functional theory) calculations. The UV/ECD spectra of each conformers are Boltzmann averaged, and the final calculated UV/ECD spectrum is obtained. At this point, by comparison of the calculated ECD spectra with the experimental ECD of the natural product, the determination of the absolute stereochemistry can be performed.

The calculations reported in my thesis have been performed using Gaussian 16 W (Gaussian *et al.*, 2004).

1.3 General experimental procedures

IR spectra were registered on an Avatar 370 FT-IR Techno-Nicolet apparatus. 1D and 2D NMR experiments were recorded on a Varian INOVA 700 and 500 (Agilent, USA) and Bruker Avance NEO 400 (Bruker, USA) spectrometers with a RT-DR-BF/1H-5mm-OZ SmartProbe. Chemical shifts are referenced to the residual solvent signal ($CDCl_3$: δ_H 7.26, δ_C 77.0; $(CD_3)_2CO$: δ_H 2.09, δ_C 205.9, 30.6; CD_3OD: δ_H 3.31, δ_C 49.0). Homonuclear ^1H connectivities were determined by COSY experiments; one-bond heteronuclear ^1H-^{13}C connectivities by the HSQC experiment; and two - and three-bond ^1H-^{13}C connectivities by gradient-HMBC experiments optimized for a $^{2,3}J$ value of 8 Hz. Through-space ^1H connectivities were obtained using a ROESY experiment with a mixing time of 500 ms. Low- and high-resolution ESIMS were performed on LTQ OrbitrapXL (Thermo Scientific) mass spectrometer. ECD spectra were obtained in a Jasco J-815 CD spectropolarimeter (Jasco, Mary's Court, Easton, MD, USA) with a 0.1 mm cuvette and eight accumulations. Medium-pressure liquid chromatography was performed on a Buchi (Switzerland) apparatus using

a silica gel (70-230 mesh) column; separations were monitored by TLC on Macherey-Nagel 60 F_{254} (0.20 mm) plates and were visualized by UV inspection and/or staining with Pancaldi mixture and heating. RP-HPLC-UV-vis separations were performed on an Agilent instrument, using, 1260 Quat Pump VL system, equipped with a 1260 VWD VL UV-vis detector, a Supelco Ascentis C18, 5 µ 10 × 250 mm column 2.5 mL/min as flow rate and a Rheodyne injector. HPLC-RI separations were performed on a Knauer (Berlin, Germany) 1800 apparatus equipped with a refractive index detector and Luna (normal phase, SI60, or reverse-phase RP18, 250×4.6 mm) (Phenomenex) column, with 0.8 mL/min as flow rate.

Reactions were monitored by TLC on Merck 60 F254 (0.25 mm) plates, visualized by staining with 5% H_2SO_4 in ethanol and heating. Organic phases were dried with anhydrous Na_2SO_4 before evaporation. Chemical reagents and solvents were purchased form Sigma-Aldrich (Germany) and were used without any further purification. Petroleum ether with boiling point of 40–60 °C was used. Silica gel 60 (70–230 mesh) was used for gravity column chromatography (CC). HPLC purifications were carried out on Agilent 1260 Infinity apparatus equipped with Sunfire C18 3.5 µm, 4.6×150mm column and UV detector set at λ_{max} 227 nm.

References

Atanasov A. G., Waltenberger B., Pferschy-Wenzig E.-M., Linder T., Wawrosch C., Uhrin P., Temml V., Wang L., Schwaiger S., Heiss E. H., Rollinger J. M., Schuster D., Breuss J. M., Bochkov V., Mihovilovic M. D., Kopp B., Bauer R., Dirscha V. M., Stuppner H. (**2015**). *Biotechnology Advances*, *33*, 1582–1614.

Banerjee S., Mazumdar S. (**2012**). Electrospray ionization mass spectrometry: a technique to access the information beyond the molecular weight of the analyte. International journal of analytical chemistry, 2012.

Butler M. S. (**2004**). The role of natural product chemistry in drug discovery. *Journal of Natural Products*, *67*, 2141–2153.

Campbell S. F. (**2000**). Science, art and drug discovery: A personal perspective. *Clinical Science*, *99*, 255–260.

Cragg G. M., Newman D. J. (**2013**). Natural products: a continuing source of novel drug leads. *Biochim Biophys Acta*, *1830*, 3670-95.

Croteau R., Kutchan T. M., Lewis N. G. (**2000**). Natural products (secondary metabolites). *Biochemistry and molecular biology of plants*, *24*, 1250-1319.

De la Torre B. G., Albericio F. (**2019**). The pharmaceutical industry in 2018. An analysis of FDA drug approvals from the perspective of molecules. *Molecules*, *24*, 809.

Demarque D. P., Crotti A. E., Vessecchi R., Lopes J. L., & Lopes N. P. (**2016**). Fragmentation reactions using electrospray ionization mass spectrometry: an important tool for the structural elucidation and characterization of synthetic and natural products. *Natural product reports*, *33(3)*, 432-455.

Gaussian 16, Revision C.01, Frisch M. J., Trucks G. W., Schlegel H. B., Scuseria G. E., Robb M. A., Cheeseman J. R., Scalmani G., Barone V., Petersson G. A., Nakatsuji H., Li X., Caricato M., Marenich A. V., Bloino J., Janesko B. G., Gomperts R., Mennucci B., Hratchian H. P., Ortiz J. V., Izmaylov A. F., Sonnenberg J. L., Williams-Young D., Ding F., Lipparini F., Egidi F., Goings J., Peng B., Petrone A., Henderson T., Ranasinghe D., Zakrzewski V. G., Gao J., Rega N., Zheng G., Liang W., Hada M., Ehara M., Toyota K., Fukuda R., Hasegawa J., Ishida M., Nakajima T., Honda Y., Kitao O., Nakai H., Vreven T., Throssell K., Montgomery J. A. Jr., Peralta J. E., Ogliaro F., Bearpark M. J., Heyd J. J., Brothers E. N., Kudin K. N., Staroverov V. N., Keith T. A., Kobayashi R., Normand J., Raghavachari K., Rendell A. P., Burant J. C., Iyengar S. S., Tomasi J., Cossi M., Millam J. M., Klene M., Adamo C., Cammi R., Ochterski J. W.,

Martin R. L., Morokuma K., Farkas O., Foresman J. B., and Fox D. J., Gaussian, Inc., Wallingford CT, (**2016**).

Griffin M. O., Fricovsky E., Ceballos G. and Villarreal F. (**2010**). Tetracyclines: a pleitropic family of compounds with promising therapeutic properties. Review of the literature. *Am J Physiol Cell Physiol*., *299*, C539–C548.

Hamilton G. R., Baskett T. F. (**2000**). In the arms of Morpheus the development of morphine for post-operative pain relief. *Can J Anaesth*, *47*, 367-374.

Hu Q., Noll R. J., Li H., Makarov A., Hardmanand M., Cooks R. G. (**2005**). *J. Mass Spectrom*, *40*, 430-443.

Karplus M. (**1959**). Contact ElectronSpin Coupling of Nuclear Magnetic Moments. *J. Chem. Phys.*, *30*, 11-15.

Kelly S. M., Price N.C. (**2000**). The Use of Circular Dichroism in the Investigation of Protein Structure and Function. *Current Protein and Peptide Science*, *1*, 349-384.

Mukherjee A.K., Basu S., Sarkar N., Ghosh A.C. (**2001**). Advances in cancer therapy with plant based natural products. *Current Medicinal Chemistry*, *8*, 1467–1486.

Palmer III A. G., Cavanagh J., Wright P. E., Rance M. (**1991**) Sensitivity improvement in proton-detected two-dimensional heteronuclear correlation NMR spectroscopy. *J. Magn. Reson*, 151-170.

Ronn M., Zhu Z., Hogan P. C., Zhang W.-Y., Niu J., Katz C. E., Dunwoody N., O. Gilicky N., Deng Y., Hunt D. K., He M., Chen C.-L., Sun C., Clark R. B., Xiao X.-Y. (**2013**). Process R&D of eravacycline: the first fully synthetic fluorocycline in clinical development. *Org. Process Res. Dev.*, *17*, 838-845.

Salim A. A., Chin Y.-W., Kinghorn A. D., Drug discovery from plants. (**2008**) In: Ramawat, K. G., Merillon, J.M. editors. Bioactive Molecules and Medicinal Plants. Springer-Verlag, Heidelberg, pp. 1–24.

Srivastava V., Negi A. S., Kumar J. K., Gupta M. M., Khanuja S.P.S. (**2005**). Plantbased anticancer molecules: A chemical and biological profile of some important leads. *Bioorganic and Medicinal Chemistry*, *13*, 5892–5908.

Steinberg D., Gotto-Jr. A. M. (**1999**). Preventing coronary artery disease by lowering cholesterol levels: Fifty years from bench to bedside. *Journal of the American Medical Association*, *282*, 2043–2050.

Willcox M. L., Cosentino M. J., Pink R., Wayling S., Bodeker G. (**2001**). Natural products for the treatment of tropical diseases. *Trends in Parasitology*, *17*, 58–60.

Chapter 2: Antimalarial transmission-blocking potential of *Lophira lanceolata*

2.1 Malaria is still an alarming problem

Malaria is a mosquito-borne protozoal infection caused by parasites of the genus *Plasmodium* with five species currently known to cause the disease in humans: *P. falciparum*, *P. vivax*, *P. malariae*, *P.ovale* and *P.knowlesi*, which usually infects macaque monkeys, as recently reported in South-east Asia (Kantele A, Jokiranta TS, 2011). Among them, *P. falciparum* and *P. vivax* represented the greatest threat for humans.

The diffusion of the parasites to people occurs through the bites of infected female *Anopheles* mosquitoes, considered as "malaria vectors". In agreement with WHO data, the geographical areas where most of malaria cases and deaths are sub-Saharan Africa, South-East Asia, Eastern Mediterranean, Western Pacific and the Americas. The population groups, considered as at higher risk of contracting malaria, include infants, children under 5 years of age, pregnant women and patients with HIV/AIDS, as well as non-immune migrants, mobile populations and travellers. Despite efforts to eradicate malaria in the past century, the disease remains a major global health problem. The most recent global malaria report published by the WHO estimated 228 million cases of malaria which caused 405000 deaths in 2018 (World malaria report 2019).

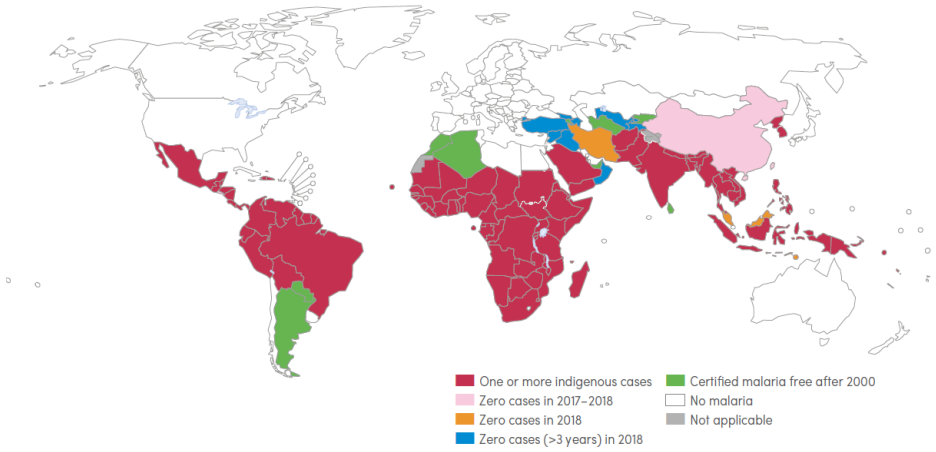

Figure 2.1. Distribution of malaria cases according to World Malaria Report 2019.

2.1.1 *Plasmodium* life cycle

The life cycle of malaria parasites takes place inside two hosts, including humans, where its asexual stages develop and the mosquitoes, for its sexual phases (Sharma and Awasthi, 2015). It starts when an infected female mosquito, belonging to the genus *Anopheles*, injects infective forms of the parasite (named sporozoites) into the human bloodstream during a blood meal. Within 15−30 min, the human liver is reached by sporozoites, causing the hepatocytes infection and then the development into schizonts. After mitosis process, thousands of infective merozoites are produced.

With the rupture of the hepatic tissue, these merozoites are dispersed into the bloodstream and they are able to penetrate and disintegrate red blood cells. This step is defined as the asexual erythrocytic phase of the parasite lifecycle that is responsible for the clinical symptoms of fever, fatigue, and chills that can lead to coma and even death.

Eventually, some asexual merozoites will evolve into sexual gametocytes. Gametocytes undergo five stages of maturation (from stage I to V) and only mature (stage V) gametocytes are capable of infecting *Anopheles* mosquitoes by ingestion of the next blood meal (Peatey, *et al.*, 2012). In the mosquito, gametocytes will sexually reproduce until the formation of ookinete first and then oocyst, in the midgut. From the oocyst are originated thousands of sporozoites that migrate to insect salivary glands, ready to achieve a new vertebrate host by the infected mosquito bite (Fernández-Álvaro E., *et al.*, 2016).

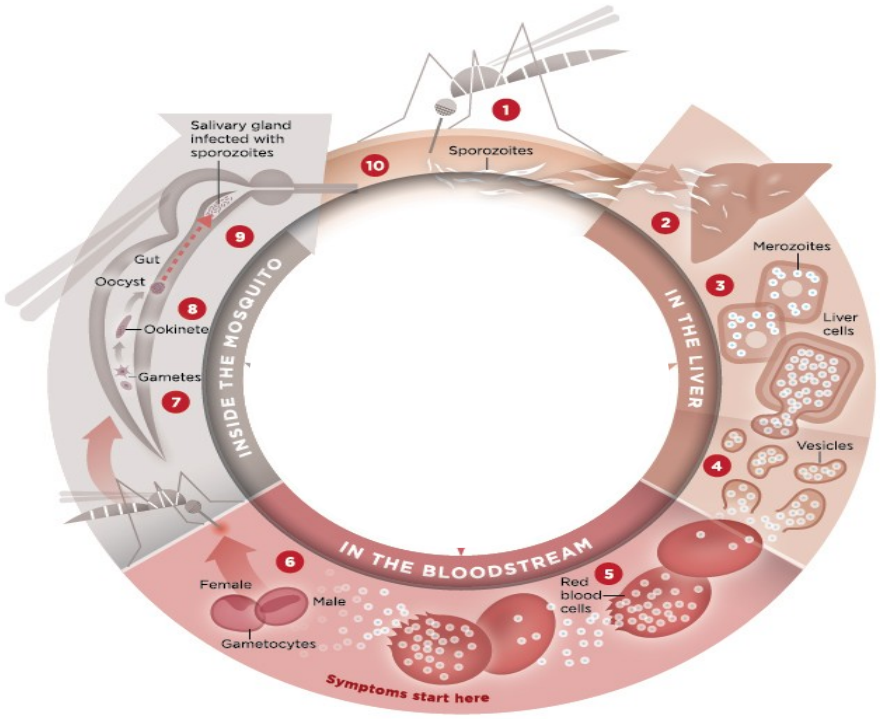

Figure 2.2. Malaria life cycle (modified from https://www.malariavaccine.org/malaria-and-vaccines/vaccine-development/life-cycle-malaria-parasite)

2.2 The new anti-malaria challenge: transmission-blocking activity

The history of antimalarial drugs dates back to 1820, when French scientists Pelletier and Caventou attributed antimalarial properties to quinine, the major alkaloid isolated from the barks of *Cinchona* species (Rubiaceae). The quinine template has later inspired the development of the most marketed antimalarials, such as chloroquine and its derivative 4-aminoquinoline, developed in the 1940s. Although they are still today considered as antimalarial drugs, their effectiveness has decreased since 1960s, due to the diffusion of *P. falciparum* resistance. Another example of quinine derivatives is mefloquine that was introduced as the antimalarial drug in 1985 and used to threat only mild or moderate malaria (Fidock *et al.*, 2004).

Nowadays, in according to WHO, the first-line treatment against malaria is based on artemisinin, a sesquiterpene lactone and endoperoxide-containing natural product, identified from the leaves of *Artemisia annua* L. (Asteraceae), also denominated as Qinghao, in 1970s. Artemisinin exhibited strong antimalarial activity against chloroquine-resistant *P. falciparum* strains and several artemisinin derivatives were synthesized, such as artemether, arteether

(artemotil), artesunate and artenimol (-dihydroartemisinin, DHA) (Sriram, D. *et al.*, 2004). Artemisinin and its derivatives are used in combination with other drugs, known as artemisinin-based combination therapy (ACT), mainly to avoid the spread of artemisinin-resistance if it is used in monotherapy, despite some cases artemisinin drug resistance has been already detected in some Southern Asian countries. Moreover, the association of different drugs revealed to be the most effective antimalarial weapon. Five currently available ACTs are artemether in combination with lumefantrine, and four other forms based on artesunate in combination with amodiaquine (two formulations), mefloquine and sulfadoxine + pyrimethamine (World malaria report 2019). Few data are reported in literature about the mode of action of these drugs, but it was established that they are able to especially inhibit the parasite asexual life stages, that are responsible for the typical malaria symptoms (e.g. fever) and resulting in their disappearance in the vertebrate hosts (Ginsburg, H. *et al.*, 1994). However, although there are several weapons to fight against malaria burden, it seems not to be enough since our world is still threateningly assailed from a huge number of malaria cases and deaths, as described from WHO data.

Recent studies have demonstrated that even if current antimalarial drugs are effective (if correctly used) in the treatment of malaria symptoms, leading to the full recovery of patients, they cannot accomplish a complete parasite clearance in humans. Indeed mature gametocytes are able to remain silent in the peripheral blood of the vertebrate host for more than one week, becoming a vector of infection for *Anopheles* mosquitoes. Indeed, within 24 h after a blood meal, all the sexual processes are completed: gametogenesis, macrogamete fecundation and zygote formation until the development of elongated ookinetes (Sinden *et al.*, 2007). Subsequently, these motile forms move from the midgut lumen to the outer midgut wall and finally produce salivary gland sporozoites. In quantitative terms, sexual forms, i.e. gametocytes in the human host and gametes and zygotes in the insect host are present in relatively low numbers, thus representing a bottleneck of the parasite's reproductive life cycle and ideal targets for pharmacological attack. Metabolism of mature gametocytes is restricted to "housekeeping" processes, whereas gamete to ookinete development involves various complex biological processes, offering a plethora of enzymes and receptors as possible drug targets (Sinden *et al.* 2012).

For this reason, the main research effort has been undergoing a challenging shift in global malaria management programs, moving from control toward elimination of the disease. It means that to achieve malaria eradication, it is necessary to produce interventions that can interrupt the transmission of parasites from humans to mosquitoes and *vice versa*.

Actually, ACT indicated to reduce gametocyte density (WWARN Gametocyte Study Group, 2016), but it cannot provide a sterilizing effect on mature stage-V gametocytes and consequently cannot block malaria transmission. Recently, the World Health Organization (WHO) suggested the addition of a single dose of primaquine (0.25 mg/kg of body weight) to the ACT administration to eliminate mature *P. falciparum* gametocytes (World malaria report 2019). At a population level, the use of primaquine as post-treatment not only contributes to reduce transmission intensity but also to slow down the emergence and diffusion of artemisinin resistant *P. falciparum* strains. However, its adverse effects restrict the use of primaquine in patients with G6PD deficiency (White *et al.* 2012).

In this scenario, medicinal plant research may contribute to develop new drug leads with anti-malarial potential, especially active against the stages responsible for *Plasmodium* transmission, i.e. the gametocytes in the vertebrate host and the sporogonic stages in the mosquito. For this reason, thanks to the modern availability of robust and reproducible screening methods to expand the arsenal of transmission-blocking drugs, part of my Ph.D. work was focused on the investigation of medicinal plants, looking for new lead compounds active against gametocytes and possibly also against the sporogonic stages, for the inclusion in multi-stage combination medicines (Abay *et al.*, 2015; Tapanelli *et al.*, 2016; Sirignano *et al.*, 2017).

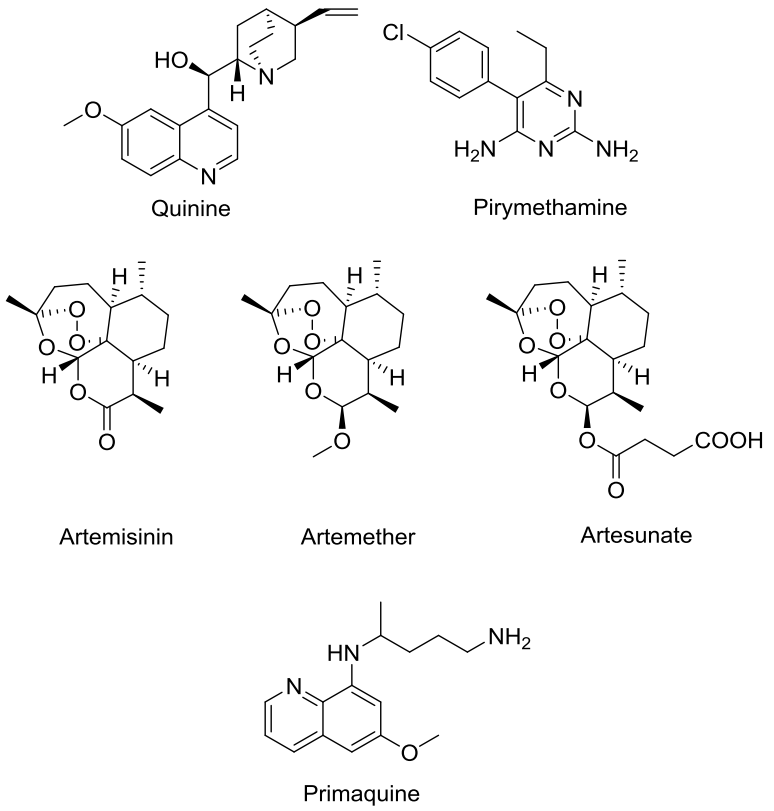

Figure 2.3. Structures of major antimalarial drugs.

2.3 Screening of plants based on their transmission-blocking properties

The recent availability of robust and reproducible screening methods for antimalarial transmission-blocking agents has permitted a preliminary screening of extracts obtained from plants traditionally used as a folk medicine for treatment of malaria or similar diseases, in order to achieve small molecules endowed with this stage-specific activity to be included in a multi-stage remedy. For this study, the selection of these plants was sustained by an ethnopharmacological approach as well as by antimalarial (*Plasmodium* asexual stages) activity of plant extract, enriched fractions or pure compounds, already reported in literature. In particular, as discussed in Chapter 1, there are two main approaches to select plants in order to find new bioactive natural compounds, namely a random screening approach or a knowledge-based approach, such as ethnopharmacology. In this case, it appears quite evident that ethnopharmacology is not able to predict a trasmission-blocking activity, anyway it was considered as a suitable starting point for this study. Following

this direction, twelve plants (reported in table 2.1) were selected, on the basis of their traditional use as remedy for malaria in Burkina Faso.

Table 2.1. List of plants (grouped according to their families) selected to evaluate for their inhibition activity on *Plasmodium*.

FAMILY	Plants
CAESALPINIACEAE	*Cassia sieberiana*
COMBRETACEAE	*Anogeissus leiocarpus*
	Combretum collinum
	Combretum fragrans
	Terminalia avicennioides
	Terminalia macroptera
OCHNACEAE	*Lophira lanceolata*
PAPAVERACEAE	*Argemone mexicana*
RUBIACEAE	*Mitragyna inermis*
	Pavetta crassipes
	Zanthoxylum zanthoxyloïdes
VERBENACEAE	*Vitex doniana*

Different parts of these plants (leaves, stems or roots) were extracted with two solvents: water and ethanol and their extracts were evaluated for their inhibition on parasite's specific life stage, namely gametocytes, early sporononic stage and ookinetes development. The study on *Plasmodium* gametocytes and asexual stage was carried out at the Department of Pharmaceutical and Biomolecular Science of University of Milano, while early sporogonic stage and ookinete-stage (ookinete Development Assay, ODA) at the School of Pharmacy at University of Camerino. Preliminary results allowed to select the ethanolic extract of *Lophira lanceolata* stem barks as a promising source of bioactive compounds, worthy of further investigation. Indeed, *L. lanceolata* stem barks revealed active on both investigated *Plasmodium* sexual life stages.

Table 2.2. Inhibitory activity of plants extracts on stage V gametocytes of the transgenic 3D7elo1-pfs16-CBG99 strain.

Plant name	Plant Part	Percentage of viability at the dose 100µg/mL	
		Ethanolic extract	Aqueous extract
Anogeissus leiocarpus	Leaves	88.75±15.04	73.50±13.07
Argemone mexicana	Leaves	55.5±16.67	66.25±17.26
Cassia sieberiana	Leaves	68.5±13.34	88.25±16.96
Combretum collinum	Leaves	65.5±18.74	75.13±13.97
Combretum collinum	Stem barks	97.63±21.53	83.88±14.06
Combretum fragrans	Leaves	63.75±19.80	55±21.75
Lophira lanceolata	Leaves	72.88±13.30	76.88±18.54
Lophira lanceolata	Stem barks	7±5.83	61.38±24.62
Mitragyna inermis	Leaves	91.25±23.88	75.88±12.26
Mitragyna inermis	Stem barks	83.38±24.25	85.75±8.1
Pavetta crassipes	Leaves	107.5±20.58	52.13±28.88
Terminalia avicennioides	Leaves	91.38±20.18	74±12.71
Terminalia avicennioides	Stem barks	65.5±15.68	80.63±9.44
Terminalia macroptera	Leaves	7.14±30.79	72.25±17.56
Terminalia macroptera	Stem barks	67.75±15.1	82.63±13.41
Vitex doniana	Root barks	101.63±33.26	89.71±26.99
Vitex doniana	Stem barks	81.88±21.51	98.5±22.78
Zanthoxylum zanthoxyloïdes	Stem barks	56.38±13.87	79.33±21.2

As illustrated in Table 2.2, the evaluation of the anti-gametocytes activity of the selected plants indicated a negligibile response of the aqueous extracts of all plants, but emphasized a great potential of the ethanolic extract of two plants: *Lophira lanceolata* stem bark and of *Terminalia macroptera* leaves. These extracts reduced the viability of *P. falciparum* gametocytes more than 90%, showing more promising than the other considered plants.

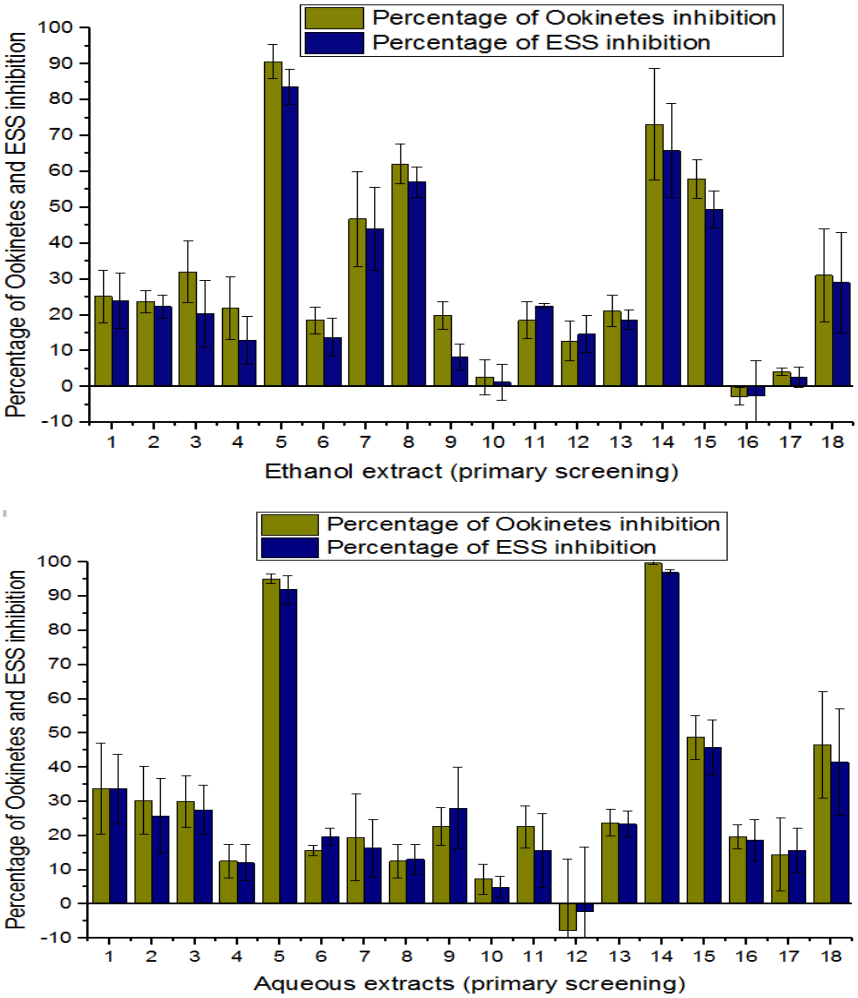

Figure 2.4. Screening of ethanolic and aqueous extracts of 12 plants for inhibition of ookinets and Early Sporogonic Stages (ESS). Inhibition percentage at 50 µg/mL is shown. Plant parts are: 1. *Terminalia avicennioides* stem barks. 2. *Terminalia avicennioides* leaves. 3. *Terminalia macroptera* stem barks. 4. *Terminalia macroptera* leaves. 5. *Combretum collinum* stem barks. 6. *Combretum collinum* leaves. 7. *Mitragyna inermis* stem barks. 8. *Mitragyna inermis* leaves. 9. *Anogeissus leiocarpus* leaves. 10. *Argemone mexicana* leaves. 11. *Pavetta crassipes* leaves. 12. *Zanthoxylum zanthoxyloïdes* stem barks. 13. *Combretum fragrans* leaves. 14. *Lophira lanceolata* stem barks. 15. *L. lanceolata* leaves. 16. *Vitex doniana* stem barks. 17. *Vitex doniana* roots. 18. *Cassia sieberiana* leaves.

On the other hand, the measurement of the early sporogonic stages and ookinetes (stages occurring in mosquito) inhibition activity by the same extracts suggested a different trend. First, as showed in figure 2.4, both aqueous and ethanolic extracts exhibited remarkable results. However, also in this case, plants showed more interesting than others were substantially two, namely the

stem barks of *L. lanceolata* and *Combretum collinum*; instead, the extracts of *Termalia macroptera* leaves dispayed now insignificant performance, compared to its activity on the gametocytes stage. The ethanolic extracts of few others plants demonstrated an inhibition activity slightly higher than 50%. In table 2.3, the IC_{50} values, calculated for *C. collinum* and *L. lanceolata* are provided.

Table 2.3. IC_{50} values (μg/mL) of crude extracts from stem barks of *L. lanceolata* and *C. collinum* on counts of early sporogonic stages and developing ookinetes.

Plant part	Extracts	DO[a] counts	ESS[b] counts
C. collinum	aqueous	17.95±1.50	22.38±1.87
	ethanolic	7.77±0.59	9.02±0.68
L. lanceolata	aqueous	16.81±1.11	18.81±0.92
	ethanolic	16.27±1.75	21.86±3.08

Data are expressed as means ± SD. [a]DO= developing ookinetes: considering counts of retort forms, elongating and fully mature ookinetes. [b]ESS= early sporogonic stages: considering counts of all forms: zygotes, retort forms, elongating and mature ookinetes.

Results showed in table 2.2 and figure 2.4 highlighted that, among the twelve investigated plants, only a couple expressed transmission-blocking properties, despite their use in traditional medicine as antimalarial remedy. Although also *T. macroptera* as well as *C. collinum* will be worthy of further investigation, we decided to address our research toward *L. lanceolata*. Indeed, this plant, unlike the other screened plants, showed promising activity both as anti-gametocydal agent and ookinetes and early sporogonic stage inhibitor.

2.4 *Lophira lanceolata*, a plant with countless powers (Prota, 2007)

L. lanceolata (Van Tiegh ex Keay) belongs to the Ochnaceae family, that is characterized as a great source of biflavonoids, with the most representative genera being *Lophira*, *Luxemburgia*, *Ochna* and *Ouratea*. Among them, the genus *Lophira* is found throughout tropical regions of Africa. The genus *Lophira* includes two known species: *Lophira alata* Banks ex P.Gaertn., from which the popular timber azobé is obtained, and *L. lanceolata*. The main difference between the two species is their habitat: *L. alata* is found in dense forest, while

Lophira lanceolata in savanna woodland. In particular, *L. lanceolata* is widely distributed in the Sudan-Guinea savannah zone, growing up in Northeast and West Tropical Africa, in regions like Sudan, Guinea, Nigeria, Senegal, Cotê d'Ivoire. *L. Lanceolata* is a tall tree that can reach up to 60 feet, straight or twisted. Its leaves are alternate, clustered at the end of short branches and elongate lanceolate. The stem bark of the *L. lanceolata* plant, that was analyzed in this study, appears harsh, broken into thin corky patches and grey in colour. The leaves are rounded at the top and extended in nature. Flowers blossom from December to February.

Figure 2.5. *Lophira lanceolata*.

About the traditional uses related to this plant, *L. lanceolata* is considered as a multi-purpose tree. The seeds were consumed more commonly in the past than at present; now from them the edible oil, called 'méni oil' is extracted, also employed for its cosmetic or medicinal properties. The wood is especially applied for mortars, railway sleepers and in bridge construction, thanks to its hardness and heaviness. It is also useful in house construction and to produce agricultural and household tools. It provides great firewood generating hot flames and little smoke and is also a large source of charcoal. The bark of the plant is used as a colourant in West Africa to inhibit cooked yam from becoming dark. Cattle browses on leaves during the dry season, while the odorous flowers are attractive to honey bees, e.g. in Nigeria.

All of the parts of *L. lanceolata* are used in traditional medicine to treat several diseases, such as constipation, diarrhoea, dysentery, menstrual pain (women) as concoction and infusion of the bark of roots and trunk. Specifically, the méni oil is used to treat dermatosis, toothache and muscular tiredness. The oil is also

a good remedy against dryness, or it is combined with porridge and given to children as a tonic. The roots are then prepared in a concoction and utilized as relief from menstrual pain, intestinal troubles. In addition, the infusion of the young twigs treats fever, respiratory tract infections and dysentery. Concoctions of young fresh or dried leaves are drunk to treat pain caused by intestinal worms, dysentery and diarrhoea in children; while young red leaves are also employed in the treatment of headache, hypertension and syphilis.

About the phytochemical content, previous analysis of the genus *Lophira* has resulted in the isolation of biflavonoids and tetraflavonoids, nitrile glycosides, benzamides, a benzoylglucoside, triterpenoids. In particular, the stem bark extract of *L. lanceolata* has been shown to contain flavonoids, tannins resin, saponin and alkaloids. They include a group of related biflavonoids called lophirones A-J, the biflavonoid isombamichalcone and the tetraflavonoid lanceochalcone (Ghogomu Tih *et al.*, 1987, 1989, 1990, 1994). The wood contains the nitrile glycoside esters lanceolin A and B, while the leaves contain lanceolatin A and B and additionally, the benzoyl glycoside lanceoloside A and the prenylated isoflavone lanceolone (Pegnyemb *et al.*, 1998). The presence of benzamide has been reported in the root bark (Persinos *et al.* 1967).

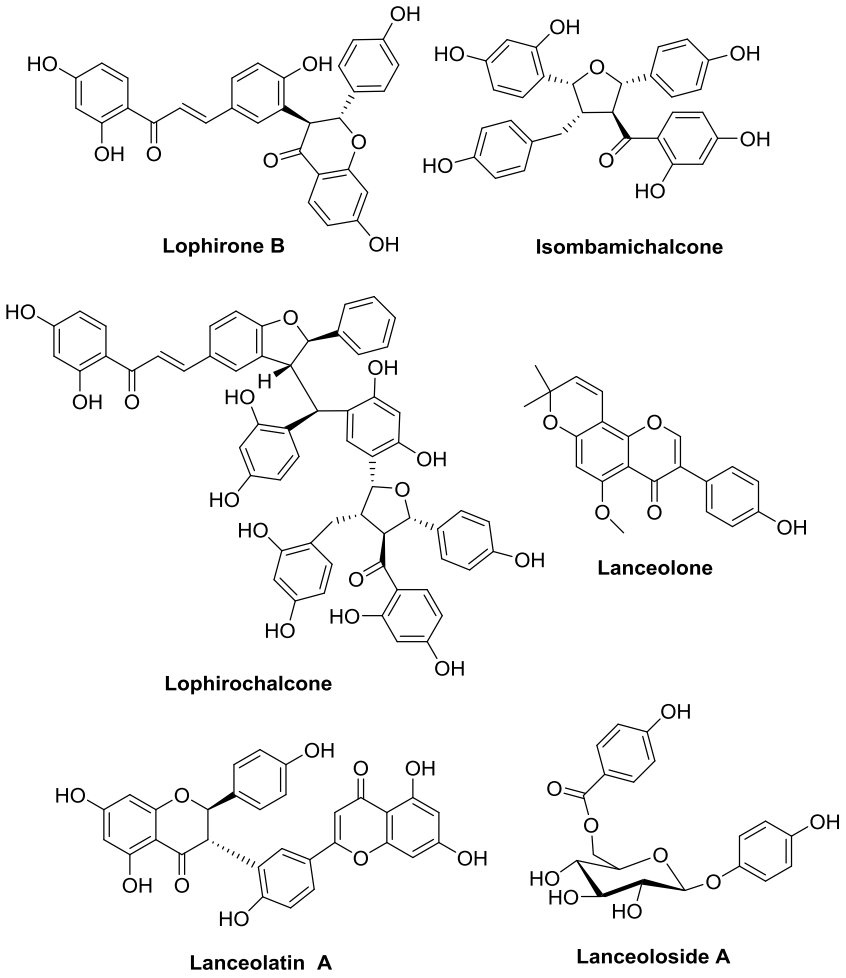

Figure 2.6. Some of reported metabolites from *L. lanceolata*.

2.5 Bioassay guided purification of *Lophira lanceolata* stem barks

The preliminary screening of plants based on their transmission-blocking properties allowed to select *L. lanceolata* stem barks (ethanolic extract) as the most promising plant species and part, demonstrating a potent activity against all *Plasmodium* investigated sexual stages. In fact, *L. lanceolata* stem bark ethanolic extract reduced gametocyte viability by more than 90% at a dose of 100 µg/mL and early sporogonic stages by more than 90% at a dose of 50 µg/mL.

The investigation of *L. lanceolata* started from the extraction in a larger scale of powder of stem bark with methanol. Methanol was used instead of etanol due to its lower cost and has the same efficiency as ethanol. Then the methanolic extract was subjected to a partitioning scheme that eventually afforded hexane, ethyl acetate and butanol sub-extracts. Following the bioassay-guided analysis, from the antimalarial evaluation of these three sub-extracts, the ethyl acetate

sub-extract proved to be the most promising. In particular, as shown in Table 2.3, the hexane phase and butanol phases indicated a negligible activity against asexual stages as well as against stage V gametocytes; in contrast, butanol phases exhibited such good activity against sexual stages that occur in the mosquito. However, the medium polar phase was considered the most suitable to start the isolation of bioactive compounds eventually active against the inquired plasmodium stages.

The preliminary results confirmed the activity of the crude methanolic extract against stage V gametocytes, with an IC_{50} value of 7.74 µg/mL (Table 2.4), while neither the methanolic extract nor any of the three sub-extracts showed significant activity (IC_{50} >30 µg/mL) against 3D7 and W2 asexual stages. Testing *L. lanceolata* butanol, hexane and ethyl acetate phases for activity against stage V gametocytes revealed that the plant gametocytocidal activity was conserved in the ethyl acetate phase, displaying an IC_{50} of 13.38 µg/mL (Table 2.4).

Table 2.4. *In vitro* antiplasmodial activity of the crude methanolic extract and sub-extracts of *L. lanceolata* stem barks against *P. falciparum* asexual blood stages of the CQ-sensitive 3D7 and CQ-resistant W2 strain and on late stage gametocytes of the 3D7elo1CBG99 strain.

Crude extracts/Phases	3D7 asexual stage IC_{50} (µg/mL)	W2 asexual stage IC_{50} (µg/mL)	Gametocyte[a] IC_{50} (µg/mL)
Methanolic extract	38.18±5.6	30.33±1.7	7.74±3.45
Butanol sub-extract	35.59±3.64	33.92±3.00	30.80±7.55
Ethyl Acetate sub-extract	39.77±7.97	33.49±8.39	13.38±2.48
Hexane sub-extracts	44.82±5.42	49.44±14.84	54.76±13.49
Chloroquine	0.005±0.002	0.178±0.056	NT
Methylene blue	NT	NT	0.020±0.003

IC_{50} values are given as the mean ± SD from at least three independent dose-response experiments conducted in duplicate or triplicate wells. Chloroquine (CQ) was used as positive control against asexual parasites and methylene blue (MB) against gametocytes. NT= not tested. [a]3D7elo1CBG99 stage V.

Besides, the ethyl acetate sub-extract, tested at 50 µg/mL, also reduced total early sporogonic stages (ESS) counts by more than 70% showing slightly stronger effects on ookinete development (OD counts) than on gametogenesis and/or fecundation processes (total ESS counts). The hexane sub-extract was practically inactive, while the butanol sub-extract exhibited a promising activity, inhibiting more than 80% of ookinete and ESS development.

Table 2.5. Preliminary results of *L. lanceolata* stem barks phases at 50 µg/ml against *P. falciparum* ookinetes and ESS development.

Phases	Percentage of ookinetes inhibition	Percentage ESS inhibition
Ethyl Acetate sub-extract 50 µg/mL	73.67±6.01	71.22±5.16
Butanol sub-extract 50µg/mL	85±10.02	81±9.57
Hexane sub-extract 50 µg/mL	10.28±6.77	10.28±6.42

Based on these results, the ethyl acetate sub-extract was selected for further fractionation studies, since this sub-extract exhibited antimalarial transmission-blocking potential on all *Plasmodium* sexual investigated stages.

Chromatographic purification by MPLC of the ethyl acetate sub-extract afforded ten subfractions, namely LL1-LL10, that were then tested (Table 2.6) and as expected, none of them showed significant activity against asexual parasites.

In contrast, a surprising difference emerged from the activity on the sexual stages: less polar fractions (LL2-LL4) significantly blocked the viability of stage V gametocytes with IC_{50} ranging from 0.79 to 7.94 µg/mL, while the inhibition activity against OD and ESS was mostly concentrated in fractions LL7 to LL10 (Table 2.6). These sub-fractions were therefore selected for isolation and identification of the bioactive compounds and characterization of their antimalarial transmission-blocking activity.

Table 2.6. *In vitro* antiplasmodial activity of sub-fractions obtained from ethyl acetate sub-extract against *P. falciparum* asexual parasites of the CQ-sensitive 3D7 and CQ-resistant W2 strain and on stage V gametocytes of the 3D7elo1CBG99 strain; and against *P. berghei* early sporogonic development.

Sub-fractions	3D7 asexual stage IC_{50} (µg/mL)	W2 asexual stage IC_{50} (µg/mL)	3D7elo1CBG99 stage V gametocyte IC_{50} (µg/mL)	Impact on OD[a] counts IC_{50} (µg/mL)	Impact on ESS[b] counts IC_{50} (µg/mL)
LL1	41.00±3.33	34.83±10.92	12.61±2.78	>100	>100
LL2	40.00±6.77	21.34±5.63	0.79±0.15	>100	>100
LL3	14.52±0.39	7.09±1.31	2.22±0.32	>100	>100
LL4	39.40±3.98	32.50±5.74	7.94±0.15	>100	>100
LL5	39.75±9.41	32.19±6.39	24.06±6.97	>100	>100
LL6	33.80±10.31	24.93±7.08	16.92±2.25	>100	>100
LL7	38.10±7.23	24.51±7.17	14.71±3.67	13.34 ± 2.50	14.38 ± 2.25
LL8	44.19±4.94	50.32±15.41	24.70±5.01	13.01 ± 2.08	15.31 ± 1.68
LL9	36.06±5.40	29.37±6.79	15.76±2.24	3.41 ± 0.34	4.11 ± 0.42
LL10	43.46±5.33	49.49±14.30	17.47±4.47	10.09 ± 1.38	11.80 ± 0.32
CQ	0.005±0.002	0.178±0.056	NT	NT	NT
MB	NT	NT	0.020±0.003	NT	NT

Data are the means ± SD from at least three independent experiments in duplicate or triplicate. Chloroquine (CQ) was used as positive control against asexual parasites and Methylene blue (MB) against gametocytes. NT= not tested. [a]OD= ookinete development: considering counts of retort forms, elongating and fully mature ookinetes. [b]ESS= early sporogonic stages: considering counts of all forms: zygotes, retort forms, elongating and mature ookinetes.

2.5.1 Chemical characterization of fractions active against stage V of *P. falciparum* gametocytes

Normal-phase HPLC purification of the bioactive fractions LL2, LL3 and LL4 afforded seven compounds (**1**–**7**) in their pure form, whose chemical structures were fully characterized employing NMR and MS analysis.

This isolated compounds were found to belong to the class of biflavonoids, characteristic of this plant. In particular, lophirones A (**1**) (Tih *et al.*, 1987), F (**2**) (Tih *et al.*, 1990), E (**3**), D (**4**) (Tih *et al.*, 1989), and C (**7**) (Tih *et al.*, 1989) were identified based on the comparison of their spectral data with those reported in the literature. In addition, minute amounts of the new derivatives **5** and **6** were also obtained.

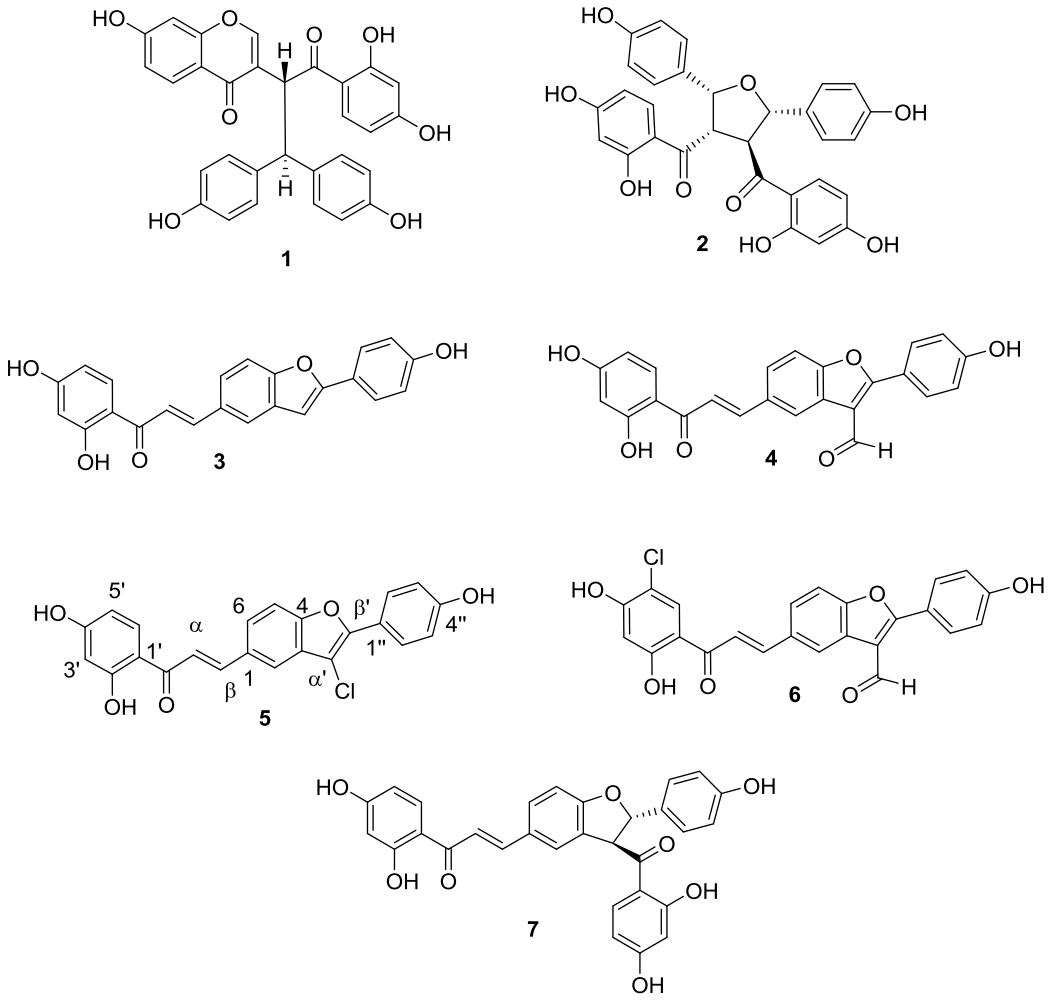

Figure 2.7. Chemical structures of **1**-**7**

From a biogenetic point of view, lophirones are considered as biflavonoids, which come from dimerization of flavonoids. Lophirone A (**1**) presents an unusual bi-flavonoid skeleton, defined by Abderamane *et al.* (2011) as an iso-biflavonoid, because of a different sequence of carbon atoms, possibly due to a 1,4-aryl group migration (Figure 2.8) similar to that of the 1,2-aryl shift in isoflavonoid biogenesis. Interestingly, isoflavonoids, as well as iso-biflavonoids, normally occur in leguminous plants, especially in the subfamily Papilionoideae (Dewick, 1994). In non-leguminous plants, isoflavonoid derivatives have been very rarely found and described only in a few isolated plant genera belonging to the families Chenopodiaceae, Compositae, Moraceae, Iridaceae, Cupressaceae, Podocarpaceae, and Bryaceae (Mackova *et al.*, 2006).

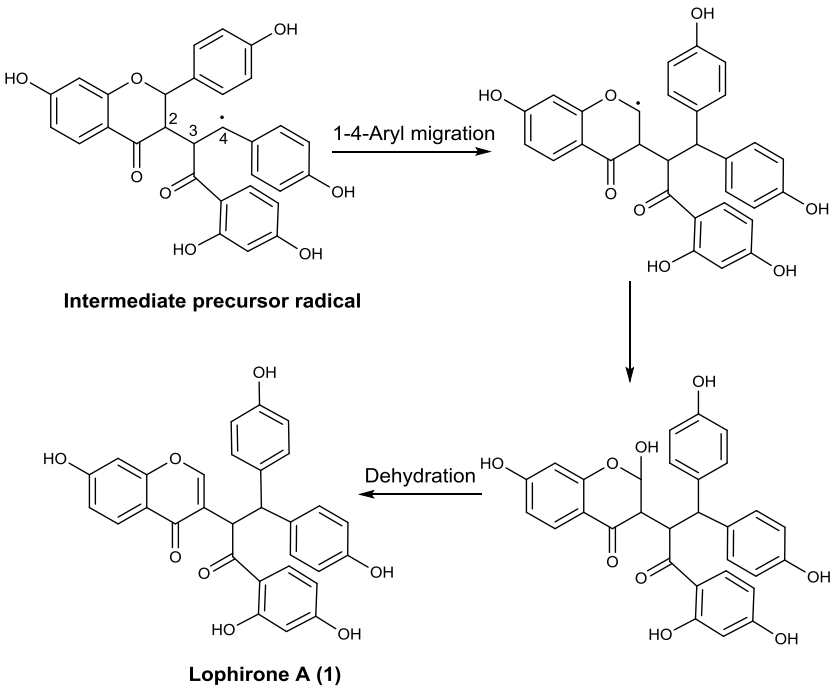

Figure 2.8. Possible biogenesis pathway for lophirone A (**1**)

Lophirone A (**1**) as well as other lophirone-type compounds were isolated from more than one plant belonging to Ochaceae family (*Lophira alata*, *Ochna sp.*, *Ouratea flava*) (Tih *et al.*, 1987; Murakami *et al.*, 1991; Messanga *et al.*, 1992; Mbing *et al.*, 2003), to confirm that the Ochnaceae family is also one of the best sources of isoflavonoids in non-leguminous plants.

Regarding lophirone C (**7**), in 1996 Shimamura *et al.* proposed a biogenetic scheme for this compound, as shown in figure 2.9, in which lophirone C (**7**) apparently is derived from one electron-oxidation of isoliquiritigenin chalcone (*a*), followed by a subsequent regioselective dimerization to give a dienone (*b*). (*b*) is converted to its enol form, generating a chalcone dimer intermediate (*c*), which can be cyclized to a dihydrofuran ring as in **7**. (Shimamura *et al.*, 1996)

Relatively more simple analogues, as lophirones D (**4**) and E (**3**), likely derive from oxidative cleavage on the structure of lophirone C. Finally, lophirones F (**2**) is composed of two trihydroxy-4,2',4'chalcone units (isoliquiritigenin) linked by an initial carbon-to-carbon bond between the two α-carbon atoms of the chalcone units, followed by various cyclization pathways. It thus differ from lophirones C-E, which arise from a carbon-to-carbon linkage between the α-carbon atom of one chalcone unit with the C-3 atom of the second unit. (Tih *et al.*, 1990, b)

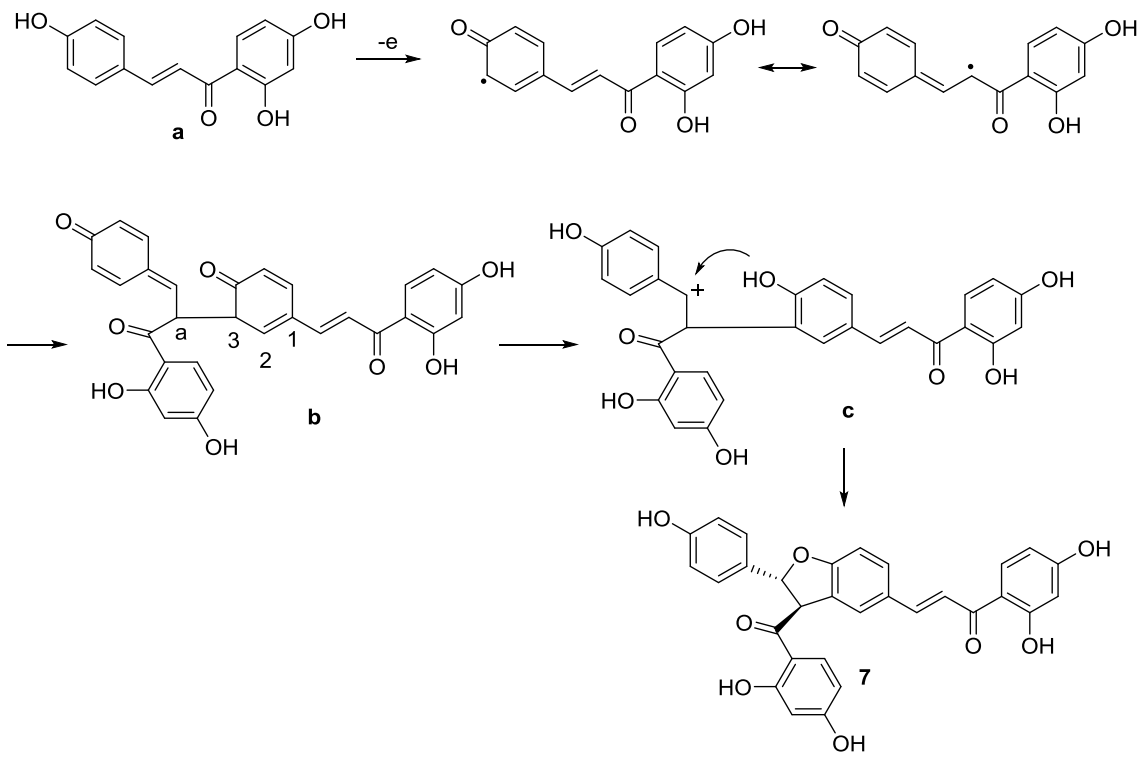

Figure 2.9. Biogenesis of lophirone C (**7**)

This family of metabolites has attracted the interest of the scientific community for its interesting bioactivities, such as antioxidant and antimutagenic activities, with protection of liver cells by upregulation of redox transcription factors (Aliyu *et al.*, 2018). Not surprisingly, total syntheses have been reported for several lophirones, and, among them, the very recent syntheses of lophirones F (Le *et al.*, 2019) and H (Abas *et al.*, 2017) represent noticeable examples.

HPLC purifications also afforded small amounts of two new chlorinated lophirone derivatives, α′-chlorolophirone E (**5**, 0.9 mg) and 5′-chlorolophirone D (**6**, 1.0 mg) (Fig. 2.6). 1D NMR data of **5**, $C_{23}H_{15}ClO_5$ by HR-ESIMS (*m/z*=405.0533, $[M-H]^-$), closely paralleled those of lophirone E ($C_{23}H_{16}O_5$) (**3**), and this greatly helped its structural assignment. An obvious difference between the two series of spectra was the lack of the furan proton, which was likely replaced by a chlorine atom. This was also suggested by the concomitant shift of neighboring protons (Fig. 2.10). Placement of the chlorine atom at the position α′ was further confirmed by the HMBC correlation from H-2 (δ_H=8.12, s) to the relatively deshielded unprotonated carbon α′ (δ_C=115.5).

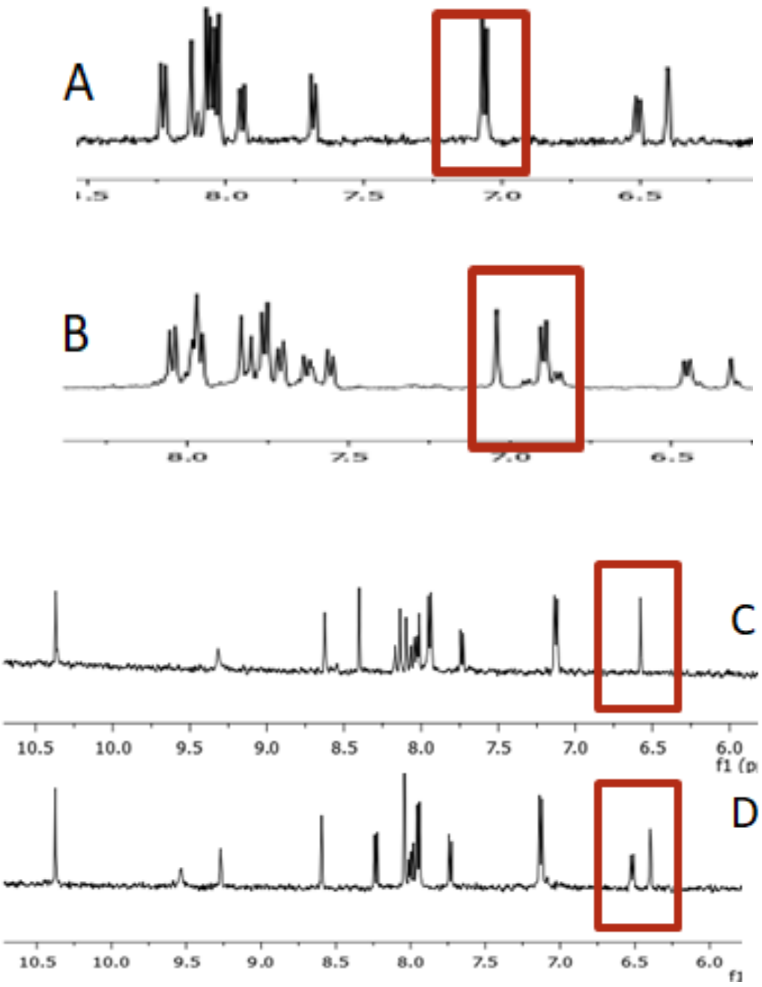

Figure 2.10. *Up:* comparison between ^{1}H NMR spectra of α'-chlorolophirone E (A) and lophirone E (B), *down*: comparison between ^{1}H NMR spectra of 5'-chlorolophirone D (C) and lophirone D (D)

Complete assignment of NMR data of **5** is reported in Table 2.8 Similarly, **6**, $C_{24}H_{15}ClO_6$ by HR-ESIMS (*m/z*=433.0480, $[M-H]^-$), was readily identified as a chlorinated analogue of lophirone D ($C_{24}H_{16}O_6$) (**4**) by inspection of 1H NMR spectrum. The most significant changes of this spectrum, compared to lophirone D (**4**), were the lack of the doublet at δ_H 6.50 (H-5′, *J*= 8.9 Hz) (Fig. 2.9) and the replacement of H-6′ doublet (δ_H 8.20, *J*= 8.9 Hz) with a singlet at δ_H 8.42. The structure of **6** was further secured upon inspection of the 2D HMBC correlations, and, in particular, correlations from both H-3′ (δ_H 6.59, brs) and H-6′ (δ_H 8.42,s) to the chlorinated C-5′ (δ_C=117.3). Complete assignment of NMR data of **6** is reported in Table 2.7.

Table 2.7. ^{1}H (700 MHz) and ^{13}C (175 MHz) NMR data of α'-chlorolophirone E (**5**) and 5'-chlorolophirone D (**6**) in $(CD_3)_2CO$.

Pos.	**5**		**6**	
	δ_C, type.	**δ_H, mult., *J* in Hz**	**δ_C, type.**	**δ_H, mult., *J* in Hz**
1	130.7, C		128.4, C	
2	120.9, CH	8.12, s	121.9, CH	8.62, s
3	118.8, C		131.5, C	
4	156.9, C		154.1, C	
5	112.6, CH	7.68, d, 8.5	111.6, CH	7.73, d, 8.7
6	125.9, CH	7.94, d, 8.5	126.2, CH	8.03, d, 8.7
α	119.8, CH	8.07, overl.	120.8, CH	8.12, d, 16.5
β	145.7, CH	8.05, overl.	143.9, CH	8.08, d, 16.5
-CO	193.7, C		191.2, C	
1'	114.3, C		116.0, C	
2'	167.9, C		165.1, C	
3'	104.6, CH	6.40, brs	108.3, CH	6.59, brs
4'	167.2, C		160.2, C	
5'	111.2, CH	6.51, dd, 9.0, 2.1	117.3, C	
6'	133.3, CH	8.22, d, 9.0	132.3, CH	8.42, s
α'	115.5, C		114.0, s	
β'	153.1, C		165.2, C	
1"	122.8, C		119.2, C	
2"-6"	127.7, CH	8.04, d, 8.6	129.7, CH	7.94, d, 8.3
3"-5"	116.9, CH	7.06, d, 8.6	116.1, CH	7.13, d, 8.3
4"	159.8, C		160.8, C	
-CHO			187.5, CH	10.39, s

The unusual presence of two chlorinated derivatives of biflavonoids could raise doubts about their possible artifact origin. Halogenated solvents were not used for extraction, partition or chromatographic purification; however, a halogenated solvent ($CDCl_3$) has been used to register NMR spectra of extracts, sub-extracts and sub-fractions. Thus, in principle, we cannot completely exclude that **5** and **6** are artifacts formed in the NMR tube. To test this hypothesis, we have left lophirones D and E for 24 h in $CHCl_3$ at room temperature but no formation of artifacts was observed. Regardless the ambiguous natural origin, compounds

5 and **6** have the advantage of increasing the chemodiversity within the small library of metabolites obtained from the bioactive sub-fractions and were therefore evaluated for their gametocytocidal activity and their effects on asexual blood stages.

2.5.2 Chemical characterization of the fractions active on sporogonic stages

Extensive reversed-phase HPLC purifications of the most active fraction on *Plasmodium* sporogonic stages (LL9) afforded three compounds (**8**–**10**) in their pure form (Figure 2.11). Lanceolins A (**8**) and B (**9**) were identified based on the comparison of their spectral data with those reported in the literature (Tih *et al.*, 1994). For these compounds the assignment in deuterated methanol is reported here for the first time (Experimental section, paragraph 2.7); in this solvent they showed a better peak resolution compared to deuterated acetone, commonly reported in the literature. Lanceolins belong to a rare class of cyanoglucosides containing a cyanomethylene group which occurrs in *Lophira* genus. In particular, this group is represented by lanceolins A and B isolated from *L. lanceolata* stem heartwook (Tih A.E., *et al.*, 1994); lanceolin C (Messanga, B. B., *et al.* 1998) and lophirosides A1, A2, B1, B2, obtained from *Lophira alata* bark. (Murakami A., *et al.*, 1993) These molecules differ from each other in two main aspects: the first one is the number of –OH groups, which have undergone an esterification process; the latter is the chemical group used for this process: benzoyl or cinnamoyl moiety (Figure 2.12).

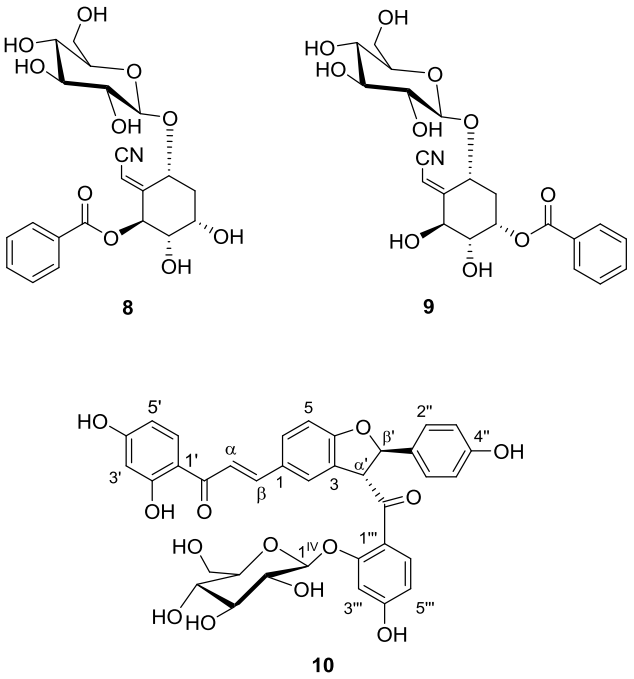

Figure 2.11. Chemical structures of **8**-**10**.

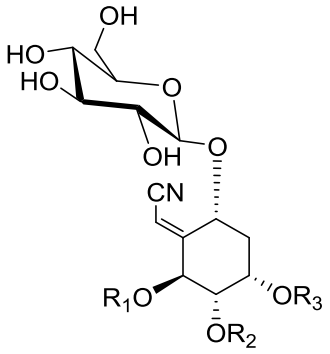

lanceolin A (8): R_1=Bz; R_2=R_3=H
lanceolin B (9): R_1=R_2=H; R_3=Bz
lanceolin C: R_1=Bz; R_2=R_3=H
lophirosides A1: R_1=H; R_2=R_3=Bz
lophirosides A2: R_1=R_3=Bz; R_2=H
lophirosides B1: R_1=H; R_2=Cinn; R_3=Bz
lophirosides B2: R_1=R_3=Cinn; R_2=Bz

Figure 2.12. Structure of nitrile glycoside esters from *Lophira* genus.

To date, the biosynthesis of these compounds has not been explored. However, it is possible that lanceolins and lophirosides derive from menisdaurin, after a natural *trans* dihydroxylation at C-4 and C-5. A subsequent esterification of C-4 hydroxyl by benzoic acid gives lanceolin A, of C-6 hydroxyl gives lanceolin B and of C-5 hydroxyl gives lanceolin C (Tih *et al.* 1994). In the case of lophirosides, the esterification occurs on two hydroxyl groups, with two benzoyl units or with one benzoyl and one cinnamoyl unit at C-4, C-5 or C-6 (Figure 2.12).

The same fractions yielding lanceolins A (**8**) B (**9**) also afforded a new biflavonoid glycoside, named glucolophirone C (**10**), $C_{36}H_{32}O_{13}$ by HR-ESIMS. The ^{1}H NMR

spectrum of **10** in $(CD_3)_2CO$ clearly evidenced the presence of signals attributable to a biflavonoid moiety (a series of singlets and multiplets between δ_H 8.12 and 5.55) and those of a sugar unit (signals from δ_H 5.19 to 3.71). The proton signal at δ_H 5.19 (d, J = 7.7) Hz showed a clear HSQC cross-peak with the carbon signal at δ_C 100.3, thus confirming its anomeric nature. Inspection of the COSY spectrum allowed us to identify the sugar spin system, which, on the basis of the available proton−proton coupling constants ($J_{H\text{-}1/H\text{-}2}$ = 7.7 Hz; $J_{H\text{-}2/H\text{-}3}$ = 7.7 Hz; $J_{H\text{-}3/H\text{-}4}$ = 6.9 Hz; $J_{H\text{-}4/H\text{-}5}$ = 7.7 Hz) and of the ^{13}C NMR chemical shift values, deduced from the HSQC spectrum, could be confidently assigned as β-glucopyranosyl unit. The remaining signals of the ^{1}H NMR spectrum of **10** could be assigned to the biflavonoid lophirone C (**7**) by comparison of its $^{1}H/^{13}C$ NMR data obtained by detailed inspection of 2D NMR spectra with those reported in the literature (Tih *et al.*, 1989, a). Cross-peaks of the 2D NMR HMBC spectrum not only supported the structural assignment of this moiety but also provided key evidence to link it to the sugar unit. Thus, correlation H-1^{IV}/C-2''' unambiguously indicated attachment of the β-glucopyranosyl unit at C-2'''. A ROESY cross-peak between H-1^{IV} and H-3''' further supported this structural assignment. The *trans* configurations of the double bond (positions α/β) and of the dihydrobenzofuran moiety (positions α'/β') of the aglycone unit of **10** were both deduced by the $^{1}H/^{1}H$ vicinal coupling constants which are in agreement with literature data (Tih *et al.*, 1989, b).

To completely define the stereostructure of the new glucolophirone C (**10**), the absolute configurations of the stereogenic carbons (C-α' and C-β') of lophirone C (**7**), which were not established when it was first isolated in 1996, have to be determined. Shimamura *et al.* described the synthesis of lophirone C (**7**), obtained through an oxidative dimerization strategy; however, this approach was not stereospecific and produced a racemic mixture (Shimamura *et al.*, 1996). The absolute configuration of only two natural lophirone-type compounds has been determined, namely 6'''-hydroxylophirone B (Kaewamatawong *et al.* 2002), and lophirone H (Abas *et al.* 2017), but both of these bioflavonoids are structurally unrelated to lophirone C.

Thus, in order to determine the absolute configuration of its stereogenic carbons, **10** was treated with 0.3 M HCl in 85% MeOH for 2h at 60 °C. (Figure 2.13) The resulting mixture was neutralized, centrifuged, and the supernatant was concentrated to dryness under nitrogen. The residue was then partitioned

between water and dichloromethane. The aqueous layer was found, by ^{1}H NMR analysis, to be composed of glucose methyl glucosides, while the organic layer, purified by HPLC afforded lophirone C (**7**) in pure form but in low yields, due to partial degradation in acidic media. The ^{1}H-NMR spectrum and the $[\alpha]_D$ value of the methanolysis product were identical to those reported for lophirone C (**7**) in the literature (Tih *et al.*, 1989, b).

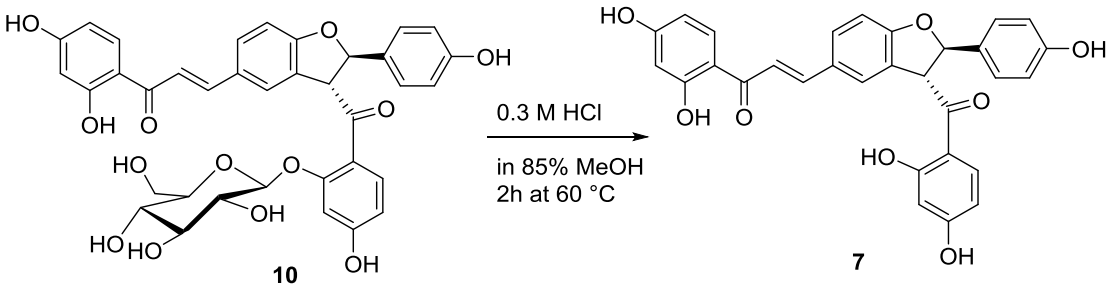

Figure 2.13. Methanolysis of glucolophirone C (**10**)

The structure of lophirone C (**7**) contains only two stereogenic carbons (C-α'/C-β') and the determination of absolute configuration at these centers could not rely on derivatization methods. Thus, taking advantage of the availability of powerful computational tools for prediction of spectroscopic properties, we decided to solve this issue by comparing calculated and experimental ECD spectra (Figure 2.14). This experiment has been carried out at the Institute of Biomedical Science Abel Salazar (University of Porto), thanks to the collaboration with Prof. Anake Kijjoa and Prof. José Augusto Pereira.

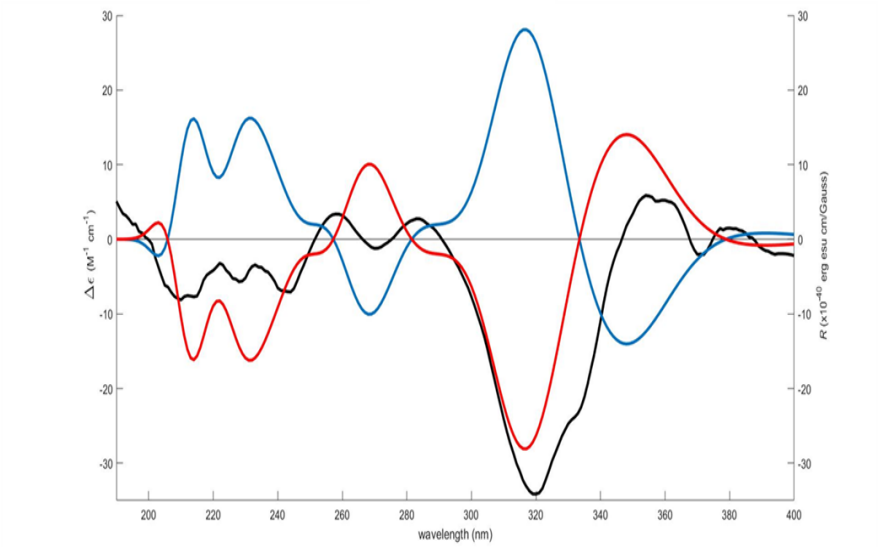

Figure 2.14. Experimental ECD spectrum (black line) of lophirone C and simulated ECD spectra of α'*R*,β'*R*-lophirone C (red line) and of α'*S*,β'*S*-lophirone C (blue line), in EtOH.

The conformational analysis of lophirone C (**7**) by molecular mechanics (MM2 and MMFF95 force fields) afforded 48 conformations that were energetically minimized and ranked using a faster DFT model (smaller basis set, B3-LYP/6-31G). Then, the most populated (lowest energy) conformations (some of which are illustrated in figure 2.15, while their energies are showed in table 2.9), spanning a window of 2 kcal/mol, were considered to calculate the first 70 ECD transitions (TD-DFT) for each model. Comparison of the experimental ECD spectrum with the spectra calculated by averaging the contribution of each conformer on the basis of the Boltzmann population, revealed a good match for the spectrum obtained from the (*R,R*) stereoisomer (Figure 2.14). Thus the α'*R*,β'*R* configuration can be assigned to lophirone C and to glucolophirone C (**10**), fully defining the stereostructrures of these compounds.

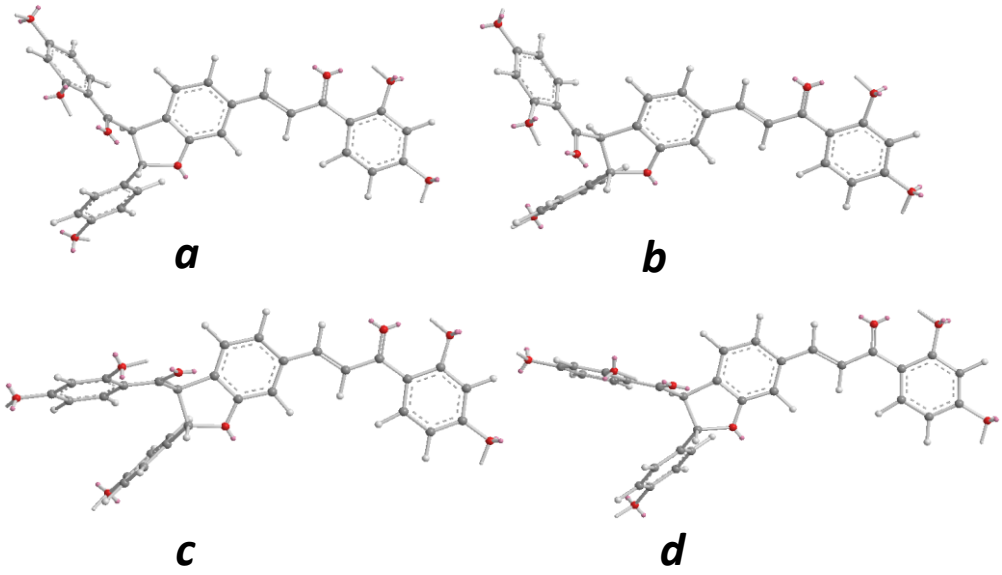

Figure 2.15. The four most populated conformers of lophirone C (**7**)

Table 2.8. Energies and population of the four most populated conformers of lophirone C.

Conformer name	ΔE[a]	ΔG[b]	P%[c]
a	-1757.385065	0.000	6.318
b	-1757.384890	0.110	5.249
c	-1757.384890	0.110	5.249
d	-1757.384877	0.115	5.205

[a]Relative energy (Ha/molecule). [b]Relative Gibbs free energy (kcal/mol). [c]Population calculated at the at the B3-LYP/6-31G(d) level in the ethanol solution.

2.5.3 Activity of pure compounds against mature gametocytes and asexual blood stages

Compounds **1**–**7** obtained from the purification of gametocytocidal subfractions (LL2-LL4) were evaluated for their activity against asexual stages using a chloroquine-resistant (W2) and a chloroquine-sensitive (3D7) strain (pLDH assay) and against stage V *P. falciparum* gametocytes using the luminescent assay. Results, expressed as IC_{50}, are reported in Table 2.9. Remarkably, lophirone E (**3**) proved to be a very potent agent against stage V gametocytes with a micromolar IC_{50} value (IC_{50} = 0.14 μM), comparable to that of methylene blue (MB). None of the tested compounds showed significant activity against asexual stages, with only lophirone C (**7**) displaying an IC_{50} value<10 μM. Thus,

different from MB (Delves *et al.* 2013), lophirone E (**3**) exhibited a unique stage-specific activity, proving to be about 100 times more active on stage V gametocytes than on asexual stages (IC_{50}=12.2 and 38.5 μM against D10 and W-2 strains, respectively). Fig. 2.16 shows the dose-response curve of lophirone E (**3**) compared to methylene blue.

Table 2.9. *In vitro* antiplasmodial activity of pure compounds **1**-**7** against *P. falciparum* asexual blood stage parasites of the CQ-sensitive 3D7 and CQ-resistant W2 strain and on stage V gametocytes of the 3D7elo1CBG99 strain.

Compounds	3D7 asexual stage IC_{50} (μM)	W2 asexual stage IC_{50} (μM)	3D7elo1CBG99 stage V gametocyte IC_{50} (μM)
Lophirone A (1)	> 50	> 50	49.4 ± 3.20
Lophirone F (2)	29.90 ± 3.94	26.74 ± 2.42	52.9 ± 1.69
Lophirone E (3)	38.47 ± 3.21	12.23 ± 2.08	0.14 ± 0.04
Lophirone D (4)	47.75 ± 4.75	45.47 ± 7.84	> 100
Compound 5	> 50	17.88 ± 5.03	4.11 ± 1.14
Compound 6	> 50	> 50	81.38 ± 9.56
Lophirone C (7)	14.23 ± 3.27	7.34 ± 0.78	8.07 ± 0.97
Chloroquine	0.0259 ± 0.0059	0.608 ± 0.22	NT
Methylene blue	NT	NT	0.08 ± 0.039

Data are the mean ± SD of IC_{50} values derived from at least three independent dose-response experiments in duplicate or triplicate wells. Chloroquine was used as positive control against asexual parasites and methylene blue against gametocytes. NT= not tested.

To investigate further the characteristics of the molecule, the cytotoxicity of lophirone E (**3**) was assessed *in vitro* on the human microvascular endothelial cell line HMEC-1. Dose-response experiments revealed the molecule to be negligibly cytotoxic, as evidenced by an IC_{50} value of 79.7 μM, that is more than 500-fold higher than that determined against stage V gametocytes (selectivity index=570).

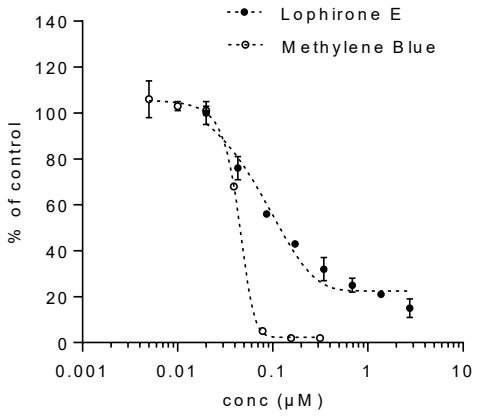

Figure 2.16. Dose-response curve of lophirone E (black circle) compared to methylene blue (empty circle) on gametocytes of the 3D7elo1CBG99 strain. Representative experiment out of three.

Although the library of tested compounds is somewhat limited, it is possible to draw some preliminary structure-activity relationships, taking advantage of the close similarity among some of them. Compounds **4** and **5** differ from lophirone E (**3)** only for the replacement of the furan hydrogen (position α') with a formyl group (in **4**) and a chlorine atom (in **5**), respectively. This change causes a marked decrease of activity for **5** (40 times less active than **3**) and a complete loss of activity for **4**, thus highlighting the crucial importance of a nonsubstituted furan ring. Lophirone C (**7**), characterized by a phenylketone substituent at α' and saturation of the furan double bond, exhibited a moderate activity against stage V gametocytes (IC_{50}=8.1 µM); however, it exhibited an activity of the same magnitude also against asexual stages.

2.5.4 Activity of pure compounds against early sporogonic stages

Having also fully defined the structures of the main components of the bioactive fraction LL9, we conducted dose-range experiments in the ODA within these isolated compounds (Table 2.10).

Table 2.10. Activity of **8**-**10** on *Plasmodium* early sporogonic development.

Compounds	Impact on DO[a] counts IC_{50} (µM)	Impact on ESS[b] counts IC_{50} (µM)
Lanceolin A (**8**)	91.15 ± 13.61	113.58 ± 22.51
Lanceolin B (**9**)	10.95 ± 0.44	12.75 ± 0.82
Glucolophirone C (**10**)	79.94 ± 9.05	90.16 ± 12.51

Data are expressed as means ± SD, testing phases in a concentration range of 3.5 – 50 µg/ml.[a] DO= developing ookinetes: considering counts of retort forms, elongating and fully mature ookinetes; [b] ESS= early sporogonic stages: considering counts of all forms: zygotes, retort forms, elongating and mature ookinetes.

The sporontocidal of activity one of the three isolated compounds, namely lanceolin B (**9**) revealed a considerable activity. ESS counts were reduced by 50% at 12.75 µM, indicating its activity on processes of gamete formation and/or fecundation. Similarly, a 50% reduction was found for OD counts at 10.95 µM, showing that lanceolin B (**9**) is also active on ookinete development. In contrast, lanceolin A (**8**) and glucolophirone C (**10**) showed a very low inhibitory activity on early sporogonic development, evidenced by high IC_{50} values of both, OD and ESS counts (IC_{50} > 50 µM). Comparing the IC_{50} values of the isolated molecule lanceolin B (**9**) with those obtained for fraction LL9 (3 to 4 µg/mL), the fraction appears slightly more active which might be explained by synergistic interactions among the components and / or the presence of other active molecules at low concentrations.

As described in paragraph 2.4.3, lanceolins belong to a rare class of cyanoglucosides, containing a cyanomethylene group. They were isolated for the first time in 1994 by Tih *et al.* from *L. lanceolata* stem barks. Actually, no pharmacological data have been reported in the literature about these compounds, except for the slight bitterness of the related dibenzoate derivatives lophirosides (Murakami *et al.*, 1993). Thus, this is the first report of a stage-selective antimalarial activity for these compounds. Noteworthy, the marked difference of activity exhibited by the two lanceolins clearly indicates that the position of benzoylation is a critical factor to determine the activity. Indirectly, this different bioactivity for isomeric products, suggests the existence of a well-defined biological target, still yet to be identified. This is particularly interesting,

given that lanceolin B (**9**) is interfering at two different moments of early sporogonic development, once before zygote formation, i.e. acting on gamete formation and/or fecundation and once after zygote formation acting on ookinete maturation. Lanceolins A (**3**), B (**4**) and glucolophirone C (**2**) were not cytotoxic against human fibroblast cell line (IC_{50} > 250 μM).

2.6 Conclusions

A screening of African plants, traditionally used as folk medicine, led to a selection of *Lophira lanceolata* as a promising source of antimalarial transmission blocking properties, showing interesting potential on all investigated *Plasmodium* sexual stages. The following bioassay-guided fractionation of organic extract obtained from stem barks led to the identification of bioactive compounds able to specifically inhibit *Plasmodium* sexual stages. In particular, the chalcone lophirone E (**3**) was identified as a potent, stage-specific gametocytocidal agent with an IC_{50} value in the micromolar range. Lophirone E (**3**) is about 100 times more active against *P. falciparum* stage V gametocytes (IC_{50}=0.14 μM) than on asexual blood stages (IC_{50}=12 μM on W2 strain). Moreover, the molecule displays negligible cytotoxicity (SI=570). The isolation of structural analogues has also allowed identifying the critical positions on the chemical scaffold of lophirone E (**3**). The existence of strict structure-activity relationships points toward the existence of a defined molecular target, whose identification would be of crucial importance. More interesting, the chemical structure of lophirone E (**3**) possesses several features (MW < 500, relative simplicity, absence of stereogenic carbons) that could facilitate a straightforward total synthesis, thus overcoming to resort to plant material as the only source. A synthetic approach to lophirone E (**3**) could also allow the preparation of analogues aiming at further improving the potency and optimizing the druggability parameters of the compound.

Regarding the activity on *Plasmodium* early sporogonic development stages and ookinetes development, lanceolin B (**9**) showed to be a transmission-blocking agent targeting *Plasmodium* stages in the mosquito. Interestingly, also a new compound, namely glucolophirone C (**10**), was identified, a 2'''-glucosylated lophirone C. Moreover, from the analysis of its pharmacological property it could be hypothesized that the glucosylation causes a loss of anti-

gametocydal activity, exhibited by lophirone C (**7**) (IC_{50} = 8.07 ± 0.97 μM), since the fraction containing **10** did not display any inhibition activity on this stage.

To summarize, these results evidence that *L. lanceolata* contains two different antimalarial transmission-blocking leads, selectively acting on sexual forms in the human host or on sporogonic stages in the mosquito host. Target identification and mode of action studies may allow further clarifying the prospective of the *L. lanceolata* molecules as transmission blocking components of new anti-malarial combination drugs.

More generally, these results also confirm the potential of the biological screening of antimalarial plants for the discovery and development of new drugs active against *Plasmodium* transmissible stages. Alternatively, the use of such plants in standardized phytomedicines could be highly beneficial for malaria control. Employed in an integrated approach with modern drugs, antimalarial transmission blocking phytomedicines may contribute to decrease transmission intensity as well as help delaying the development and diffusion of *Plasmodium* strains resistant to currently used ACTs, since the transmission blocking activities are crucial to interrupt disease transmission.

2.7 Experimental section

2.7.1 Plant material

Twelve medicinal plants were selected on the basis of ethno-botanical information on their use as antimalarial remedies in western Burkina Faso and were identified and authenticated at Comoé regional department of forestry and confirmed on www.theplantlist.org. For this study, barks of *L. lanceolata* were collected in Banfora, western Burkina Faso on January 2016 and immediately dried at the temperature of 25°C for two weeks. After drying, the stem bark material was powdered and then stored in dry and dark conditions. A voucher specimen of the bark (Cnrfp16Ll) was deposited in the herbarium of "Centre National de Recherche et de Formation sur le Paludisme CNRFP" (Ouagadougou, Burkina Faso).

2.7.2 Extraction and isolation of the compouds

Crude organic extracts for the twelve investigated plants were prepared by maceration of powdered plant (50 g) for 24 hours in 500 mL of ethanol. After filtration, the residues were re-extracted twice under the same conditions to ensure complete extraction. Aqueous extracts were prepared by boiling 50 g of powdered plant in 500 mL of distilled water for 30 minutes. After cooling, solutions were filtered on cotton wool and freeze-dried with a lyophilizer. The various dry extracts obtained were stored in sterile containers at 4°C. The powdered *L. lanceolata* stem barks (1.1 Kg) was exhaustively extracted by maceration in methanol (5×2 L) to afford 157 g of a crude extract after removal of the solvent under reduced pressure. The methanolic extract thus obtained was dissolved in water and then partitioned subsequently with *n*-hexane, EtOAc, and n-butanol to yield 3.0, 9.1, and 18.5 g of sub-extracts, respectively. The EtOAc sub-extract (9.1 g) was subjected to MPLC over a silica gel column (70-230 mesh) and eluted with a solvent gradient of increasing polarity from n-hexane to EtOAc, EtOAc-MeOH (1:1), and finally MeOH. Altogether, ten fractions were obtained, which were then subjected to bioactivity evaluation. Fraction LL2 (41 mg), eluted with n-hexane-EtOAc, 6:4, was separated by normal-phase HPLC (n-hexane-EtOAc, 65:35, flow rate 0.8 mL/min), yielding lophirone D (**4**, 1.3 mg), lophirone E (**3**, 1.8 mg), 5′-chlorolophirone D (**6**, 1.0 mg) and α′-chlorolophirone E (**5**, 0.9 mg). Fraction LL3 (175 mg), eluted with n-

hexane-EtOAc 1:1, was partially separated by HPLC (n-hexane-EtOAc, 1:1, flow rate 0.8 mL/ min) to afford pure lophirone C (**7**, 7.6 mg) and lophirone F (**2**, 9.8 mg). Fraction LL4 (2 g), eluted with n-hexane-EtOAc, 4:6, was first purified by GCC over a silica gel column (70–230 mesh) using n-hexane-EtOAc (from 8:2 to EtOAc) and then EtOAc-MeOH (1:1) and finally MeOH, to afford lophirone A (**1**, 121.0 mg). A portion of fraction LL9 (80 mg), eluted with EtOAc-MeOH, 90:10, was separated by semi-preparative RP-18 HPLC performed on an Agilent instrument, using Supelco Ascentis C18, 5µm 250 × 10 mm column. The mobile phase was a mixture of A: water, and B methanol with a gradient programmed as follows: starting conditions: 70%A- 30%B; t_{10} min: 40%A-60 % B; t_{15} min 25%A- 75%B; t_{25} min 0%A- 100%B; t_{30} min 40%A- 60%B; t_{35} min 70%A- 30%B. The injected volume was 500 µL and flow-rate was 2.5 mL/min. The UV detection wavelength was set at 254 nm. This separation led to the isolation of glucolophirone C (**10**) (12.5 mg, Rt 25.1 min) and a mixture of lanceolins which was further purified by reversed-phase HPLC with MeOH-H_2O (35:65 flow rate 0.8 mL/min) to yield lanceolins A (**8**, 6.9 mg) and B (**9**, 4.1 mg).

2.7.3 Spectroscopic data for the isolated compounds

α′-Chloro-Lophirone E (**5**): Colorless amorphous solid. ESIMS *m/z* 405 $[M-H]^-$; HR-ESIMS: *m/z* 405.0533$[M-H]^-$ (calcd for $C_{23}H_{13}ClO_5$, 405.0535). ^1H and ^{13}C NMR [$(CD_3)_2CO$] are reported in Table 2.7.

5′-chloro-Lophirone D (**6**): Colorless amorphous solid. ESIMS *m/z* 433 $[M-H]^-$; HR-ESIMS: *m/z* 433.0480 $[M-H]^-$ (calcd for $C_{24}H_{13}ClO_6$, 433.0484). ^1H and ^{13}C NMR [$(CD_3)_2CO$] are reported in see Table 2.7.

Glucolophirone C (**10**): Yellowish amorphous solid. $[\alpha]_D$= -28.7 (*c* = 0.1, MeOH); ^1H NMR ($(CD_3)_2CO$, 700 MHz): δ_H 13.54 (1H, s, OH), 8.12 (1H, d, *J* = 9.0 Hz, H-6'), 7.91 (1H, d, *J* = 8.8 Hz, H-6'''), 7.79 (1H, overlapped, H-6), 7.78 (1H, overlapped, H-β), 7.65 (1H, s, H-2), 7.64 (1H, overlapped, H-α), 7.32 (2H, d, *J* = 8.4 Hz, H-2''-6''), 6.98 (1H, d, *J* = 8.3 Hz, H-5), 6.87 (2H, d, *J* = 8.4 Hz, H-3''-5''), 6.78 (1H, d, *J* = 9.0 Hz, H-5'), 6.63 (1H, s, H-3'''), 6.52 (1H, d, *J* = 8.8 Hz, H-5'''), 6.32 (1H, s, H-3'), 6.26 (1H, d, *J* = 6.9 Hz, H-β'), 5.55 (1H, d, *J* = 6.9 Hz, H-α'), 5.19 (1H, d, *J* = 7.7 Hz, H-1^{IV}), 3.89 (1H, d, *J* = 11.8 Hz, H-6^{IV}a), 3.71 (1H, dd, *J* = 11.8, 5.4 Hz, H-6^{IV}b), 3.62 (1H, m, H-5^{IV}), 3.59 (1H, d, *J* = 7.7 Hz,

H-4^{IV}), 3.52 (1H, t, *J* = 7.7 Hz, H-2^{IV}), 3.48 (1H, t, *J* = 7.7 Hz, H-3^{IV}); ^{13}C NMR $(CD_3)_2CO$, 175 MHz): δ_C 192.3 (C-1'''a), 190.9 (C-1'a), 167.3 (C-2′), 165.6 (C-2'''), 164.4 (C-4′), 164.3 (C-4'''), 161.2 (C-4), 157.4 (C-4''), 142.8 (C-β), 134.0 (C-3), 133.6 (C-6'), 132.1 (C-6'''), 131.8 (C-6), 129.9 (C-1''), 127.8 (C-2''-6''), 127.1 (C-1), 125.5 (C-2), 117.7 (C-α), 115.5 (C-3''-5''), 111.0 (C-5), 108.9 (C-5′), 108.1 (C-5'''), 104.1 (C-3'''), 103.0 (C-3'), 100.3 (C-1^{IV}), 87.5 (C-β′), 77.2 (C-5^{IV}), 77.0 (C-4^{IV}), 73.8 (C-2^{IV}), 70.4 (C-3^{IV}), 61.6 (C-6^{IV}), 57.0 (C-α′); ESIMS *m/z* 671 $[M - H]^-$; HRESIMS *m/z* 671.1764 $[M - H]^-$ (calcd. for $C_{36}H_{31}O_{13}$, 671.1770).

Lanceolin A (**8**): amorphous white solid δ_H 8.13 (2H, d, *J* = 7.3 Hz, H-2"-6"), 7.62 (1H, t, *J* = 7.3 Hz, H-4"), 7.49 (2H, t, *J* = 7.3 Hz, H-3"-5"), 5.80 (1H, s, H-2), 5.05 (1H, overlapped, H-4), 5.04 (1H, overlapped, H-8), 4.57 (1H, bs, H-5), 4.46 (1H, d, *J* = 7.6 Hz, H-1'), 4.36 (1H, brs, H-6), 3.85 (1H, m, H-6'a), 3.73 (1H, m, H-6'b), 3.39 (1H, overlapped, H-3'), 3.36 (1H, overlapped, H-5'), 3.28 (1H, overlapped, H-4'), 3.27 (1H, overlapped, H-2'), 2.48 (1H, d, *J* = 15.1 Hz, H-7a), 1.97 (1H, d, *J* = 15.1 Hz, H-7b).

Lanceolin B (**9**): amorphous white solid δ_H 8.13 (2H, d, *J* = 7.3 Hz, H-2"-6"), 7.59 (1H, t, *J* = 7.3 Hz, H-4"), 7.47 (2H, t, *J* = 7.3 Hz, H-3"-5"), 5.81 (1H, brs, H-2), 5.47 (1H, d, *J* = 2.0 Hz, H-6), 5.04 (1H, d, *J* = 9.6 Hz, H-8), 4.95 (1H, bs, H-4), 4.33 (1H, d, *J* = 7.7 Hz, H-1'), 3.87 (1H, m, H-6'a), 3.74 (1H, m, H-6'b), 3.68 (1H, dd, *J* = 11.8, 5.8 Hz H-5), 3.34 (1H, overlapped, H-3'), 3.28 (1H, overlapped, H-4'), 3.21 (1H, m, H-5'), 3.08 (1H, t, *J* = 8.2 Hz, H-2'), 2.63 (1H, d, *J* = 15.5 Hz, H-7a), 1.99 (1H, d, *J* = 15.5 Hz, H-7b).

2.7.4 Methanolysis of glucolophirone C (10)

Glucolophirone C (**10**, 8 mg) was dissolved in 0.3 M HCl in 85% MeOH and the solution was heated at 60 °C in a shielded reaction vial for 2 hours. After being cooled, the reaction mixture was neutralized with Ag_2CO_3 solution, centrifuged, and the supernatant was evaporated to dryness under N_2 stream. This was then partitioned between water (2 x 5 mL) and $CHCl_3$ (2 x 5 mL) yielding 1.1 mg from the aqueous layer and 6.0 mg from the chloroform layer. The organic layer was purified by HPLC (*n*-hexane−EtOAc, 1:1, flow rate 0.8 mL/ min) to afford pure lophirone C (**7**, 1.0 mg).

2.7.5 ECD calculation for lophirone C (7)

The dihedral driver and MM2 minimizations for lophirone C (**7**) were done in Chem3D Ultra (Perkin-Elmer Inc., Waltham, MA, USA). All DFT minimizations with model chemistries B3-LYP/6-31G as well as ECD spectral calculations (TD-DFT, 70 transitions) were performed with Gaussian 16W (Gaussian Inc., Wallingford, CT, USA) using an IEFPCM solvation model for ethanol. The simulated spectral lines for **7** were obtained by summation of Gaussian curves, as reported by Stephens and Harada, 2010. A line broadening of 0.3 eV was applied to all transitions to generate the calculated line.

2.7.6 *Plasmodium falciparum* parasite cultures

Asexual blood-stage cultures. *P. falciparum* CQ-sensitive 3D7 and CQresistant W2 strains were cultured according to the method of Trager & Jensen, with minor modifications (Trager and Jensen, 1976). Briefly, parasites were cultured using human erythrocytes (type O-positive red blood cells for 3D7 and A positive red blood cells for W2) at 5% hematocrit in parasite culture medium (RPMI 1640 supplemented with 20mM HEPES, 2mM glutamine, 0.01% hypoxanthine and 1% of lipid-rich bovine serum albumin-Albumax II). Parasite cultures were kept at 37 °C in the presence of a fixed gas composition (1% O_2, 5% CO_2, 94% N_2).

Gametocyte cultures. The transgenic 3D7 strain 3D7elo1-pfs16-CBG99 expressing the luciferase CBG99 under the gametocyte specific promoter pfs16 was used in all the gametocytocidal experiments and the luciferase activity was taken as measure of gametocyte viability (D'Alessandro *et al.*, 2016). To obtain constant and high gametocyte production, culture medium was supplemented with 10% naturally clotted heat-inactivated 0-positive human serum (Interstate Blood Bank, Inc.) instead of Albumax.

Briefly, cultures of *P. falciparum* 3D7 asexual parasites were diluted to 0.5% parasitemia and maintained up to day 15 with daily media changes without fresh red blood cells (RBC) addition. When early gametocytes (stages I and II) and dead asexual forms were found, cultures were treated with 50mM N-acetyl-D-glucosamine (NAG) for 72 h, to block reinvasion of remaining asexual parasites and obtain pure and nearly synchronous gametocytes. All the cultures were maintained at 37 °C in a standard gas mixture consisting of 1% O_2, 5% CO_2, and 94% N_2. Gametocyte stages were routinely checked by Giemsa-

stained smears. The day of the experiment, stage V gametocytes were counted and when their percentage was higher than 90% the experiment was performed.

2.7.7 *P. falciparum* drug susceptibility assay

Extracts, fractions and pure compounds were dissolved in DMSO and diluted with medium to achieve the required concentrations (final DMSO or ethanol concentration ≤1%, which is not toxic to the parasites). Chloroquine (CQ) and methylene blue (MB) were used as positive control for the assessment of asexual or gametocyte stages, respectively. Test compounds were placed in 96-well plates (EuroClone) and serial dilutions were performed in a final volume of 100 µL/well. 100 µL of asexual parasite or gametocyte cultures with parasitemia of 1–1.5% were distributed into each well to achieve a final volume of 200 µL and final hematocrit of 1%. The plates were put into an incubating chamber and inflated with the proper gas mixture for 2 min before putting in the incubator at 37 °C for 72 h. The growth of the asexual stages was determined spectrophotometrically by measuring the activity of the parasite lactate dehydrogenase (pLDH), according to a modified version of Makler's method (Makler *et al.*, 1993). Briefly, the drug-treated culture was re-suspended and 20 µL/well were transferred into a new plate containing 100 µL of Malstat reagent (0.11% [vol/vol] Triton-100, 115.7mM lithium L-lactate, 30.27mM Tris, 0.62mM 3-acetylpyridine adenine dinucleotide [APAD] [Sigma-Aldrich], adjusted to pH 9 with 1M HCl) and 25 µL of PES/NBT (1.96mM nitroblue tetrazolium chloride and 0.24mM phenazine ethosulfate). The plate was incubated in the dark at room temperature (20 °C) for 15 min and then read at a wavelength of 650 nm using a microplate reader Synergy4 (BioTek). Results were analyzed and expressed as the 50% inhibitory concentration in respect to control wells (IC_{50}). For the determination of gametocytes viability, the luciferase assay was used as described previously (D'Alessandro *et al.*, 2016). Briefly, at the end of the incubation, 100 µL of supernatant were discarded from each well of the experimental plate. The remaining culture at 2% hematocrit was then re-suspended and 70 µL were transferred into a black plate. The luciferase substrate D-luciferin (1mM in 0.1M citrate buffer, pH 5.5) was added in each well at the 1:1 (v/v) and the plate was incubated in the dark for 10 min. The luminescence signal was read using a luminescence reader Synergy4 (BioTek)

with integration time 500 ms. The results of the chemo-sensitivity assays were expressed as the percent viability compared to the untreated controls, calculated with the following formula: 100×([Readout of treated sample- blank]/ [Readout of untreated sample- blank]); Readout is OD for asexual parasites and ALU for gametocytes. As blank, uninfected RBC and gametocytes treated with a high dose of MB (300 ng/mL) were used for the asexual and gametocyte assay, respectively. The percentage of viability was plotted as a function of drug concentrations and the curve fitting was obtained by nonlinear regression analysis using a four-parameter logistic method (software Gen5 1.10 provided with the Synergy4 plate reader [Biotek]). The IC_{50}, which is the dose capable of inducing 50% inhibition of parasite viability, was obtained by extrapolation. At least three experiments in duplicate were performed with the test extract/compounds against each investigated parasite stage and strain.

2.7.8 *In vitro* mammalian cell toxicity assay

Cytotoxicity was evaluated in human dermal microvascular endothelial cells (HMEC-1). The cells were maintained under standard conditions at 37 °C in a 5% CO_2 incubator in MCDB 131 medium supplemented with 10% fetal calf serum, 10 ng/mL epidermal growth factor, 1 µg/mL hydrocortisone, 2mM glutamine, 100 U/mL penicillin, 100 mg/mL streptomycin, and 20mM HEPES buffer (pH 7.3). For the toxicity experiments, HMEC-1 cells were plated in 96-well plates at 104 cells/100 µL/well and incubated at 37 °C and 5% CO_2 overnight. Test compounds were dissolved in DMSO and diluted with medium to achieve the required concentrations. 100 µL/well of herbal products were added to the plate to reach a final volume of 200 µL/ well. Cells were incubated for 72 h before measuring cell viability by the MTT test, as described previously (D'Alessandro *et al.*, 2007). Cytotoxicity was expressed as the 50% inhibitory concentration (IC_{50}). Three independent experiments were performed in duplicate wells.

2.7.9 Activity against early sporogonic stages (ESS)

The rodent malaria model *Plasmodium berghei* /BALB/c mice/*Anopheles stephensi* mosquitoes was employed. The *P. berghei* CTRPp.GFP strain, which expresses a constitutive green fluorescent protein during zygote to ookinete development (PbCTRPp.GFP) (Vlachou *et al.* 2004), was used and maintained

in the laboratory of Parasitology, at the University of Camerino (Italy) through mouse to mouse acyclic passages and mouse to mosquito to mouse cyclic passages. Aliquots of PbCTRPp.GFP infected blood were stored in glass capillaries in liquid nitrogen (-70°C). Male and female BALB/c mice (3-4 weeks old; 20 ± 3 g), were used as gametocytemic blood donor for the Ookinete Development Assay (ODA). Mice were reared and maintained in the animal breeding facilities of the University of Camerino (Italy) and experiments and handling of animals were performed in accordance with the Italian Legislative Decree on the "Use and protection of laboratory animals" (D. Lgs. 116 of 10/27/92).

2.7.10 Ookinete development assay (ODA)

The *P.berghei* ODA was employed as described by Tapanelli *et al.*, 2016. Briefly, two mice were infected with PbCTRPp.GFP infected RBCs (iRBCs) from capillaries. On the same day, six mice were treated with phenylhydrazine (Sigma-Aldrich, Austria) at 120 mg/kg, to stimulate erythropoiesis. Four days later, the phenylhydrazine pre-treated mice were inoculated i.p. 10^7 iRBCs using the blood from one of the capillary infected mice (~5% parasitemia). At day 4 after mouse infection, gametocytemia was determined on Giemsa thin smears and maturity of microgametocytes, i.e. their capacity to form gametes checked by the exflagellation assay (Blagborough *et al.*, 2012). Briefly, 5 µL of blood were taken from the tail tip of the mice and diluted (~1:30) with exflagellation medium (RPMI 1640 (Sigma-Aldrich, USA) containing 25 mM HEPES, 25 mM sodium bicarbonate, 50 mg/L hypoxanthine, 100 µM xanthurenic acid (Sigma-Aldrich, USA), pH 8.3). Samples of diluted blood (7 µL) were then placed in hand-made glass slide chambers and incubated for 20 min at 19°C. Numbers of flagellated gamete extruding microgametocytes, visible as vibrating "exflagellation centers" were counted under the microscope (400 ×). Mice showing more than 3 exflagellation centers per 1000 RBCs and the presence of female and male gametocytes on thin smears were selected as blood donors for the ODA.

Stock solutions of extracts, sub-extracts or fractions were prepared at 10 mg/mL in DMSO and diluted in ookinete medium i.e. exflagellation medium adjusted to pH 7.4 and supplemented with 20% heat inactivated fetal bovine serum, 10000 IU/mL of penicillin and 10000 µg/mL of streptomycin (Sigma-Aldrich, USA). Ten

µL of pre-diluted extracts (fractions) were dispensed to the wells of 96 wells micro-plates (Falcon, USA) containing 80 µL of ookinete medium. DMSO (0,1%) served as negative control. 10 µL of blood obtained from gametocytemic donor mice by cardiac puncture were then transferred to the wells at a dilution of 1:20 (corresponding to a hematocrit of 1-2%) in a total volume of 100 µl. Final DMSO concentration in test wells was below 0.1%, considered not to be cytotoxic. The plate was quickly transferred to a 19°C chamber and incubated for 22–24hr. Subsequently, each well content was mixed thoroughly (to disintegrate aggregations of ookinetes) and diluted 1:50 in PBS (pH 7.4) in a new plate to obtain a cell monolayer. After sedimentation of ESS and blood, GFP-expressing zygotes and ookinetes were counted at the fluorescent microscope (FITC fluorescent filter, 400 × magnifications). All samples were tested in triplicate wells using blood from at least 2 mice on different plates.

2.7.11 Assessment of the ESS morphological alterations

To assess morphological alterations of active extracts on early sporogonic forms thin blood smears were prepared from the plate wells at the end of the ookinete assay. Briefly, the content of triplicate wells was transferred into an Eppendorf tube and centrifuged at 1500 rpm for 10 min. Thin blood smears were prepared with the cell pellet, fixed with methanol and stained with Giemsa (10% in PBS pH 7.4) for 90 min. Smears were examined under the light microscope (1000×) and early sporogonic stages examined over a slide area corresponding to 80,000 red blood cells. Early sporogonic forms on treatment and control slides were differentially counted as zygotes, retort forms, fully matured ookinetes, denatured zygotes and residual cells.

2.7.12 Statistical Analysis

Excel 2007 spreadsheet (Microsoft office) was employed for data analysis. $IC_{50,}$ values, i.e. compound concentrations capable of inducing 50% inhibition of parasite viability, were calculated from the sigmoidal dose-response curve using Originlab Originpro 9.1 statistical software. Confidence intervals at 95% are given for IC_{50} values and percent inhibition data referred to controls, obtained at primary screening. Graphs were plotted using Graph Pad prism 5.10 and data comparison was performed by analysis of variances (one way - ANOVA). Values of $P < 0.05$ were considered statistically significant.

References

Abas H., Linsdall S.M., Mamboury M., Rzepa H.S., Spivey A.C. (**2017**). Total synthesis of (+)-Lophirone H and its pentamethyl ether utilizing an oxonium–prins cyclization. *Org. Lett.*, *19*, 2486–2489.

Abay S.M., Lucantoni L., Dahiya N., Dori G., Dembo E.G., Esposito F., Lupidi G., Ogboi S., Ouedraogo R.K., Sinisi A., Taglialatela-Scafati O., Yerbanga R.S., Bramucci M., Quassinti L., Ouedraogo J.B., Christophides G., Habluetzel A.. (**2015**). *Plasmodium* transmission blocking activities of *Vernonia amygdalina* extracts and isolated compounds. *Malar. J., 14*, 288.

Abderamane B., Tih A. E., Ghogomu R. T., Blond A. and Bodo B. (**2011**). Isoflavonoid Derivatives from *Lophira alata* Stem Heartwood. *Z. Naturforsch.*, *66 c*, 87 – 92.

Aliyu N.O., Ajala-Lawal R.A., Ajiboye T.O. (**2018**). Lophirones B and C halt acetaminophen hepatotoxicity by upregulating redox transcription factor Nrf-2 through Akt, PI3K, and PKC pathways. *J. Biochem. Mol. Toxicol.*, *32*, e22055.

Cao H., Chen X., Jassbi A.R., Xiao J. (**2015**). Microbial biotransformation of bioactive flavonoids. *Biotechnol. Adv.*, *33*, 214–223.

D'Alessandro S., Gelati M., Basilico N., Parati E.A., Haynes R.K., Taramelli D. (**2007**). Differential effects on angiogenesis of two antimalarial compounds, dihydroartemisinin and artemisone: Implications for embryotoxicity. *Toxicology*, *241*, 66–74.

D'Alessandro S., Camarda G., Corbett Y., Siciliano G., Parapini S., Cevenini L., Michelini E., Roda A., Leroy D., Taramelli D., Alano P. (**2016**). A chemical susceptibility profile of the *Plasmodium falciparum* transmission stages by complementary cell-based gametocyte assays. *J. Antimicrob. Chemother, 71,* 1148–1158.

Dewick P. M. (**1994**). Isoflavonoids. In: The Flavonoids: Advances in Research since 1986 (Harborne, J. B., ed.). Chapman and Hall, London, p. 202.

Fernández-Álvaro E., David Hong W., Nixon G. L., O'Neill P. M., Calderón F. (**2016**). Antimalarial Chemotherapy: Natural Product Inspired Development of Preclinical and Clinical Candidates with Diverse Mechanisms of Action. *J. Med. Chem.*, *59*, 5587−5603.

Fidock, D., Rosenthal, P., Croft, S. *et al.* (**2004**). Antimalarial drug discovery: efficacy models for compound screening. *Nat. Rev. Drug. Discov*, *3*, 509–520.

Ginsburg, H.; Atamna, H. (**1994**). The redox status of malaria-infected erythrocytes: An overview with an emphasis on unresolved problems. *Parasite*, *1*, 5–13.

https://www.malariavaccine.org/malaria-and-vaccines/vaccine-development/life-cycle-malaria-parasite

Kantele A and Jokiranta TS. (**2011**). Review of cases with the emerging fifth human malaria parasite, *Plasmodium knowlesi*. *Clin Infect Dis.*, *52*, 1356–1562.

Mackova Z., Koblovska R., and Lapcik O. (**2006**). Distribution of isoflavonoids in non-leguminous taxa – an update. *Phytochemistry*, *67*, 849 – 855.

Makler M.T., Ries J.M., Williams J.A., Bancroft J.E., Piper R.C., Gibbins B.L., Hinrichs D.J. (**1993**). Parasite Lactate Dehydrogenase as an Assay for *Plasmodium falciparum* Drug Sensitivity. *Am. J. Trop. Med. Hyg., 48*, 739–741.

Mbing J. N., Pegnyemb D. E., Ghogomu Tih R., Sondengam B. L., Blond A., Bodo B. (**2003**). Two biflavonoids from Ouratea flava stem bark. *Phytochemistry*, *63(4)*, 427–431.

Messanga B.B., Ghogomu Tih R., Kimbu S.F., Sondengam B.L. (**1992**). Calodenone, a new isobiflavonoid from *Ochna calodendron*. *J.Nat.Prod.*, *55(2)*, 245-248.

Messanga B. B., Ghogomu R., Sondengam B. L., Blond A., Bodo B. (**1998**). Lanceolin C, a new nitrile glycoside from *Lophira alata*. *Fitoterapia*, *69(5)*, 439-442.

Murakami A., Ohigashi H., Nozaki H., Tada T., Kaji M.and Koshimizu K. (**1991**). Possible Inhibitor of Tumor Promotion and Related Polyphenol from *Lophira alata*, a Medicinal Plant in Tropical West Africa. *Agric. Biol. Chem.*, *55 (4)*, 1151-1153.

Murakami A., Ohigashi H., Tanaka S., Hirota M., Irie R., Takeda N., Tatematsu A. and Koshimizu K. (**1993**). Bitter cyanoglycosides from *Lophira alata. Phytochemistry*, *32(6)*, 1461-1466.

Peatey C.L., Leroy D., Gardiner D.L., Trenholme K.R. (**2012**). Anti-malarial drugs: how effective are they against *Plasmodium falciparum* gametocytes?. *Malar J.*, *11*, 34.

Pegnyemb D. E., Messanga B. B., Ghogomu R., Sondengam B. L., Martin M. T., Bodo B. (**1998**). A new benzoylglucoside and a new prenylated isoflavone from *Lophira lanceolata*. *J. Nat. Prod.*, *61(6)*, 801-803.

Persinos G. J., Quimby M. W., Mott A. R., Farnsworth N. R., Abraham D. J., Fong H. H. S., Blomster R. N. (**1967**). Nigerian plants. III. Biological and phytochemical screening of *Lophira lanceolata* and the isolation of benzamide. *Planta Medica*, *15(4)*, 361-365.

*PROTA. **2007**.* Volume 14 of Plant resources of tropical Africa: Vegetable oils*. PROTA. 2007. pp. 115–117.* ISBN 978-90-5782-191-2.

Sharma C. and Awasthi S. K. (**2015**). An Overview of Tropical Diseases, edited by Amidou Samie. Chapter 3, Recent Advances in Antimalarial Drug Discovery - Challenges and Opportunities.

Shimamura T., Arakawa Y., Hikita K., Niwa M. (**1996**). Biogenetic synthesis of biflavonoids, lophirone B and C, from *Lophira lanceolata*. *Heterocycles*, 43(10), 2223-2227.

Sirignano C., Snene A., Rigano D., Tapanelli S., Formisano C., Luciano P., El Mokni R., Hammami S., Tenoh A.R., Habluetzel A., Taglialatela-Scafati O. (**2017**). Angeloylated Germacranolides from *Daucus virgatus* and Their Plasmodium Transmission Blocking Activity. *J. Nat. Prod.*, *80*, 2787–2794.

Sinden R.E., Dawes E.J., Alavi Y., Waldock J., Finney O., Mendoza J., Butcher G.A., Andrews L., Hill A. V., Gilbert S.C., Basáñez M. G. (**2007**). Progression of *Plasmodium berghei* through *Anopheles stephensi* is density-dependent. *PLoS Pathog.*, *3*, 2005–2016.

Sriram D., Rao V.S., Chandrasekhara K.V., Yogeeswari P. (**2004**). Progress in the research of artemisinin and its analogues as antimalarials: An update. *Nat. Prod. Res.*, *18*, 503–527.

Tapanelli S., Chianese G., Lucantoni L., Yerbanga R.S., Habluetzel A., Taglialatela-Scafati O. (**2016**). Transmission blocking effects of neem (*Azadirachta indica*) seed kernel limonoids on *Plasmodium berghei* early sporogonic development. *Fitoterapia*, *114*, 122–126.

Tih R.G., Sondengam B.L., Martin M.T., Bodo B. (**1987**). Lophirone A, a biflavonoid with unusual skeleton from *Lophira lanceolata*. *Tetrahedron Lett., 28*, 2967-2968.

(a) Tih R.G., Sondengam B.L., Martin M.T., Bodo B. (**1989**). Lophirones D and E: Two New Cleaved Biflavonoids from *Lophira lanceolata*. *J. Nat. Prod.*, *52*, 284-288.

(b) Tih R.G., Sondengam B.L., Martin M.T., Bodo B. (**1989**). Structure of lophirones B and C, biflavonoids from the bark of *Lophira lanceolata*. *Phytochemistry*, *28*, 1557-1559.

Tih R.G., Sondengam B.L., Martin M.T., Bodo B. (**1990**). Structure of the chalcone dimers lophirone F, and H from *Lophira lanceolata* stem bark. *Phytochemistry*, *29*, 2289-2293.

Tih R.G., Ewola Tih A., Sondengam B.L. (**1994**). Structures of Lophirones I and J, Minor Cleaved Chalcone Dimers of *Lophira lanceolata*. *J. .Nat. Prod.*, *57 (1)*, 142-145.

Tih A. E.,. Ghogomu R. T., Sondengam B. L., Martin M.T. and Bodo B. (**1994**) 'Lanceolins A and B: nitrile glycoside esters from *Lophira lanceolata*. *J. Nat. Prod.*, *57(7)*, 971-974.

Tih A. E.,. Ghogomu R. T., Sondengam B. L., Caux C., and Bodo B. (**2006**). Minor Biflavonoids from *Lophira alata* Leaves. *J. Nat. Prod., 69,* 1206-1208.

Trager W., Jensen J.B. (**1976**). Human malaria parasites in continuous culture. *Science*,193, 673–675.

White N.J., Qiao L.G., Qi G., Luzzatto L. (**2012**). Rationale for recommending a lower dose of primaquine as a *Plasmodium falciparum* gametocytocide in populations where G6PD deficiency is common. *Malar. J., 11*, e418.

World malaria report 2019. Geneva: World Health Organization; 2019. Licence: CC BY-NC-SA 3.0 IGO.

WWARN Gametocyte Study Group. (**2016**). Gametocyte carriage in uncomplicated *Plasmodium falciparum* malaria following treatment with artemisinin combination therapy: a systematic review and meta-analysis of individual patient data. *BMC Med*, *14*, 79.

Appendix A: Spectral data of chapter 2

^{1}H NMR spectrum (500 MHz) of lophirone A (**1**) in $(CD_3)_2CO$.

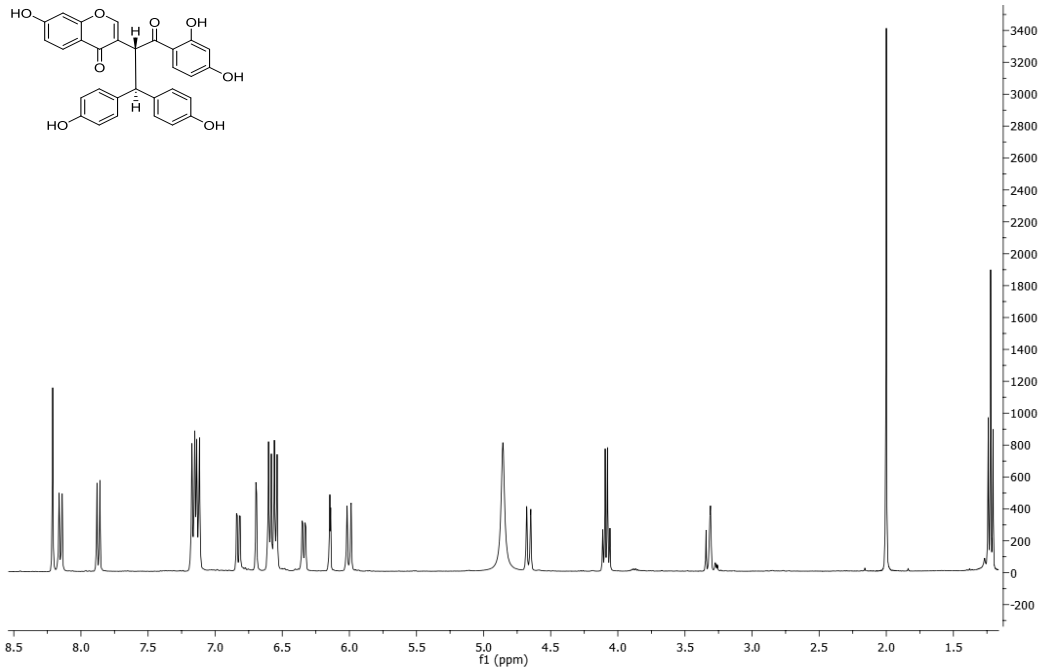

^{1}H NMR spectrum (500 MHz) of lophirone F (**2**) in $(CD_3)_2CO$.

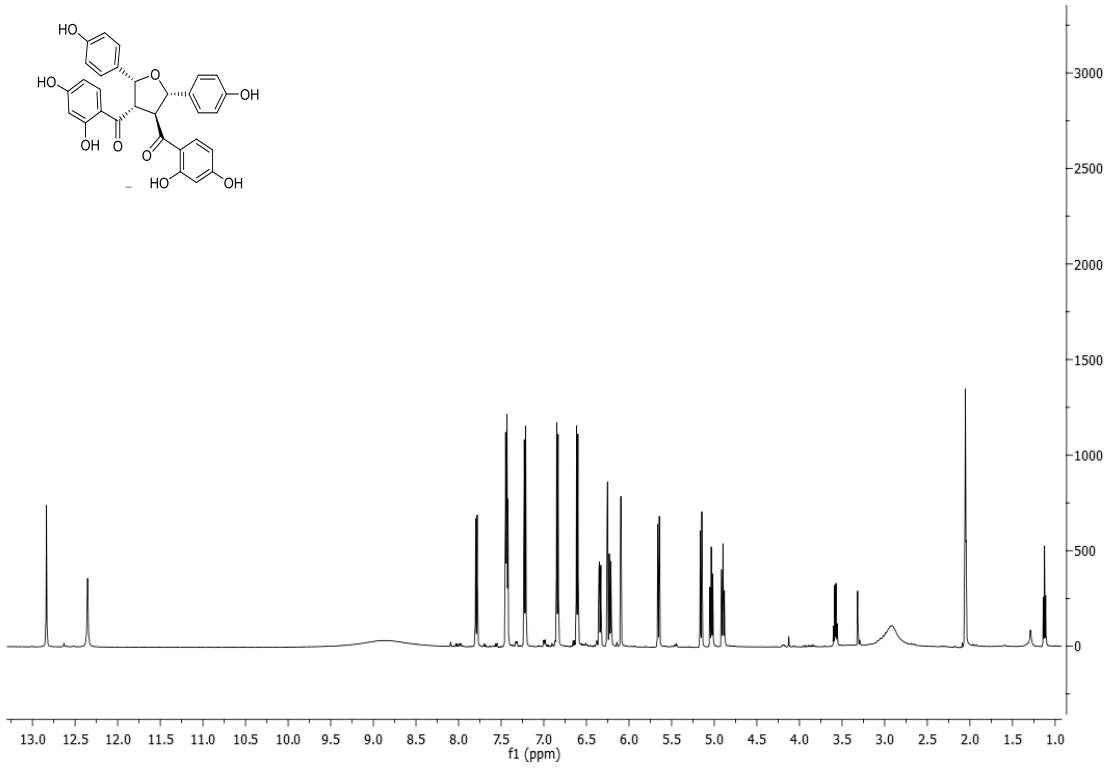

^{1}H NMR spectrum (500 MHz) of lophirone E (**3**) in $(CD_3)_2CO$.

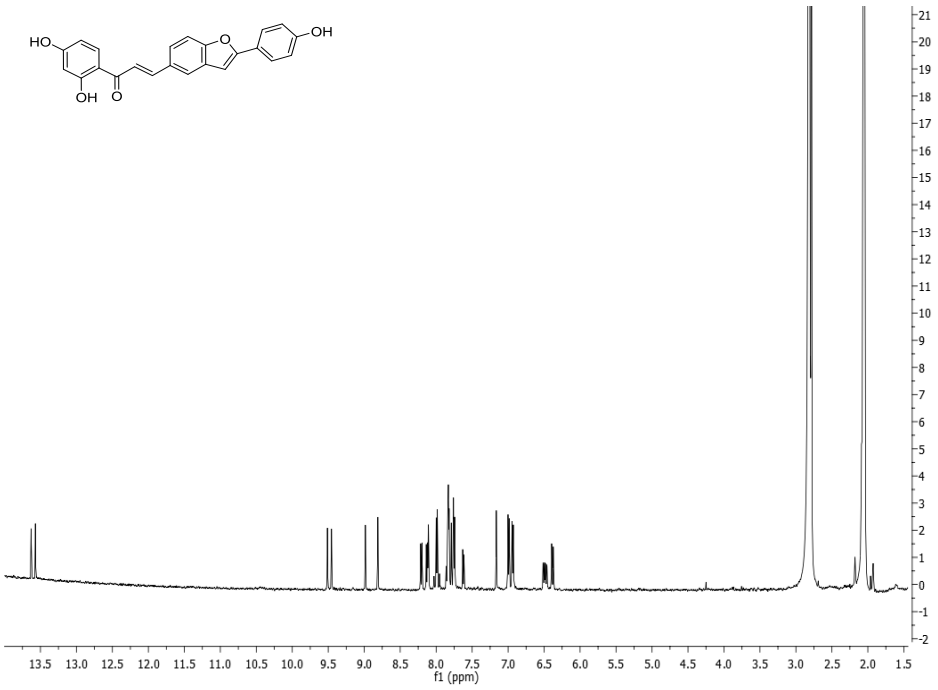

^{1}H NMR spectrum (500 MHz) of lophirone D (**4**) in $(CD_3)_2CO$.

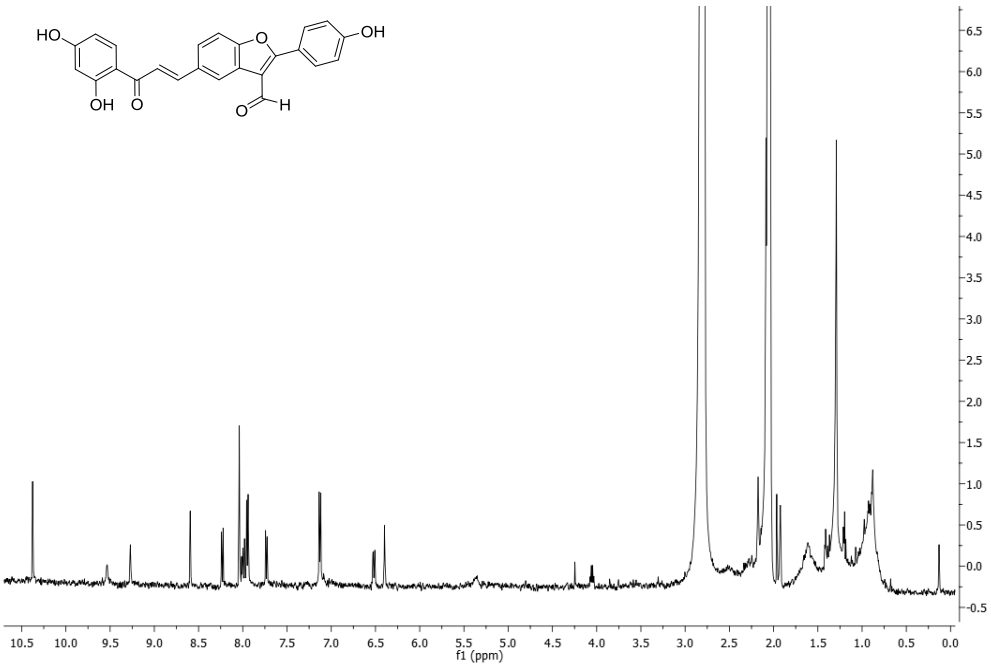

^{1}H NMR spectrum (500 MHz) of α'-chlorolophirone E (**5**) in $(CD_3)_2CO$.

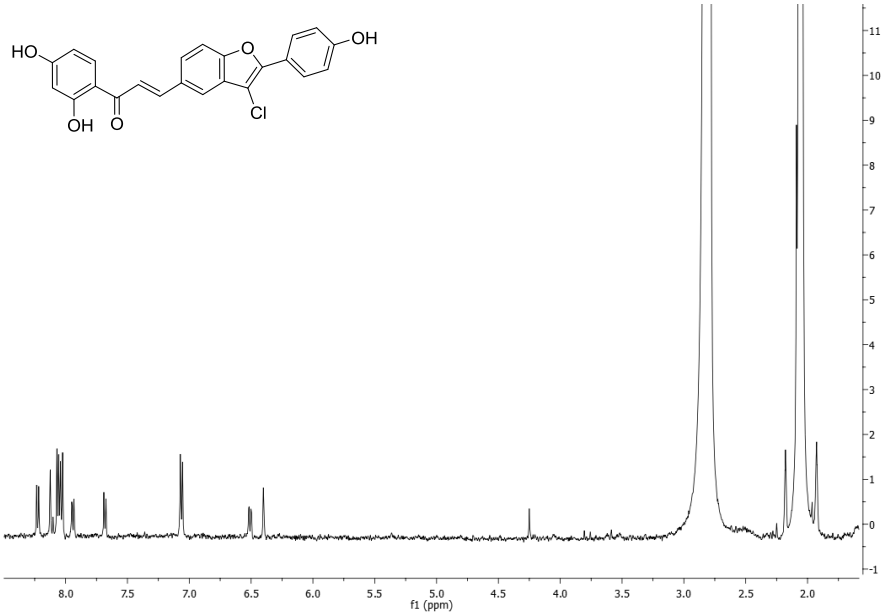

^{1}H NMR spectrum (500 MHz) of 5'-chlorolophirone D (**6)** in $(CD_3)_2CO$.

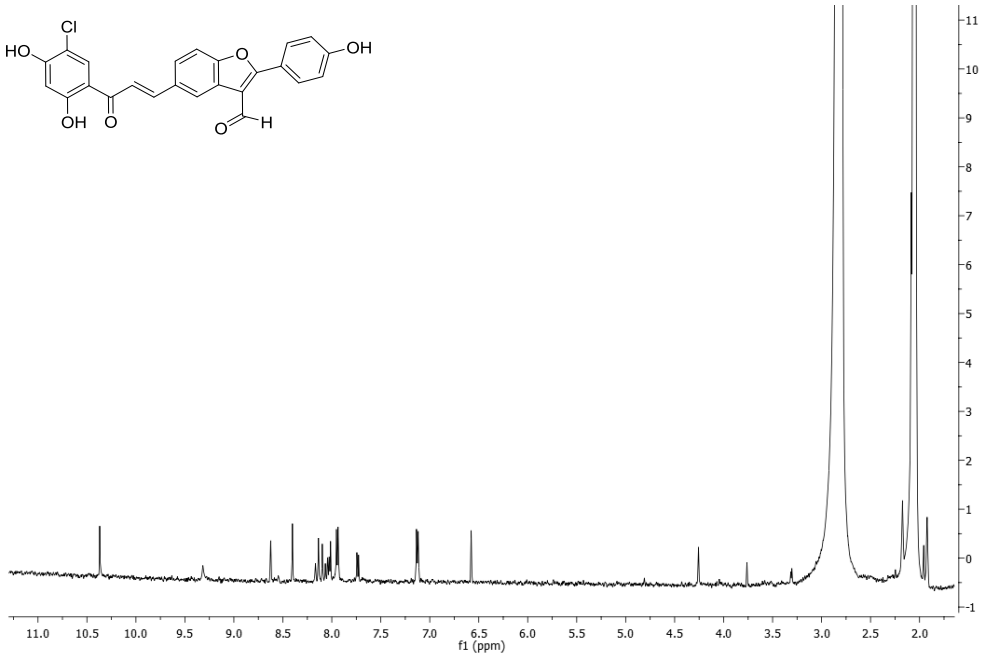

^{1}H NMR spectrum (500 MHz) of lophirone C (**7**) in $(CD_3)_2CO$.

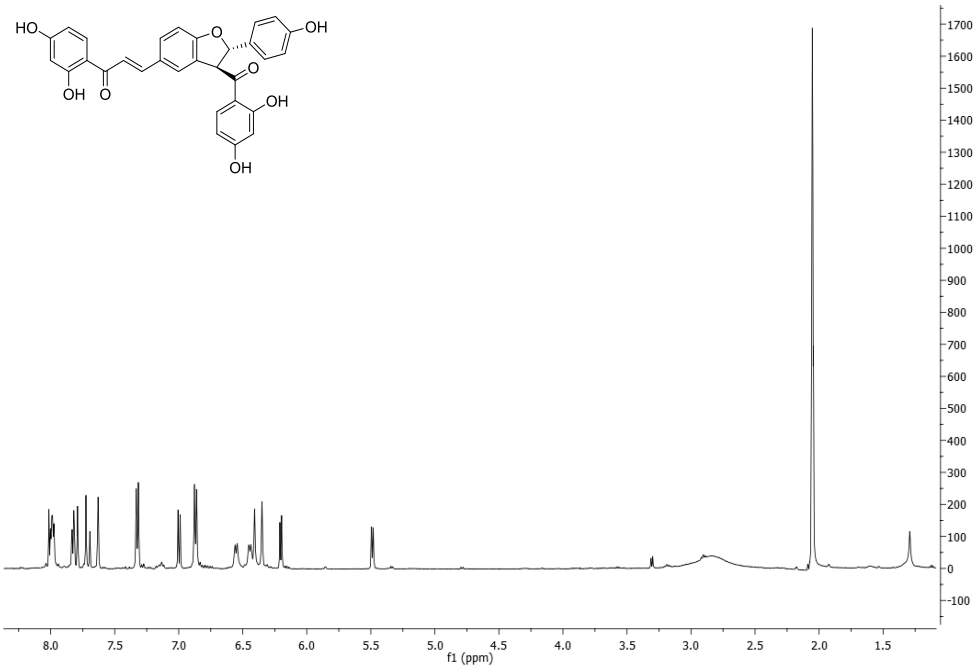

^{1}H NMR spectrum (700 MHz) of lanceolin A (**8**) in (CD_3OD).

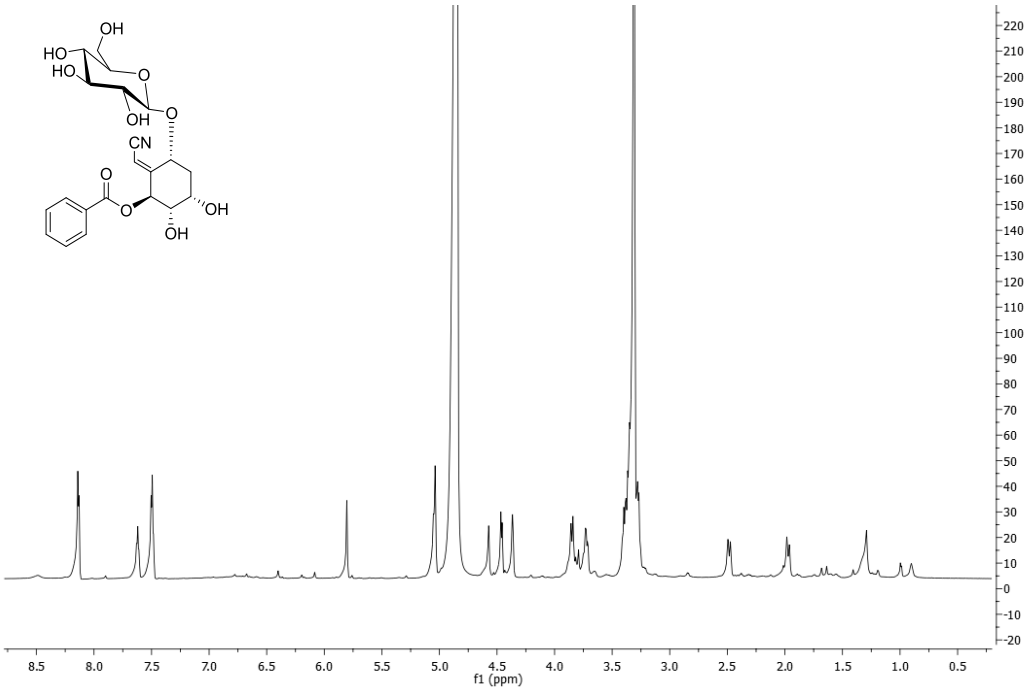

^{1}H NMR spectrum (700 MHz) of lanceolin B (**9**) in (CD_3OD).

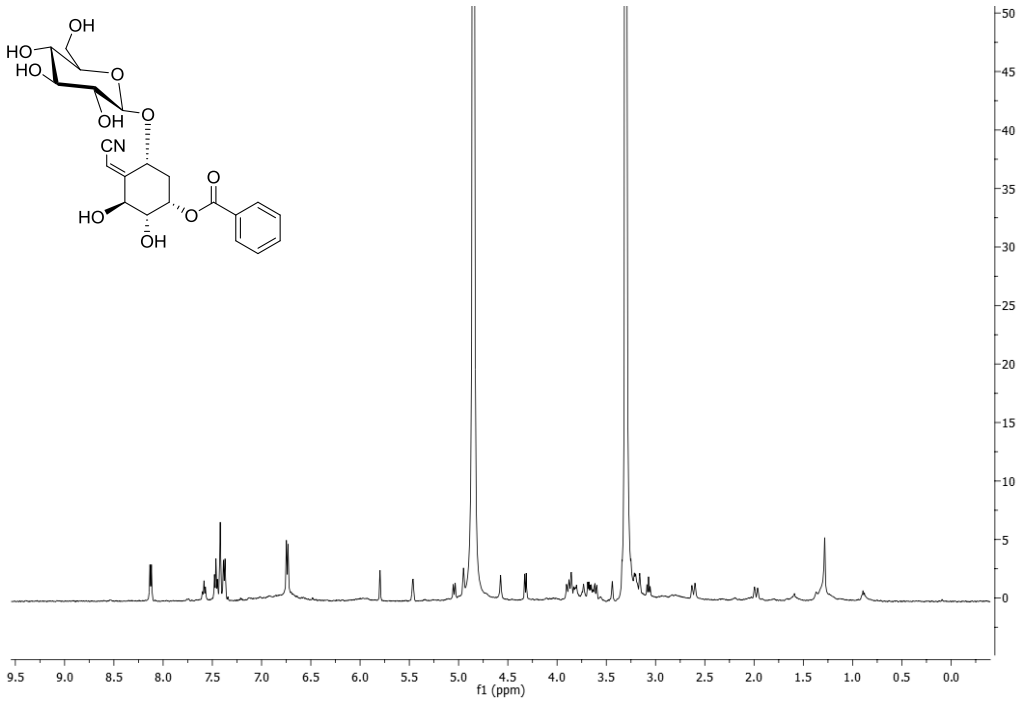

^{1}H NMR spectrum (700 MHz) of glucolophirone C (**10**) in ($(CD_3)_2CO$).

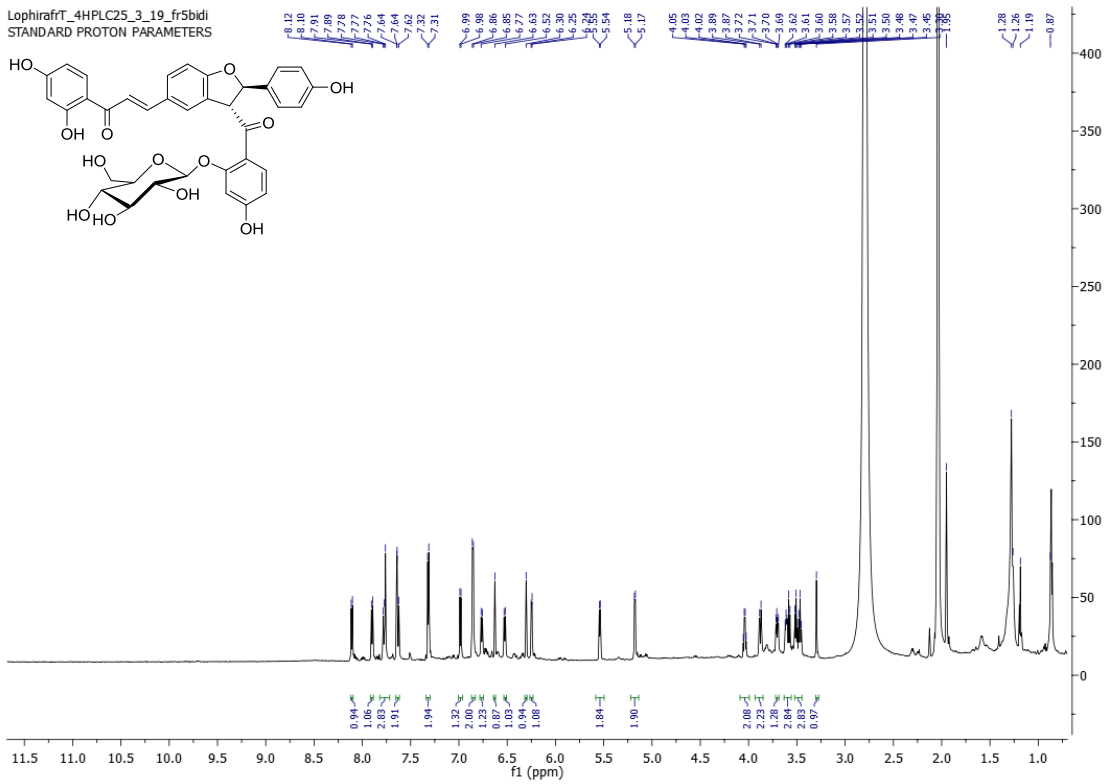

COSY spectrum (700 MHz) of glucolophirone C (**10**) in $(CD_3)_2CO$.

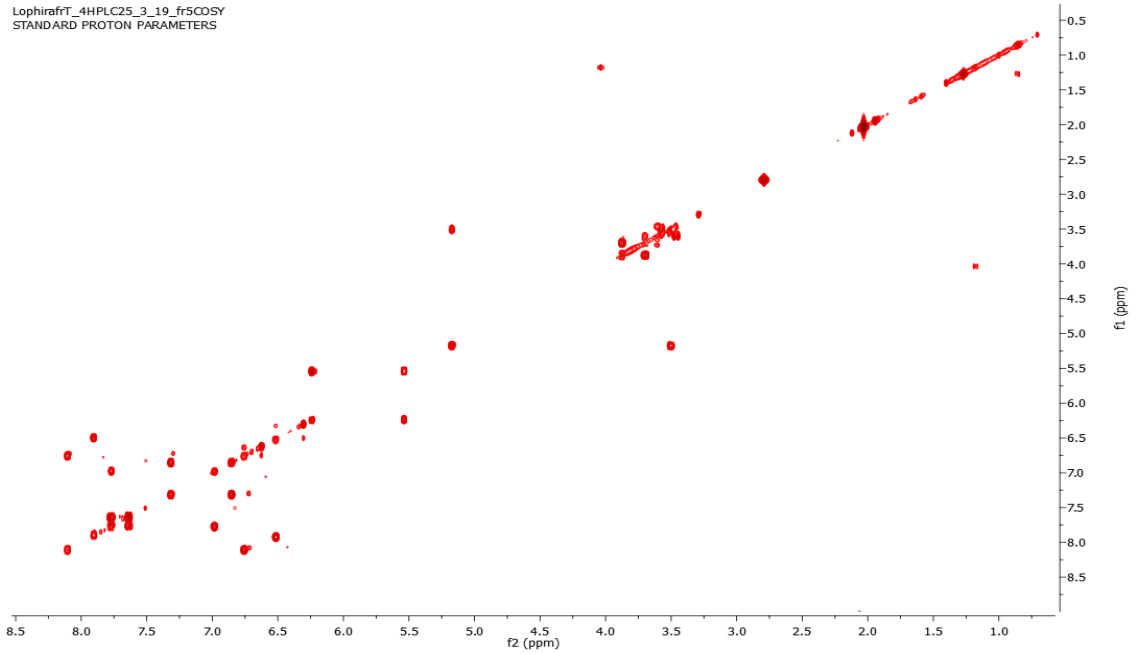

ROESY spectrum (700 MHz) of glucolophirone C (**10**) in $(CD_3)_2CO$.

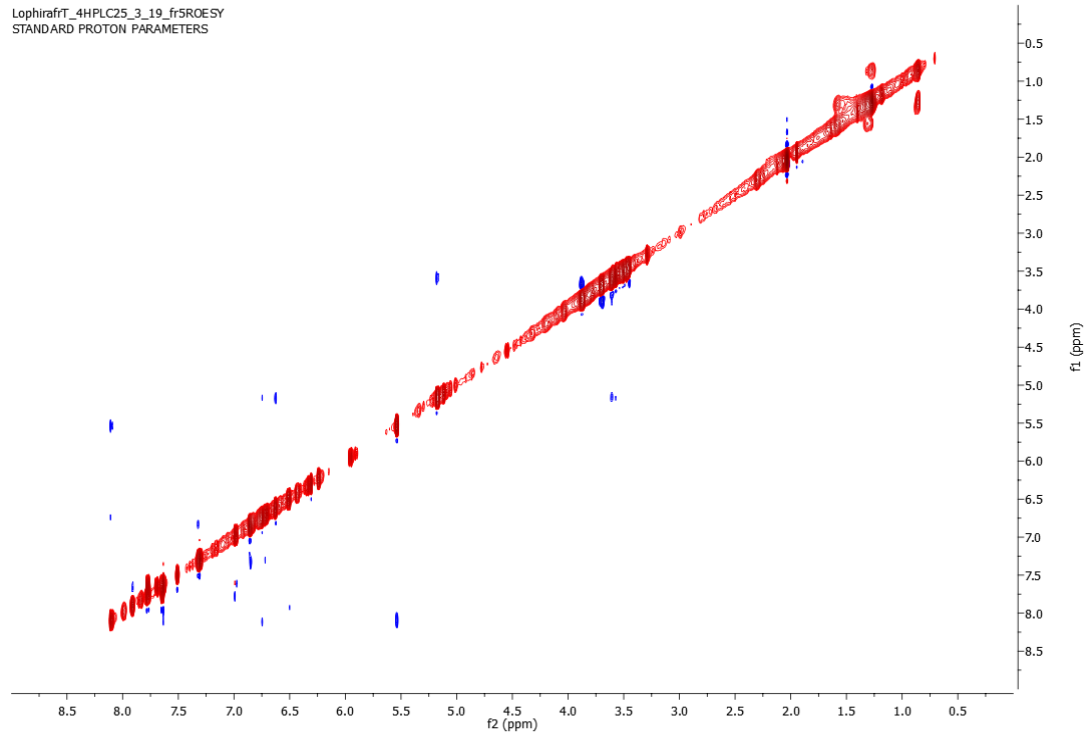

HSQC spectrum (700 MHz) of glucolophirone C (**10**) in $(CD_3)_2CO$.

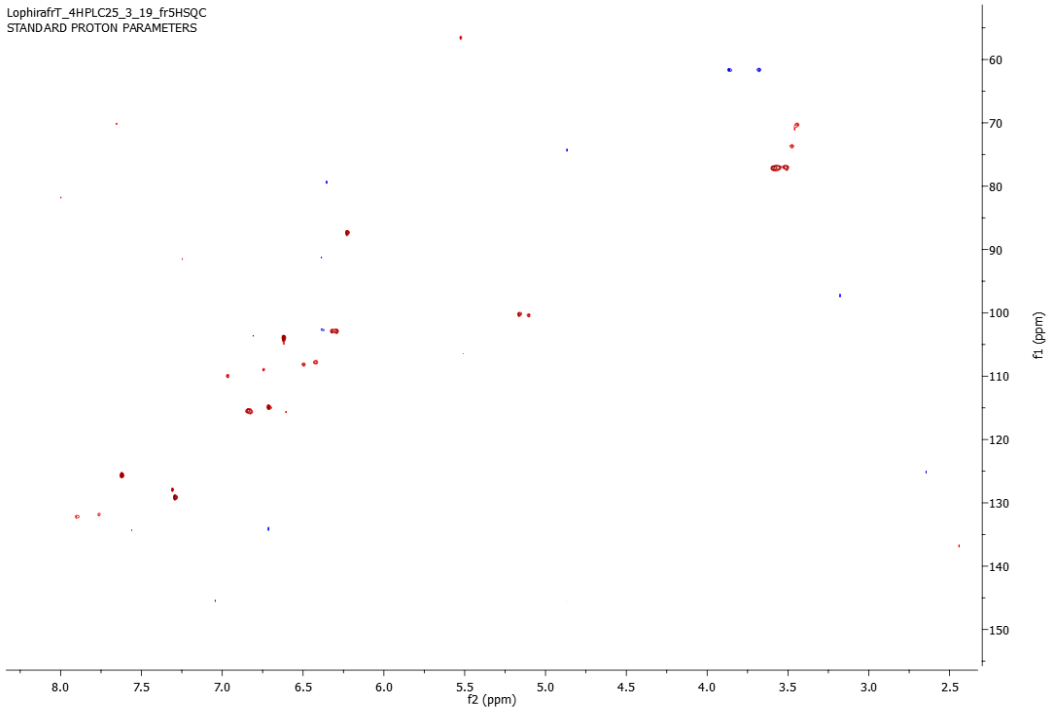

HMBC spectrum (700 MHz) of glucolophirone C (**10**) in $(CD_3)_2CO$.

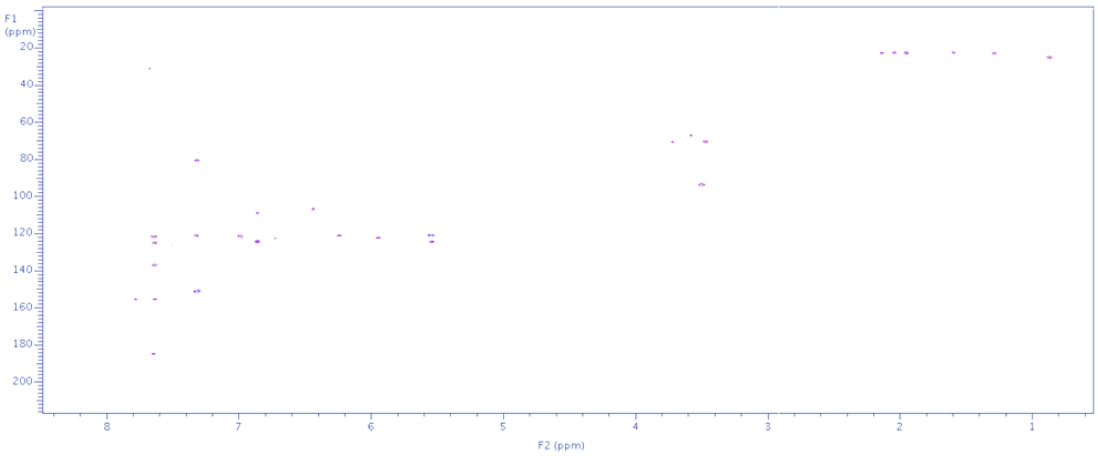

Chapter 3: Exploration of the phytocannabinoid chemical and biological space

3.1 Introduction

Cannabis sativa has always been considered as a disputed plant. Although it revealed to perform beneficial effects for several pathologies, including glaucoma and epilepsy, a precious source of nutrients, sustainable raw material for manufacturing and textiles, it is also the most widely spread illegal drug in the world, especially among young adults (Citti *et al.*, 2019). From a taxonomic point of view, *C. sativa* is a considerably peculiar plant, belonging to the family Cannabaceae, which includes only two genera: *Cannabis* and *Humulus*. In addition, the genus *Cannabis* is represented by only one species. However, several chemotypes of *C. sativa* have been recognized (Hillig *et al.*, 2015), essentially differing from each other in their geographical origin and/or phytochemical composition, especially for the concentration of the substance responsible for its narcotic effect,(-)-Δ^9-tetrahydrocannabinol (Δ^9THC, **4a**). For the reason of simplification, it is possible to distinguish two main *Cannabis* phenotypes in the medicinal community: a medicinal/psychotropic type of *Cannabis*, containing high concentration of Δ^9-THC (**4a**) (generally > 6%). A fiber-type *Cannabis*, well known as hemp and used for textile or seed oil purposes, which contains Δ^9-THC (**4a**) at concentrations lower than 0.2% (dry weight). The major phytocannabinoid of hemp is cannabidiol (CBD, **3a**), whose concentration ranges from 5 to 20%. In addition, other minor non-psychotropic cannabinoids occur in both varieties, including cannabigerol (CBG, **1a**) and cannabichromene (CBC, **2a**) (Figure 3.1).

The recreational use of the Δ^9-THC-rich variety of *C. sativa* started about 5000 years ago, becoming nowadays the most widely utilized illicit narcotic plant in the world. In ancient times, documents about rites and uses of cannabis, as a medicinal or ludic drug, were distributed to a large range of cultures. For instance, one of the first historical descriptions of *C. sativa* was attributed to the Atharvaveda, a Hindu ancient paper, which dates from 1500–1000 BCE. In this text, *Cannabis sativa* was designated as a sacral plant, to be utilized in numerous rituals and ceremonies. Indeed, Herodotus illustrated a ceremonial burning of Cannabis seeds during a Scythian funeral, near the Black Sea, in one of his works, namely “Histories” (400 BCE) (Schafroth and Carreira, 2017).

However, the psychotropic variety of cannabis was completely unknown to the ancient Mediterranean civilizations, becoming noted in Europe only at the times of the Crusades in the XII-XIII centuries (Appendino *et al.*, 2011). In more recent times, in the West, medicinal uses of cannabis were introduced by O'Shaughnessy in 1839, who suggested its application in the treatment of tetanus and as well as for analgesic sedative, anti-inflammatory, antispasmodic and anti-convulsant effects (Doyle and Spence, 1995).

Only in the 1960s the cannabis key ingredient, Δ^9-THC, **4a**, was isolated and synthesized, along with other structurally related compounds, with very potent biological properties, such as nabilone, commercially available as Cesamet™ (Makriyannis and Rapaka, 1987). At the same time, the interest in developing cannabis-based therapies never led to additional medications and, therefore, was extremely reduced. The reason for this decline can be ascribed to the new compounds' narcotic effects and to the absence of any well-defined pharmacological mode of action for newer analogs (Vemuri and Makriyannis, 2015).

The discovery of the endocannabinoid system in 1988 and, in particular, cannabinoid receptor 1 (CB_1) and five years later, cannabinoid receptor 2 (CB_2) as the main targets of phytocannabinoids, led to a renovated attention to this plant (Reekie *et al.*, 2017). In this context, further exploration of *C. sativa* secondary metabolites led to the revelation of the richness of this plant, in terms of pharmacological activities and making it one of the hottest topics in current medicinal chemistry research (Hanuš *et al.*, 2016).

To date, more than 500 different natural products have been identified in *C. sativa*, revealing its peculiar complex mixture of compounds, encompassing the classes of polyketides, terpenoids (a mixture of about 120 mono- and sesquiterpenoids are responsible for the characteristic odor of the plant), modified sugars, alkaloids, flavonoids, stilbenoids, and quinones. Among these, the secondary metabolites, to which still today the scientific community is more interested, are called phytocannabinoids. They represent the main bioactive ingredients in cannabis plant extracts, accumulated in the secretory cavity of the glandular trichomes, which largely occur in female flowers and in most aerial parts of the plants (Andre *et al.*, 2016). Various definitions for phytocannabinoids have emerged, but in these studies, phytocannabinoids are

considered as the natural products or their derivatives that share a chemical similarity to cannabinoids.

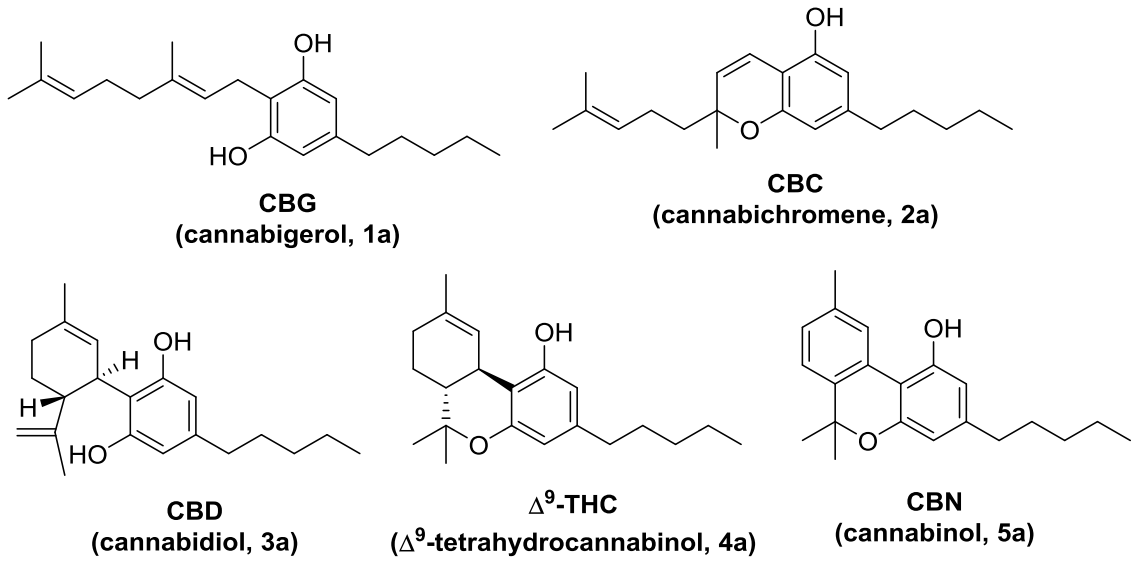

Figure 3.1. Structure of some well-known phytocannabinoids.

The phytochemical composition as well as the pharmacological potential of phytocannabinoids from *C. sativa* appears to be not exhaustively unravelled still today. Indeed, only recently several new phytocannabinoids were identified from medicinal cannabis, they are homologs of cannabidiol (**3a**) and Δ^9-THC (**4a**) (the two major metabolites from *C. sativa*), sharing the same structural scaffold, but with a different length of the alkyl side chain (Citti *et al.*, 2019). On the other side, the application of phytocannabinoids and their derivatives in therapeutics is growing. Several medications based on phytocannabinoids are currently approved around the world, including: Marinol® (AbbVie Products) approved by the FDA, which contains as its active compound the synthetic form of Δ^9-THC (**4a**), dronabinol, as antiemetic and appetite stimulator in patients treated with cancer chemotherapy or for AIDS-associated anorexia and weight loss. Sativex® (GW Pharmaceuticals) the first cannabinoid-based drug approved in Italy in 2013 as a remedy against muscle spasticity caused by multiple sclerosis, its active ingredients is nabiximols, consisting of a 1:1 mixture of Δ^9-THC (**4a**) and CBD (**3a**). Epidiolex® (GW Pharmaceuticals), approved in USA in 2018 and EU in 2019, based exclusively on CBD (**3a**) and employed for the treatment of pediatic epilepsy.

Our research group is currently involved in the phytochemical study of Cannabis varieties and, more generally, of phytocannabinoid chemistry and biology. In

this context, during my Ph.D activity, I have investigated the phytochemical content of a fiber hemp variety as well as the reactivity of the major phytocannabinoids with iodine and other oxidant reagents.

3.1.1 Phytochemistry of phytocannabinoids

As described in the previous section, in Cannabis plants, phytocannabinoids are the most interesting components from a pharmacological and chemical point of view. They belong to a class of mono- to tetracyclic C_{21} (or C_{22}, for the carboxylated forms) meroterpenoids and biogenetically derive from an enzymatic reaction between resorcinol and the isoprenoid group. The diversity of the almost 150 known phytocannabinoids is particularly due to the various combination of these two parts, that for the most commonly naturally occurring phytocannabinoids correspond to olivetolic acid, namely a C_{12} polyketide unit and geranyl pyrophosphate (GPP), originating from the deoxyxylulose phosphate / methylerythritol phosphate pathway.

Phytocannabinoids are usually characterized by a *para*-orientation of terpenyl and pentyl groups, although, compounds with a different degree of isoprenylation (prenyl, sesquiterpenyl) or with an alkyl group (methyl, propyl, or more rarely ethyl and butyl) were also found in *C. sativa*. Phytochemical studies of terrestrial and marine organisms revealed that cannabinoids have a larger distribution in Nature, including higher plants, as well as liverworts and fungi. They could be mainly distinguished based on their aliphatic or an aromatic ketide starter (alkyl- and aralkyl phytocannabinoids, respectively). For instance, *C. sativa* and *Rhododendrons* produce exclusively alkyl phytocannabinoids, while aralkyl phytocannabinoids are typical of some leguminous plants from the genera *Amorpha*, *Glycyrrhiza*, *Helichrysum* and *Macherium*, as well as in some lower plants, such as liverworts from the genus *Radula*. In particular, the South-African plant, namely *Helichrysum umbraculigerum* (Less.), is a good producer CBG (**1a**), CBGA (**1b**) and, interestingly, of abnormal CBGA (**1g**), along with other cannabinoids, which differ for the substitution of the *n*-pentyl (or *n*-propyl) C-3 side chain with a β-phenylethyl group (e.g. H-CBG, **1h**), referred to in the literature as prenylated bibenzyls. Besides, these compounds have been also found in the genus *Radula*, where they occur with their *ortho*-derivatives (defined as abnormal cannabinoids) (Hanuš *et al.*, 2016). Surprisingly, few data

are reported in literature about the pharmacological activities of the prenylated bibenzyl and abnormal cannabinoids, so far (Pollastro et al, 2017).

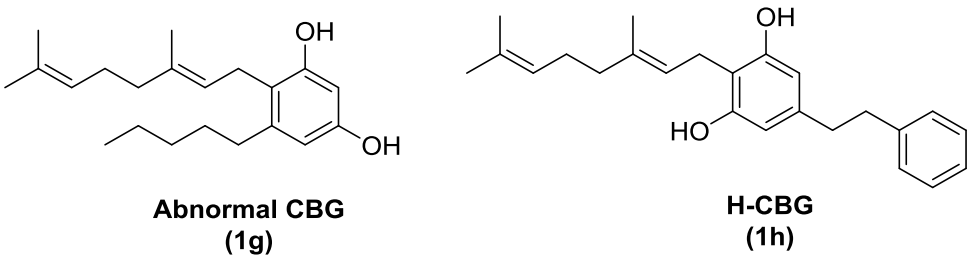

Figure 3.2. Structure of **1g** and **1h**.

3.1.1.1 Cannabigerol-type compounds

The first product, formed by the condensation reaction of olivetolic acid and a C_{12} polyketide unit and GPP, leads to the formation of cannabigerolic acid (CBGA, **1b**). As shown in Figure 3.3, the polyketide moiety of CBG (**1a**) and more generally of cannabinoids are produced by *n*-hexanoylCoA, through the three-fold addition of malonyl-derived acetate units, followed by cyclization and aromatization to provide olivetolic acid. The enzyme responsible for the condensation between olivetolic acid and GPP is a specific prenyltransferase, discovered in the expanding leaves of *C. sativa* (Fellermeier and Zenk, 1998). It is widely admitted that the obtained cannabigerolic acid (CBGA), as well as other cannabinoid acids undergo a non-enzymatic decarboxylation step to achieve their neutral form, by heat.

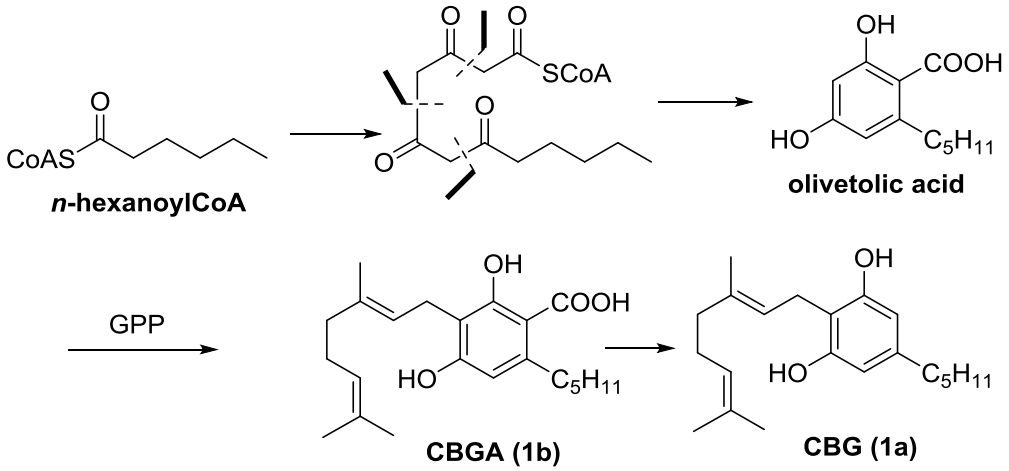

Figure 3.3. Biogenesis of cannabigerolic acid (CBGA, **1b**) and cannabigerol (CBG, **1a**)

The structural trademark of CBG-type compounds is the presence of a linear isoprenyl residue. CBG was not identified as the major constituent of *C. sativa*, although, as already specified, another *non*-cannabis plant, *Helichrysum*

umbraculigerum Less., produces CBG (**1a**) and CBGA (**1b**) as the main secondary metabolites (Hanuš *et al.*, 2016). Several minor analogs of cannabigerol have been identified, presenting a shorter alkyl side chain, with C_4, C_3 or C_1 side chains. Among them, cannabigerovarin (**1c**) (Shoyama *et al.*, 1975) (C_3H_7 side chain) or more generally cannabivarins could be mentioned. It is possible that they derive from an enzymatic reduction of the CBG pentyl chain or a shorter starter unit (butanoyl CoA) for the ketide homologation.

Further CBGA analogues include cannabinerolic acid (Taura *et al.*, 1995), characterized by a different configuration (*Z*) of the double bond in the prenyl unit; carmagerol, extracted from the Carma variety of *C. sativa* (Appendino *et al.*, 2008, a); and several hydroxylated and oxidized quinone derivatives of cannabigerol, reported from a high-potency Δ^9-THC-rich variety of *C. sativa* (Radwan *et al.*, 2009).

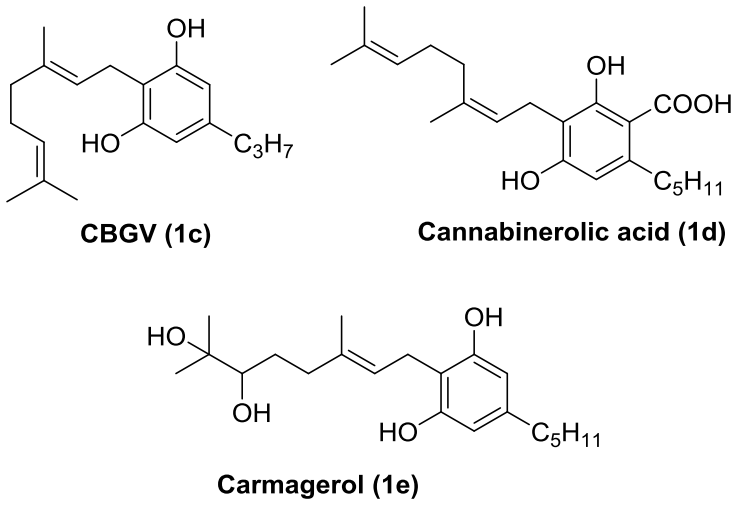

Figure 3.4. Structure of some CBG analogues.

3.1.1.2 Cannabichromene (CBC) and cannabicyclol-type compounds

In this type of phytocannabinoids, the isoprenyl residue is oxidatively fused to the resorcinyl ring. Natural CBC (**2a**) is only isolated as a racemate and it is the unique major phytocannabinoid that shows a bluish fluorescence under UV light (Hanuš *et al.*, 2016).

A [2 + 2] intramolecular cycloaddition of CBCA (**2b**), the acidic precursor of CBC (**2a**), causes the concomitant constitution of two additional rings (four- and five-membered, respectively) providing the tetracyclic system of cannabicyclolic acid (CBLA, **6b**), switched into cannabicyclol (CBL, **6a**) by decarboxylation (figure 3.5) (Appendino *et al.*, 2011). The formation of CBL (**6a**) remains, actually, not

resolved. It is possible that cannabicyclol (**6a**) is a result of natural irradiation on the plant or it is an artifact formed in the crude extract. In any case, the photocycloaddition occurs with peculiar diastereoselectivity, and the product is obtained from the approach of the terminal double bond from the face *anti* to that of the angular pyrane oxygen. Also cannabicyclol was isolated from *Cannabis* as a racemate, whose relative configuration was established by X-ray analysis of the dibromoderivative (Bengley *et al.*, 1970) and showed in Figure 3.5.

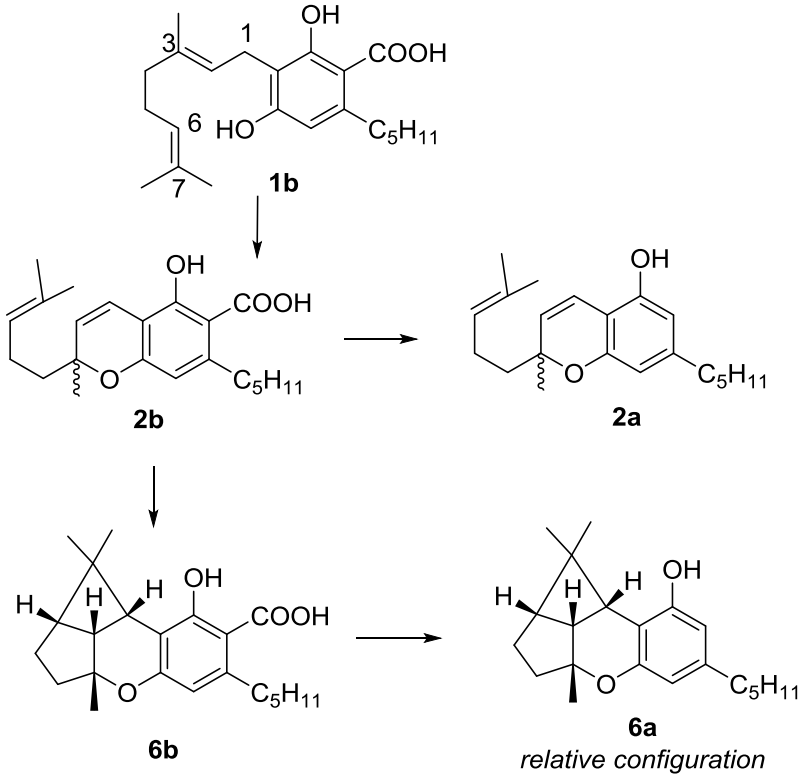

Figure 3.5. Biogenesis of cannabichromene- and cannabicylol-type compounds

3.1.1.3 Cannabidiol (CBD)-type compounds

CBD (**3a**) was the first phytocannabinoid to be isolated in 1940 (Adams *et al.*, 1940, *a*; Jacob and Todd, 1940); however, its precise structure elucidation was only reported more than two decades later, revising the location of the endocyclic double bond (originally reported at C-3, C-5 and C-8 by different authors), and establishing its relative configuration. The study of the correlation between natural (-)-menthol and CBD (Figure 3.6), led to the determination of the absolute configuration of its stereogenic carbons (Mechoulam and Shvo, 1963; Santavy, 1964).

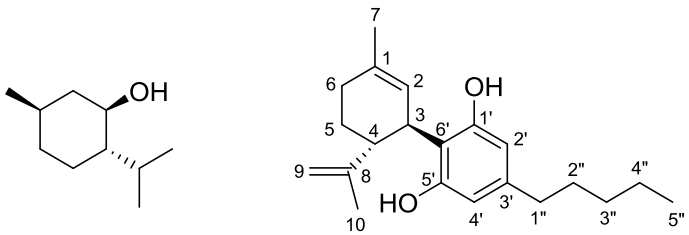

Figure 3.6. Structures of (-)-menthol and CBD (**3a**).

CBD (**3a**) is a major constituent of the fiber hemp, along with its carboxylated form, representing the first pre-cannabinoid to be isolated. These compounds are the result of an oxidative cyclization of CBGA (**1b**)**,** catalyzed by cannabidiolic acid synthase and resulting in the formation of a link between C-1 and C-6 of the prenyl unit. In addition, the aromatized analogue of CBD, namely cannabinodiol (CBDN, **3c**), was isolated and considered as a possible artifact, since its concentration increases with the age of the stored plant. Among the naturally occurring analogues of CBD (**3a**), several compounds possess interesting structure features: an alkyl residue with an even number of carbons, such as CBDB, namely cannabidiol with a butyl side-chain (**3d**) (Linciano *et al.*, 2019), or *O*-alkylation with propyl- and pentyl residues.

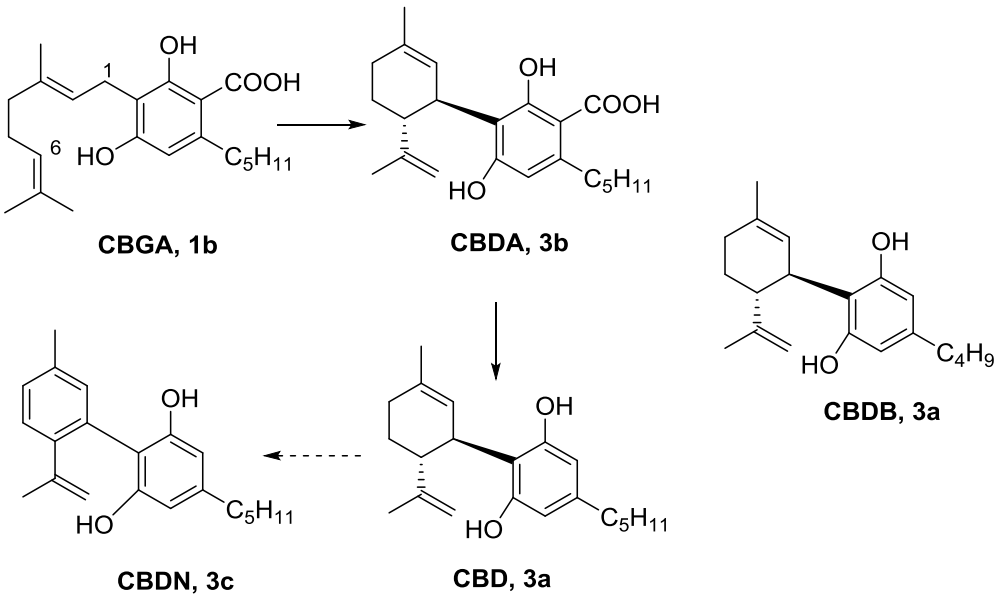

Fig. 3.7. *(left)* Biogenesis of cannabidiol (**3a**) and cannabinodiol (**3c**); *(right)* structure of CBD analogue, with an butyl side-chain.

Besides, cannabielsoin (**7a**) is the major pyrolysis product obtained from CBD (**3a**) or CBDA (**3b**), leading to CBEA (**7b**) and the CBE (**7a**), but they also isolated from Cannabis. It is formed by the attachment of one of the two

phenolic oxygen atoms at the endocyclic double bond of the monoterpene unit generating the dihydrofuran ring of cannabielsoins. The acidic type of cannabielsoin exists in two isomeric forms, having the carboxylate located *ortho* or *meta* to the oxygen bridge. (Hanuš *et al.*, 2016)

Related to CBD (**3a**) are dihydrocannabifuran (**7c**) and cannabifuran (CBF, **7d**) (Friedrich-Fiechtl and Spiteller, 1975), produced by the same process of CBE (**7a**) and all these three compounds have been detected in the smoke condensate of the hashish.

Finally, cannabimovone (CBM, **7e**), also isolated from the non-psychotropic variety of *C. sativa* (Carma), represented the first cannabinoid with an *abeo*-menthane terpenoid structure. It seems that CBM derived from CBD through a stereoselective dihydroxylation of the endocyclic double bond, followed by oxidative cleavage of the glycol system and then aldolyzation of the resulting dicarbonyl intermediate (Taglialatela-Scafati *et al.*, 2010).

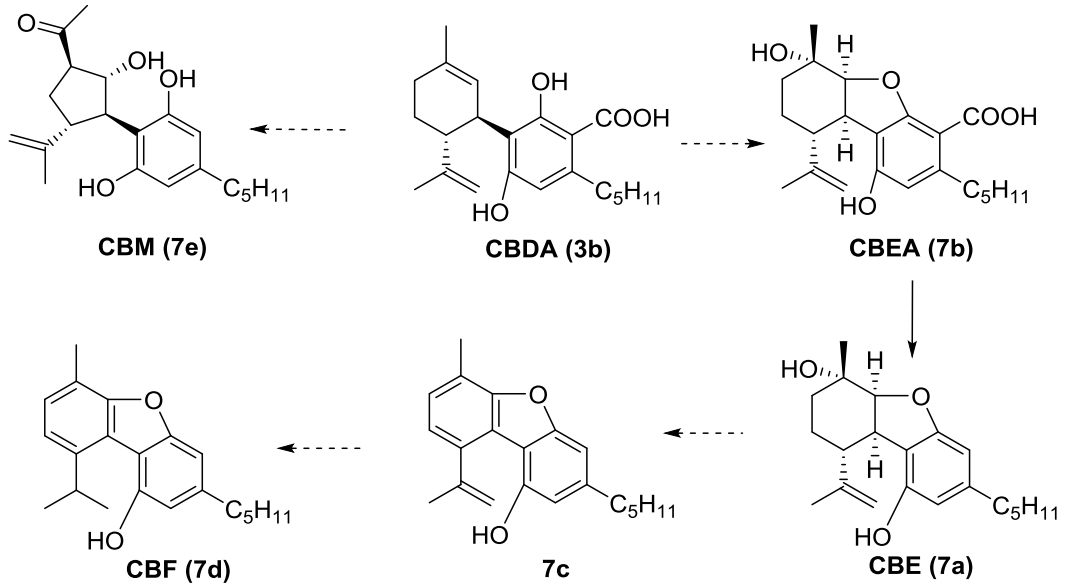

Figure 3.8. Cannabielsoin- and cannabimovone-type compounds

3.1.1.4 Tetrahydrocannabinol-type compounds

The major constituent of the narcotic phenotype of *C. sativa* is *trans*- Δ^9-THC (Δ^9-THC, **4a**), along with its acidic precursor, delete tetrahydrocannabinolic acid. Their biogenesis was defined after isolation and characterization of the specific FAD-dependent enzyme THCA synthase. This enzyme is responsible for the cyclization of CBGA (**1b**) by a cationic intermediate with positive charge

at C-3 (Taura *et al.*, 1995). Attachment of the phenolic oxygen at C-7 of the monoterpene unit and the linkage C-6/C-2 resulted in the formation of the tricyclic system of THCA (**4b**) and its decarboxylated analogue Δ^9-THC (Figure 3.9).

Regio- and stereoisomers also occur in cannabis, but as minor constituents (Taylor *et al.*, 1966; Schafroth *et al.*, 2014; Zias et al, 1993). It is not clear if these compounds are enzymatically produced or if, conversely, they are artifacts originating from the degradation of Δ^9-THC (**4a**) or of CBD (**3a**). Δ^8-THC (**4f**) corresponds to an example of numerous isomers of Δ^9-THC; besides, chemically it is more stable because of the location of the double bond, for this reason the isomerisation happens. Additionally, also *cis*- Δ^9-THC was isolated from cannabis, detected only in traces in narcotic cannabis, while in larger amount in fiber cannabis.

In the figure 3.9, hydroxylated derivatives (Qureshi *et al.*, 2012), along with the epoxide form (Ross *et al.*, 2010) of Δ^9-THC are also illustrated as products isolated from cannabis. Among the tetrahydrocannabinol-type compounds that are mentioned in this chapter, cannabicitran (**17**) represents a *cis*-THC epoxide, probably obtained through a Makovnikov-type protonation of the endocyclic double bond, followed by the addition of the free hydroxyl group at C-1 (Hanuš *et al.*, 2016).

Finally, the completely aromatized analogues of Δ^9-THC are named cannabinol (**5a**) and cannabinolic acid (**5b**).

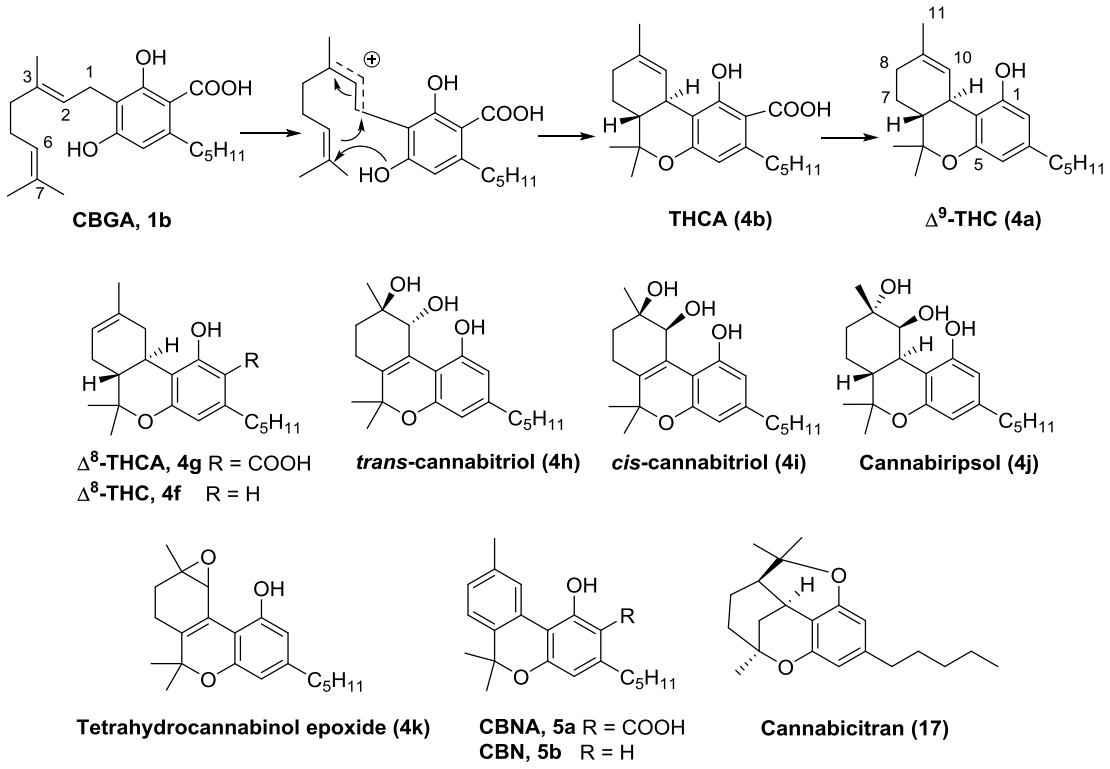

Figure 3.9. Structure of tetrahydrocannabinol-type compounds.

3.1.2 Pharmacology and medicinal applications

Normally, the pharmacological research has focused its main efforts in the study of the affinity performed by cannabinoids to the two GPCR known as cannabinoid receptors (CB_1 and CB_2). In effect, within the almost 200 known cannabinoids, only Δ^9-THC, its isomer Δ^8-THC, and, to a less extent, their aromatized derivative CBN (**5a**) (Figure 3.1), bind, significant affinity, to the ligand recognizing site of these receptors and in particular, the psychoactive effect assigned to marijuana is mediated by their interactions with CB_1 receptors (Hanuš *et al.*, 2016).

Phytocannabinoids have a pleiotropic bioactivity profile. Indeed targets of cannabinoids include glycine receptors (ligand-gated ion channels that have a role in mediating inhibitory neurotransmission in the central nervous system); transient receptor potential (TRP) channels (expressed in many cell types and tissues that play a role in physical senses such as temperature); G protein-coupled receptors (GPRs; species that activate signal transduction); 5-hydroxytryptamine (5-HT) or serotonin receptors (neurotransmitter GPRs); peroxisome proliferator-activated receptors (PPARs function as transcription factors regulating gene expression) and cytochrome P450 (a biological oxidant) (Reekie *et al.*, 2017).

Thus, the cannabis potential extends well beyond its narcotic effect, since non-THC cannabinoids might determine several therapeutic benefits. On the other hand, the therapeutic use of THC is limited by its psychoactive property and potential for inducing dependence and tolerance.

Thanks to the collaboration with two distinct groups (Endocannabinoid Research Group of the CNR, Italian National Research Council of Naples, and Departement of Physiology and Immunology, at the University of Córdoba) phytocannabinoids obtained during my PhD's research were investigated for interaction on TRPs channels and PPAR-γ:

3.1.2.1 Phytocannabinoids and TRPs receptors

The transient receptor potential (TRP) proteins constitute a large group of non-selective cation permeable channels, which display an extraordinary diversity of roles in sensory signaling to regulate several cell functions (Montell *et al.*, 2002). TRP channels were initially discovered in a mutant *Drosophila melanogaster* (Montell and Rubin, 1989) that, when exposed to intense light, showed transient calcium influx into their photoreceptor cells; this is the explanation why the mutant gene was called *trp*, 'transient receptor potential'. They are ubiquitous in the human organism, with six *trans*-membrane (TM) domains and area subdivided into six subfamilies: TRPA (ankyrin), TRPC (canonical), TRPM (melastatin), TRPML (mucolipin), TRPP (polycystin), and TRPV (vanilloid), varying in the motifs of their amino and carboxyl termini. Normally, TRP channels perceive changes in the cellular content, in particular, temperature, stretch/pressure, chemicals, oxidation/reduction, osmolarity and pH, both acidic and alkaline. (Tsagareli and Nozadze, 2019) However, TRP channels have been demonstrated to mediate pain, taste, hot or cold sensations, which has encouraged an intense research activity aimed at developing TRP channel modulators with potential therapeutic value (Appendino *et al.*, 2008). Consequently, TRP agonists/antagonists could provide interesting pharmacological opportunities in several pathologies (Appendino *et al.*, 2008 b).

Because of their involvement in the detection of pain evoking noxious stimuli, TRPA1 and TRPM8 are among the most intensely investigated TRP channels. The transient receptor potential ankyrin 1 (TRPA1) is a channel characterized

by the presence of 17 ankyrin-repeats and a calcium-binding site in its N-terminus, along with a zinc-binding site in the *C*-terminus (Fig. 3.6). It can be defined as a pain sensor because it is mainly expressed in sensory neurons (where it is co-expressed with TRPV1), however, recent works outlined that functional TRPA1 is also present in non-neuronal tissues such as heart, lung, small intestine, and pancreas. Many studies carried out using TRPA1 knockout mice and specific antagonists, have related the function of TRPA1 in noxious cold perception, and is also involved in neuropathic and inflammatory pain (Baraldi *et al.*, 2010), qualifying as a target for the discovery of novel analgesic and anti-inflammatory agents. It is activated by many stinging natural products, such as allyl isothiocyanate, cinnamaldehyde and allicin, contained in mustard oil, cinnamon and garlic respectively, or by environmental irritants, such as acrolein or formalin. Interestingly, TRPA1 is also stimulated by a non-psychotropic cannabinoid such as cannabichromene, considered to play a critical role in the anti-inflammatory and analgesic activities of cannabis extracts.

The transient receptor potential vanilloid (TRPV1-4) is thermosensitive but has different temperature activation profiles. Among these, TRPV1 is activated by temperatures in the noxious range (>43 °C) with an activation threshold of 40 °C along with various noxious chemicals, including eicosanoids, capsaicin (the active constituent of chili peppers), protons and peptide toxins. The activation of TRPV1 plays a key role in the detection of a large array of noxious stimuli. TRPV1 antagonists have advanced to clinical trials where findings of drug-induced hyperthermia and loss of heat sensitivity have raised the question about the viability of a therapeutic approach (Bevan *et al.*, 2014). TRPV2 recently revealed an important role as a potential biomarker in glioblastoma prognosis and therapy. TRPV3 appears to be critical for skin barrier formation, hair growth, wound healing, keratinocyte mutation, and cutaneous pain, itch, and temperature sensation. Naturally occurring genetic mutations with augmented TRPV3 function lead to hairless, skin inflammation, severe itchiness, and dermatitis, suggesting the potential use of TRPV3 blockers in the treatment of skin disease. Hypoxia/ischemia increases TRPV4 expression and function in astrocytes and pulmonary arterial smooth muscle cells of mice exposed to chronic hypoxia-induced pulmonary hypertension (Tsagareli and Nozadze, 2019)

Finally, the transient receptor potential melastatin 8 (TRPM8) is a nonselective cation channel activated by cold and agents like menthol (an active constituent of peppermint) and several other chilling compounds such as eucalyptol, and icilin (a synthetic compound), which induce a cool sensation (De Petrocellis et al, 2007). It is considered as a neuronal sensor that plays a role in cold and mechanical allodynia associated to traumatic neuropathy, in conjunction with TRPA1. However, TRPM8 and TRPV1 are expressed also in nervous and non-nervous tissues that are not subjected to temperatures changes, thus suggesting other important functional roles beyond those temperature sensors. For example, TRPM8 is aberrantly expressed in a variety of malignant solid tumors (especially prostate), and that its overexpression correlates with tumor progression (Borrelli *et al.*, 2014). Among the non-THC cannabinoids, cannabidiol and cannabigerol are significant antagonists of TRPM8, suggesting underlying the analgesic, anti-inflammatory and anticancer potentials.

3.1.2.2 PPAR and phytocannabinoids

In the past few years it has been demonstrated that peroxisome proliferator-activated receptors (PPARs), a family of nuclear receptors able to regulate lipid turnover and metabolism, are also targeted by phytocannabinoids (Pistis & Melis, 2010). Nuclear receptors (NRs) act as ligand-inducible transcription factors and are classified into two categories (www.nursa.org). Type I NRs includes estrogen, glucocorticoid, progesterone, mineralocorticoid, and androgen receptors, which undergo nuclear translocation upon ligand activation and bind as homodimers to DNA. Type II NRs are located in the nucleus binding to DNA as heterodimers with the retinoid X receptor (RXR). PPARs, thyroid hormone receptor, liver X receptors and Vitamin D receptors fall into this category (Sladek, 2011). The complex between PPARs and RXR binds to PPAR responsive element (PPRE) and determines the expression of genes acting on diverse biological processes, such as lipid metabolism, insulin sensitivity, cell growth and differentiation and immune response. They are also the targets of drugs that are effective in the treatment of metabolic syndrome including insulin resistance, glucose intolerance, obesity, dyslipidemia, hypertension, atherosclerosis and renal dysfunction (Chen *et al.*, 2014). So far, three isoforms of PPARs have been recognized, including PPARα PPARδ (also

known as PPARβ), and PPARγ (PPARγ$_1$ and PPARγ$_2$), considered as attractive targets to treat type 2 diabetes (T2D). Despite their structural similarity and display strong homology in amino acid sequence, the three isoforms are differentially distibuted among tissues. Generally, PPARα is profuse in the brown adipose tissue, heart, liver and kidney; PPARγ is highly expressed in the adipose tissue and other tissues and PPARδ is expressed everywhere. PPAR ligands differ from endogenous fatty acids such as leukotriene B4, 8-S-hydroxy eicosatetraenoic acid and prostaglandin J2, to pharmaceutical drugs such as fibrates and thiazolidinediones (TZDs), in particular, insulin sensitizers TZDs are selective agonists of PPARγ (Willson *et al.*, 2000). In addition to the beneficial effects in diabetes specific PPARγ agonists have also been investigated as a potential therapy against several chronic diseases such as rheumatoid arthritis, liver fibrosis, inflammatory bowel diseases, neurodegenerative and neuroinflammatory disorders and some type of cancers (Lehrke and Lazar, 2005). In this sense although TZDs are potent PPARγ full agonists (PPARγ-fa) their mechanism-based side effects have limited the full therapeutic potential of these compounds (Ciudin *et al.*, 2012). Thus, new studies have developed new classes of molecules able to reduce or eliminate adverse effects, they are defined as selective PPARγ modulators (PPARγ-m). In this sense natural and synthetic cannabinoids are considered PPARγ-m that readily transverse the BBB because of their lipophilicity. Preclinical evidence shows that cannabinoids alleviate neuroinflammatory and neurodegenerative processes through the activation of PPARγ (Fernández-Ruiz *et al.*, 2013). Thus, a number of cannabinoids and endocannabinoids have been reported to be PPARγ agonists. In general, the potency of cannabinoids is several orders of magnitude lower at PPARγ than the reference drugs pioglizatone and rosiglitazone, which act at low nanomolar concentrations. For example, Δ^9-THC stimulates PPARγ at higher concentrations than those needed to activate CB_1 and CB_2 (Granja *et al.*, 2005). In the CNS there is a clear evidence that Δ^9-THC mediates neuroprotective effects by acting on CB_1 and PPARγ. (Carroll *et al.*, 2012). Thus, it is possible that the neuroprotective effects of Δ^9-THC may be mediated not only through CB_1 signalling, but also through activation of PPARγ, thereby exemplifying the polypharmacological profile of the major phytocannabinoids. CBD targets PPARγ (Pertwee *et al.*, 2010) with an EC_{50} ranging from 5 to 20 μM (O'Sullivan

and Kendall, 2010; Granja *et al.*, 2012), but there is a mounting evidence that many biological activities of CBD are mediated through PPARγ. CBD was found to stimulate hippocampal neurogenesis through a PPARγ-dependent pathway. CBD and Δ^9-THC also exert adipogenesis and vasorelaxant effect, in part inhibited by a PPARγ antagonist. More recently, it has been shown that CBD increases the expression of COX-2 and PPARγ at the protein level in lung cancer cells.(Ramer *et al.*, 2013). CBG outperforms Δ^9-THC and CBD in the binding to PPARγ, showing an EC_{50} of 12,7 μM (Granja *et al.*, 2012). Several reports have suggested that PPARγ is a potential target for the development of novel anti-HD drugs. In this sense, CBG was showed to be neuroprotective in mice intoxicated with 3-nitropropionate, improving motor deficits and preserving striatal neurons. (Valdeolivas *et al.*, 2014). Another class of cannabinoids that exhibited interesting activity related to PPARγ, are cannabinoid quinones. The oxidation of CBD and CBG to HU-311 and VCE-003 (the quinoid form of CBD and CBG, respectively) demostrated greatly enhances of its binding activity to PPARγ (Granja *et al.*, 2012). More recently, a class of CBD quinones, chromenopyrazolediones, inspired on HU-345 (cannabinol quinone) have also been described and shown to exert antitumor activity on prostate cancer cells and on tumor xenografts prossibly due to a mechanism involving ROS generation and PPARγ activation (Morales *et al.*, 2013).

3.2 Phytochemical investigation of *Cannabis sativa*

Dried female flowerheads of *Cannabis sativa* were extracted with acetone at room temp. Solvent evaporation yielded a gummy residue that was partitioned between 1:1 aqueous methanol and petroleum ether in order to eliminate fatty substances. The polar phase was then concentrated and extracted with CH_2Cl_2 and the dried organic phase (over anhydrous Na_2SO_4) was then purified by column chromatography on RP-18 silica gel affording pure cannabidiol (**3a**), cannabigerol (**1a**) and cannabichromene (**2a**).

A less polar fraction was separated by semi-preparative HPLC-UV affording the new phytocannabinoid, named dicannabidiol (DCBD, **8**, 2.3 mg).

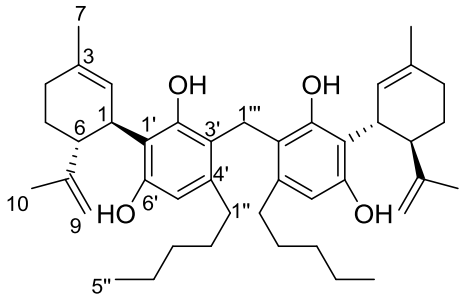

Figure 3.10. Structure of dicannabinol (**8**)

Dicannabidiol (**8**) was isolated as an optically active colorless oil with the molecular formula $C_{43}H_{60}O_4$, determined on the basis of HR-ESIMS. ^{1}H NMR spectrum of **8** (Table 3.1) closely resembled the parallel data for cannabidiol in the same solvent, with a couple of significant exceptions: a) the presence of a single aromatic proton signal, resonating slightly downfield shifted (δ_H 6.13, s); b) the presence of an additional proton signal resonating at δ_H 3.85, brs. The COSY spectrum confirmed the presence of cannabidiol-type spin systems and allowed the assignment of the corresponding signals. Furthermore, the HSQC spectrum was instrumental to assign the resonances of protonated carbons, which also resembled those of CBD (Table 3.1). Interestingly, the additional signal at δ_H 3.85 was associated to a carbon atom resonating at δ_C 30.1, indicating its likely non-oxygenated nature. All the MS and NMR data pointed to a dimeric CBD structure for dicannabidiol (**8**), with a methylene bridge to connecting the two CBD units.

Table 3.1. ^{1}H and ^{13}C NMR data of dicannabidiol (**8**) in CD_3OD.

Pos.	δ_C, type	δ_H, mult., *J* in Hz
1	35.9, CH	3.97, m
2	124.9, CH	5.43, brs
3	134.8, C	-
4a	29.9, CH_2	2.22, m
4b		2.05, m
5a,b	30.5, CH_2	1.73, overlapped
6	46.2, CH	2.66, m
7	22.0, CH	1.74, brs
8	149.1, C	-
9a	109.9, CH	4.39, brs
9b		4.41, brs
10	22.0, CH_3	1.62, s
1’	117.0, C	-
2’	157.3, C	-
3’	114.2, C	-
4’	141.3, C	-
5’	107.9, C	6.13, s
6’	153.8, C	-
1’’	33.1, CH_2	2.42, m
2’’	30.4, CH_2	1.58, overlapped
3’’	33.5, CH_2	1.30, overlapped
4’’	25.7, CH_2	1.28, overlapped
5’’	14.2, CH_3	0.88, t, 7.1
1’’’	30.1, CH_2	3.85, brs

Both HMBC and ROESY spectra (Figure 3.11) supported this hypothesis, indicating the dimerization positions and contributed to the assignment of the remaining ^{13}C NMR resonances.

Particularly diagnostic were the HMBC correlations from H-1''' to C-2', C-3' and C-4' and the ROESY correlation of H-1''' with H-1'', unambiguously supporting the attachment of a methylene bridge at C-3' connecting two cannabidiol units.

Due to a symmetric nature of the molecule, the NMR data of only one unit are presented and have been discussed. The relative configurations of the cannabidiol stereogenic centers was also supported by the ROESY spectrum.

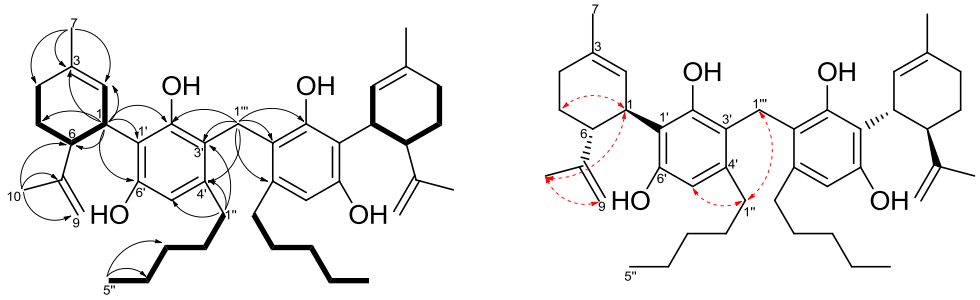

Figure 3.11. Key COSY (bold lines), HMBC (black arrows) and ROESY (red arrows) correlations for **8.**

Dicannabidiol (**8**) is a dimeric cannabidiol belonging to a quite small class of phytocannabinoids which also includes cannabisol (**8a**), reported by Zulfiqar *et al.* in 2012 from a high-potency THC-rich *C. sativa* strain. Since we analyzed a CBD-rich strain, it is logical to presume that the two compounds are formed by the same mechanism.

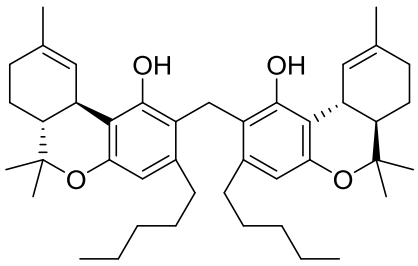

8a

Figure 3.12. Structure of cannabisol.

Following the Zulfiqar's hypothesis for cannabisol, dicannabidiol could derive from a Claisen-type reaction between two cannabidiolic acid units, followed by reduction of the resulting ketone. Alternatively, these compounds could derive from a dicumarol-type pathway, possibly involved an external fungal interaction as a source of formaldehyde. Further experiments would be needed to obtain information on the biogenetic origin of dicannabidiol and of cannabisol.

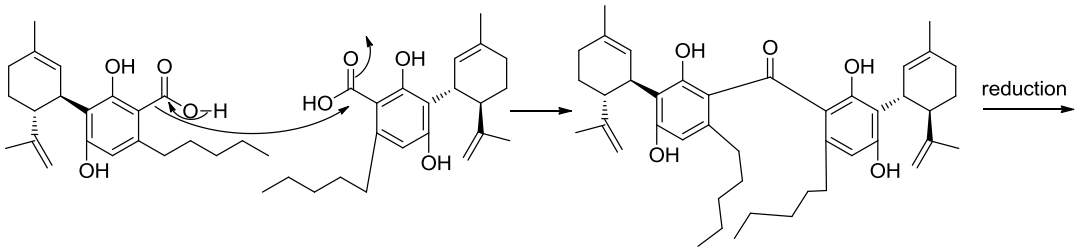

Figure 3.13. Hypothetical origin of dicannabidiol following a Claisen-type reaction.

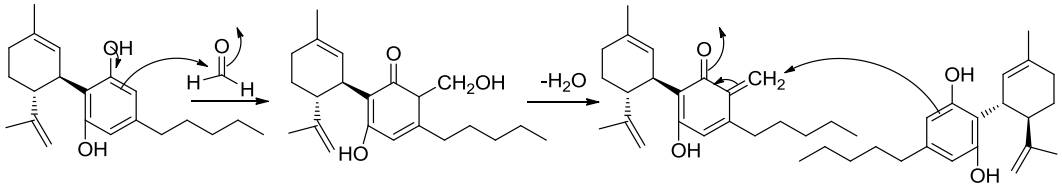

Figure 3.14. Hypothetic biogenetic origin of dicannabidiol from a dicumarol-type pathway.

Given its CBD-dimeric nature, cannabisol was evaluated for its modulating activity on TRP channels. Results are reported in Tables 3.2-3.4.

Table 3.2. Activity of CBD (**3a**) and dicannabidiol (**8**) on calcium influx in HEK293 cells transfected with rTRPA1. Allylisothiocyanate (AITC) was used as a control on TRPA1.

	hTRPA1		
	Efficacy (%AITC 100µM)	**Potency EC_{50} µM**	**IC_{50} inh TRPA1 µM (AITC 100µM)**
CBD (3a)	108.9 ± 2.8	0.48 ± 0.03	0.45 ± 0.01
8	96.7 ± 1.4	3.0 ± 0.2	4.95 ± 0.4

Table 3.3. Efficacy and potency of CBD (**3a**) and dicannabidiol (**8**) on hTRPV1 channel and inhibitory (Inh.) effect on rTRPM8 channel.

	hTRPV1			**rTRPM8**
	Efficacy (% ionomycin 4µM)	**Potency EC_{50}**	**IC_{50} inh TRPV1 µM (capsaicin 0.1 µM)**	**IC_{50} inh TRPM8 µM (icilin 0.25µM)**
CBD (3a)	78.4 ± 2.0	4.1 ± 0.3	3.7 ± 0.3	2.8 ± 0.2
8	12.3 ± 0.4	4.55 ± 0.4	> 20	3.9 ± 0.4

Table 3.4. Efficacy and potency of CBD (**3a**) and dicannabidiol (**8**) on rTRPV2 and rTRPV3 channels.

	rTRPV2			rTRPV3		
	Efficacy (% ionomycin 4μM)	**Potency EC_{50} μM**	**IC_{50} inh TRPV2 μM (LPC 3μM)**	**Efficacy (% ionomycin 4 μM)**	**Potency EC_{50} μM**	**IC_{50} inh TRPV3 μM (Thymol 100μM)**
CBD (3a)	67.5 ± 2.2	1.2 ± 0.1	1.1 ± 0.1	53.6 ± 1.3	0.51 ± 0.06	0.75 ± 0.01
8	< 10	NA	> 20	66.5 ± 0.8	4.6 ± 0.2	11.8 ± 0.4

Cannabisol (**8**) is completely inactive on TRPV1 and TRPV2, while it activates TRPA1 and inhibits TRPM8 with a similar potency to that of CBD. This implies that its dimeric structure confers to dicannabidiol a higher selectivity for modulation of TRPA1 and TRPM8.

3.3 Semi-synthetic modifications of phytocannabinoids

The second part of my research activity on phytocannabinoids was addressed to expand their chemical and biological space through semi-synthetic modifications. It can be considered that the huge inventory of *Cannabis sativa* secondary metabolites is the result of the intrinsic reactivity of some of the major phytocannabinoids, namely Δ^9-THC (**4a**), CBD (**3a**), CBG (**1a**) and CBC (**2a**). However, several other "non-natural" reactions can be exploited on the phytocannabinoid scaffold and their effects on bioactivity is certainly worthy of being explored. During my PhD thesis, I have investigated reactivity of cannabinoids in three differet conditions, and the results obtained will be the subject of the following discussion. First, iodination of *non*-psychotropic cannabigerol and cannabichromene has been investigated; in addition the use of hypervalent iodine on cannabidiol has been selected as an efficient way to produce cannabinoquinoids, and finally pyrolysis of cannabichromene has been explored.

The use of iodine as an inexpensive, non-toxic, readily available catalyst for various organic transformations has recently been well reviewed. Iodine reagents could possess an oxidation state of -I or +I, becoming sources of nucleophilic or electrophilic iodine, respectively. In addition, in organic chemistry also polyvalent iodine compounds are currently receiving an upswing in a wide

range of application areas. They constitute a separate class of iodine-containing reagents, where the iodine oxidation state ranges from +III to +VII, thus rendering it highly electrophilic. Howewer, the use of iodine reagents is proved to play a key role in the development of modern synthetic methodologies, including iodocyclization, electrophilic or nucleophilic iodination of organic compounds, transformation of molecules containing oxygen functional groups and some aromatization processes (Parvatkar *et al.*, 2012).

In particular, Domingo *et al.* reported an iodine-promoted method of aromatizing a number of different terpenoids (Domingo *et al.*, 2016), including some *p*-menthene alchool or *p*-menthandienes, such as terpen-4-ol, the main component of the essential oil extracted from *Melaleuca alternifolia* (tea tree oil) (Hart *et al.*, 2000) or limonene, a natural product that accumulates in the citrus peel, respectively. The aromatization of limonene, along with other *p*-menthanes, to yield *p*-cymene was achieved by the treatment of iodine in DDQ (2,3-dichloro-5,6-dicyano-1,4-benzoquinone) as solvent.

This aromatization method was recently exploited by our research group (Pollastro *et al.*, 2018, b) to aromatize various *p*-menthane-type phytocannabinoids and their carboxylated precursors, leading to their efficient conversion into cannabinol (CBN, **5a**). In that case, DDQ was found to be superfluous and for this reason, it was replaced by refluxing in toluene. The reaction was showed to be preferable comparing to the previously reported protocols for the synthesis of CBN, in terms of simplicity and substrate range. It includes not only *p*-methandiene phytocannabinoids such as cannabidiol (CBD), but also tricyclic tetrahydrocannabinols such as Δ^9-THC as well as their lower analogues from the viridin series, from which cannabivarin (CBV, **5c**) was obtained, in stead of CBN. Since the purification of CBN and CBV from aged and partially degraded marijuana samples is particularly complicated, the main result of this work was the achievement of an easier availability of CBN and CBV, especially starting from non-narcotic biomasses (source of CBD) and providing the incentive for further investigation in terms of bioactivity.

However, the versatility of iodine as a tool in natural product manipulation substantially extends beyond these described applications and the impressive diversity of the phytocannabinoid constituents of cannabis (cannabinome) (Hanuš *et al.*, 2016) allowed the investigation of the chemical behavior of the other two main components of this plant, cannabigerol and cannabichromene.

They were exposed to iodine and also the biological space around thermo-transient receptor potential (TRP) channels was eventually explored.

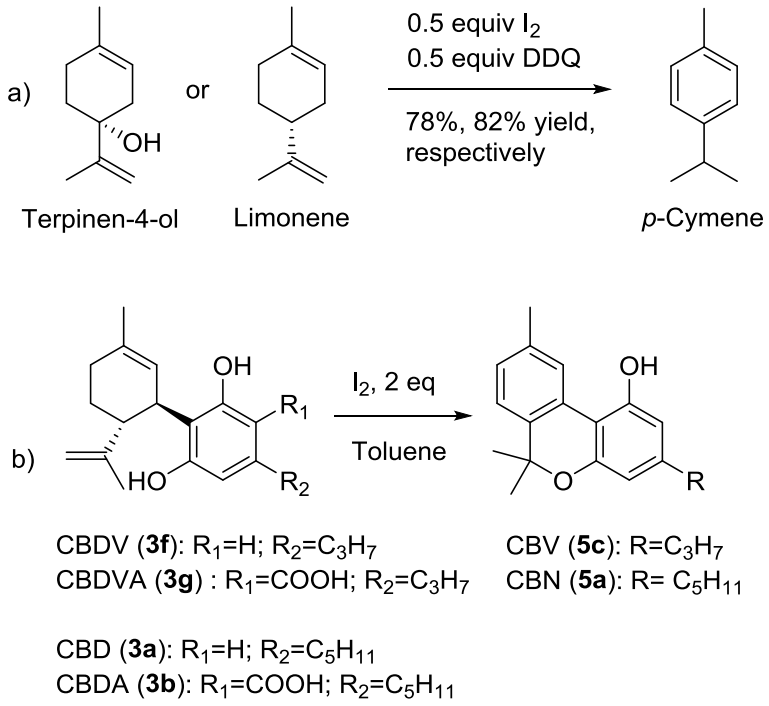

Figure 3.15. a) Aromatization of *p*-menthane terpenoids. b) Aromatization of *p*-menthane-type phytocannabinoids. Abbreviations: CBDV = cannabidivarin; CBDVA = cannabidivarinic acid; CBD = cannabidiol; CBDA = cannabidiolic acid; CBV = cannabivarin; CBN = cannabinol.

3.3.1 Iodine-mediated cyclization of cannabigerol (CBG)

Among the isolated phytocannabinoids from hemp, cannabigerol (**1a**) possesses a different terpenyl moiety. Indeed, cannabigerol (**1a**) could not be classified as a *p*-menthandiene type phytocannabinoids, like CBD (**3a**) or as a tricyclic analogue, similar to Δ^9-THC. However, the terpenyl portion of cannabigerol (as well as cannabigerolic acid) corresponds to polyenes that play a key role in the biogenesis of isoprenoids, generating their cascade cyclization, systematically investigated and popularized in the organic chemistry community by Johnson at Stanford in the sixties and seventies of the past century (Yoder *et al.*, 2005).

Polyolefins successfully react when the possibility exists to trap cationic intermediates intramolecularly by attack of a nucleophilic heteroatom (namely, the hydroxyl groups on the aromatic ring), as in the case of isoprenylated phenolics like cannabigerolic acid (CBGA, **1b**) and its decarboxylated and

thermally stable analogue cannabigerol (CBG, **1a**). Actually, few data are reported in the literature about the classic electrophilic-triggered polyolefin cascade cyclization in cannabis (Hanuš *et al.*, 2016), except for the easy cyclization of CBG (**1a**) to the diastereoisomeric tetrahydroxanthanes **9a** and **9b** upon refluxing with *p*-toluenesulfonic acid in benzene (Mechoulam and Yagen, 1969; Gaoni and Mechoulam, 1971).

Since, there is growing evidence that iodine, either alone or in combination with oxidants or phosphines, can trigger interesting reactions of polyolefins (Barluenga *et al.*, 2004), similar to the chloronium and bromonium-induced polyene cyclizations described by Snyder and coworkers, during my Ph.D. studies, I have investigated the reactivity of CBG (**1a**) with iodine, applying the same protocol used by Pollastro *et al.*, for the aromatization of *p*-menthane-type phytocannabinoids.

The iodine-reaction on CBG (**1a**) was performed by refluxing a toluene solution of CBG (**1a**) with two equivalents of iodine and the formation of a single, less polar TLC spot was observed. Actually, spectroscopic and HPLC analysis revealed that it corresponded to a mixture of six compounds (**9a**, **9b**, **10**, **11a**, **11b**, **12**), which were then purified. The purification processes were accomplished by the utilization of HPLC on complementary phases (silica gel and RP18 columns), and all mixture constituents were obtained in their pure form.

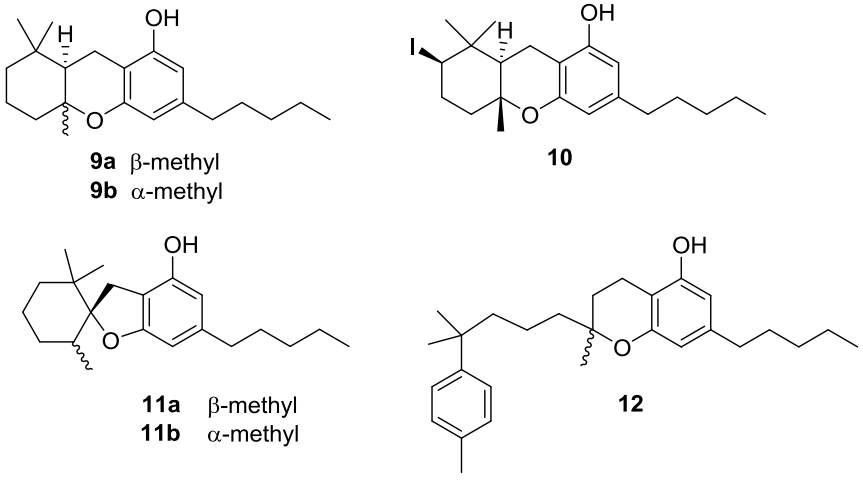

Figure 3.16. Stuctures of products obtained by the reaction of CBG with I_2

Among the purified products, iodocyclocannabigerol A (**10**) (Fig. 3.16) was the major constituent of the reaction mixture, accounting for ca. 60% of it, and

was isolated in high diastereomeric purity. Conversely, compounds **9** and **11** (Fig. 3.16) were almost equimolecular mixtures of two diastereomers. Indeed, since CBG (**1a**) is achiral, all these compounds were obtained as racemate form. Compounds **9a** and **9b** had already been reported from the reaction of CBG by refluxing *p*-toluenesulfonic acid, but they had not yet been spectroscopically fully characterized, hence in the experimental section their NMR assignments are reported. All the other compounds were previously unreported, until this study.

The HR-ESIMS spectrum analysis revealed the molecular formula $C_{21}H_{32}IO_2$ for iodocyclocannabigerol A (**10**). It included one iodine atom and, just like CBG (**1a**), six unsaturation degrees, but the two double bonds of the terpenyl moiety in **1a** are replaced by a bicyclic system in **10**. The inspection of the ^{1}H NMR spectrum of **10** showed the typical phytocannabinoids resonances of pentenyl resorcinol moiety, in addition to a series of signals resonating between δ_H 1.08 (s) and 4.24 (dd, *J*=12.8, 3.8 Hz). Extensive analysis of the 2D NMR spectra allowed a complete elucidation of the structure of **10**.

Analysis of the COSY correlations revealed that the proton signals whose chemical shifts are between δ_H 1.08 and 4.24 belong to two spin systems (H_2-1′/H-2′ and H_2-4′ to H-6′). While the HSQC spectrum allowed not only the identification of the protons directly connected to the carbons but also the identification of the methine proton (δ_H 4.24) on the iodine-bearing carbon (δ_C 39.2). Finally, the whole structure of **10** was deduced on the basis of the HMBC cross-peaks. Indeed the correlations exhibited from H_3-8′ (δ_H 1.08) and H_3-9′ (δ_H 1.16) to C-2′ (δ_C 51.4), C-7’ (δ_C 46.4) and C-6′ (δ_C 39.2) and from H_3-10′ (δ_H 1.24) to C-2′ (δ_C 51.4), C-3′ (δ_C 75.8) and C-4′ (δ_C 42.4) confirmed the presence of tricyclic planar arrangement of **10** (figure 3.17).

The relative configuration was easily assessed based on the $J_{H\text{-}H}$ values and the spatial proximities in the ROESY spectrum. In particular, the *cis* diaxial orientation of H-2′ (δ_H 1.86, dd, *J*=11.5, 3.6 Hz) and H-6′ (δ_H 4.24, dd, *J*=12.8, 3.8 Hz) was evidenced by their large vicinal coupling constants (J > 10 Hz), while the ROESY correlations from Me-10′ to H_2-1′ indicated the *β*-axial orientation of the methyl group.

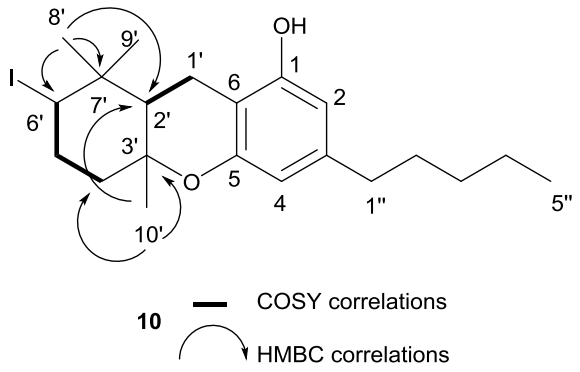

Figure 3.17. Key COSY and HMBC for **10**.

Spirocannabigerols A (**11a**) and B (**11b**) (Fig. 3.18), with $C_{21}H_{33}O_2$ as molecular formula by HR-ESIMS, represented an unprecedented scaffold within both natural and synthetic cannabinoids. They were identified as a pair of non-iodinated diastereomeric derivatives, characterized by the rearranged terpenyl moiety of an oxaspiro[4.5]decane system. Among the recorded spectra, the COSY cross-peaks clearly evidenced, in addition to the resonances of the pentyl moiety, a large spin system (from H_3-10′ to H_2-6′) and an isolated and relatively deshielded diastereotopic methylene (δ_H 2.93 d, J=16.0 Hz; 2.84 d, J=16.0 Hz). The HMBC correlations from these protons to C-3′ (δ_C 37.7), the dimethylated C-7′ (δ_C 38.1) and the markedly deshielded quaternary C-2′ (δ_C 93.3) led to the proposed planar structure (Figure 3.18). The ^{1}H and ^{13}C NMR data of **11b**, assigned based on a full set of 2D NMR spectra, closely resembled those of **11a** and clearly identified its diastereomeric relationship. The relative arrangement of the two adjacent stereogenic centers (C-2′ and C-3′) was deduced by the ROESY correlations from H_3-10′ (**11a**) or H-3’ (**11b**) to H_2-1′.

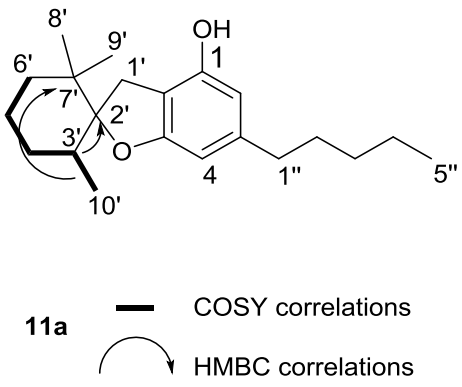

Figure 3.18. Key COSY and HMBC correlations for **11a**.

The molecular formula of **12**, $C_{28}H_{41}O_2$ was determined by HR-ESIMS, clearly included an additional C7 unit, compared to CBG (**1a**). Inspection of the ^{1}H NMR spectrum of **12** revealed the presence of a *p*-disubstituted phenyl unit (δ_H 7.19, d, *J*=8.2 Hz and δ_H 7.08, d, J=8.2 Hz) and of a benzylic methyl (δ_H 2.27, s), suggesting that a toluene unit had reacted with the substrate. The COSY spectrum of **12** assigned all the multiplets of the terpenyl moiety to –CH_2CH_2– and –$CH_2CH_2CH_2$– fragments, while the HSQC spectrum associated all the directly linked H/C resonances. These data along with the HMBC cross-peaks, shown by the methyl singlets, unambiguously defined the structure of the racemic mixture of **12**: H_3-10′ (δ_H 1.10, s) to C-2′ (δ_C 30.7), C-3′ (δ_C 75.8) and C-4′ (δ_C 39.8); H_3-8′ and H_3-9′ (δ_H 1.24, s) to C-6′ (δ_C 45.0), C-7′ (δ_C 37.1), C-1‴ (δ_C 146.3); H_3-7‴ (δ_H 2.27, s) to C-3‴ (δ_C 128.6) and C-4‴ (δ_C 134.6) (Figure 3.19).

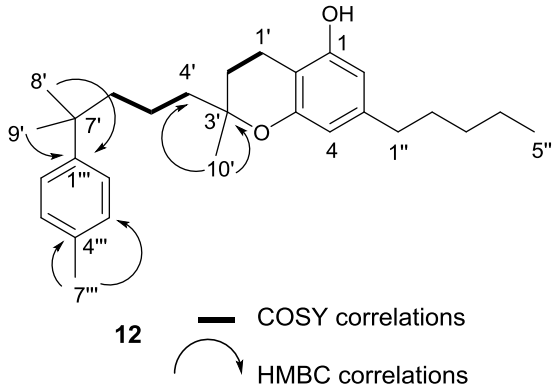

Figure 3.19. Key COSY and HMBC correlations for **12**.

CBG (**1a**) was also subjected to other different conditions of iodine-manipulation of organic compounds. For instance, a larger excess of iodine (3–5 equivalents), as well as the use of iodonium sources like *N*-iodosuccinimide (NIS) was added to the CBG-toluene solution, but an extremely complex reaction mixtures were obtained and therefore, not further analyzed. The use of HI gave exclusively the same products (**9a**,**b**) obtained by Mechoulam with *p*-toluenesulfonic acid (Mechoulam and Yagen, 1969; Gaoni and Mechoulam, 1971). While, under refluxing toluene, the cannabigerolic acid (CBGA, **1b**) gave only the thermal decarboxylation to CBG, which, after the addition of iodine, afforded the same reaction mixture obtained from CBG (**1a**).

Figure 3.20 mechanistically rationalizes the formation of the main reaction products.

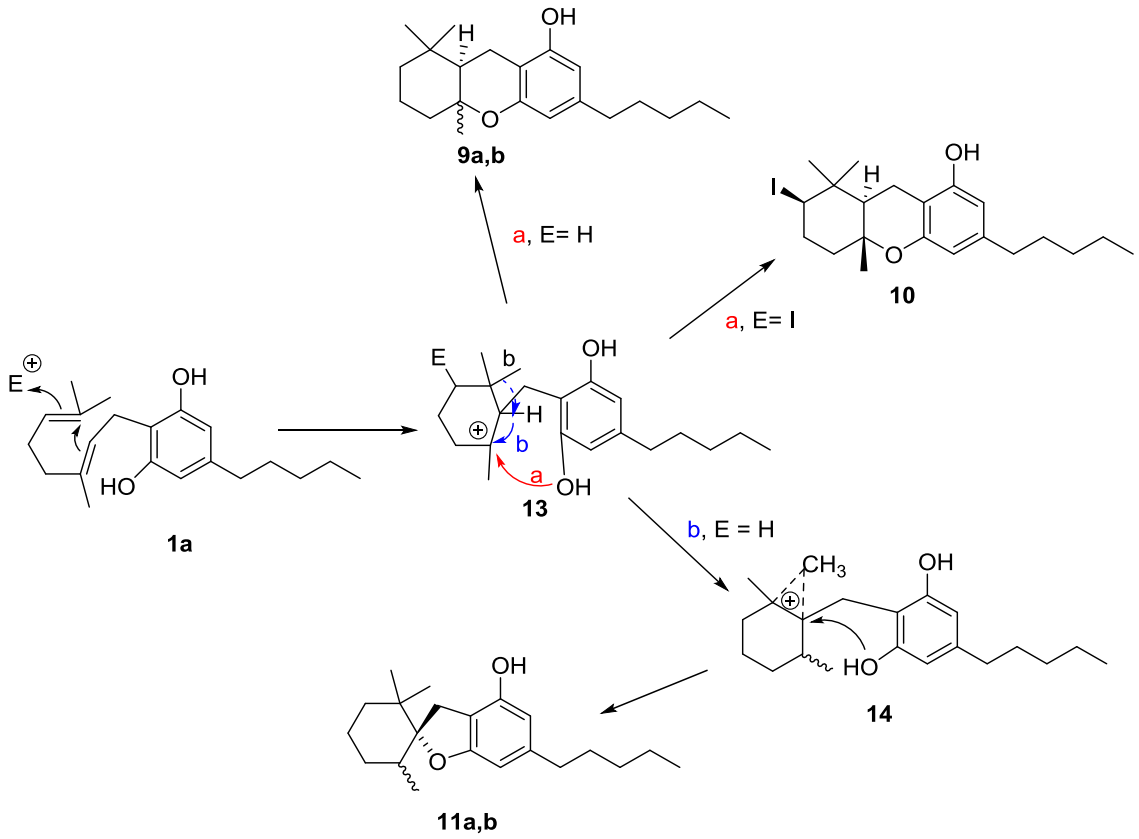

Figure 3.20. Possible mechanisms leading to the formation of **9-12** from CBG (**1a**).

As illustrated, compound **10** results from a pathway similar to that leading to **9a**, **9b**, the only difference being the nature of the electrophilic trigger (iodine vs proton) (Mechoulam and Yagen, 1969; Gaoni and Mechoulam, 1971). Surprisingly, none of the other compounds contained iodine, rather deriving from the action of hydrogen iodide slowly generated in the course of the formation of **10**.

The spirocannabinoids **11a** and **11b** are the results of a process involving protonation of the distal double bond, cyclization and rearrangement, by hydride migration, of the classic tertiary cation to the non-classic, corner-protonated cyclopropyl cation **14** (Dewar *et al.*, 1987). Rather than evolving by proton loss and formation of a cyclopropane ring, the corner-protonated cyclopropyl cation **14** is trapped by the ortho-phenolic hydroxyl group (Figure 3.20). Formation of the strong carbon–oxygen bond presumably drives this unusual rearrangement, not unprecedented, however, in natural meroterpenoids, since a prenylated flavonoid with the same oxaspiro[4,5]decyl moiety of spirocannabigerols (**11a**, **11b**) is known (Huang *et al.*, 2017). The dihydrochromene derivative **12**, which is the result of the involvement of the ω-double bond of the geranyl moiety of

CBG (**1a**) in a Friedel-Crafts alkylation of the solvent toluene prevents its participation in the cascade-type cyclization that leads, via the tertiary cation **13**, to all other reaction products.

3.3.1.1 Biological evaluation of the 'manipulated products': modulation of TRPs

As mentioned in section 3.1.2.1, the TRP proteins constitute a superfamily of non-selective cation channels ubiquitous in the human organism, where they regulate several cell functions (Montell *et al.*, 2002). In this context, CBG (**1a**), a non-psychotropic constituent of *Cannabis*, has a complex biological profile, whose hallmark is TRPM8 antagonist activity (IC_{50} = 0.16 μM, against icilin 0.25 μM) (Cascio *et al.*, 2010; De Petrocellis *et al.*, 2011; Borrelli *et al.*, 2014). The activity on TRPM8 and other thermo-TRPs has been suggested to underlie the analgesic and anti-inflammatory properties and its anticancer potential (Borrelli *et al.*, 2014). Therefore, the evaluation of its cyclic analogues **9**–**12** against a battery of thermo-TRPs was performed (Tables 3.5-3.7), providing some interesting considerations. First of all, the performance of compound **10**, on all investigated endpoints, suggested that the introduction of an iodine atom could cause different effects for the activity, depending on the target; while the effect of the non-iodinated analogues and the difference of activity between the two diastereomers **9a**/**9b** and **11a**/**11b** is remarkable. Comparing with the activity of CBG (**1a**) on TRPM8 (IC_{50} = 0.16 ± 0.02 μM, against against icilin 0.25 μM)**,** all compounds showed a general decrease of affinity for TRPM8 (Table 3.5).

Table 3.5. Efficacy and potency of compounds **9**-**12** on rTRPV2 channel and inhibitory (Inh.) effect on rTRPM8 channel. Desensitizing behavior was evaluated against lysophosphatidylcholine (LPC) for TRPV2.

	rTRPM8		**rTRPV2**	
Comp.	**IC_{50} inh TRPM8 μM (icilin 0.25μM)**	**Efficacy (% ionomycin 4μM)**	**Potency EC_{50} μM**	**IC_{50} inh TRPV2 μM (LPC 3μM)**
9a	> 100	41.3 ± 0.9	8.4 ± 1.3	> 100
9b	17.1 ± 2.2	31.7 ± 0.1	5.8 ± 0.1	> 100
10	7.2 ± 0.6	< 10	NA	2.3 ± 0.3
11a	> 50	37.7 ± 0.1	4.7 ± 0.5	13.7 ± 2.1
11b	> 50	27.5 ± 0.1	6.4 ± 0.1	> 50
12	> 100	< 10	NA	4.5 ± 0.4

On the contrary, they exhibited high activity on TRPA1 (Table 3.6), which is not a major target of CBG. In this case, the two diastereomers **11a** and **11b** displayed different effects, with EC_{50}= 0.49 ± 0.02 μM and 1.3 ± 0.1 μM, respectively. In addition, their potency was comparable to that of mustard oil (AITC, allylisothiocyanate), and all the compounds could efficiently desensitize TRPA1 from activation by AITC (Table 3.6). This profile of activity is interesting, since these CBG cyclized derivatives add to our limited inventory of non-covalent activators of TRPA1 (Del Prete *et al.*, 2015).

Table 3.6. Activity of **9**-**12** on calcium influx in HEK293 cells transfected with rTRPA1 and hTRPV1. Allylisothiocyanate (AITC) was used as a control on TRPA1. Further details, are showed in the experimental section.

	rTRPA1			hTRPV1		
Cp.	**Efficacy (% AITC 100μM)**	**Potency EC_{50} μM**	**IC_{50} inh TRPA1 μM (AITC 100μM)**	**Efficacy (% ionomycin 4μM)**	**Potency EC_{50} μM**	**IC_{50} inh TRPV1 μM (capsaicin 0.1μM)**
9a	95.2 ± 1.1	0.23 ± 0.02	0.26 ± 0.01	< 10	NA	> 100
9b	98.5 ± 0.7	0.29 ± 0.01	0.27 ± 0.01	48.5 ± 2.4	2.6 ± 0.8	5.9 ± 0.7
10	90.0 ± 2.0	2.0 ± 0.3	4.8 ± 0.6	< 10	NA	> 100
11a	108.1 ± 1.3	0.49 ± 0.02	0.45 ± 0.02	43.9 ± 0.1	1.8 ± 0.1	7.1 ± 0.5
11b	101.6 ± 3.3	1.3 ± 0.1	1.7 ± 0.1	32.3 ± 0.4	4.9 ± 0.3	37.0 ± 2.7
12	120.3 ± 2.2	0.35 ± 0.05	0.32 ± 0.02	< 10	NA	> 50

A significant difference of activity was observed for the interaction with TRPV1 (Table 3.6), with **9b** and **9a** being more efficacious and potent than their diastereomers (**9a** and **11b**, respectively). In addition, **10** was inactive, indicating that the introduction of the bulky iodine atom at C-6′ has a negative impact on the interaction with both TRPA1 and TRPV1 channels. Conversely, the same structural change is able to confer a potent inhibitory activity of the activation of TRPM8 by icilin (0.25 μM). Compound **10** was the only member of the series able to modulate this channel (Table 3.5).The overall activity of **9**–**12** on TRPV2, TRPV3 and TRPV4 was almost negligible (Tables 3.5 and 3.7), with the exception of the moderate activity of **9a**/**9b** and **11a**/**11b** on TRPV2 (Table 3.5), a clinically validated cardiovascular target.

Table 3.7. Efficacy and potency of **9**-**12** on TRPV3 and TRPV4 channels.

	rTRPV3			rTRPV4		
Comp	**Efficacy (% ionomycin 4μM)**	**Potency EC_{50} μM**	**IC_{50} inh TRPV3 μM (Thymol 100μM)**	**Efficacy (% ionomycin 4μM)**	**Potency EC_{50} μM**	**IC_{50} inh TRPV4 μM (GSK1016790 A 10 nM)**
9a	< 10	NA	> 50	< 10	NA	> 100
9b	17.5 ± 0.2	6.7 ± 0.1	8.0 ± 1.3	< 10	NA	3.9 ± 0.4
10	< 10	NA	> 50	< 10	NA	> 100
11a	< 10	NA	12.8 ± 1.4	13.9 ± 0.1	3.3 ± 0.2	4.3 ± 0.2
11b	< 10	NA	> 50	< 10	NA	39.7 ± 2.1
12	< 10	NA	> 50	18.0 ± 0.4	18.0 ± 2.6	> 100

In summary, unlike the parent compound, the cyclized analogues of CBG mainly target TRPA1, showing also, with variable selectivity, activity on TRPV1 and TRPM8. Among these compounds, potency depends on the configuration of the stereogenic centers, and the presence of a bulky iodine substituent is detrimental for activity.

The iodine-induced cyclization of CBG (**1a**) exemplifies how a simple chemical operation (refluxing in toluene with iodine) can generate remarkable novel chemical diversity within a bioactive scaffold, modulating its biological profile and exploring its chemical areas.

3.3.2 Thermal and Iodine-mediated rearrangement of cannabichromene

Cannabichromene (CBC, **2a**) is a *non*-narcotic constituent of hemp, mainly accumulated in leaves. It was first isolated from *Cannabis sativa* L. in 1966, while its corresponding acid (cannabichromenoic acid, CBCA, **2b**) was isolated two years later from the same plant source. These compounds are the first members of a group of 5-hydroxy-7- alkyl(aralkyl)benzo[*2H*]pyrans spread in Nature, including not only from plants but also from fungi.

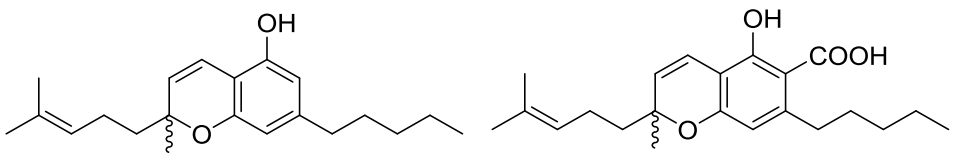

CBC: cannabichromene (2a) **CBCA: cannabichromenoic acid (2b)**

Figure 3.21. Structures of cannabichromene (**2a**), and cannabicromenoic acid (**2b**).

It is traditionally considered, along with Δ^9-THC, cannabidiol (CBD) and cannabigerol (CBG), a major phytocannabinoid, although its content is much lower than that of other "major" phytocannabinoids (0.2-0.3% on dry weight basis). Besides, chromatographic studies on chiral stationary phases demonstrated that cannabichromene, unlike the other major phytocannabinoids, is scalemic (Pollastro *et al.*, 2018, a).

Our interest in cannabichromene, in the framework of the exploration of phytocannabinoid chemical space, came out from a hypothesized connection between this compound and Δ^9-THC. Briefly, the investigation of medicinal marijuana, that is, the inhaling of vapors of crude Cannabis products (flowerheads, cannabis oil, hashish), is still receiving considerable attention, especially regarding the conversion of phytocannabinoids that occurs when crude Cannabis products are vaporized (Hazekamp *et al.*, 2006). Indeed, heating, which causes the decarboxylation of acidic cannabinoids to their neutral forms (Wang *et al.*, 2016), could drastically modify the profile of Cannabis products. More complex reactions generate new phytocannabinoids and/or interconvert existing ones, because of their propensity to undergo complex rearrangements (Hanuš,*et al.*, 2016).
In this context, a research proposed a mechanism for thermal isomerization of the dihydrochromenone model **15** to the corresponding THC analogue **16**, through *in silico* and experimental results (Figure 3.22).

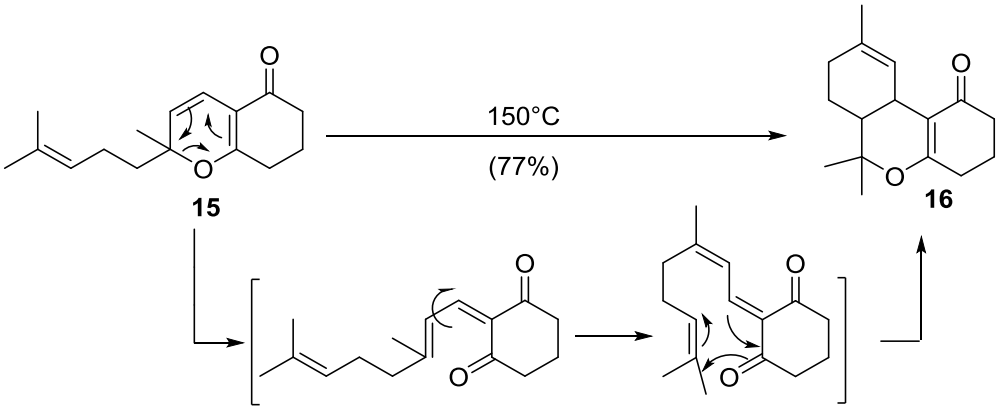

Figure 3.22. Thermal rearrangement of the cannabichromene (CBC) model **15** to afford a mixture of *cis/trans* Δ^9-THC analogues (**16**).

Based on a mechanism of electroreversion to a quinonemethide and intramolecular cycloaddition to the terminal isoprenyl double bond, consecutive calculations postulated that cannabichromene, could determine the formation of

narcotic tetrahydrocannabinols with a hypotetical yield of 77% (Figure 3.22). This claim, if proven, would have the important consequence that also leaves of fiber hemp could be considered potentially narcotic (Garcia *et al.*, 2009). Since the regulatory considerations associated with the generation of THC, a compound listed on the Schedule I in the USA, didn't allow the experimental application of the reaction CBC, the French group used only the *non*-aromatic model (Garcia *et al.*, 2009). Surprisingly, this study had no follow-up, and the possibility that THC could be generated from CBC under pyrolytic conditions was not further investigated.

Several considerations motivated the analysis of the thermal degradation of CBC under the same conditions of the conversion of **15** to **16**. First, the use of *non*-aromatic CBC results in the omission of the importance associated with the aromaticity loss, for the electrocyclic opening that provokes the deconstructive annulation. Besides, it appeared surprising that modern studies on the chemistry of cannabichromene have escaped this reaction, especially if the yield was so high (77%) as claimed for **15** (Garcia *et al.*, 2009).

In an attempt to clarify this issue, CBC underwent the conditions used for the model compound **15**, with silica gel (Figure 3.23) (Garcia *et al.*, 2009). This treatment led to the formation of three compounds (Figure 3.23), and the potential formation of any THC isomer was monitored by ^{1}H NMR spectrum (700 MHz).

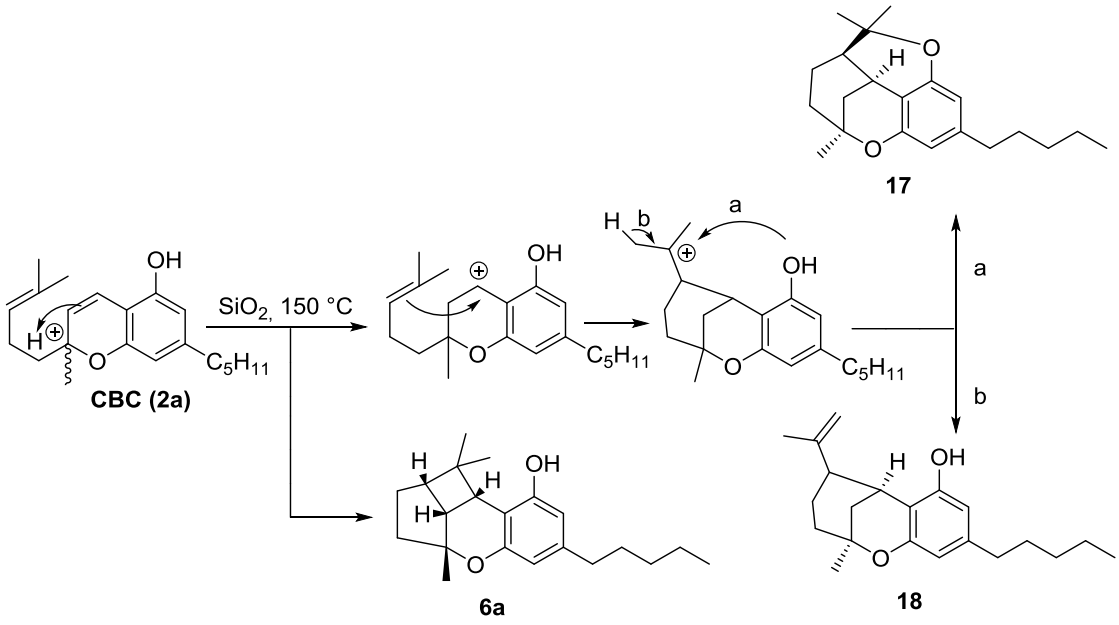

Figure 3.23. Pyrolysis of cannabichromene (150 °C, microwave 300 W, 210 min) in the presence of silica gel.

In figure 3.23 we postulate the formation of the main products of cannabichromene pyrolisis. Cannabicitran (citrylidene-cannabis, bicyclo-CBC, **17**) (Crombie *et al.*, 1979) and Δ^8-iso-*cis*-THC (cyclo-CBC, **18**) (Yagen and Mechoulam, 1969) could derive from the protonation of the chromene double bond and formation of a benzyl cation, which was further trapped by the terminal isoprenyl double bond, concluding with the proton loss in the case of Δ^8-iso-*cis*-THC (**18**) or intramolecular oxygen trapping for cannabicitran (**17**). The third product cannabicyclol (CBL, **6a**) is a well-known product of intramolecular [2 + 2] photocycloaddition of CBC (**2a**, 45% yield) (Crombie et al, 1968) and CBC (**2a**) treatment with $FeCl_3$ (65% yield) (Li and Lee, 2014). The acid mediated formation of CBL from CBC has been considered a Gassman-type cationic [2π + 2π] cyclization (Gassman and Lottes, 1992), but the *anti*-Markovnikov regiochemistry is in contrast with the carbocation stability that guides this type of cycloaddition (Gassman and Lottes, 1992; Roberts *et al.*, 1967). Therefore, a different mechanism was proposed during this study for the thermal degradation of CBC (**2a**) to CBL (**6a**), and illustrated in Figure 3.24. The reaction might implicate the formation of a cyclopropane intermediate (**19**) after a concerted process caused by electrophilic (acidic) activation of the carbonyl tautomer of the resorcinyl moiety, and terminated by electrophilic Markovnikov addition to the electron-rich homoisoprenyl terminal double bond (Figure 3.24). This process, similar to the santonine−desmotroposantonine rearrangement (Andreocci, 1893), generates a tertiary cation and successively the opening of the cyclopropane ring produces an oxonium ion. Eventually, the restoring of aromaticity by decomplexation and tautomerization concludes the reaction.

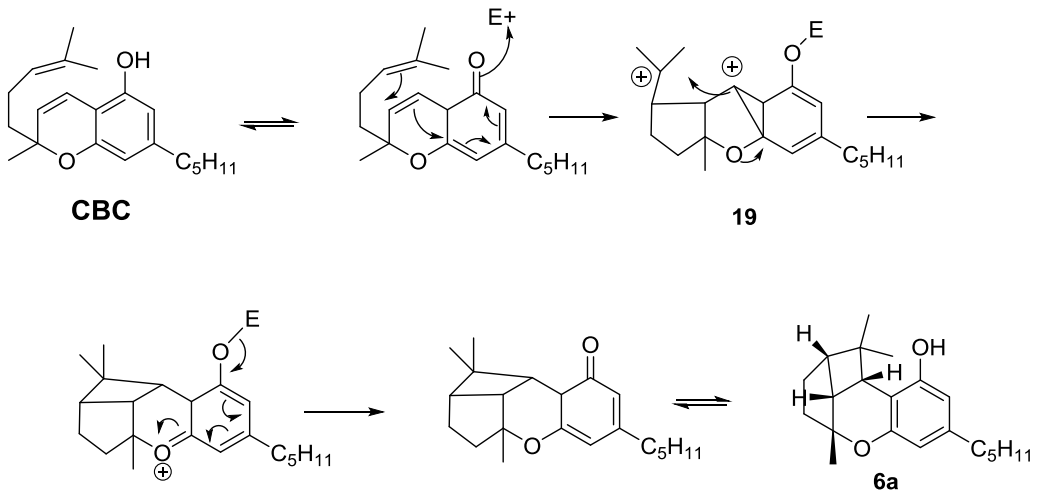

Figure 3.24. Possible rationalization for the formation of cannabicyclol (CBL, **6a**) from the acidic thermolysis of cannabichromene (CBC, **2a**) (E^+ = H^+ or a Lewis acid, R = n-C_5H_{11}). The reaction is a mechanistic pericyclic "false friend", just like the Staudinger β-lactam synthesis.

After these considerations, we can conclude that the thermal degradation of the model compound **15** significantly differ from that of CBC, where a series of cationic processes replaces the electrocyclic opening of the chromene ring that characterized the former process. Trying to rationalize this different results, we hypothesized that the conversion of CBC to THC in pyrolytic condition failed because of the well-known poor stability of this product. Taking advantage of the iodine-mediated aromatization of THC to CBN (Domingo *et al.*, 2016; Pollastro *et al.*, 2018, b), we proposed that the aromatization of the carbocyclic moiety could guide the reaction toward the electrocyclization, overcoming, or at least balancing, the disadvantageous initial de-aromatization step. Thus, iodine, rather than acids, could accomplish the chemistry postulated for the model compound, but turning CBC into cannabinol (CBN, **5a**), the aromatized version of Δ^9-THC. As supposed, the treatment of CBC under the conditions developed for the aromatization of Δ^9-THC (refluxing in toluene with two equivalents of iodine) (Pollastro *et al.*, 2018, b) led, in a spot-to-spot fashion, to its conversion to CBN in 82% yield.

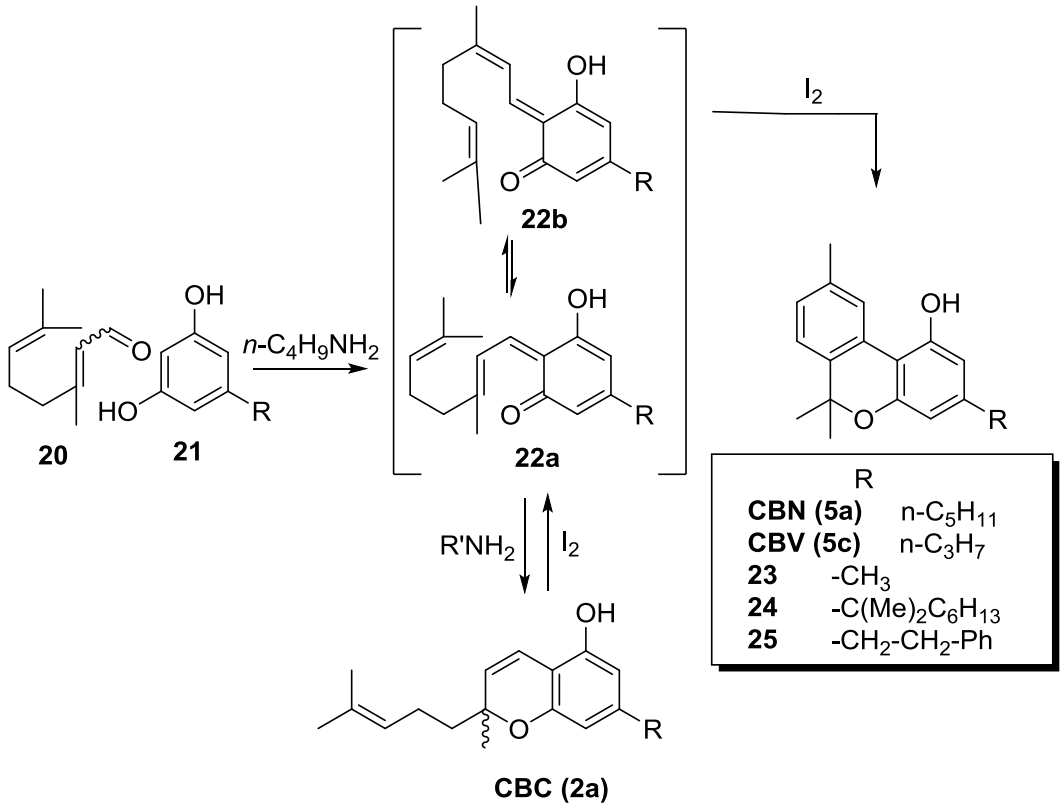

Figure 3.25. Total synthesis of cannabinol (**5a**) and analogues. In the one-pot procedure for cannabinol (**5a**), Dowex 50 WX8 was added after the first step, and after filtration over Celite, iodine was added. CBN was obtained in 55% yield.

With these results, the delicate role of the iodine source to produce the deconstructive annulations seems to be quite clear. The capacity of iodine to generate HI by interaction with hydroxyl groups from the substrate or from traces of protic solvents (Laurence *et al.*, 2011) was discarded as a possible mechanism since treatment of CBC (**2a**) with Brönsted acids affords compounds resulting from the formation of a benzyl cation and not by cycloreversion (Pollastro *et al.*, 2018, b). A soft polarizability/polarization of the I−X bond seems, conversely, critical to avoid electrophilic attack to the electron-rich aromatic ring and the dihydropyran double bond. Therefore, the electroreversion could then be promoted by halogen bonding to the chromene oxygen and/or to its aromatic ring (Breugst and von der Heiden, 2018), while the final aromatization conducts the various equilibria in favour of the generation of dibenzochromenes. It is remarkable that, despite the plethora of reaction pathways available, only the deconstructive annulation was observed, at least within the limit of ^{1}H NMR sensitivity, by analysis of the crude reaction mixture.

At this point, for a further development of this reaction, it was hypothesized to synthesize CBN (**5a**) directly from the the condensation of citral (**20**) and resorcinols (**21**) by a iodine-promoted aromatization, redirecting the reaction from the generation of chromenes (**2a**) to benzochromenes (**5a**, **5c**, **23**, **24**, **25**). In this way, the same quinine methide intermediate **22**, proposed for the deconstructive annulation of chromenes to benzochromenes (Figure 3.25), is formed and iodine has been reported to promote the condensation of cyclic β-dicarbonyls and unsaturated aldehydes to dihydrochromenes (Jung *et al.*, 2009).

Unfortunately, the direct treatment of citral (**20**) and olivetol (**21**, R = n-C_5H_{11}) with iodine only produced a complex mixture, confirming that cyclohexadiones are not good models of resorcinols, and amine catalysis is required for the initial condensation step. At the same time, amines (pK_{BI2} ca. 3.8) (Laurence *et al.*, 2011) exhibit a stronger affinity for iodine than ether oxygen or an aromatic ring (pK_{BI2} ca. 0 in both cases) (Laurence *et al.*, 2011), and complexation with an amine completely neutralizes the σ-hole electrophilicity of iodine (Breugst and von der Heiden, 2018). To overcome this obstacle, the amine (n-butylamine) was used in association with an acidic ion resin (Elsohly *et al.*, 1982), adding the iodine to the filtered solution and continuing refluxing. In this way, after aqueous workup of the reaction, CBN (**5a**) could be achieved in a rewarding 55% yield directly from olivetol and citral (Figure 3.25).

This procedure solves a long-standing problem in cannabinoid chemistry and natural product synthesis, since aryl coupling of a resorcinyl benzoate, the most obvious retrosynthetic strategy to cannabinol, gives the wrong regioisomer (unnatural CBN) (Adams *et al.*, 1940,a). Thus, in his classic studies on cannabinoids, Adams et al. managed to synthesize CBN (**5a**) via aryl coupling of resorcinyl benzoates all possible regioisomers of CBN except the natural one (Adams *et al.*, 1940,b). This regiochemical issue was only recently solved by Hertweck using a different tether and a different aryl coupling strategy (photosplicing of a benzylsulfonamidic precursor) (Kloss *et al.*, 2018). The one-pot synthesis of dibenzochromenes, developed in this study, is general for 5-alkylresorcinols, a relevant and strongly populated class of plant and microbial secondary metabolites (Kozubek *et al.*, 1999), and citral (Figure 3.25). In this way, the structure of cannabinol was rearranged, expeditiously generating natural (**5c**, **23**) and synthetic analogues from the α,α-dimethylheptyl (**24**) and

the phenethyl (**25**) series (Hanuš *et al.*, 2016) useful to explore the biological space associated with its chemotype. However, the deconstructive annulation of homoprenylchromenes also has some limitations. The reaction was investigated with higher homologues of citral (C-10), namely, farnesal (C-15) and geranylgeranial (C-20), but in both cases, complex mixtures were formed. In addition, nonsymmetric resorcinols like 4-hexylresorcinols afford isomeric chromenes in the condensation step, and even when the single isomers were reacted with iodine, the reactions produce mixtures. Conjugating groups, like double bonds or a carbonyl, on the resorcinol moiety are not tolerated, and regrettably, the reaction could not be applied to resorcinol flavonoids and stilbenoids, two very common classes of natural products. Attempts to expand the application of the reaction to heteroaromatic analogues of alkylresorcinols also met with limited success. Thus, the pyranocoumarin ferprenin (**26**) (Appendino *et al.*, 1988) gave the corresponding dibenzochromene (**27**) in a mixture with two "benzylic" cyclization products (**28 a,b**) that became the exclusive reaction products with the pyranopyrone **30** (Figure 3.26).

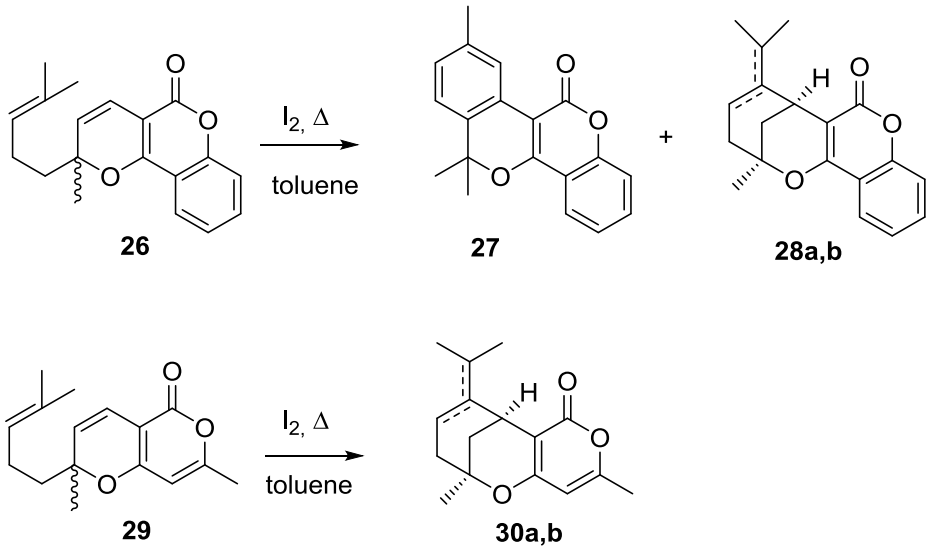

Figure 3.26. Attempts to extend the chromene deconstructive annulations to isosteric cannabichromene analogues.

3.3.3 The oxidation of phytocannabinoids to cannabinoquinoids

As part of a study on the phytocannabinoid chemical space, the effect of their oxidation to cannabinoquinoids was also investigated. In particular, since cannabidiolquinone (CBDQ, HU-313, **31**) is considered as a degradation marker and alleged hepatotoxic metabolite of cannabidiol (CBD, **3a**), a systematic study

on the oxidation of CBD (**3a**) to CBDQ (**31**), under a variety of experimental conditions (base-catalyzed aerobic oxidation, oxidation with metals, oxidation with hypervalent iodine reagents), was developed.

Hemp tissues have long been known to give a purple color when treated with bases (Lkam, 1911). This unique color reaction is at the basis of the Beam test, one of the simplest forensic test to detect marijuana. The chemistry underlying this color reaction was elucidated by Mechoulam, who, in a seminal work published almost fifty years ago (Mechoulam *et al.*, 1968) identified the colored pigment as a mixture of monomeric and dimeric cannabinoid quinols, characterizing the structure of the compounds formed from CBD (Figure 3.27). Paradoxically, Δ^9-THC and CBN, the psychoactive principles of marijuana, do not give this color reaction, which requires the presence of a resorcinyl moiety with free hydroxyls. Therefore, the Beam test actually detects the presence of the *non*-psychotropic cannabinoids, typical of fiber hemp rather than the psychotropic cannabinoids typical of marijuana.

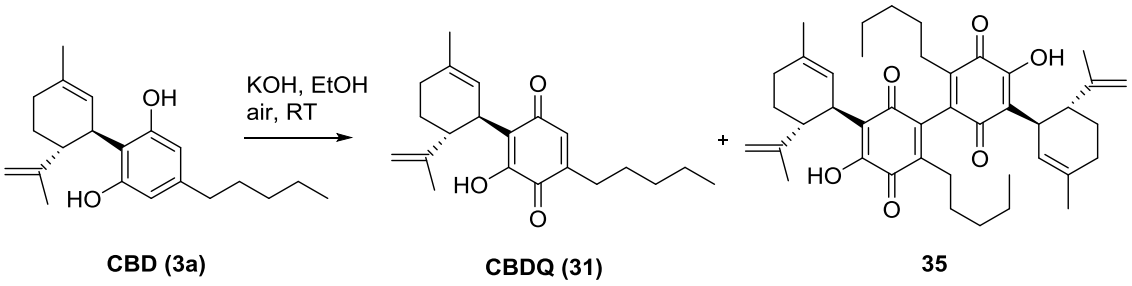

Figure 3.27. Base-catalyzed air oxidation of CBD.

Despite the forensic relevance of cannabinoid quinones, the biological profile of these compounds has long been overlooked because of the difficulty of their purification, their chemical instability, and uncertainties on their structure, long debated between a *p*- or *o*-quinone nature. Interest in cannabinoid quinols was rekindled in the past decade by Mechoulam, who confirmed their *p*-quinone structure by X-ray crystallography, improved their synthesis, and discovered the potent cytotoxic activity of the quinol from CBD, a compound known under the name of HU-331 (Kogan *et al.*, 2004). HU-331 is a selective and potent (nanomolar IC_{50}) inhibitor of DNA topoisomerase II, with antitumor activity (Peters and Kogan, 2007). Interestingly this compound was described previously to be generated during hepatic microsomal metabolism of CBD and capable of generating ROS inducing cell toxicity. (Watanabe *et al.*, 1991; Usami

et al., 2008). While the development of **31** as a drug was abandoned, possibly because of unfavorable stability properties and cellular toxicity (del Río *et al.*, 2016), distinct lines of research stimulated interest for this compound**.** For instance, microsomial formation of **31** from CBD (**3a**) has been associated to P450 covalent inhibition and perturbation of hepatic xenobiotics metabolism (Bornheim and Grillo, 1998), and a similar process could also underlie the liver toxicity reported for high dosages of CBD (Ewing *et al.*, 2019). Furthermore, **31** is formed during long-term storage of CBD (**3a**) under aerobic conditions, and its availability is therefore important for quality control of this API (Active Pharmaceutical Ingredient).

Although there is a confluence of interest for CBDQ (**31**) from various areas of cannabinoid research, the only report of its synthesis is the one inspired by the Beam test. Under these conditions, yields are incostant, scale-dependent, and modest (ca 20% at best), while significant amounts of the dimeric quinone **32** are also formed by oxidative dimerization of CBDQ. Both reaction products, especially **32**, are unstable and rapidly turn into a complex mixture of polar compounds (Mechoulam *et al.*, 1968). Furthermore, in an attempt to reproduce this reaction in laboratory, the oxidation reaction was poorly reproducible, and could not be scaled up over a few hundred milligrams of starting material, even when air or 80% oxygen were bubbled into the biphasic reaction system. A more reproducible behaviour was observed with KH or LiH in THF or toluene under heterogeneous conditions but scale up was still problematic.

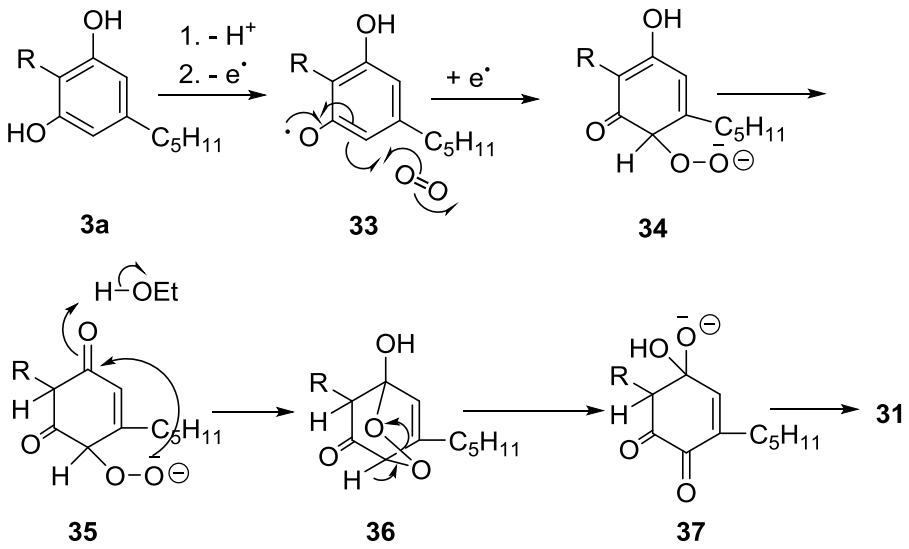

Figure 3.28. Possible mechanism for the aerobic base-mediated formation of cannabiquinone (CBDQ, **31**) from cannabidiol (CBD, **3a**) in ethanolic KOH. (R= 3-*p*-mentha-1,8-dienyl).

The reaction is presumably triggered by a formation of a phenate anion, next oxidized to an electrophilic radical (**33**) that adds to dioxygen to form a peroxyl radical, next reduced to **34** by an additional phenate ion. After tautomerization to **35**, the hydroperoxyl anion is trapped by the *para*-carbonyl group. This generates the bridged keto-peroxyhemiacetal **36**, whose α-deprotonation triggers cleavage of the peroxidic bond, eventually affording the hydroxylated quinone **31** via the hydrate **37** (Figure 3.28). This process is reminiscent of the transformation of vitamin K hydroquinone into its epoxyquinone form (Dowd *et al.*, 1995), and could explain the sensitivity of the reaction to radical traps like BHT as well as the unreactivity of mono-alkylated phytocannabinoids, like Δ^9-tetrahydrocannabinol (Δ^9-THC) and cannabichromene (CBC), where the prototropic equilibrium required for the formation of the peroxyhemiacetal is not possible (cf. the formation of **35** from **34** in figure 3.28).

The reaction profile of the Beam test was basically replicated, without any substantial improvement of yield, by metal oxidants [$FeCl_3$, $K_3[Fe(CN)_6]$, MnO_2, Cr^{6+}-based reagents, CuCl, $CuCl_2$, Ag_2O, $NH_4Ce(NO_3)_5$] under both catalytic and stoichiometric conditions, as well as by peroxides (TBHP, basic H_2O_2), with significant amounts of the dimer **32** being always formed under basic conditions or during the long reaction times required for conversion. A surprising and notable exception was the behaviour of the Takehira complex ($CuCl_2$-hydroxylamine) (Takehira *et al.*, 1989), that afforded a mixture of the

hydroxyimino quinone **38** and the chlororesorcinol **39**. The regioselectivity in the formation of **38** was deduced from the diagnostic ^{3}J HMBC cross-peaks of H-1" with the hydroxyimino carbonyl carbon.

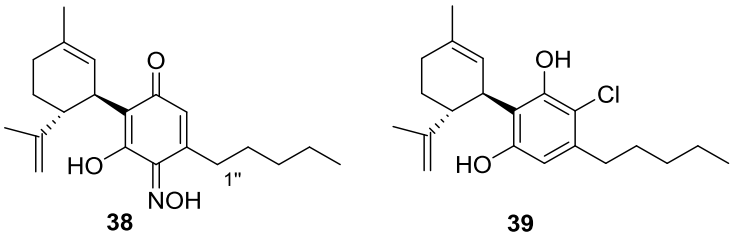

38 **39**

Figure 3.29. Structures of **38** and **39**.

The Takehira complex was originally developed for the oxidation of methylpolyphenolics to their corresponding hydroxyquinones, a reaction of relevance for the industrial synthesis of vitamin E, and was later modified by replacement of hydroxylamine with other nitrogen bases (Takehira *et al.*, 1989). In control experiments, copper (II) chloride alone gave CBDQ (**31**) and the dimer **32** as the only reaction products, while the quinone **31** did not react with hydroxylamine, suggesting a role for hydroxylamine in the chemoselective halogenation reaction, possibly via the generation of an *N*-chlorinated species, and of copper (II) in the activation of the quinone carbonyl toward nucleophilic attack by hydroxylamine.

Hypervalent iodine derivatives have become increasingly popular for a wide range of oxidative reactions (Nicolaou *et al.*, 2002), and bis(trifluoroacetoxy)iodobenzene (BTIB) was reported to be able to oxidize the mono-*O*-alkylated cannabinoid Δ^{9}-THC (**4a**), otherwise unreactive in Beam-type oxidations, to its corresponding hydroxyquinone (Kogan *et al.*, 2004). This λ_3-iodane was also able to oxidize CBD (**3a**) to CBDQ (**31**), but λ_5 iodanes like 2-iodoxybenzoic acid (IBX, **40**) (Frigerio *et al.*, 1999) and the Dess-Martin periodinane (DMP) (Dess and Martin, 1983) gave much better and more reproducible yields, with a stabilized and not explosive version of IBX (SIBX) emerging as the reagent of choice. The superior behavior of SIBX compared to IBX might be related to the acidity of the stabilizing matrix (isophtalic- and benzoic acids), that could help the hydrolytic cleavage of iodic esters formed in the reaction (Ozanne *et al.*, 2003).

The oxidation is presumably initiated by the sigmatropic rearrangement of the iodineoxygen bond in the mixed λ_5 iodane ester **41** formed by interaction of IBX

(**40**) and the C-1′ phenolic hydroxyl (Figure 3.30). The resulting C-2′ λ_3-quinol **42,** after oxidation to the corresponding λ_5-iodane **43**, is turned by [3.3]-sigmatropic rearrangement of the carbon-oxygen bond into the C-4′ λ_5-iodinane **44**, with β-elimination eventually generating the hydroxyquinone **31** and a reduced λ_3-iodinane.

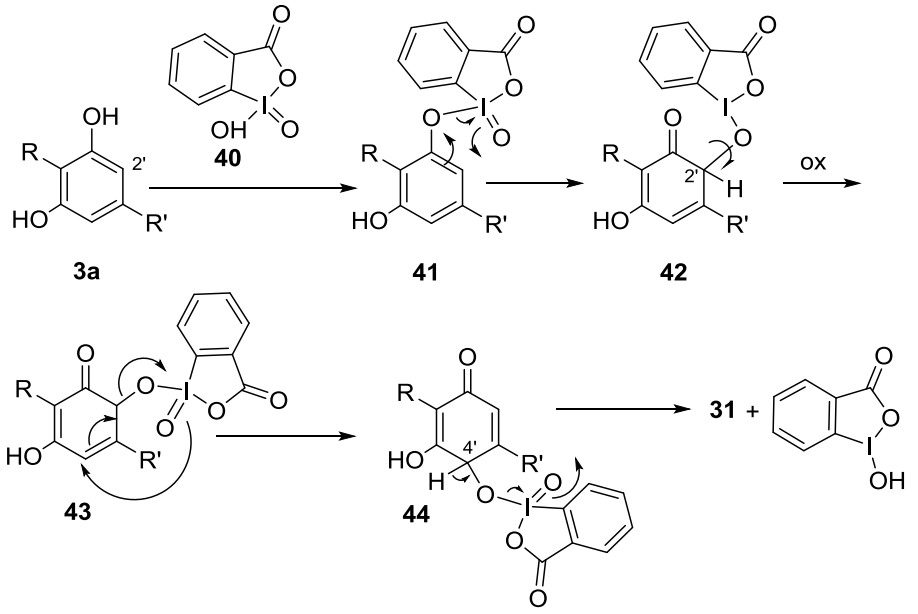

Figure 3.30. Possible mechanism for thr SIBX-mediated formation of cannabiquinone (CBDQ, **31**) from cannabidiol (CBD,**3a** (R= 3-*p*-mentha-1,8-dienyl, R' = *n*-pentyl).

Remarkably, dimerization was completely suppressed under iodinane oxidation, and yields in the range of 50-60% could be obtained under multigram reaction scale. CBDQ (**31**), an orange powder (the product resulting from the Beam-type oxidation was reported by Kogan *et al.*, 2004 as a brown powder. In this work this observation was confirmed, presumably related to the formation of highly colored impurities under the basic conditions of the Beam oxidation that could not be removed by hexane washing or recrystallization), is unstable in solution, rapidly degrading in both protic (methanol) and aprotic (acetone, $CHCl_3$) solvents, with generation of the more polar dimer **32** and next of a host of uncharacterized more polar products. On the other hand, it could be stored for at least ten months as a powder at – 18 °C in a sealed flask, or for additional time as a frozen benzene or DMSO solution at 4 °C (Appendino *et al.*, 2009). The oxidation with SIBX is general for phytocannabinoids, and, apart from cannabigerol (**1a**), it could also be applied to mono-etherified compounds [cannabichromene (CBC, **2a**), cannabinol (**5a**)] that are unreactive under Beam-test conditions, obtaining their corresponding hydroxyquinones **45**-**47.**

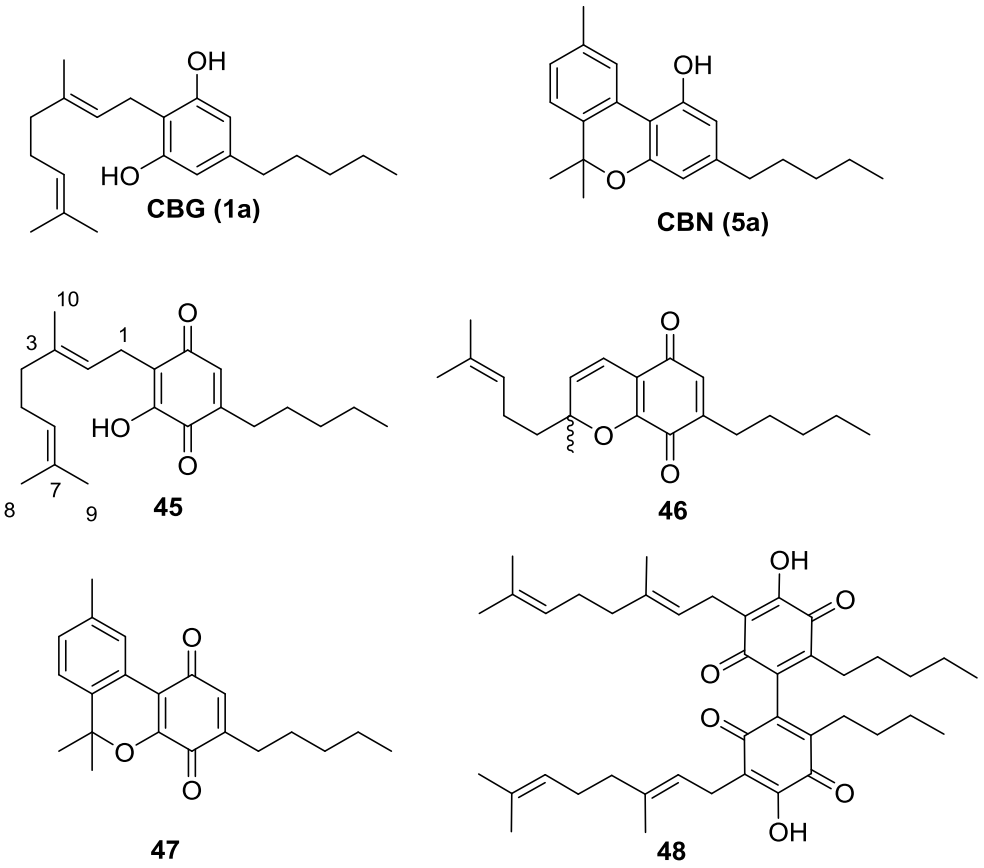

Figure 3.31. The oxidation with SIBX of cannabigerol (**1a**), cannabichromene (CBC, **2a**) and cannabinol (**5a**) led to the formation of **46** and **47**.

CBDQ (**31**) has been reported to be *non*-narcotic (Kogan *et al.*, 2004), and indeed it lacked significant affinity for CB_1 and CB_2 (del Río *et al.*, 2016). Nevertheless, as described in the section 3.1.2.2, it showed powerful modulating activity on PPAR-γ and various degree of PPAR-γ activating activity were also shown by the other cannabinoquinoids (Granja *et al.*, 2012), but dimerization was detrimental for activity, and dimeric quinones were devoid of significant activity in PPARγ-activity assays (compounds were considered inactive if unable to induce 5-fold PPARγ-induction at 50 μM concentration). Dimeric quinones are axially chiral, and, since enantiomeric cannabinoids can show markedly different profiles of bioactivity (Hanuš *et al.*, 2005), one of them, the one from CBG (**48**), was resolved by chiral chromatography on a chiral column packed with amylosetris (5-chloro-2-methylphenylcarbamate). However, both the *aR* and the *aS* enantiomers turned out to be inactive. Similarly, the hydroxyiminoquinone **38** and the chlorinated resorcinol **39** were also devoid of activity.

3.4 Conclusion

The exploration of phytocannabinoid chemistry carried out in this study, led to several interesting results. First, an unprecedented dimeric CBD-type phytocannabinoid was isolated from a fiber hemp chemotype of Cannabis. Its pharmacological evaluation revealed a peculiar profile on TRP channels.

Moreover, semi-synthetic modification on some phytocannabinoids led to expansion of the chemical space related to the cannabinoid chemotype. Addition of iodine agents on the terminal isoprenyl double bond of cannabigerol (CBG, **1b**) as well as the thermally stable decarboxylated version of CBGA (**1a**), essentially caused a cascade cyclization, providing some unprecedented compounds. Biological evaluation of these compounds on six thermo-transient receptor potential channels (TRPs) showed a remodeling of bioactivity compared to CBG (**1b**), with emphasis on TRPA1 rather than TRPM8, the major target of CBG.

Furthermore, this study allowed to elucidate mechanistically the thermal degradation of cannabichromene (CBC, **2a**), dominated by cationic reactions and not by the pericyclic rearrangements as postulated by Garcia *et al.* in 2009. However, if the thermal conditions are flanked by iodine addition, the reaction proceeds to CBN, thus providing an alternative source to obtain this overlooked phytocannabinoid. Even with some limitations, starting from simple and easily available starting material, it is possible to convert homoisoprenylchromenes to benzo[c]chromenes, through an iodine-mediated deconstructive annulations. Besides, the generation of biologically relevant chemical diversity from simple building blocks could encourage the biological evaluation of compounds of limited availability by isolation.

Finally, a reproducible and scalable synthesis of cannabinoquinoids, including CBDQ (**31**), was developed, making significantly easier the access to this compound of relevance not only for its bioactivity profile, but also for the analysis of CBD, the study of its binding to P450 apoproteins, and its effects on liver function.

3.5 Experimental section

3.5.1 Extraction and Isolation of *Cannabis sativa*

The isolation and manipulation of all cannabinoids were carried out in accordance with their legal status (Authorization SP/101 of the Ministero della Salute, Rome, Italy).

Dried female flowerheads of *Cannabis sativa* (750 g) were heated at 120°C for 2.5 h in a ventilated oven, to decarboxylate pre-cannabinoids. After cooling to room temp., the plant material was extracted with acetone at room temp (2 × 10 L). Solvent evaporation yielded a gummy residue that was partitioned between 1:1 aqueous methanol and petroleum ether in order to eliminate fatty acids. The polar phase was then concentrated and extracted with CH_2Cl_2 and the dried organic phase (over anhydrous Na_2SO_4) was then purified by column chromatography on RP-18 silica gel linear gradient, from MeOH/H_2O 55:45 to 90:10) affording pure cannabidiol (**3a**, 210 mg), cannabigerol (**1a,** 61 mg) and cannabichromene (**2a**, 22 mg). A methanolic solution of Fraction 2 (700 mg) was separated by semipreparative HPLC-UV performed on an Agilent instrument, using Phenomenex Luna C18, 10 µm 250 mm × 10 mm column. The mobile phase was a mixture of A (acetonitrile), B (water with 10 ppm (v/v) of formic acid) using the following gradient: starting conditions, A 70% B 30%; 15 min, B 100%; 25 min, B 100%; 30 min, A 70% B 30%; 35 min, A 70% B 30%. The injected volume was 500 µL, and flow rate was 3 mL/min. The UV detection wavelength was set at 275 nm. This separation afforded 9 fractions (A-I). Fraction I was identified as dicannabidiol (**8**, 2.3 mg, Rt 26.6 min).

Dicannabidiol (**8**): colorless oil, $[\alpha]_D$ -44.8 (c 0.23, CH_3OH); ^1H NMR (CD_3OD, 700 MHz) and ^{13}C NMR (CD_3OD, 125 MHz), see Table 3.1; ESIMS *m/z* 639 [M - H]$^-$; HRESIMS *m/z* 639.4501 [M - H]$^-$ (cald for $C_{43}H_{59}O_4$, 639.4492).

3.5.2 Reaction of cannabigerol (CBG, 1a) with iodine

To a solution of CBG (**1a**, 1.0 g, 3.160 mmol, coming from my research group library) in toluene (10 mL) iodine (802 mg, 6.3 mmol, 2M equivalents) was added. The reaction was refluxed for 5 h, and then worked up by cooling to room temp., dilution with hexane, and washing with 5% $Na_2S_2O_3$. The residue was purified by gravity column chromatography on silica gel (10g, petroleum

ether – EtOAc: 95:5) to afford 590 mg of a yellowish oil. A sample of which (180 mg) was fractionated by semi-preparative HPLC on silica gel (petroleum ether-EtOAc: 85:15) to afford three fractions, Fr.1 (72 mg), Fr. 2 (63 mg) and Fr. 3 (50 mg). Fr. 2 contained pure iodocyclocannabigerol A (**10**, 14.8% yield). Fr. 1 was purified by HPLC on Sunfire C18 column (eluent gradient from CH_3CN/H_2O 7:3 to CH_3CN, flow rate 0.8 mL/min) to obtain cyclocannabigerol A (7.1 mg, 2.3% yield, **9a**) and cyclocannabigerol B (25.1 mg, 8.1% yield, **9b**). Fr. 3 was purified by HPLC on Sunfire C18 column (eluent gradient from CH_3CN/H_2O 8:2 to CH_3CN, flow rate 0.8 mL/min) to obtain spirocannabigerol A (2.1 mg, 0.7% yield, **11a**), spirocannabigerol B (4.1 mg, 1.3% yield, **11b**), and compound **12** (12.6 mg, 3.2% yield).

*3.5.2.1 Cyclocannabigerol A (**9a**)*

Colorless amorphous solid. $[\alpha]_D$=0. ^{1}H NMR (CD_3OD, 400 MHz): δ_H 6.15 (1H, s, H-4), 6.04 (1H, s, H-2), 2.68 (1H, dd, *J*=16.7, 4.7 Hz, H-1′a), 2.40 (2H, t, *J*=7.7 Hz, H-1″), 2.25 (1H, dd, *J*=16.7, 13.4 Hz, H-1′b), 1.89 (1H, d, *J*=10.3 Hz, H-4′a), 1.61 (1H, overlapped, H-5′a), 1.55 (4H, overlapped, H-2″, H-3″), 1.51 (1H, overlapped, H-4′b), 1.49 (1H, overlapped, H-2′), 1.42 (2H, H-5′b, H-6′a, overlapped), 1.33 (1H, overlapped, H-6′b), 1.32 (2H, overlapped, H-4″), 1.17 (3H, s, H'-10), 1.08 (3H, s, H′-9), 0.94 (3H, s, H'-8), 0.89 (3H, s, H-5″); ^{13}C NMR (CD_3OD, 100 MHz) δ_C 153.8 (C-5), 152.7 (C-1), 139.4 (C-3), 106.2 (C-2), 105.0 (C-6), 104.2 (C-1), 71.8 (C-3′), 41.6 (C-2′), 39.5 (C-6′), 37.3 (C-4′), 33.9 (C-1″), 32.3 (C-7′), 30.0 (C-9′), 29.7 (C-4″), 29.3 (C-2″-3″), 24.1 (C-10′), 19.0 (C-8′), 15.8 (C-1′, C-5′), 11.7 (C-5″); ESIMS *m/z* 317 $[M+H]^+$; HRESIMS *m/z* 317.2469 $[M+H]^+$ (calcd for $C_{21}H_{33}O_2$, 317.2481).

*3.5.2.2 Cyclocannabigerol B (**9b**)*

Colorless amorphous solid. $[\alpha]_D$=0. ^{1}H NMR (CD_3OD, 400 MHz): δ_H 6.17 (1H, s, H-4), 6.06 (1H, s, H-2), 2.78 (1H, d, *J*=17.7 Hz, H-1′a), 2.66 (1H, dd, *J*=17.7, 7.8 Hz, H-1′b), 2.42 (2H, t, *J*=7.6 Hz, H-1″), 1.96 (1H, d, *J*=13.8 Hz, H-4′a), 1.85 (1H, m, H-5′a), 1.57 (2H, m, H-2″), 1.57 (2H, m, H-3″), 1.51 (1H, dd, *J*=13.8, 4.3 Hz, H-4′b), 1.47 (1H, d, *J*=7.8 Hz, H-2′), 1.42 (2H, overlapped, H-5′b, H-6′a), 1.33 (1H, overlapped, H-6′b), 1.32 (2H, overlapped, H-4″), 1.18, s (3H, s, H-10′), 0.98 (3H, s, H-9′), 0.91 (3H, t, *J*=7.0 Hz, H-5″), 0.65 (3H, s, H-8′);

^{13}C NMR (CD_3OD, 100 MHz): δ_C 153.8 (C-5), 152.6 (C-1), 139.7 (C-3), 106.4 (C-2), 105.1 (C-6), 104.6 (C-1), 73.0 (C-3′), 42.4 (C-2′), 39.9 (C-6′), 37.7 (C-4′), 33.9 (C-1″), 32.1 (C-7′), 30.1 (C-9′), 29.7 (C-4″), 29.3 (C-2″-3″), 24.5 (C-10′), 19.0 (C-8′), 16.2 (C-1′, C-5′), 11.7 (C-5″); ESIMS *m/z* 317 $[M+H]^+$; HRESIMS *m/z* 317.2479 $[M+H]^+$ (calcd for $C_{21}H_{33}O_2$, 317.2481).

*3.5.2.3 Iodocyclocannabigerol A (**10**)*

Pale yellow amorphous solid. $[\alpha]_D$=0. ^{1}H NMR ($CDCl_3$, 500 MHz): δ_H 6.23 (1H, s, H-4), 6.17 (1H, s, H-2), 4.24 (1H, dd, *J*=12.8, 3.8 Hz, H-6′), 2.83 (1H, dd, *J*=16.5, 4.9 Hz, H-1′a), 2.45 (1H, overlapped, H-5′a), 2.44 (1H, overlapped, H-1′b), 2.44 (2H, overlapped, H-1″), 2.33 (1H, dd, *J*=13.6, 3.8 Hz, H-5′b), 1.86 (1H, dd, *J*=11.5, 3.6 Hz, H-2′), 1.82 (1H, m, H-4′a), 1.75 (1H, brdd, *J*=13.6, 3.8 Hz, H-4′b), 1.55 (2H, m, H-2″), 1.55 (2H, m, H-3″), 1.30 (2H, m, H-4″), 1.24 (3H, s, H-10′), 1.16 (3H, s, H-9′), 1.08 (3H, s, H-8′), 0.88 (3H, t, *J*=6.6 Hz, H-5″); ^{13}C NMR ($CDCl_3$, 100 MHz): δ_C 153.4 (C-5), 152.6 (C-1), 142.9 (C-3), 109.5 (C-4), 108.4 (C-2), 105.1 (C-6), 75.8 (C-3′), 51.4 (C-2′), 46.4 (C-7′), 42.4 (C-4′), 39.2 (C-6′), 35.6 (C-1″), 34.3 (C-5′), 32.2 (C-9′), 31.5 (C-4″), 30.8 (C-2″-3″), 20.1 (C-1′), 19.7 (C-10′), 19.6 (C-8′), 14.0 (C-5″); ESIMS *m/z* 443 $[M+H]^+$; HRESIMS *m/z* 443.1439 $[M+H]^+$ (calcd for $C_{21}H_{32}IO_2$, 443.1447).

*3.5.2.4 Spirocannabigerol A (**11a**)*

Colorless amorphous solid. $[\alpha]_D$=0. ^{1}H NMR (CD_3OD, 500 MHz): δ_H 6.06 (1H, s, H-2), 6.03 (1H, s, H-4), 2.93 (1H, d, *J*=16.0 Hz, H-1′a), 2.84 (1H, d, *J*=16.0 Hz, H-1′b), 2.43 (2H, t, *J*=7.7 Hz, H-1″), 2.20 (1H, overlapped, H-3′), 1.62 (1H, overlapped, H-5′a), 1.61 (1H, overlapped, H-6′a), 1.56 (2H, q, *J*=7.41 Hz, H-2″), 1.55 (1H, overlapped, H-4′a), 1.54 (1H, overlapped, H-5′b), 1.45 (1H, overlapped, H-4′b), 1.34 (2H, overlapped, H-3″), 1.32 (2H, overlapped, H-4″), 1.18 (1H, dd, *J*=13.2, 3.2 Hz, H-6′b), 1.12 (3H, s, H-8′), 0.90 (3H, t, *J*=6.8 Hz, H-5″), 0.79 (3H, s, H-9′), 0.75 (3H, d, *J*=6.7 Hz, H-10′); ^{13}C NMR (CD_3OD, 100 MHz): δ_C 162.8 (C-5), 152.7 (C-1), 144.2 (C-3), 110.0 (C-6), 106.1 (C-2), 99.3 (C-4), 93.3 (C-2′), 38.1 (C-7′), 37.7 (C-3′), 36.4 (C-6′), 35.7 (C-1″), 31.5 (C-1′), 31.3 (C-3″), 31.1 (C-2″), 30.0 (C-4′), 24.3 (C- 9′), 22.6 (C-4″), 21.4 (C-8′), 21.3 (C-5′), 14.2 (C-10′), 13.2 (C-5″); ESIMS *m/z* 317 $[M+H]^+$; HRESIMS *m/z* 317.2473 $[M+H]^+$ (calcd for $C_{21}H_{33}O_2$, 317.2481).

*3.5.2.5 Spirocannabigerol B (**11b**)*

Colorless amorphous solid. $[\alpha]_D$=0. ^{1}H NMR (CD_3OD, 500 MHz): δ_H 6.06 (1H, s, H-2), 6.05 (1H, s, H-4), 3.06 (1H, d, *J*=16.0 Hz, H-1′a), 2.74 (1H, d, *J*=16 Hz, H-1′b), 2.43 (2H, t, *J*=7.6 Hz, H-1″), 1.80 (1H, overlapped, H-3′), 1.76 (1H, dd, *J*=13.0, 3.6 Hz, H-6′a), 1.63 (1H, m, H-5′a), 1.56 (2H, m, H-2″), 1.55 (1H, overlapped, H-5′b), 1.53 (1H, bd, *J*=10.5 Hz, H-4′a), 1.46 (1H, overlapped, H-4′b), 1.33 (2H, overlapped, H-4″), 1.30 (2H, overlapped, H-3″), 1.23 (2H, bd, *J*=13.0 Hz, H-6′b), 1.02 (3H, s, H-8′), 0.90 (3H, t, *J*=7.0 Hz, H-5″), 0.81 (3H, s, H-9′), 0.73 (3H, d, *J*=6.6 Hz, H-10′); ^{13}C NMR (CD_3OD, 125 MHz): δ_C 162.8 (C-5), 152.8 (C-1), 144.2 (C-3), 110.2 (C-6), 106.6 (C-2), 99.8 (C-4), 94.6 (C-2′), 38.2 (C-7′), 37.1 (C-3′), 36.4 (C-6′), 35.8 (C-1″), 31.7 (C-1′), 31.5 (C-3″), 31.3 (C-2″), 30.6 (C-4′), 24.0 (C-9′), 22.6 (C-4″), 21.7 (C-8′), 21.3 (C-5′), 14.8 (C-10′), 13.2 (C-5″); ESIMS *m/z* 317 $[M+H]^+$; HRESIMS *m/z* 317.2469 $[M+H]^+$ (calcd for $C_{21}H_{33}O_2$, 317.2481).

*3.5.2.6 Toluene adduct **12***

Colorless powder. $[\alpha]_D$=0. ^{1}H NMR (CD_3OD, 500 MHz): δ_H 7.19 (2H, d, *J*=8.2 Hz, H-2‴ and H-6‴), 7.08 (2H, d, *J*=8.2 Hz, H-3‴ and 5‴), 6.12 (1H, s, H-4), 6.00 (1H, s, H-2), 2.46 (1H, ddd, *J*=13.2, 6.8, 2.4 Hz, H-1′a), 2.38 (1H, t, *J*=7.7 Hz, H-1″), 2.27 (3H, s, H-7‴), 1.65 (2H, m, H-2′), 1.59 (2H, dd, *J*=13.0, 3.6 Hz, H-6′), 1.56 (2H, m, H-2″), 1.46 (2H, m, H-4′), 1.33 (2H, m, H-4″), 1.30 (1H, m, H-3″), 1.24 (6H, s, H-8, H-9), 1.10 (3H, s, H-10′), 1.18 (2H, m, H-5′), 0.88 (3H, t, *J*=6.3 Hz, H-5″). ^{13}C NMR (CD_3OD, 125 MHz): δ_C 155.0 (C-5), 154.6 (C-1), 146.3 (C-1‴), 144.2 (C-3), 134.6 (C- 4‴), 128.6 (C-3‴ and C-5‴), 125.7 (C-2‴ and C-6‴), 108.3 (C-2), 106.1 (C-6), 106.0 (C-4), 75.8 (C-3′), 45.0 (C-6′), 39.8 (C-4′), 37.1 (C-7′), 35.6 (C-1″), 31.5 (C-3″), 31.3 (C-2″), 30.7 (C-2′), 28.6 (C-8′), 18.5 (C-9′), 22.6 (C-4″), 20.0 (C-7‴), 19.1 (C-5′), 16.5 (C-1′), 14.8 (C-10′), 13.5 (C-5″); ESIMS *m/z* 409 $[M+H]^+$; HRESIMS *m/z* 409.3099 $[M+H]^+$ (calcd for $C_{28}H_{41}O_2$, 409.3107).

3.5.3 Pyrolysis of cannabichromene (2a) in the presence of silica gel

CBC (**2a**, 100 mg, 0.32 mmol, coming from my research group library) was adsorbed onto silica (200 mg) and heated to 150 °C by microwave (CEM

Discover SP Microwave, 300 W) at regular intervals of 30 minutes for a total of 210 minutes, until complete consumption of the starting material as monitored by TLC (PE-EtOAc 9:1, Rf CBC= 0.27, Rf product mixture= 0.43). The crude reaction mixture was first purified by gravity column chromatography on silica gel using 9:1 PE-EtOAc solution as eluent to afford 68 mg of brown oil. Further HPLC purification (UV detector set at λ_{max} 227 nm; flow 0.8 mL/min) using as eluent a gradient from CH_3CN/H_2O (0.1% HCOOH) 7:3 to CH_3CN in 25 min afforded pure cannabicitran (**17**, 18.0 mg, 0.057 mmol, 17.8% yield), Δ^8-iso-*cis*-THC (**18**, 11.3 mg, 0.036 mmol, 11.2% yield), and cannabicyclol (**6a**, 31.3 mg, 0.10 mmol, 31.2%). The NMR data of cannabicitran (Crombie *et al.*, 1979), Δ^8-iso-*cis*-THC (Yagen and Mechoulam, 1969), and cannabicyclol (Crombie et al, 1968 are in agreement with those reported in the literature.

3.5.4 Iodine-mediated annulation of homo-isoprenylchromenes to benzo[*c*]chromenes: synthesis of CBN (5a)

To a stirred solution of CBC (**2a**, 300 mg, 0,954 mmol, coming from my research group library) in toluene (20 mL), iodine (472 mg, 1,860 mmol) was added. The mixture was refluxed and monitored by TLC (PE-EtOAc 9:1, Rf CBC= 0,27, Rf product= 0,29). After 3 hours, the reaction was quenched by addition of Na_2SO_3 s.s. and extraction with EtOAc. After drying (anhydrous Na_2SO_4) and evaporation, the residue was purified by gravity column chromatography on silica gel with PE-EtOAc 95:5 solution to afford CBN (**5**) as a brown oil (236 mg, 82% yield).

3.5.4.1 One-pot total synthesis of CBN (5a)

To a stirred solution of olivetol (**21**, 100 mg, 0,554 mmol) toluene (5mL), citral (**20**, 91 µL, 0,533 mmol) and *n*-butylamine (53 µL, 0,533 mmol) were added. The mixture was refluxed overnight, then cooled to room temperature. Dowex 50 W X 8 (200 mg) was added, and the solution was stirred for 10 minutes at room temperature then filtered over celite pad in a new round bottomed flask. To the filtered solution, iodine (268 mg, 1,066 mmol) was added. The mixture was refluxed for 3 hours, then quenched by addition of sat. Na_2SO_3 and extraction with EtOAc. After drying (anhydrous Na_2SO_4) and evaporation, the residue was purified by gravity column chromatography on silica gel and eluted with PE-EtOAc 95:5 solution to afford CBN (**5a**) as a brown

oil (94 mg, 0.305 mmol, 55% yield). The NMR data obtained for cannabinol (**5a**) matched those reported in the literature (Choi *et al.*, 2004).

*3.5.4.2 Synthesis of **5c**.*

To a stirred solution of **2a** (260 mg, 0.914 mmol, coming from my research group library) in toluene (20 mL), iodine (463 mg, 1.828 mmol) was added. The mixture was refluxed and monitored by TLC (PE-EtOAc 9:1, Rf 2a= 0.55, Rf product= 0.45). After 2 hours, the reaction was quenched by addition of sat. Na_2SO_3 and extraction with EtOAc. After drying (anhydrous Na_2SO_4) and evaporation, the residue was purified by gravity column chromatography on silica gel and eluted with PE-EtOAc 98:2 solution to obtain **5c** as a brown oil (207 mg, 80% yield). Compound **5c** was identified on the basis of a comparison of its spectral data with those reported in the literature (Pollastro et al, 2018, a).

*3.5.4.3 Synthesis of **23***

To a stirred solution of **2a** (300 mg, 1.161 mmol) in toluene (30 mL), iodine (590 mg, 2.323 mmol) was added. The mixture was refluxed and monitored by TLC (PE-CH_2Cl_2 6:4, Rf **2a**= 0.35, Rf product= 0.42). After 2 hours, the reaction was quenched by addition of Na_2SO_3 s.s. and extraction with EtOAc. After drying (anhydrous Na_2SO_4) and evaporation, the residue was purified by gravity column chromatography on silica gel with PE-EtOAc 95:5 solution to afford compound cannabiorcol (**23**) as a brown solid (188 mg, 63% yield). Compound **23** was identified on the basis of a comparison of its spectral data with those reported in the literature (Meltzer *et al.*, 1981).

*3.5.4.4 Synthesis of **24***

To a stirred solution of **2a** (200 mg, 0.540 mmol) in toluene (20 mL), iodine (273 mg, 1.080 mmol) was added. The mixture was refluxed and monitored by TLC (PE-EtOAc 9:1, Rf **2a**= 0.38, Rf product= 0.44). After 2 hours, the reaction was quenched by addition of Na_2SO_3 s.s. and extraction with EtOAc. After drying (anhydrous Na_2SO_4) and evaporation, the residue was purified by gravity column chromatography on silica gel and eluted with PE-EtOAc 95:5 solution to afford compound **24** as a brown solid (165 mg, 83% yield). Compound **24** was identified on the basis of a comparison of its spectral data with those reported in the literature (Khanolkar *et al.*, 2007).

*3.5.4.5 Synthesis of **25***

To a stirred solution of **2a** (280 mg, 0.774 mmol) in toluene (20 mL), iodine (393 mg, 1.549 mmol) was added. The mixture was refluxed and monitored by TLC (PE-EtOAc 9:1, Rf **2a** = 0.44, Rf product = 0.46). After 2 hours, the reaction was quenched by addition of Na_2SO_3 s.s. and extraction with EtOAc. After drying (anhydrous Na_2SO_4) and evaporation, the residue was purified by gravity column chromatography on silica gel and eluted with PE-EtOAc 95:5 solution to afford compound **25** as dark yellow oil (113 mg, 41% yield).
ESIMS *m/z* 343 $[M - H]^-$; HRESIMS *m/z* 343.1700 $[M - H]^-$ (calcd for $C_{24}H_{23}O_2$, 343.1704). ^{1}H NMR (CD_3OD, 700 MHz): δ_H 8.34 (1H, s, H-8), 7.26-7.14 (overlapped, H-7, H-4' to H-8'), 7.03 (1H, d, *J* = 7.0 Hz, H-8), 6.36 (1H, s, H-2), 6.26 (1H, s, H-4), 2.88 (2H, t, *J* = 7.2 Hz, H-1′), 2.78 (2H, t, *J* = 7.2 Hz, H-2′), 2.34 (3H, s, H-11), 1.53 (6H, s, H-12, H-13). ^{13}C NMR (CD_3OD, 175 MHz): δ_C 156.5 (C-1), 155.7 (C-4a), 144.2 (C-10a), 143.1 (C-3), 141.8 (C-3'), 129.5 (C-8), 129.3 (C-6'), 128.3 (C-4', C-8'), 128.2 (C-5', C-7'), 126.9 (C-10), 123.3 (C-7), 110.7 (C-4), 110.5 (C-2), 109.8 (C-10b), 78.1 (C-6), 39.0 (C-1'), 38.6 (C-2'), 27.5 (C-12, C-13), 21.6 (C-11).

3.5.5 Reaction of pyranopyrones with iodine

To a stirred solution of ferprenine (300 mg, 1.035 mmol) in toluene (20 mL), iodine (515 mg, 2.03 mmol) was added. The mixture was refluxed and monitored by TLC (PE-EtOAc 9:1, Rf ferprenine= 0.40, Rf product mix= 0.54). After 3 hours, the reaction was quenched by addition of sat. Na_2SO_3 and extraction with EtOAc. After drying (anhydrous Na_2SO_4) and evaporation, the residue was purified by gravity column chromatography on silica gel and eluted with PE-EtOAc 95:5 solution to afford 180 mg of brown oil. Further HPLC purification (UV detector set at λ_{max} 227 nm; flow rate 1.0 mL/min) using as eluent a gradient from CH_3CN/H_2O (0.1% HCOOH) 7:3 to CH_3CN in 20 min afforded pure compounds **27** (11.3 mg, 3.7%), **28a** (57.4 mg, 18.7%) and **28b** (61.9 mg, 20.2%). When the same reaction and purification conditions were applied to compound **29** (200 mg, 0.77 mmol), compounds **30a** and **30b** (mixture 66.3 mg, 33.2%) were obtained.

*3.5.5.1 Compound **27***

ESIMS *m/z* 293 $[M + H]^+$; HRESIMS *m/z* 293.1181 $[M + H]^+$ (calcd. for $C_{19}H_{17}O_3$, 293.1172). ^{1}H NMR (CD_3OD, 500 MHz): δ_H 8.41 (1H, s, H-13), 7.95 (1H, d, *J* = 8.0 Hz, H-1), 7.66 (1H, t, *J* = 8.0 Hz, H-2), 7.39 (2H, overlapped, H-3, H-4), 7.23 (1H, d, *J* = 7.8 Hz, H-16), 7.19 (1H, d, *J* = 7.8 Hz, H-15), 2.38 (3H, s, H-17), 1.77 (6H, s, H-18-19). ^{13}C NMR (CD_3OD, 125 MHz): δ_C 164.5 (C-9), 159.8 (C-7), 152.3 (C-5), 144.2 (C-11), 137.9 (C-14), 132.2 (C-2), 131.2 (C-6), 129.4 (C-15), 124.8 (C-13), 124.7 (C-3), 123.7 (C-1), 123.5 (C-12), 122.5 (C-16), 116.1 (C-4), 101.9 (C-8), 81.1 (C-10), 25.2 (C-18, C-19), 20.0 (C-17).

*3.5.5.2 Compound **28a**.*

ESIMS *m/z* 297 $[M + H]^+$; HRESIMS *m/z* 297.1501 $[M + H]^+$ (calcd for $C_{19}H_{21}O_3$, 297.1485). ^{1}H NMR (CD_3OD, 500 MHz): δ_H 7.86 (1H, d, *J* = 7.8 Hz, H-1), 7.58 (1H, t, *J* = 7.8 Hz, H-3), 7.31 (1H, t, *J* = 7.8 Hz, H-2), 7.29 (1H, d, *J* = 7.8 Hz, H-4), 4.18 (1H, bs, H-12), 2.57 (1H, dd, *J* = 14.9, 5.4 Hz, H-14a), 2.12 (1H, dt, *J* = 13.8, 2.4 Hz, H-15a), 1.96 (1H, dd, *J* = 13.3, 2.2 Hz, H-11a), 1.93 (3H, s, H-19), 1.89 (1H, overlapped, H-11b), 1.81 (1H, overlapped, H-14b), 1.69 (3H, s, H-18), 1.67 (1H, overlapped, H-15b), 1.53 (3H, s, H-17). ^{13}C NMR (CD_3OD, 125 MHz): δ_C 164.5 (C-9), 162.1 (C-7), 153.2 (C-5), 130.1 (C-3), 127.4 (C-13), 123.0 (C-16), 122.3 (C-2), 120.6 (C-1), 114.6 (C-4), 79.4 (C-10), 38.2 (C-15), 34.7 (C-11), 28.7 (C-12), 25.3 (C-17), 20.5 (C-14), 18.2 (C-18), 17.8 (C-19).

*3.5.5.3 Compound **28b**.*

ESIMS *m/z* 297 $[M + H]^+$; HRESIMS *m/z* 297.1481 $[M + H]^+$ (calcd for $C_{19}H_{21}O_3$, 297.1485). ^{1}H NMR (CD_3OD, 500 MHz): δ_H 7.81 (1H, d, *J* = 7.8 Hz, H-1), 7.57 (1H, t, *J* = 7.9 Hz, H-3), 7.32 (1H, overlapped, H-2), 7.30 (1H, overlapped, H-4), 5.32 (1H, t, *J* = 3.1 Hz, H-14), 3.69 (1H, t, *J* = 3.3 Hz, H-12), 2.54-2.51 (3H, overlapped, H-11-16), 2.11 (1H, dd, *J* = 13.02, 3.3 Hz, H-15a) 1.88 (1H, d, *J* = 13.0 Hz, H-15b), 1.65 (3H, s, H-17), 1.12 (3H, d, *J* = 6.8 Hz, H-19), 1.00 (3H, d, *J* = 6.8 Hz, H-18); ^{13}C NMR (CD_3OD, 125 MHz): δ_C 164.9 (C-9), 162.1 (C-7), 153.6 (C-5), 150.7 (C-13), 132.9 (C-3), 125.3 (C-2), 123.6 (C-1), 117.4 (C-4), 116.3 (C-14), 105.3 (C-8), 80.4 (C-10), 41.6 (C-11), 35.6 (C-15), 33.7 (C-16), 30.1 (C-12), 28.3 (C-17), 22.7 (C-18), 21.1 (C-19).

3.5.6 SIBX Oxidation of phytocannabinoids. Reaction with CBD (3a) as exemplificative.

To a cooled (ice bath) solution of CBD (**3a**, 5 g, 15,6 mmol, coming from my research group library) in EtOAc (75 mL), SIBX (21.1 g, 31,5 mmol, 2 molar equiv.) was addd in six portions of ca 5 g each. The cooling bath was removed, and the suspension was stirred at room temp. for 18 h and then filtered over a pad of Celite. The filtration cake was washed with EtOAc (50 mL), and the pooled filtrates were washed with sat. $Na_2S_2O_3$ (4 x 75 mL), and next with brine. After drying and evaporation, the residue was purified by GCC on silica gel (150 g, petroleum ether-EtOAc 9:1 as eluent) to obtain a brown oil that solidified upon storing in the refrigerator. Washing with cold petroleum ether removed the some colored impurities, and afforded an orange powder (3.17 g, 61% yield). The same protocol was used for the oxidation and the purification of the other phytocannabinoids investigated (CBC, **2a**; CBG, **1a**; CBN, **5a**). The scale was 100-200 mg, and the yield were 59% (CBCQ, **46**), 37% (CBGQ, **45**) and 58%, (CBNQ, **47**).

*3.5.6.1 Cannabigeroquinone (CBGQ, **45**)*

Red powder, IR λ_{max} (KBr disc): 3272, 2955, 2923, 2856, 1644, 1637, 1350,1316, 1191, 1175, 580 cm^{-1}; ^1H NMR ($CDCl_3$, 400 MHz): δ_H 6.94 (1H, s, OH), 6.45 (1H, bs, H-2'), 5.13 (1H, t, *J* = 7.4 Hz, H-2), 5.04 (1H, t, *J* = 6.7 Hz, H-7), 3.13 (2H, d, *J* = 7.4 Hz, H-1), 2.41 (2H, t, *J* = 7.6, H-1''), 1.99-1.90 (4H, m, H-4, H-5), 1.73 (3H, s, H-8), 1.64 (3H, s, H-9), 1.57 (3H, s, H-10), 1.50 (2H, m, H-2''), 1.33 (4H, m, H-3'', H-4''), 0.89 (3H, t, *J* = 6.8 Hz, H-5''); ^{13}C NMR ($CDCl_3$, 100 MHz): δ_C 187.7, 184.2, 150.9, 145.1, 137.3, 134.4, 131.5, 124.3, 120.2, 119.7, 39.8, 31.5, 28.3, 27.4, 26.7, 25.8, 22.5, 22.0, 17.8, 16.3, 14.0; ESIMS: *m/z* 331 $[M + H]^+$; HRESIMS *m/z* 331.2262 $[M + H]^+$, calcd. for $C_{21}H_{31}O_3$, 331.2268.

*3.5.6.2 Cannabichromenquinone (CBCQ, **46**)*

Red oil, IR λ_{max} (KBr disc): 2957, 2926, 2852,1648, 1580, 1324, 1078, 969, 891cm^{-1}; ^1H NMR ($CDCl_3$, 400 MHz): δ_H 6.47 (1H, d, *J* = 9.9 Hz, H-1), 6.40 (1H, bs, H-2'), 5.56 (1H, d, *J* = 9.9 Hz, H-2), 5.07 (1H, t, *J* = 6.9 Hz, H-6), 2.39 (2H, t, *J* = 7.6 Hz, H-1''), 2.08 (1H, m, H-5a), 1.88 (1H, m, H-5b), 1.66 (2H, overlapped, H-4), 1.64 (3H, s, H-8), 1.55 (3H, s, H-9), 1.49 (2H, m, H-2''), 1.46 (3H, s, H-10), 1.32 (4H, m, H-3'', H-4''), 0.89 (3H, t, *J* = 6.7 Hz, H-5''); ^{13}C NMR ($CDCl_3$, 100

MHz): δ_C 184.6, 181.9, 150.8, 147.7,132.2, 131.4, 128.8, 123.4, 115.4, 115.0, 83.0, 41.5, 31.4, 28.7, 27.4, 27.3, 25.6, 22.6, 22.4, 17.7, 13.9; ESIMS *m/z* 329 $[M + H]^+$; HRESIMS *m/z* 329.2107 $[M + H]^+$, calcd for $C_{21}H_{29}O_3$, 329.2111.

*3.5.6.3 Cannabinolquinone (CBNQ, **47**)*

Red oil, IR IR λ_{max} (KBr disc): 2955, 2924, 2855, 1649, 1382, 1145, 1110, 811 cm^{-1}; ^1H NMR ($CDCl_3$, 400 MHz): δ_H 8.30 (1H, s, H-2), 7.09 (1H, d, *J* = 7.9 Hz, H-6), 7.02 (1H, d, *J* = 7.9 Hz, H-5), 6.63 (1H, t, *J* = 1.4 Hz, H-2'), 2.40 (2H, t, *J* = 7.7 Hz, H-1''), 2.36 (3H, s, H-7), 1.69 (6H, s, H-9, H-10), 1.56 (2H, m, H-2''), 1.32 (4H, m, H-3'', H-4''), 0.90 (3H, t, *J* = 6.8 Hz, H-5''); ^{13}C NMR ($CDCl_3$, 100 MHz): δ_C 180.2, 175.3, 163.3, 144.7, 138.1, 133.8, 131.8, 128.9, 125.7, 122.3, 111.0, 82.7, 53.6, 31.6, 29.8, 29.0, 28.3, 27.4, 22.4, 21.4, 13.9; ESIMS *m/z* 325 $[M + H]^+$; HRESIMS *m/z* 325.1791 $[M + H]^+$, calcd. for $C_{21}H_{25}O_3$, 325.1798.

*3.5.6.4 Dimeric Cannabigeroquinone (**48**) and chiral chromatography*

Red powder, IR λ_{max} (KBr disc): 3280, 2955, 1350, 1188, cm^{-1}; ^1H NMR ($CDCl_3$, 400 MHz): δ_H 6.98 (1H, s, OH), 5.17 (1H, t, *J* = 7.4 Hz, H-2), 5.06 (1H, t, *J* = 6.7 Hz, H-7), 3.16 (2H, d, *J* = 7.4 Hz, H-1), 2.32 (2H, t, *J* = 7.6, H-1''), 2.05-1.90 (4H, m, H-4, H-5), 1.73 (3H, s, H-8), 1.64 (3H, s, H-9), 1.57 (3H, s, H-10), 1.49 (2H, m, H-2''), 1.32 (4H, m, H-3'', H-4''), 0.89 (3H, t, *J* = 6.8 Hz, H-5''). ESIMS: *m/z* 645 $[M + H]^+$; HRESIMS *m/z* 645.4159 $[M + H]^+$, calcd. for $C_{41}H_{57}O_6$, 645.4155. A sample of **48** (2.0 mg) was separated on the chiral Lux 5 µ Amylose-2 250 x 4.60 mm column, Phenomenex, eluent *n*-hexane/isopropanol 9:1 (0.2% TFA) with a flow rate 0.7 mL/min and two peaks were obtained with Rt = 8 min (0.9 mg) and Rt = 13 min (0.7 mg).

3.5.7 Oxidation of Cannabidiol (CBD, 3a) with the Takehira Reagent

To a stirred solution of CBD (**3a**, 200 mg, 0,64 mmol, coming from my research group library) in toluene – *tert*-butanol (3:1, 20 mL), copper (II) chloride (43 mg, 0,32 mmol, 0,5 molar equiv.) and hydroxylamine hydrochloride (22 mg, 0,32 mmol, 0,5 molar equiv.) were added. The solution turned from yellow to brown, and was stirred for 2 hours at room temp., and next worked up by dilution with 2N H_2SO_4 and extraction with EtOAc. The organic phase was

washed with brine, dried with anhydrous Na_2SO_4, filtered and evaporated. The residue was purified by GCC (5 g silica gel, petroleum ether-EtOAc gradient, from petroleum ether to 95:5 petroleum ether – EtOAc as eluent) to give **39** (135 mg, 34%) and **38** (20%).

*3.5.7.1 Hydroxyiminocannabiquinone (**38**)*

Brownish oil, IR λ_{max} (KBr disc): 2960, 2924, 2856, 1617, 1420, 1420, 1260, 1092, 1016, 797 cm^{-1}; ^1H NMR (CD_3OD, 400 MHz): δ_H 6.25 (1H, s, H-2′), 5.12 (1H, s, H-2), 4.50 (1H, s, H-9a), 4.49 (1H, s, H-9b), 3.82 (1H, m, H-3), 2.92 (1H, td, *J* = 11.7, 3.2 Hz, H-4), 2.70 (2H, t, *J* = 7.5 Hz, H-1”), 2.18 (1H, m, H-6a), 1.99 (1H, m, H-6b), 1.73 (2H, overlapped, H-5), 1.65 (3H, s, H-7), 1.63 (3H, s, H-10), 1.60 (2H, overlapped, H-2”), 1.34 (2H, overlapped, H-3”), 1.33 (2H, overlapped, H-4″), 0.91 (3H, t, *J* = 6.9 Hz, H-5″); ^{13}C NMR (CD_3OD, 100 MHz): δ_C 176.3 (C-1′), 168.1 (C-5′), 150.2 (C-8), 148.7 (C-3′), 148.1 (C-4′), 133.6 (C-1), 125.6 (C-2), 120.6 (C-2′), 119.1 (C-6′), 110.8 (C-9), 45.6 (C-4), 36.2 (C-3), 32.8 (C-3″), 31.6 (C-6), 31.5 (C-1″), 30.8 (C-5), 30.5 (C-2″), 23.6 (C-7), 23.5 (C-4”), 19.1 (C-10), 14.3 (C-5”) ; ESIMS *m/z* 344 $[M + H]^+$; HRESIMS *m/z* 344.2210 $[M + H]^+$ calcd for $C_{21}H_{30}NO_3$, 344.2220.

*3.5.7.2 2-Chlorocannabidiol (**39**)*

Yellow oil, IR λ_{max} (KBr disc): 3500, 3421, 2962, 2924, 2859, 1623, 1421, 1258, 1193, 1054, 888, 817, 698 cm^{-1}; ^1H NMR (CD_3OD, 400 MHz): δ_H 6.21 (1H, s, H-2’), 5.25 (1H, s, H-2), 4.46 (1H, s, H-9a), 4.44 (1H, s, H-9b), 3.99 (1H, m, H-3), 2.95 (1H, m, H-4), 2.56 (2H, t, *J* = 7.4 Hz, H-1”), 2.20 (1H, m, H-5a), 2.01 (1H, d, *J* = 17.1 Hz, H-5b), 1.76 (2H, m, H-6), 1.68 (3H, s, H-7), 1.65 (3H, s, H-10), 1.56 (2H, m, H-2”), 1.35 (4H, m, H-3”-4”). 0.91 (3H, t, *J* = 6.8 Hz, H-5”); ^{13}C NMR (CD_3OD, 100 MHz): δ_C 156.1, 152.7, 150.2, 139.3, 134.2, 126.6, 118.2, 112.8, 110.7, 109.6, 46.2, 38.3, 34.7, 32.7, 31.7, 30.7, 30.5, 23.7, 23.5, 19.3, 14.4. ESIMS *m/z* 349, 351 $[M + H]^+$ ratio 3:1; HRESIMS *m/z* 349.1919 $[M + H]^+$ (calcd for $C_{21}H_{30}{}^{35}ClO_2$, 349.1929).

3.5.8 Thermo-TRPs (TRPV1, TRPV2, TRPV3, TRPV4, TRPM8, TRPA1) receptor assays

HEK-293 cells stably over-expressing recombinant rat TRPA1, TRPM8, TRPV2-4, TRPM8 or human TRPV1 were selected by G-418 (Geneticin; 600 μgmL^{-1}), cultured on 100-mm diameter Petri dishes as monolayers in minimum

essential medium supplemented with non-essential amino acids, 10% fetal bovine serum, and 2mM glutamine, and maintained under 5% CO_2 at 37 °C. Stable expression of each channel was checked by quantitative real time-PCR. The effect of the substances on intracellular Ca^{2+} concentration $[Ca^{2+}]_i$ was determined using Fluo-4, a selective intracellular fluorescent probe for Ca^{2+}. Toward this aim, on the day of the experiment, cells overexpressing the TRP channels were loaded for 1 h in the dark at room temperature with the methyl ester Fluo4-AM (4 μM in DMSO containing 0.02% Pluronic F-127, Invitrogen) in minimum essential medium without fetal bovine serum. After the loading, cells were washed twice in Tyrode's buffer (145mM NaCl, 2.5mM KCl, 1.5mM $CaCl_2$, 1.2mM $MgCl_2$, 10mM D-glucose, and 10mM HEPES, pH 7.4), re-suspended in Tyrode's buffer, and transferred (about 100,000 cells) to the quartz cuvette of the spectrofluorimeter (Perkin-Elmer LS50B; PerkinElmer Life and Analytical Sciences, Waltham, MA) under continuous stirring. $[Ca^{2+}]_i$ was determined before and after the addition of various concentrations of test compounds by measuring cell fluorescence at 25 °C (λ_{EX}=488 nm, λ_{EM}=516 nm). Curve fitting (sigmoidal dose–response variable slope) and parameter estimation were performed with GraphPad Prism® (GraphPad Software Inc., San Diego, CA). Potency was expressed as the concentration of test substances exerting a half maximal agonist effect (i.e., half-maximal increases in $[Ca^{2+}]_i$ (EC_{50}), calculated by using GraphPad®. The efficacy of the agonists was first determined by normalizing their effect to the maximum Ca^{2+} influx effect on $[Ca^{2+}]_i$ observed with application of 4 μM ionomycin (Sigma). The increases in fluorescence in wild-type HEK293 cells (i.e. not transfected with any construct) were used as baseline and subtracted from the values obtained from transfected cells. The effects of TRPA1 agonists are expressed as a percentage of the effect obtained with 100 μM allyl isothiocyanate (AITC). In the case of TRPM8 the experiments were carried out at 22 °C with a Fluorescence Peltier System (PTP-1, Perkin-Elmer). Antagonist/desensitizing behavior was evaluated against capsaicin (0.1 μM) for TRPV1, icilin (0.25 μM) for TRPM8; AITC (100 μM) for TRPA1, lysophosphatidylcholine (LPC) (3 μM) for TRPV2, GSK1016790A 10 nM for TRPV4 by adding the compounds in the quartz cuvette 5 min before stimulation of cells with agonists. In the case of TRPV3, rat TRPV3-expressing HEK-293 cells were first sensitized with the non-selective agonist 2-aminoethoxydiphenyl borate (100 μM). Antagonist/desensitizing behavior was evaluated against

thymol (100 μM). Data are expressed as the concentration exerting a half-maximal inhibition of agonist $[Ca^{2+}]_i$ increasing effect (IC_{50}) which was calculated again using GraphPad Prism® software. The effect on $[Ca^{2+}]_i$ exerted by the agonist alone was taken as 100%. All determinations were at least performed in triplicate. Statistical analysis of the data was performed by analysis of variance at each point using ANOVA followed by Bonferroni's test.

3.5.9 PPAR-γ Activity Evaluation

Human embryonic kidney epithelial cells 293T cells were obtained from the American Type Culture Collection (CRL-3216) and cultured in DMEM supplemented with 10% FCS and antibiotics. To analyze PPAR-γ transcriptional activity HEK-293T cells were cultured in 24-well plates (2×104 cells/well) and transiently co-transfected with GAL4-PPAR-γ (50 ng) GAL4-luc (firefly luciferase, 50 ng) vectors using Roti-Fect (Carl Roth, Karlsruhe, Germany). Twenty hours after transfection the cells were stimulated with increasing concentrations of the compounds for 6 h and luciferase activities were quantified using Dual-Luciferase Assay (Promega, Madison, WI, USA). Rosiglitazone (1 μmol/L, Cayman Chemical, MI, USA), was used as a positive control for PPAR-γ activation (50-fold induction over basal activity). Test compounds and controls stocks were prepared in DMSO and the final concentration of the solvent was always less than 0.5% v/v. The plasmid GAL4-PPAR-γ was obtained from Prof. Christopher Sinal (Dalhousie University, Canada).

References

(a) Adams R., Baker B. R. and Wearn R. B. (**1940**). Structure of Cannabinol. III. Synthesis of Cannabinol, 1-Hydroxy-3-n-amyl-6,6,9-trimethyl-6-dibenzopyran. *J. Am. Chem. Soc.*, *62*, 2204–2207.

(b) Adams R., Hunt M., Clark J. H. (**1940**). Structure of Cannabidiol, a Product Isolated from the Marihuana Extract of Minnesota Wild Hemp. *J. Am. Chem. Soc.*, *62*, 196-200.

(c) Adams, R., Pease, D. C., Clark J. H., Baker B. R. (**1940**). Isolation and structure elucidation of cannabidiol. *J. Am. Chem. Soc*., *62*, 2197-2200.

Andre C. M., Hausman J.-F. and Guerriero G. (**2016**) *Cannabis sativa*: The Plant of the Thousand and One Molecules. *Front Plant Sci.*, *7,* 19.

Andreocci, A. (**1893**). *Gazz. Chim. Ital.*, *23*, 469.

Appendino G., Tagliapietra S., Nano G. M., Picci V. (**1988**). Ferprenin, a prenylated coumarin from Ferula communis. *Phytochemistry*, *27*, 944-946.

(a) Appendino G., Giana A., Gibbons S., Maffei M., Gnavi G., Grassi G., Sterner O.A. (**2008**). A Polar Cannabinoid from *Cannabis sativa* var. Carma *Nat. Prod. Commun.*, *3*, 1977-1980.

(b) Appendino G., Minassi A., Pagani A., Ech-Chadad A. (**2008**). The role of natural products in the ligand deorphanization of TRP channels. *Curr Pharm Des.*, *14*, 2–17.

Appendino G., Pollastro F., Verotta L., Ballero M., Romano A., Wyembek P., Szcuzuraszeck K., Mozrzymas J. W., Taglialatela-Scafati O. (**2009**). Polyacetylenes from Sardinian *Oenanthe fistulosa*: A Molecular Clue to *risus sardonicus*. *J. Nat. Prod., 72*, 962-965.

Appendino G., Chianese G. and Taglialatela-Scafati O. (**2011**). Cannabinoids: Occurrence and Medicinal Chemistry. *Current Medicinal Chemistry*, *18*, 1085-1099.

Barluenga J., Trincado M., Rubio E., Gonzalez J. M. (**2004**). Intramolecular Arylation Reactions of Alkenes: A Flexible Approach to Chromans and Tetrahydroquinoline Derivatives. *J. Am. Chem. Soc.*, *126*, 3416–3417.

Beam, W. (**1911**). *4th Report, Wellcome Trop. Research Lab., Rep. Sudan Gov.,* 25.

Bengley M. J., Clarke D. G., Crombie L., Whiting D. A. (**1970**). The X-Ray Structure of Dibromocannabicyclol: Structure of Bicyclomahanimbine. *J. Chem. Soc., Chem. Commun.,* 1547–1548.

Bornheim L. M., Grillo M. P. (**1998**). Characterization of cytochrome P450 3A inactivation by cannabidiol: possible involvement of cannabidiol-hydroxyquinone as a P450 inactivator.*Chem. Res. Toxicol., 10*, 1209-1216.

Borrelli F., Pagano E., Romano B., Panzera S., Maiello F., Coppola D., De Petrocellis L., Buono L., Orlando P., Izzo A. A. (**2014**). Colon carcinogenesis is inhibited by the TRPM8 antagonist cannabigerol, a Cannabis-derived non-psychotropic cannabinoid. *Carcinogenesis*, *35*, 2787–2797.

Breugst M., von der Heiden D. (**2018**). Mechanisms in Iodine Catalysis *Chem. - Eur. J.*, 24, 9187.

Carroll, C.B., Zeissler, M.L., Hanemann, C.O., Zajicek, J.P. (**2012**). $^{9}\Delta$-tetrahydrocannabinol (Δ^{9}-THC) exerts a direct neuroprotective effect in a human cell culture model of Parkinson's disease. *Neuropathol Appl Neurobiol*., *38*, 535-547.

Cascio M. G., Gauson L. A., Stevenson L. A., Ross R. A., Pertwee R. G. (**2010**). Evidence that the plant cannabinoid cannabigerol is a highly potent

α_2-adrenoceptor agonist and moderately potent $5HT_{1A}$ receptor antagonist. *Br J Pharmacol.*, *159*, 129–141.

Chen, L., Jia, Z., Yang, G. (**2014**). PPARs and Metabolic Syndrome. *PPAR Res*. 2014-832606.

Choi Y. H., Hazekamp A., Peltenburg-Looman A.M., Frédérich M., Erkelens C., Lefeber AW., Verpoorte R. (**2004**). NMR assignments of the major cannabinoids and cannabiflavonoids isolated from flowers of Cannabis sativa. *Phytochem Anal.*,*15*, 345-354.

Citti C., Linciano P., Russo F., Luongo L., Iannotta M., Maione S., Laganà A., Capriotti A. L., Forni F., Vandelli M. A., Gigli G., Cannazza G.. (**2019**). A novel phytocannabinoid isolated from *Cannabis sativa* L. with an in vivo cannabimimetic activity higher than Δ^9-tetrahydrocannabinol: Δ^9-Tetrahydrocannabiphorol. *Scientific Reports, 9, 20335.*

Ciudin, A., Hernandez, C., Simó, R. (**2012**). Update on cardiovascular safety of PPARgamma agonists and relevance to medicinal chemistry and clinical pharmacology. *Curr Top Med Chem.*, *12*, 585-604.

Crombie, L.; Ponsford, R.; Shani, A.; Yagnitinsky, B.; Mechoulam, R. (**1968**). Hashish components. Photochemical production of cannabicyclol from cannabichromene. *Tetrahedron Lett.*, *9*, 5771.

Crombie L., Redshaw S. D., Whiting D. A. (**1979**). The mechanism of intramolecular ‘citran’ bicyclisation of chromens: stereochemistry of a forward (H^+ catalysed) and a related reverse (thermal) process. *J. Chem. Soc., Chem. Commun.*, *79*, 630.

De Petrocellis L., Starowicz K., Schiano Moriello A., Vivese M., Orlando P., V. Di Marzo. (**2007**). Regulation of transient receptor potential channels of melastatin type 8 (TRPM8): Effect of cAMP, cannabinoid CB_1 receptors and endovanilloids. *Experimental Cell Research*, *313*, 1911-1920.

De Petrocellis L., Ligresti A., Schiano Moriello A., Allarà M., Bisogno T., Petrosino S., Stott C. G., Di Marzo V. (**2011**). Effects of cannabinoids and cannabinoid-enriched Cannabis extracts on TRP channels and endocannabinoid metabolic enzymes. *Br. J. Pharmacol.*, *163*, 1479–1494.

del Río C., Navarrete C., Collado J. A., Bellido M. L., Gómez-Cañas M., Pazos M. R., Fernández-Ruiz J., Pollastro F., Appendino G., Calzado M. A., Cantarero I., Muñoz E. (**2016**). The cannabinoid quinol VCE-004.8 alleviates bleomycin-induced scleroderma and exerts potent antifibrotic effects through peroxisome proliferator-activated receptor-γ and CB2 pathways. *Sci Rep.*, *6*, 21703.

Del Prete D., Caprioglio D., Appendino G. Minassi A., Schiano-Moriello A., Di Marzo V., De Petrocellis L. (**2015**). Discovery of non-electrophilic capsaicinoid-type TRPA1 ligands. *Bioorg Med Chem Lett.*, *25*, 1009–1011.

Dess D. B., Martin J. C.(**1983**). Readily accessible 12-I-5 oxidant for the conversion of primary and secondary alcohols to aldehydes and ketones. *J. Org. Chem.*, *48*, 4155-4156.

Dewar M. J. S., Healy E. F., Ruiz J. M. (**1987**). A High Level Ab Initio Study of Corner-protonated Cyclopropane . *J. Chem. Soc. Chem. Commun.*, 943–945.

Domingo V., Prieto C., Silva L., Rodilla J. M. L., Quílez del Moral J. F., Barrero A. F. (**2016**). Iodine, a Mild Reagent for the Aromatization of Terpenoids. *J. Nat. Prod.*, *79*, 831−837.

Doyle E. and Spence A. (**1995**). A Synthesis of phytocannabinoids. Cannabis as a medicine? *Br.J. Anaesth., 74*, 359–361.

Dowd P., Hershline R., Wook S., Naganathan S. (**1995**). Vitamin K and energy transduction: a base strength amplification mechanism. *Science*, *269*, 1684-1691.

Elsohly E. A., Turner C. E., Clark A. M., Elsohly M. A. (**1982**). Synthesis and antimicrobial activities of certain cannabichromene and cannabigerol related compounds. *J. Pharm. Sci.*,71, 1319-1323.

Ewing L. A., Skinner C. M., Quick C. M., Kennon-McGill S., McGill M. R., Walker L. A., ElSohly M. A., Gurley B. J., Koturbash I. (**2019**). Hepatotoxicity of a Cannabidiol-Rich Cannabis Extract in the Mouse Model. *Molecules*, *24*, pii: E1694.

Fellermeier M., Zenk M.H. (**1998**). Prenylation of olivetolate by a hemp transferase yields cannabigerolic acid, the precursor of tetrahydrocannabinol. *FEBS Lett.,* 427, 283-285.

Fernández-Ruiz J., Sagredo O., Pazos M.R., García C., Pertwee R., Mechoulam R., Martínez-Orgado J. (**2013**). Cannabidiol for neurodegenerative disorders: important new clinical applications for this phytocannabinoid? *Br J Clin Pharmacol.*, *75*, 323-333.

Friedrich-Fiechtl J., Spiteller G. (**1975**). Neue cannabinoide—1. *Tetrahedron*, 31, 479-87.

Frigerio M., Santagostino M., Sputore S. (**1999**). *J. Org. Chem.*, *64*, 4537–4538.

Garcia A., Borchardt D., Chang C.-D. A., Marsella M. J. (**2009**). *J. Am. Chem. Soc.*, *131*, 16640. For a study on the biological profile of cis-THC, see: Chicca A., Schafroth M. A., Reynoso-Moreno I., Erni R., Petrucci V., Carreira E. M., Gertsch J. (**2018**). *Sci. Adv.*, *4*, 2166.

Gaoni Y., Mechoulam R. (**1971**). Isolation and structure of Δ^1-tetrahydrocannabinol and other neutral cannabinoids from hashish. *J Am Chem Soc.*, *93*, 217–224.

Gassman, P. G.; Lottes, A. C. (**1992**). Cyclobutane formation in the 2π + 2π cycloaddition of allyl and related cations to unactivated olefins. Evidence for the second step in the proposed mechanism of the ionic diels-alder reaction. *Tetrahedron Lett.*, *33*, 157.

Granja A. G., Carrillo-Salinas F., Pagani A., Gómez-Cañas M., Negri R., Navarrete C., Mecha M., Mestre L., Fiebich B. L., Cantarero I., Calzado M. A., Bellido M. L., Fernandez-Ruiz J., Appendino G., Guaza C., Muñoz E. (**2012**). *JNeuroimmune Pharmacol.*, 7, 1002-1016.

Grlic, L. A comparative study on some chemical and biological characteristics of various samples of cannabis resin. United Nations Office of Drugs and Crime (**1962**). (https://www.unodc.org/unodc/en/data-and-analysis/bulletin/bulletin_1962-01-01_3_page005.html).

Hanuš, L. O.; Tchilibon, S.; Ponde, D. E.; Breuer, A.; Fride, E.; Mechoulam, R. (**2005**). Enantiomeric cannabidiol derivatives: synthesis and binding to cannabinoid receptors. *Org. Biomol. Chem.*, *3*, 1116-1123.

Hanuš L. O., Meyer S. M., Muñoz E., Taglialatela-Scafati O., Appendino G. (**2016**). Phytocannabinoids: a unified critical inventory. *Nat. Prod. Rep.*, *33*, 1357–1392.

Hart P. H., Brand C., Carson C. F., Riley T. V., Prager R. H. e Finlay-Jones J. J. (**2000**). Terpinen-4-ol, the main component of the essential oil of *Melaleuca alternifolia* (tea tree oil), suppresses inflammatory mediator production by activated human monocytes. (abstract). *Inflammation Research*, *49*, 11, Berlino, Springer.

Hazekamp A., Ruhaak R., Zuurman L., van Gerven J., Verpoorte R. (**2006**). Evaluation of a vaporizing device (Volcano®) for the pulmonary administration of tetrahydrocannabinol. *J. Pharm. Sci.*, *95*, 1308.

Hillig, K.W. (**2005**). Genetic evidence for separation in *Cannabis* (Cannabaceae). *Genet. Resour. Crop. Evol., 52*, 161-180.

Huang Y-L., Shen C-C., Shen Y-C., Chiou W-F. Chen C-C. (**2017**). Anti-inflammatory and Antiosteoporosis Flavonoids from the rhizomes of *Helminthostachys zeylanica*. *J. Nat. Prod*., *80*, 246–253.

Jacob A. and Todd A. (**1940**). Cannabidiol and Cannabol, Constituents of Cannabis indica Resin *Nature*, 350.

Jung E. J., Lee Y. R., Lee H.-J. (**2009**). Iodine-Catalyzed One-Pot Synthesis of 2H-Pyrans by Domino Knoevenagel/6π-Electrocylization *Bull. Korean Chem. Soc.*, 30, 2833.

Khanolkar A. D., Lu D., Ibrahim M., Duclos, Jr. R. I., Thakur G. A., Malan Jr. T. P., Porreca F., Veerappan V., Tian X., George C., Parrish D. A., Papahatjis D. P., Makriyannis A. (**2007**). Cannabilactones: A Novel Class of CB2 Selective Agonists with Peripheral Analgesic Activity. *J. Med. Chem.*, *50*, 6493.

Kinghorn A. D., Falk H., Gibbons S., Kobayashi J. (eds.) (**2017**). Phytocannabinoids, Progress in the Chemistry of Organic Natural Products, *103.*

Kloss F., Neuwirth T., Haensch V. G., Hertweck C. (**2018**). Metal-Free Synthesis of Pharmaceutically Important Biaryls by Photosplicing. *Angew. Chem.*, *57*, 14476.

Kogan N. M., Rabinowitz R., Levi P., Gibzon D., Sandor P., Schlesinger M., Mechoulam R. (**2004**). Synthesis and Antitumor Activity of Quinonoid Derivatives of Cannabinoids. *J. Med. Chem. 47*, 3800-3806.

Kozubek A., Tyman J. H. P. (**1999**). Resorcinolic Lipids, the Natural Non-isoprenoid Phenolic Amphiphiles and Their Biological Activity. *Chem. Rev.*, *99*, 1-26.

Kurdyumov A. V., Hsung R. P. (**2006**). An Unusual Cationic [2 + 2] Cycloaddition in a Divergent Total Synthesis of Hongoquercin A and Rhododaurichromanic Acid A *J. Am. Chem. Soc.*, *128*, 6272.

Laurence C., Graton J., Berthelot M., El Ghomari M. (**2011**). The diiodine basicity scale: toward a general halogen-bond basicity scale. *J.Chem. - Eur. J.*, *17*, 10431.

Lehrke, M., Lazar, M.A. (**2005**). The many faces of PPARgamma. *Cell*, 123, 993-999.

Lerner, P. (**1969**). The precise determination of tetrahydrocannabinol in marihuana and hasish. *Bull. Narcotics*, *21*, 39.

Li X., Lee Y. R. (**2014**). Efficient and novel one-pot synthesis of polycycles bearing cyclols by $FeCl_3$-promoted [2 + 2] cycloaddition: application to cannabicyclol, cannabicyclovarin, and ranhuadujuanine A. *Org. Biomol. Chem.*, *12*, 1250.

Linciano P., Citti C., Luongo L., Belardo C., Maione S., Vandelli M. A, Forni F., Gigli G.,. Laganà A, Montone C. M. and Cannazza G. (**2019**). Isolation of a High-Affinity Cannabinoid for the Human CB_1 Receptor from a Medicinal Cannabis sativa Variety: Δ^9-Tetrahydrocannabutol, the Butyl Homologue of Δ^9-Tetrahydrocannabinol. *J. Nat. Prod., in press*.

Makriyannis, A. & Rapaka, R.S. (**1987**). The medicinal chemistry of cannabinoids: an overview. *NIDA Res. Monogr*. 79, 204–210.

Mayer M., Meyer B. (**1999**). Characterization of Ligand Binding by Saturation Transfer Difference NMR Spectroscopy. *Angew Chem Int*, *38*, 1784-1788.

Mechoulam R. and Shvo Y. (**1963**). Hashish—I : The structure of Cannabidiol. *Tetrahedron*, *19*, 2073–2078.

Mechoulam, R.; Ben-Zvi, Z.; Gaoni, Y. (**1968**). Hashish—XIII : On the nature of the beam test. *Tetrahedron*, 5615-5624.

Mechoulam R., Yagen B. (**1969**). Stereoselective cyclizations of cannabinoid 1,5 dienes. *Tetrahedron Lett.*, *10*, 5349–5352.

Meltzer, P. C., Dalzell, H. C., Razdan, R. K. (**1981**). An Improved Synthesis of Cannabinol and Cannabiorcol. *Synthesis*, 985.

Mills, J. H. Cannabis Britannica: Empire, Trade, and Prohibition 1800−1928; Oxford University Press: Oxford, (**2005**). Montell C., Birnbaumer L., Flockerzi V. (**2002**). *Cell.,108*, 595–598.

Morales, P., Vara, D., Goméz-Cañas, M., Zúñiga, M.C., Olea-Azar, C., Goya, P., Fernández-Ruiz, J., Díaz-Laviada, I., Jagerovic, N. (**2013**). Synthetic cannabinoid quinones: preparation, in vitro antiproliferative effects and in vivo prostate antitumor activity. *Eur J Med Chem*., *70*, 111-119.

Nicolaou K. C., Montagnon T., Baran P. S., Zhong Y.-L. (**2002**). Iodine(V) Reagents in Organic Synthesis. Part 4. o-Iodoxybenzoic Acid as a Chemospecific Tool for Single Electron Transfer-Based Oxidation Processes *J. Am. Chem. Soc.*, *124,* 2245–2258.

O'Sullivan, S.E., Kendall, D.A. (**2010**). Cannabinoid activation of peroxisome proliferator-activated receptors: potential for modulation of inflammatory disease. *Immunobiology*, *215*, 611-616.

Ozanne, A.; Pouységu, L.; Depernet, D.; Bruno, F.; Quideau, S. (**2003**). A Stabilized Formulation of IBX (SIBX) for Safe Oxidation Reactions Including a New Oxidative Demethylation of Phenolic Methyl Aryl Ethers. *Org Lett.*, *5*, 2903-2906. The use of SIBX for the telescoped synthesis of aminoderivatives of cannabinoquinoids was previously disclosed in the proprietary literature: Appendino G., Cabello de Alba M. L. B., Muñoz, E. WO2015/158381.

Parvatkar P. T., Parameswaran P. S., Tilve S. G. (**2012**). Recent Developments in the Synthesis of Five- and Six-Membered Heterocycles Using Molecular Iodine. *Chem. Eur. J.*, *18*, 5460–5489.

Pereira, A.; Pfeifer, TA.; Grigliatti, TA.; Andersen, RJ. (**2009**). Functional cell-based screening and saturation transfer double-difference NMR have identified haplosamate A as a cannabinoid receptor agonist. *ACS Chem Biol*, *4*, 139-144.

Pertwee, R.G., Howlett, A.C., Abood, M.E., Alexander, S.P., Di Marzo, V., Elphick, M.R., Greasley, P.J., Hansen, H.S., Kunos, G., Mackie, K., Mechoulam, R., Ross, R.A. (**2010**). International Union of Basic and Clinical Pharmacology. LXXIX. Cannabinoid receptors and their ligands: beyond CB_1 and CB_2. *Pharmacol Rev., 62*, 588-631

Peters M., Kogan N. M. (**2007**). HU-331: a cannabinoid quinone, with uncommon cytotoxic properties and low toxicity. *Expert Opin. Investig. Drugs*, *16*, 1405-1413.

Pollastro F., De Petrocellis L., Schiano-Moriello A., Chianese G., Heyman H., Appendino G., Taglialatela-Scafarti O. (**2017**). Amorfrutin-type phytocannabinoids from *Helichrysum umbraculigerum*. *Fitoterapia*, *123*, 13–17.

a) Pollastro F., Caprioglio D., Del Prete D., Rogati F., Minassi A., Taglialatela-Scafati O., Minoz E. and Appendino G. (**2018**) Cannabichromene. *Natural Product Communications, 13*, 1189-1194.

b) Pollastro F., Caprioglio D., Marotta P., Schiano Moriello A., De Petrocellis L., Taglialatela-Scafati O. and Appendino G. (**2018**). Iodine-promoted aromatization of *p*-menthane-type phytocannabinoids. *J. Nat. Prod*, *81*, 630−633.

Qureshi M. N., Kanwal F., Siddique M., Rahman I.-U. and Akram M. (**2012**). Estimation of Biologically Active Cannabinoids in Cannabis indica by Gas Chromatography-mass Spectrometry (GC-MS). *World Appl. Sci. J.*, *19*, 918–923.

Radwan M. M., ElSohly M. A., Slade D., Ahmed S. A., Khan I. A., Ross S. A. (**2009**). Biologically Active Cannabinoids from High-Potency *Cannabis sativa*. *J. Nat. Prod.*, *72*, 906-911.

Ramer R., Heinemann K., Merkord J., Rohde H., Salamon A., Linnebacher M., Hinz B. (**2013**). COX-2 and PPAR-γ confer cannabidiol-induced apoptosis of human lung cancer cells. *Mol Cancer Ther.*, *12*, 69-82.

Reekie T. A., Scott M. P. and Kassiou M. (**2017**). The evolving science of Phytocannabinoids. *Nature Reviews, Chemistry, 2*, article number 0101.

Regal K. M., Mercer S. L., Dewessee J. E. (**2014**). HU-331 is a catalytic inhibitor of topoisomerase IIα. *Chem. Res. Toxicol.*, *27*, 2044-2051.

Riveira M. J., La-Venia A., Mischne M. P. (**2016**). Pericyclic Cascade toward Isochromenes: Application to the Synthesis of Alkaloid Benzosimuline. *J. Org. Chem.*, *81*, 7977−7983.

Roberts R. M., Landolt R. G., Greene R. N., Heyer E. W. (**1967**). Enolene Rearrangements. Relationship to the “Abnormal Claisen Rearrangement” and Other 1,5-Hydrogen Shift Processes *J. Am. Chem. Soc.*1404.

Ross S. A., Radwan M. M., El-Alfy A. T., Manly S. P., Ahmed S. A., Slade D., Eslinger A., Wilson L., Seale S., Dale O., Cutler S., Khan I. A. and ElSohly M. M. (**2010**). 20th Annual Symposium of the International Cannabinoid Research Society, Research Triangle Park, NC, USA, pp. P4–21.

Šantavý F. (**1964**). Notes on the structure of cannabidiol compounds. Acta Univ. Palacki. Olomuc., *Fac. Med.*, *35*, 5–9.

Schafroth M. A. and Carreira E. M. (**2017**). Synthesis of Phytocannabinoids - © Springer International Publishing Switzerland.

Schafroth M. A., Zuccarello G., Krautwald S., Sarlah D. and Carreira E. M. (**2014**). Stereodivergent total synthesis of Δ^9-tetrahydrocannabinols. *Angew. Chem.*, *Int. Ed.*, *53*, 13898–13901.

Shoyama Y., Hirano H., Oda M., Somehara T., Nishioka I. (**1975**). Cannabis. IX. Cannabichromevarin and cannabigerovarin, two new propyl homologs of cannabichromene and cannabigerol. *Chem. Pharm. Bull.*, *23*, 1894-5.

Sladek, F.M. (**2011**). What are nuclear receptor ligands? *Mol Cell Endocrinol. 334*, 3-13.

Takehira K., Shimizu M., Watanabe Y., Orita H., Hayakawa T. (**1989**). A novel synthesis of trimethyl-p-benzoquinone: copper(II)–hydroxylamine catalysed oxygenation of 2,3,6-trimethylphenol with dioxygen*J. Chem. Soc.*, *Chem. Commun.*, 1705-1706.

Takehira K., Shimizu M., Watanabe Y., Orita H., Hayakawa T. (**1989**). A novel oxygenation of 2,3,6-trimethylphenol to trimethyl-p-benzoquinone by dioxygen with copper(II) chloride/amine hydrochloride catalyst. *Tetrahedron Lett.*, *30*, 6691-6692.

Taglialatela-Scafati O., Pagani A., Scala F., De Petrocellis L., Di Marzo V., Grassi G., Appendino G. (**2010**). Cannabimovone, a cannabinoid with a rearranged terpeni skeleton from hemp. *Eur. J. Org. Chem., 11*, 2067–2072

Tsagareli M. G. and Nozadze I. (**2019**). An overview on TRP channels. *Behavioural Pharmacology*, *in press*.

Taura F., Morimoto S., Shoyama Y. (**1995**). Cannabinerolic acid, a cannabinoid from *Cannabis sativa*. *Phytochemistry*, *39*, 457-458.

Taylor E. C., Lenard K. and Shvo Y. (**1966**). Active Constituents of Hashish. Synthesis of dl-Δ^6-3,4-trans-Tetrahydrocannabinol. *J. Am. Chem. Soc.*, *88*, 367–369.

Usami N., Yamamoto I., Watanabe K. (**2008**). Generation of reactive oxygen species during mouse hepatic microsomal metabolism of cannabidiol and cannabidiol hydroxy-quinone. *Life Sci.*, *83 (21-22)*, 717-724.

Valdeolivas, S., Navarrete, C., Cantarero, I., Bellido, M.L., Muñoz, E., Sagredo, O. (**2015**). Neuroprotective Properties of Cannabigerol in Huntington's Disease: Studies in R6/2 Mice and 3-Nitropropionate-lesioned Mice. *Neurotherapeutics, 12*, 185-199.

Vemuri V. K. and Makriyannis A. (**2015**). Medicinal Chemistry of Cannabinoids. *Clinical Pharmacology & Therapeutics, 97.*

Wang M., Wang Y.-H., Avula B., Radwan M. M., Wanas A. S., van Antwerp J., Parcher J. F., ElSohly M. A., Khan I. A. (**2016**). Cannabis Cannabinoid Res., *1*, 262.

Watanabe K., Usami N., Yamamoto I., Yoshimura H. (**1991**). Inhibitory effect of cannabidiol hydroxy-quinone, an oxidative product of cannabidiol, on the hepatic microsomal drug-metabolizing enzymes of mice. *J Pharmacobiodyn*, *14(7)*, 421-427.

Willson T.M., Brown P.J., Sternbach D.D., Henke B.R. (**2000**). The PPARs: from orphan receptors to drug discovery. *J Med Chem.*, *43*, 527-550.

Wood T. B., Spivey W. T. N., Easterfield T. H. (**1896**). XL.—Charas. The resin of Indian hemp. *J. Chem. Soc.*, *69*, 539-546.

Yagen B., Mechoulam R. (**1969**). Modern numbering would locate the double bond at C-11, and the name iso-THC is, nevertheless, confusing. *Tetrahedron Lett.*, *10*, 5353.

Yeom H.-S., Li H., Tang Y., Hsung R. P. (**2013**). Total Syntheses of Cannabicyclol, Clusiacyclol A and B, Iso-Eriobrucinol A and B, and Eriobrucinol *Org. Lett.*, *15*, 3130.

Yoder R. A., Johnston J. N. (**2005**). A Case Study in Biomimetic Total Synthesis: Polyolefin Carbocyclizations to Terpenes and Steroids. *Chem. Rev.*, *105*, 4730–4756.

Zias J., Stark H., Seligman J., Levy R., Werker E., Breuer A. and Mechoulam R. (**1993**). Early medical use of cannabis. *Nature*, *363*, 215.

Zulfiqar F., Ross S. A., Slade D., Ahmed S. A., Radwan M. M., Ali Z., Khan I. A., and ElSohly M. A. (**2012**). Cannabisol, a Novel Δ^9-THC dimer possessing a unique methylene bridge, isolated from *Cannabis sativa*. *Tetrahedron Letters, 53,* 3560-3562.

Appendix B: Spectral data of chapter 3

^{1}H NMR spectrum (700 MHz) of compound **5a** (CD_3OD).

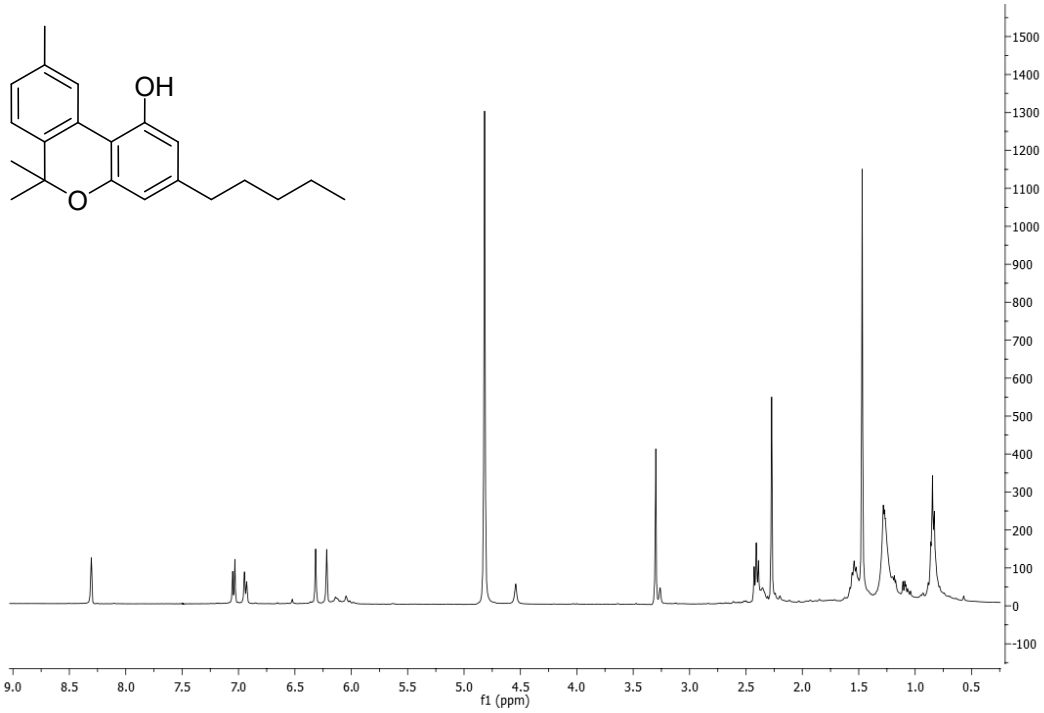

COSY spectrum (500 MHz) of **5a** (CD_3OD).

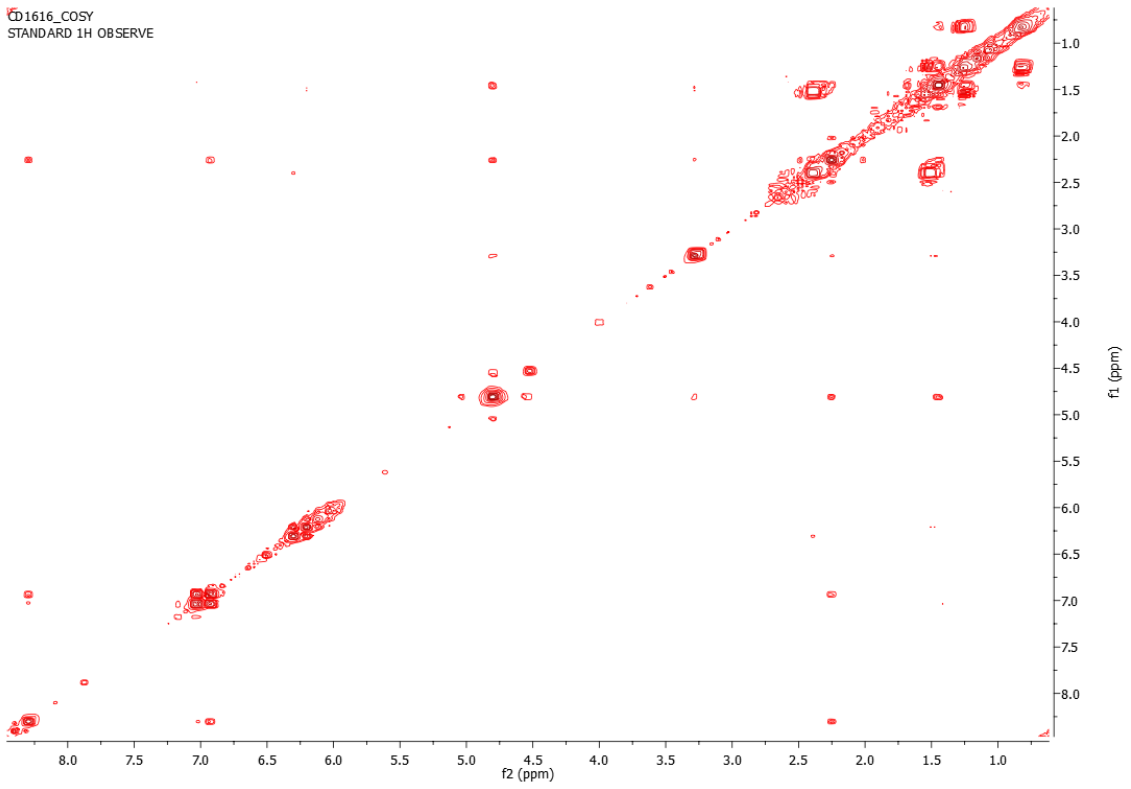

HMBC spectrum (500 MHz) of **5a** (CD_3OD).

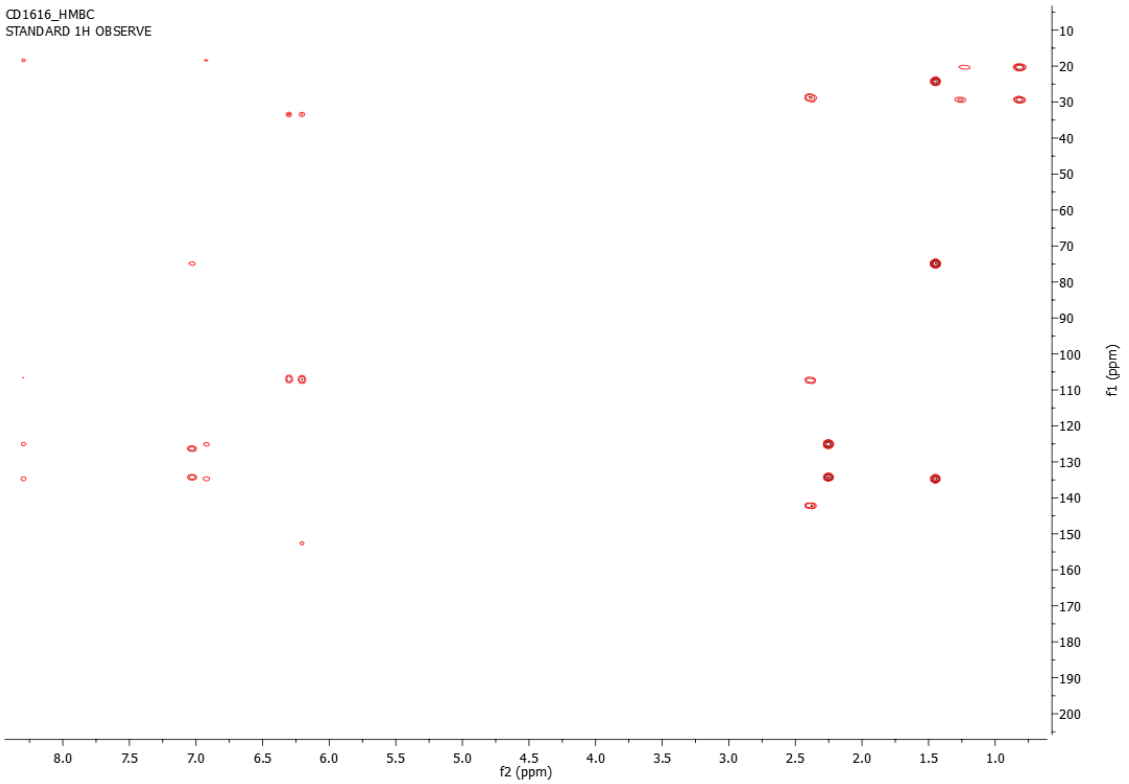

HSQC spectrum (500 MHz) of **5a** (CD_3OD).

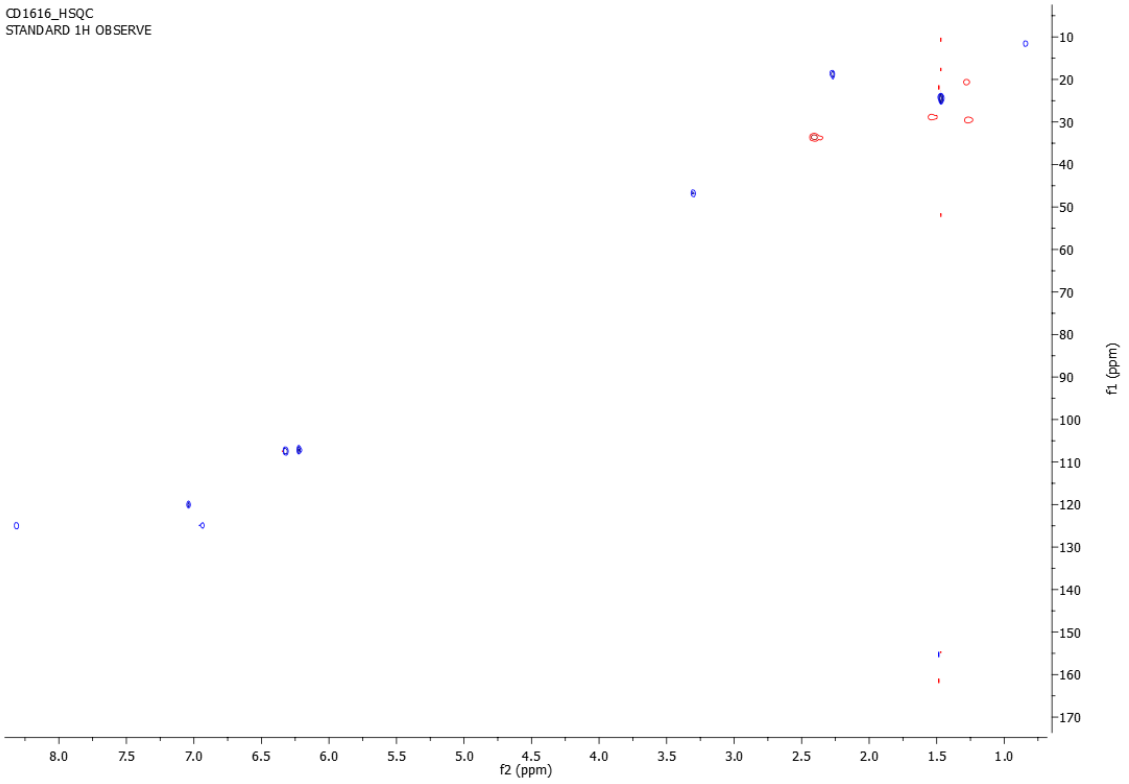

^{1}H NMR spectrum (500 MHz) of **6a** ($CDCl_3$).

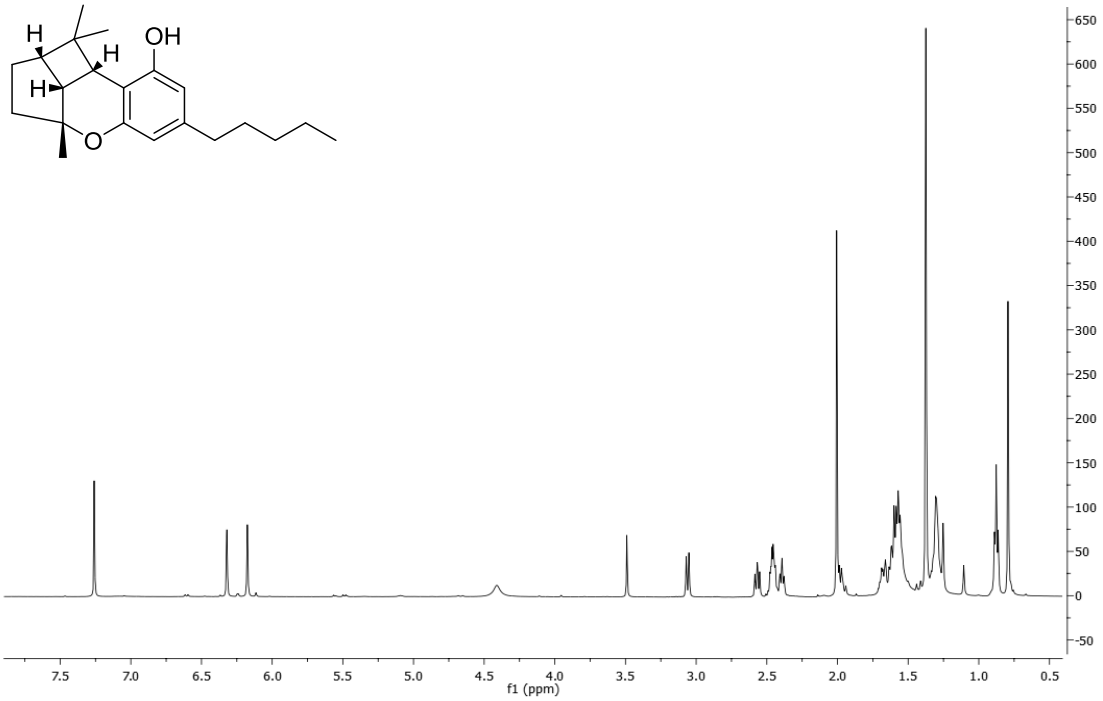

^{1}H NMR spectrum (700 MHz) of **8** (CD_3OD).

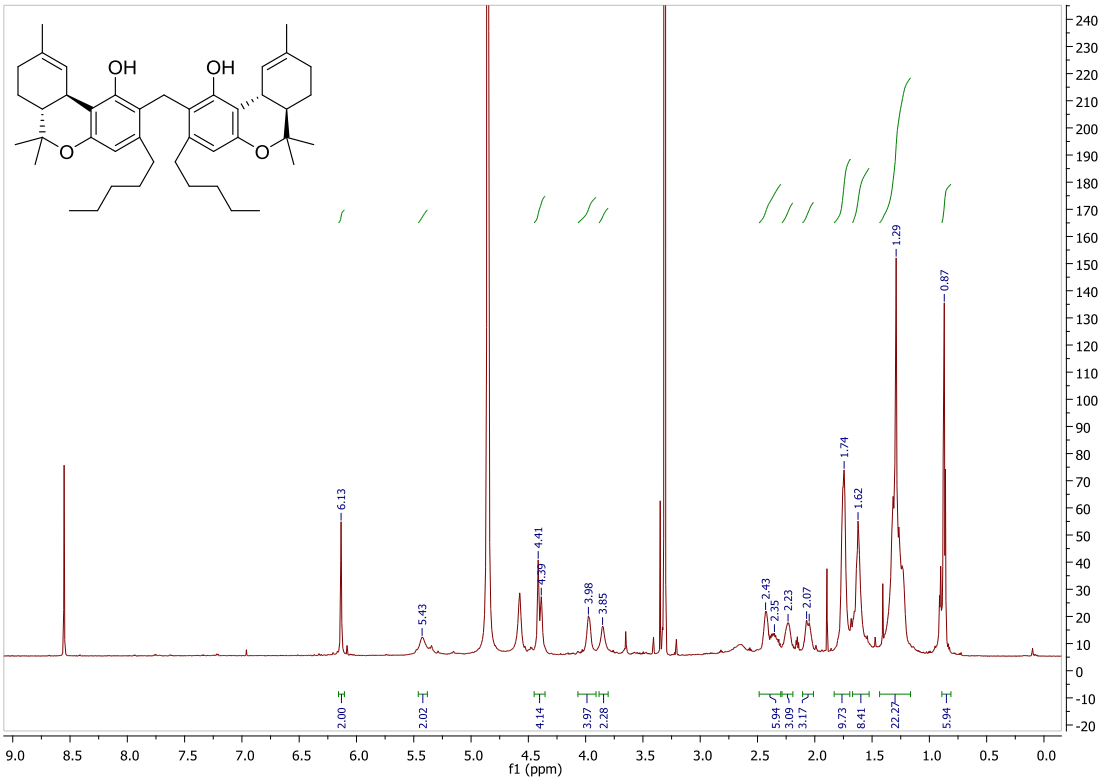

HSQC spectrum (700 MHz) of **8** (CD_3OD).

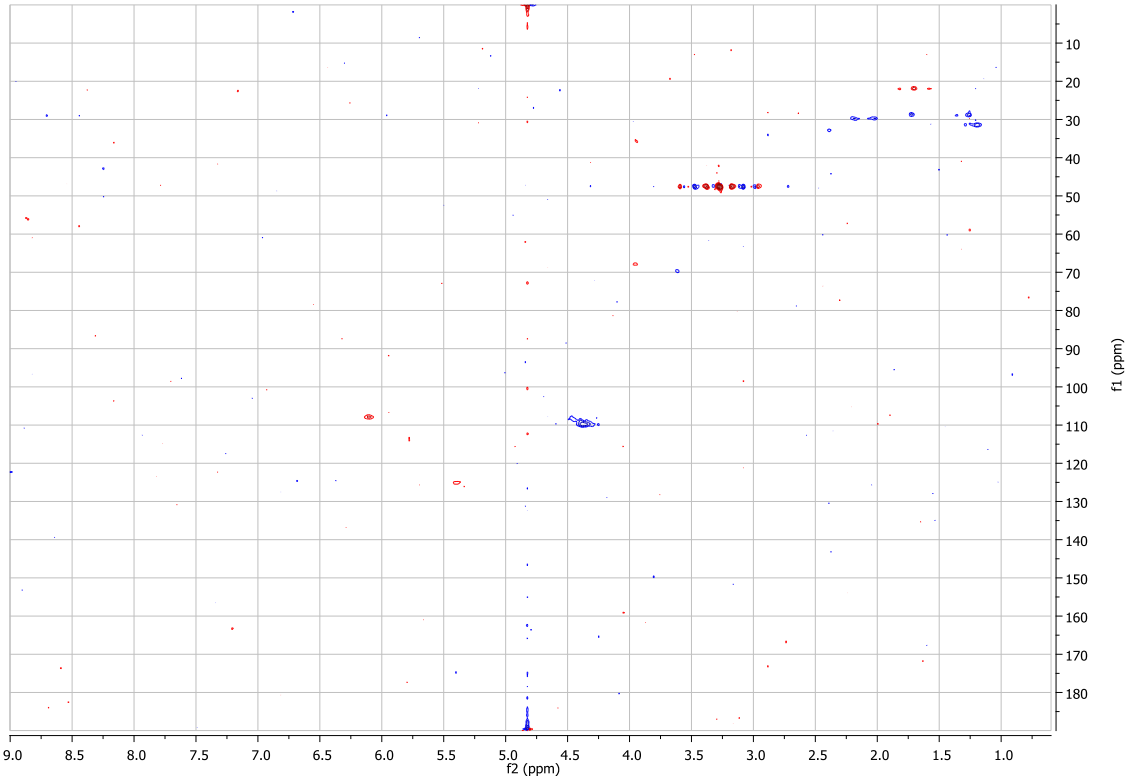

ROESY spectrum (700 MHz) of **8** (CD_3OD).

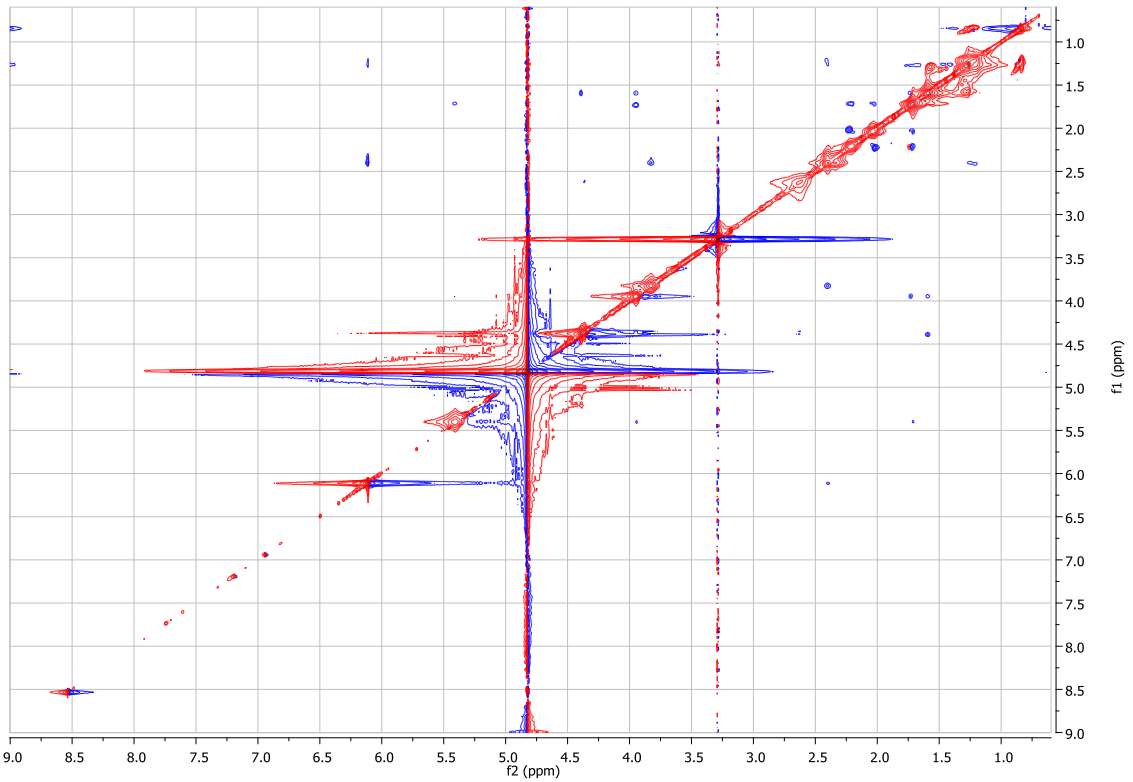

^{1}H NMR spectrum (500 MHz) of **9a** (CD_3OD).

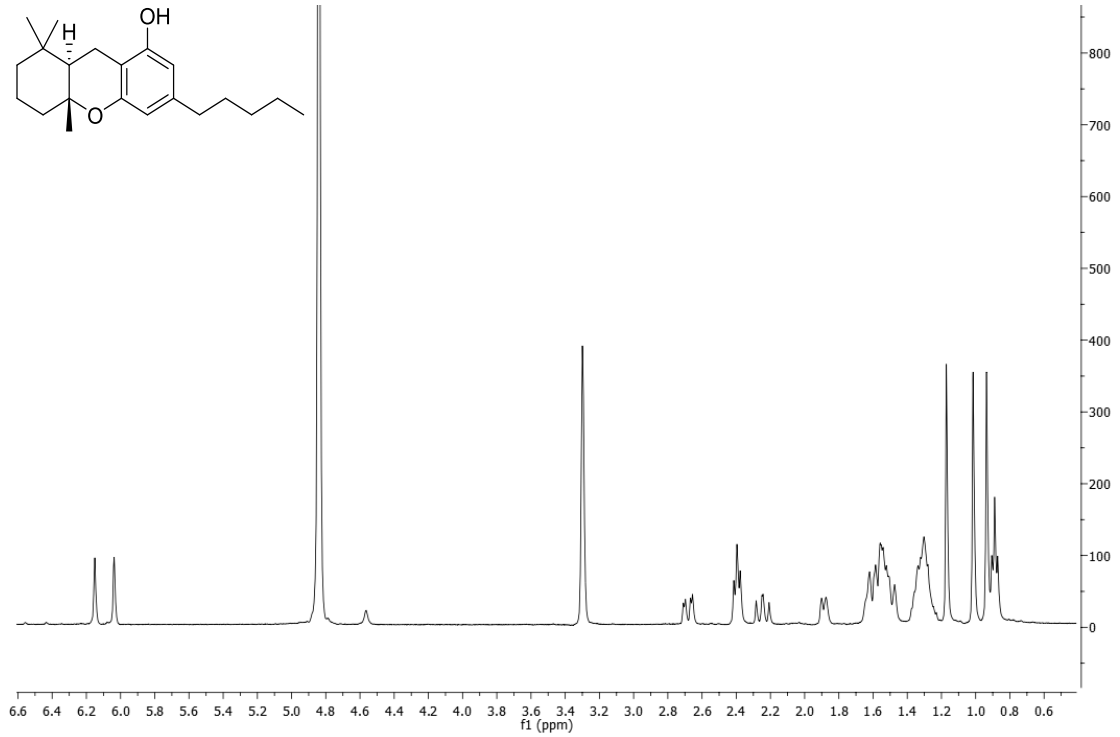

^{1}H NMR spectrum (500 MHz) of **9b** (CD_3OD).

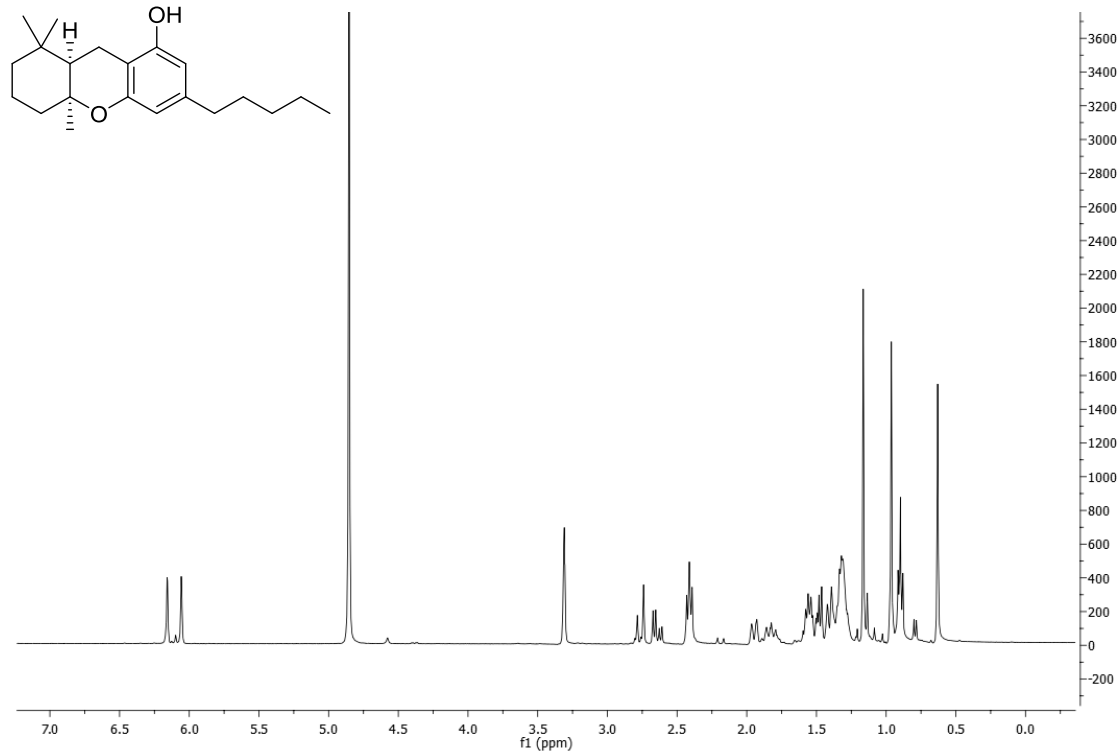

COSY spectrum (500 MHz) of **9b** (CD_3OD).

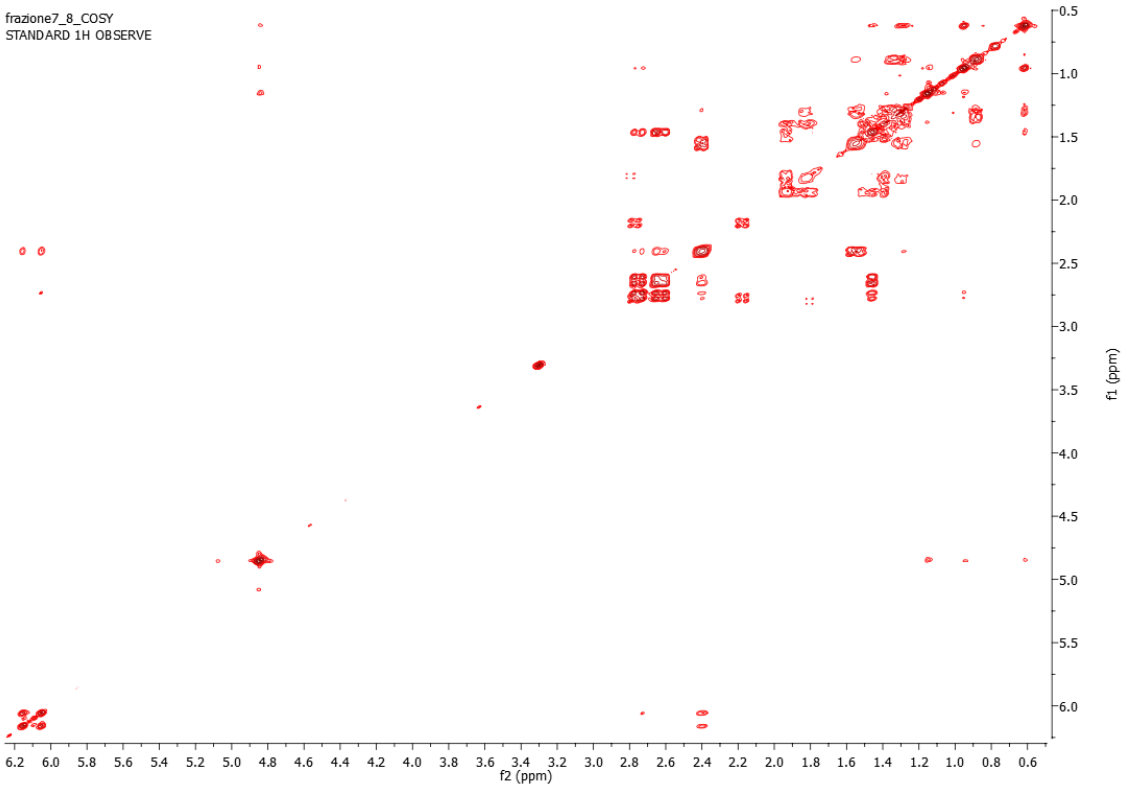

HMBC spectrum (500 MHz) of **9b** (CD_3OD).

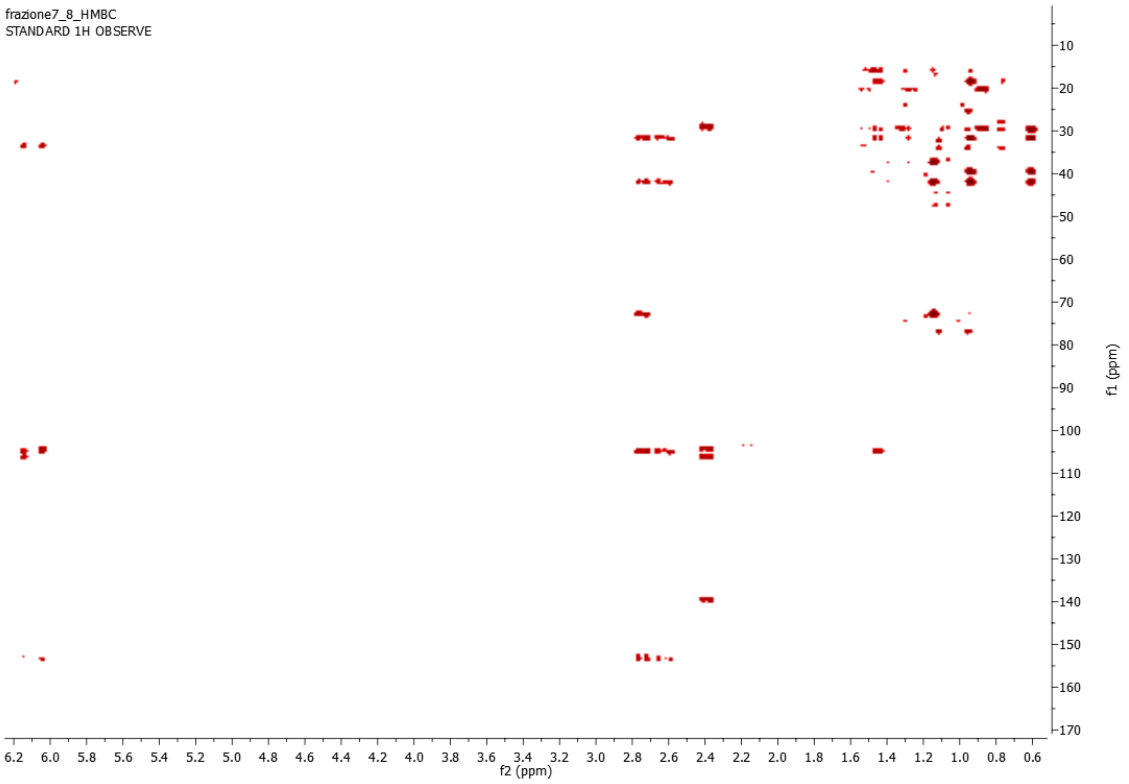

HSQC spectrum (500 MHz) of **9b** (CD_3OD).

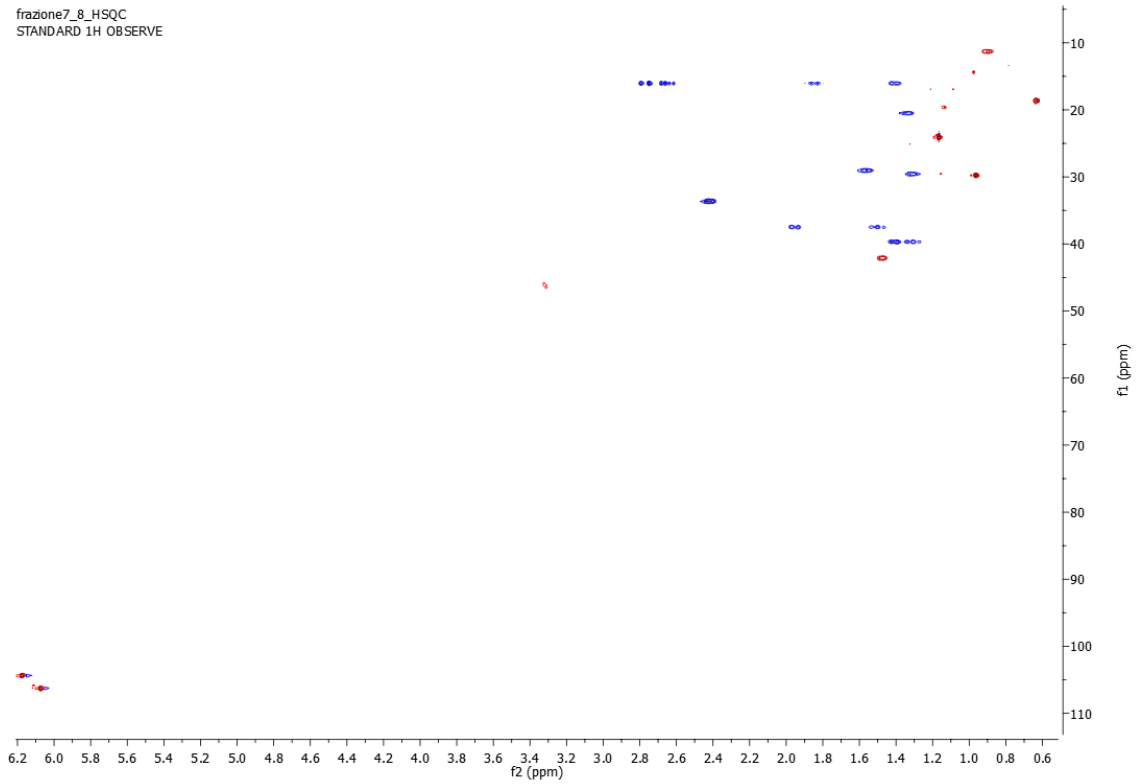

^{1}H NMR spectrum (500 MHz) of **10** (CD_3OD).

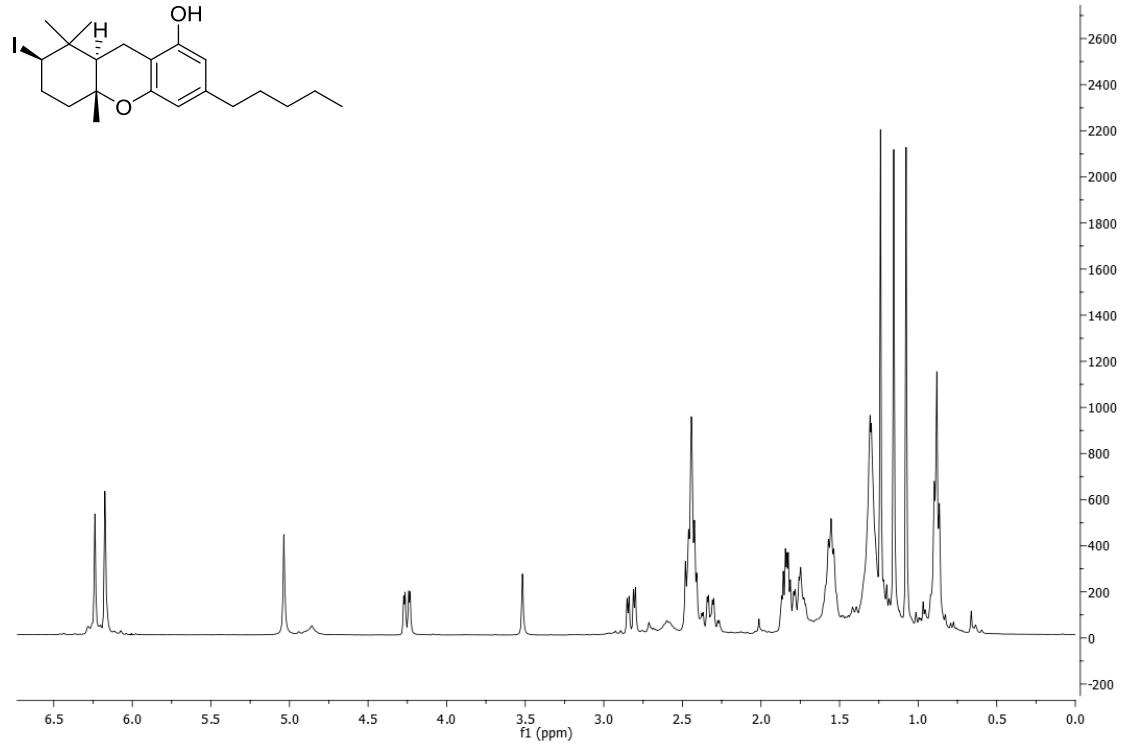

COSY spectrum (500 MHz) of **10** (CD_3OD).

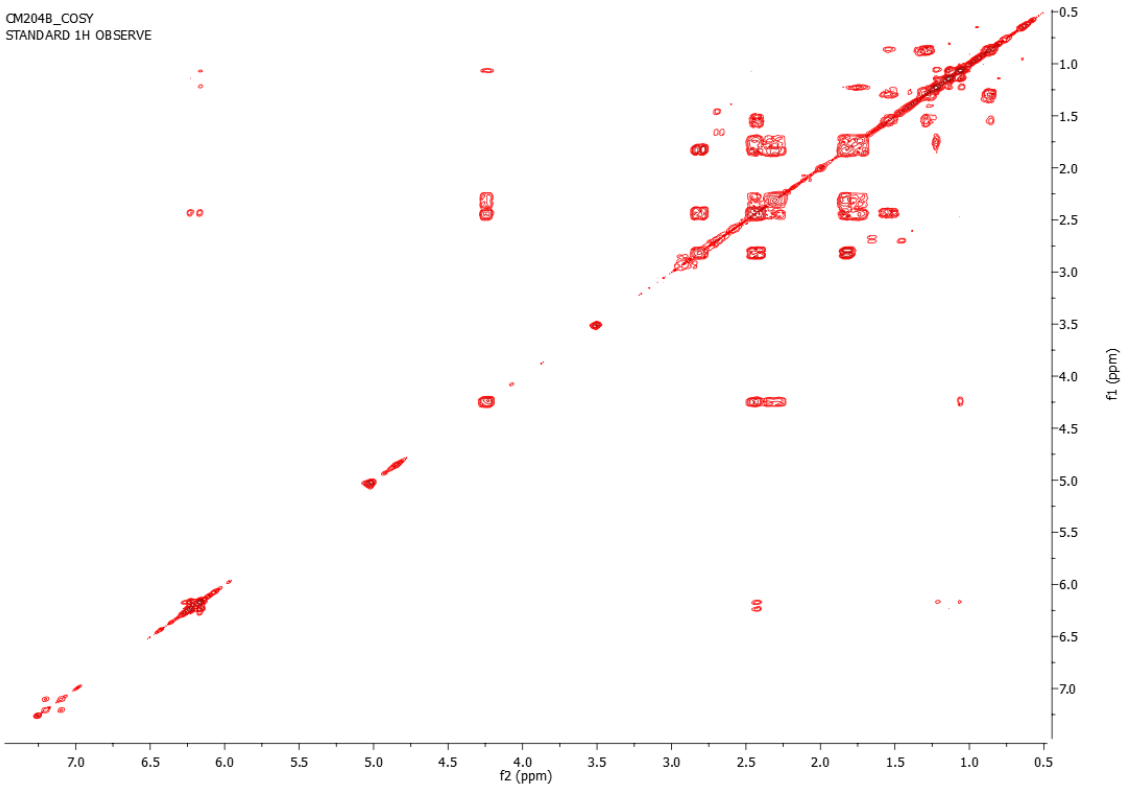

HMBC spectrum (500 MHz) of **10** (CD_3OD).

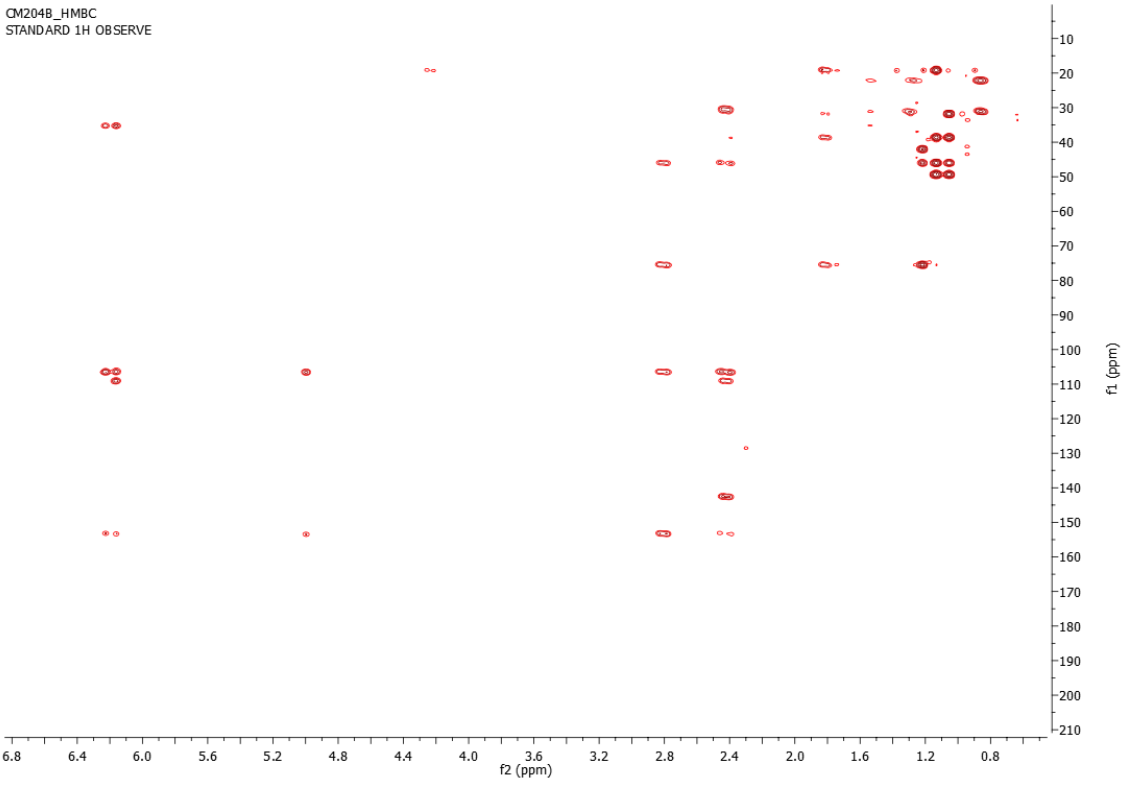

HSQC spectrum (500 MHz) of **10** (CD_3OD).

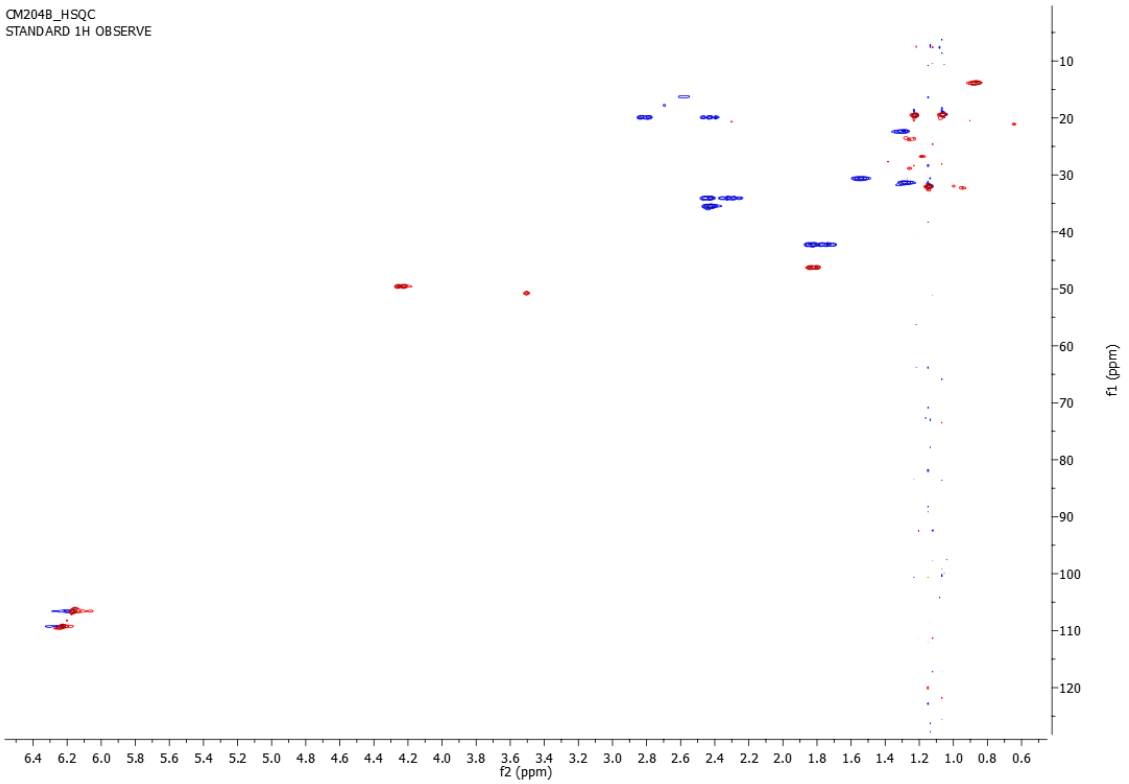

^1H NMR spectrum (500 MHz) of **11a** (CD_3OD).

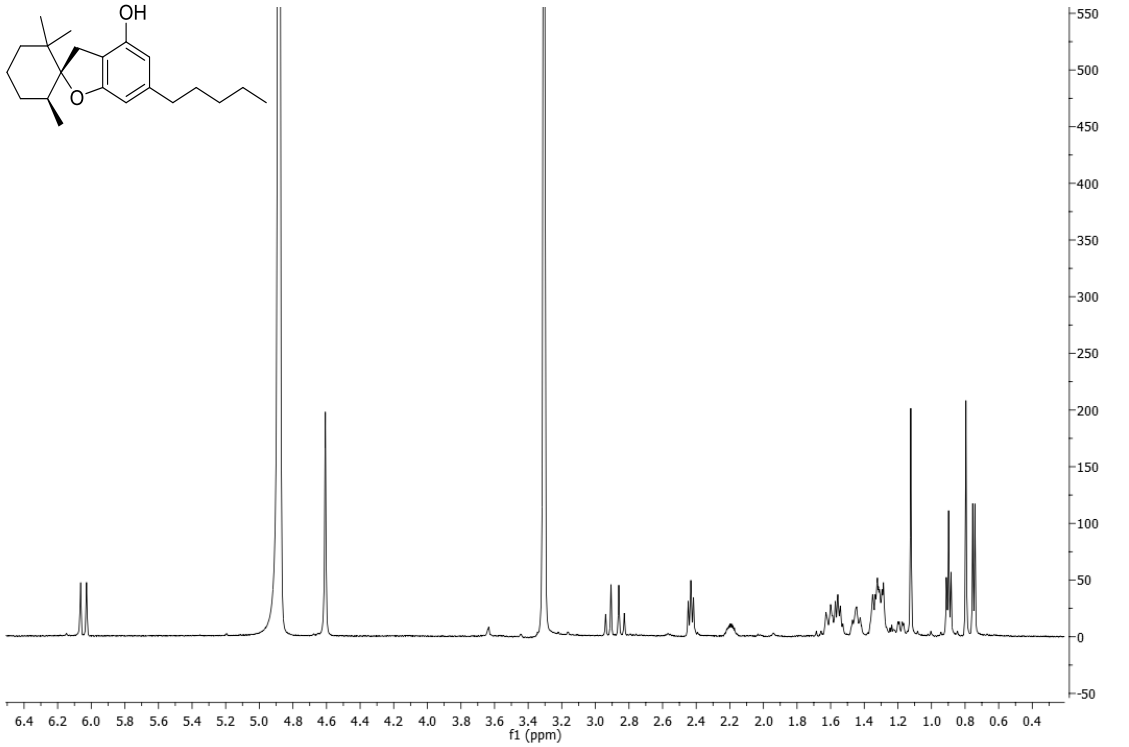

^{1}H NMR spectrum (500 MHz) of **11b** (CD_3OD).

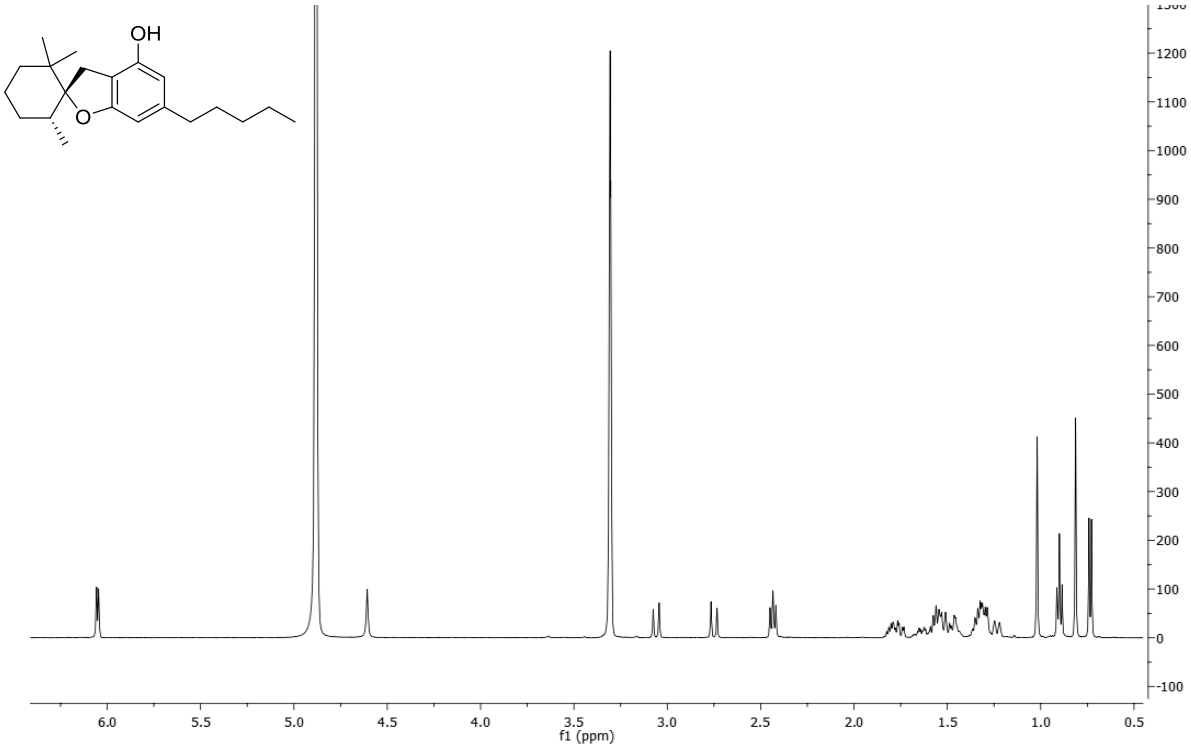

COSY spectrum (500 MHz) of **11b** (CD_3OD).

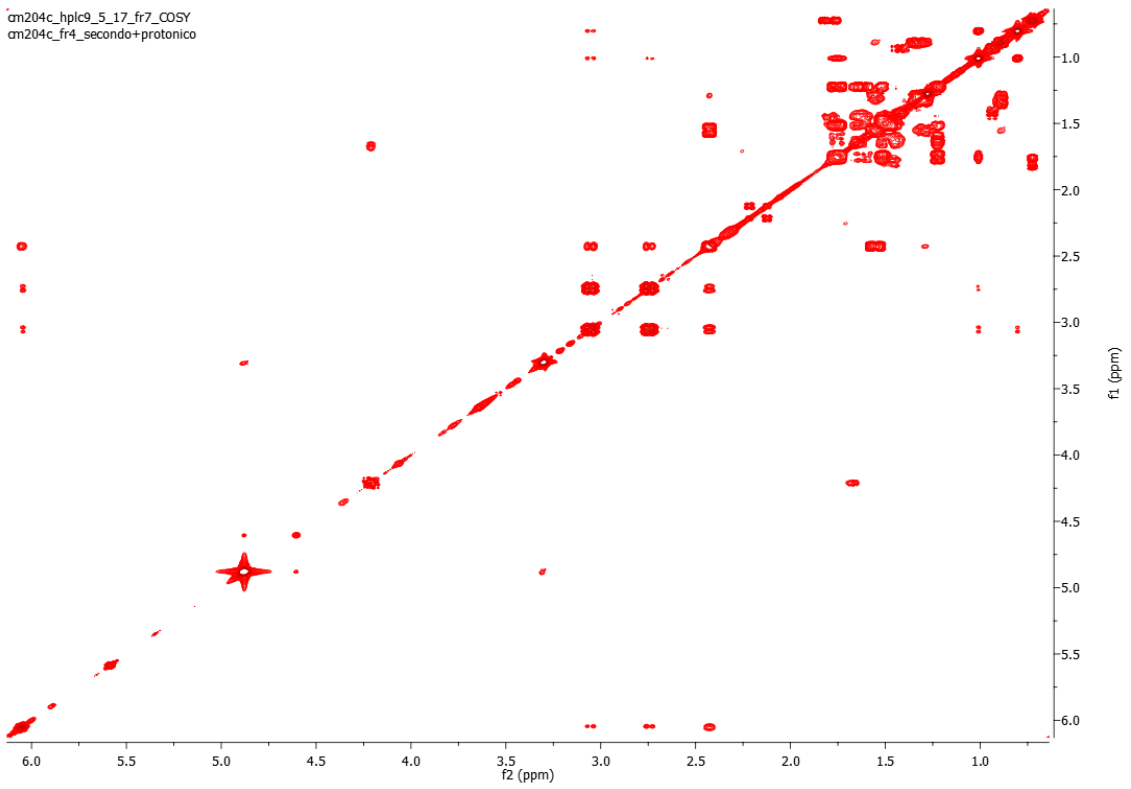

HMBC spectrum (500 MHz) of **11b** (CD_3OD).

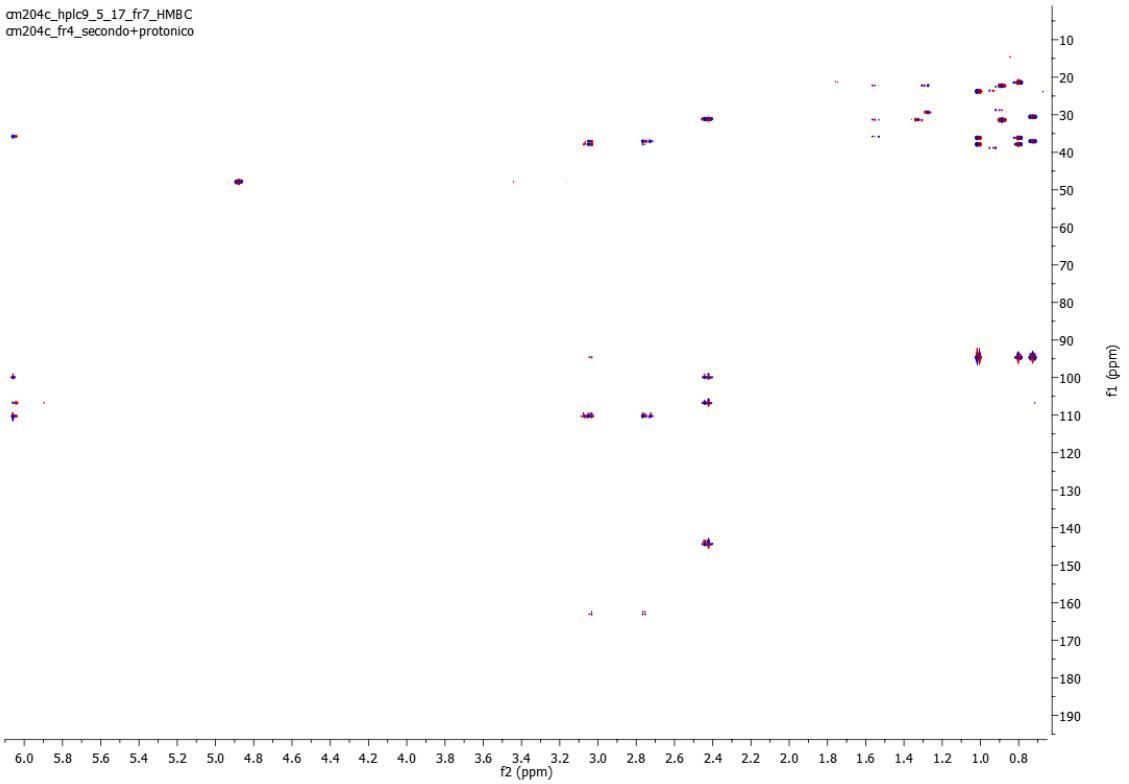

HSQC spectrum (500 MHz) of **11b** (CD_3OD).

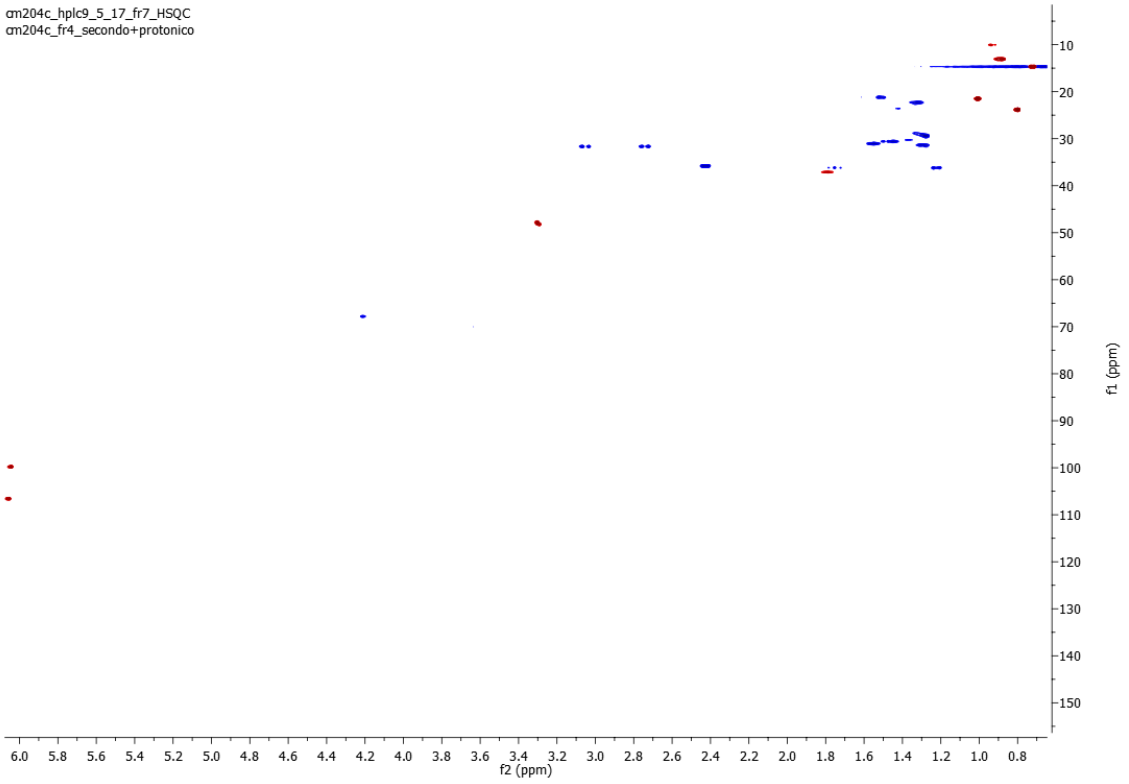

^{1}H NMR spectrum (500 MHz) of **12** (CD_3OD).

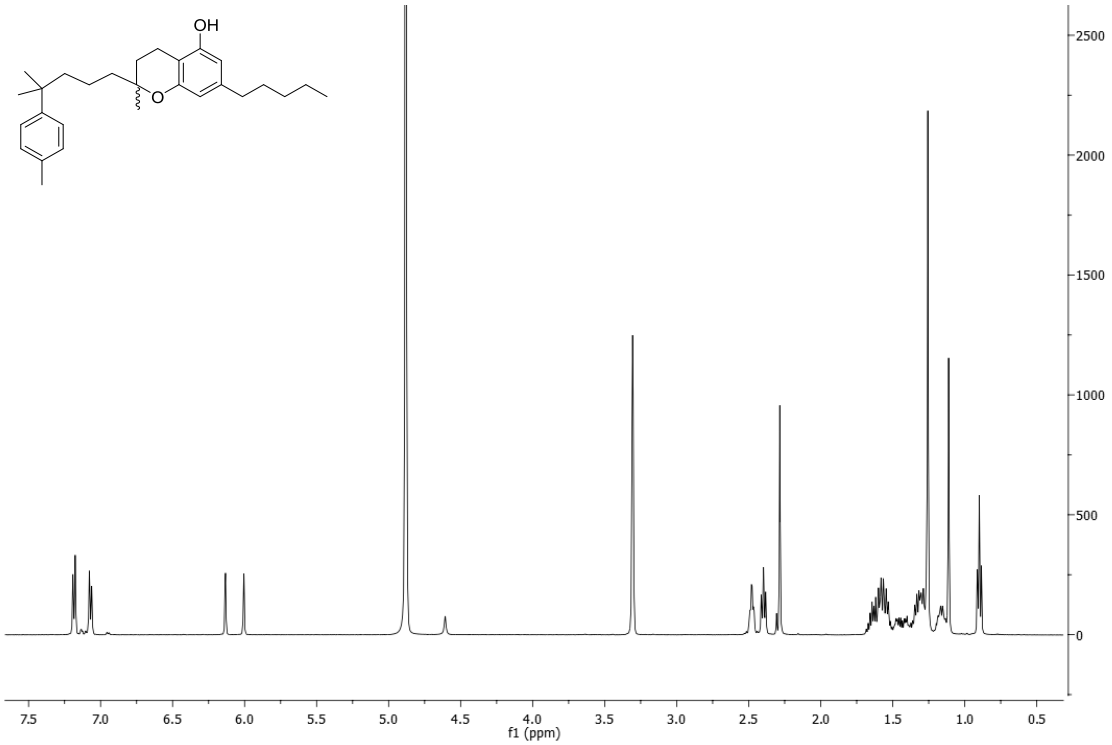

COSY spectrum (500 MHz) of **12** (CD_3OD).

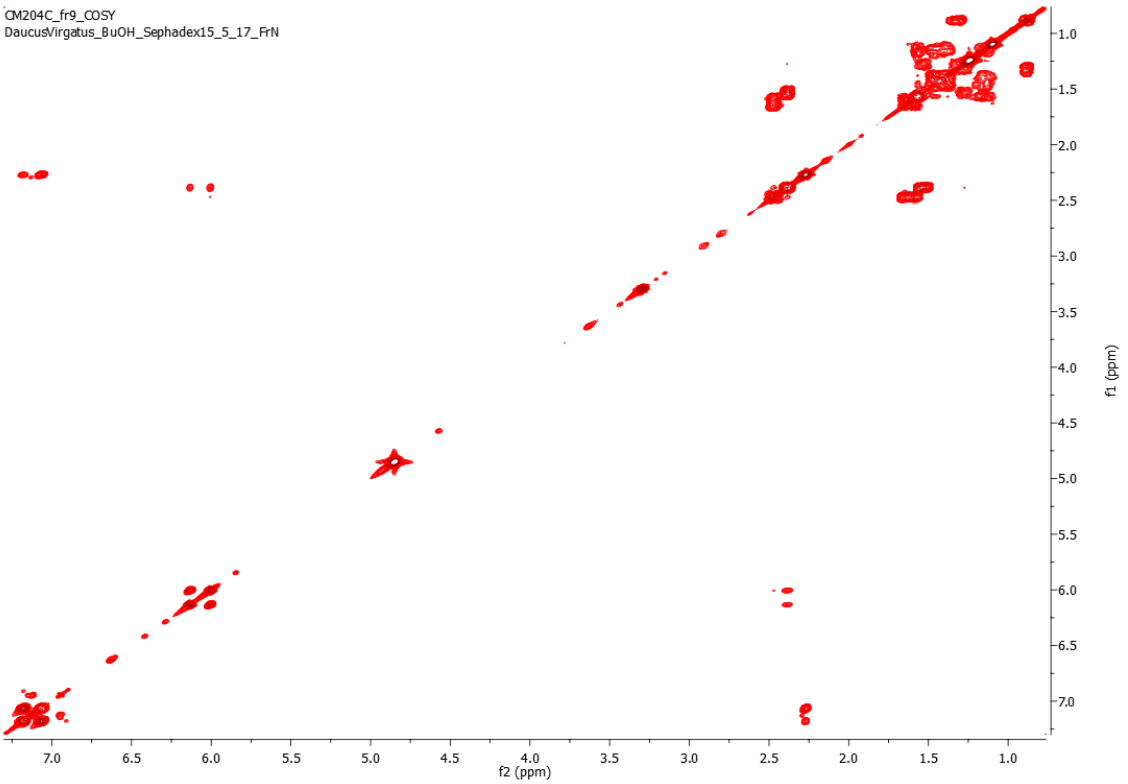

HMBC spectrum (500 MHz) of **12** (CD_3OD).

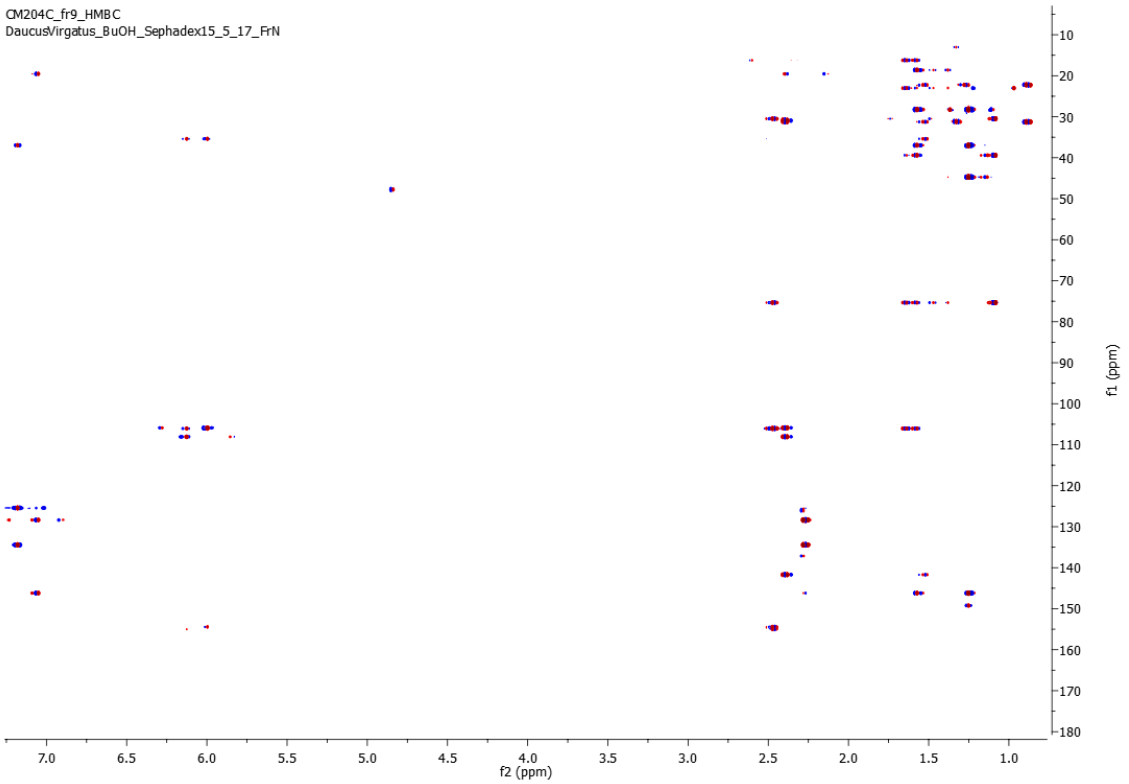

HSQC spectrum (500 MHz) of **12** (CD_3OD).

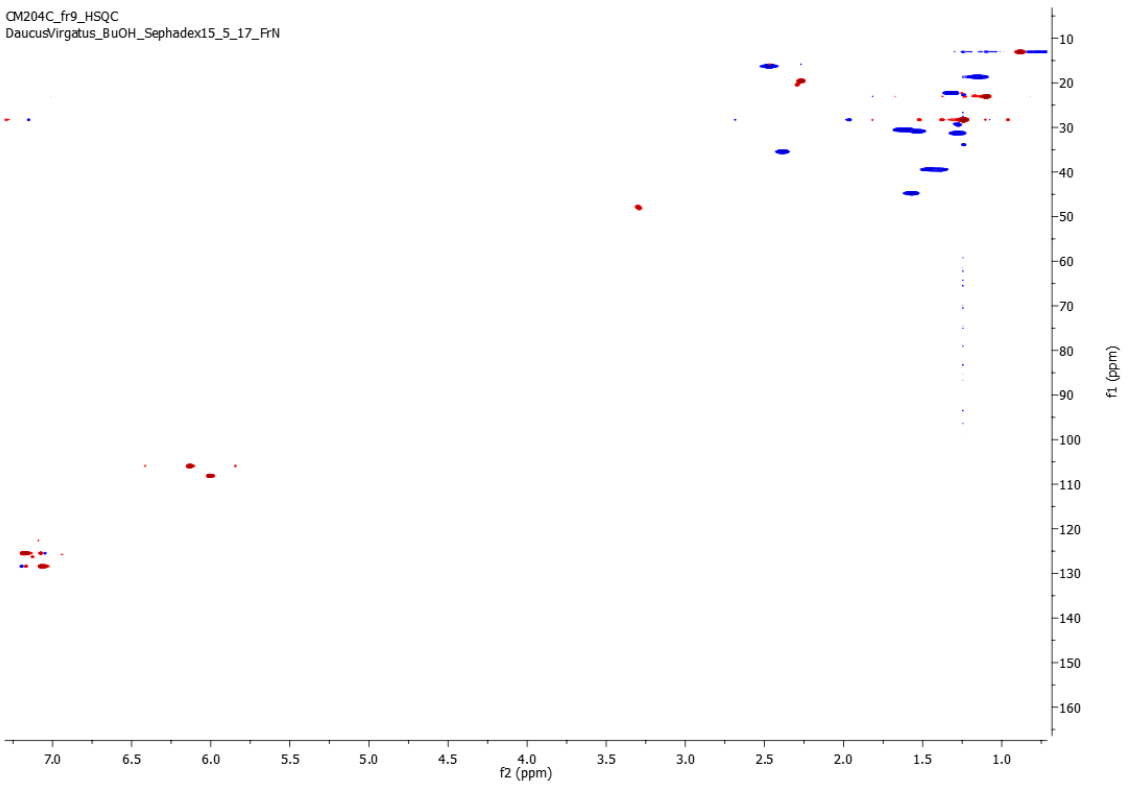

^{1}H NMR spectrum (500 MHz) of **17** ($CDCl_3$).

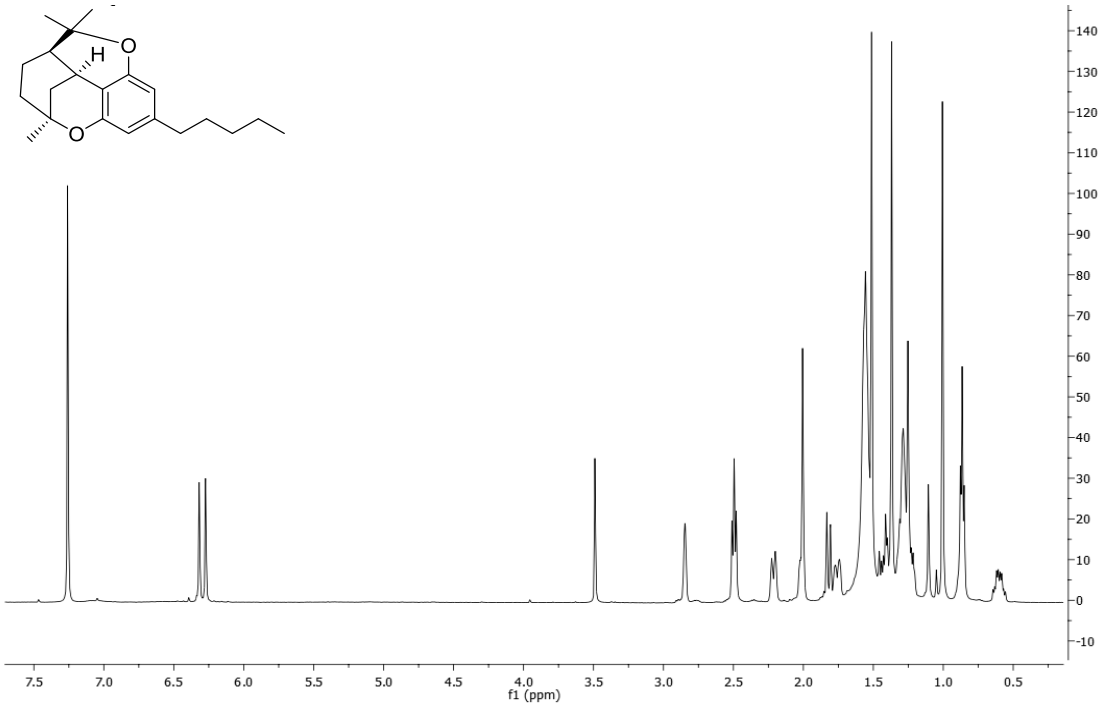

^{1}H NMR spectrum (500 MHz) of **18** ($CDCl_3$).

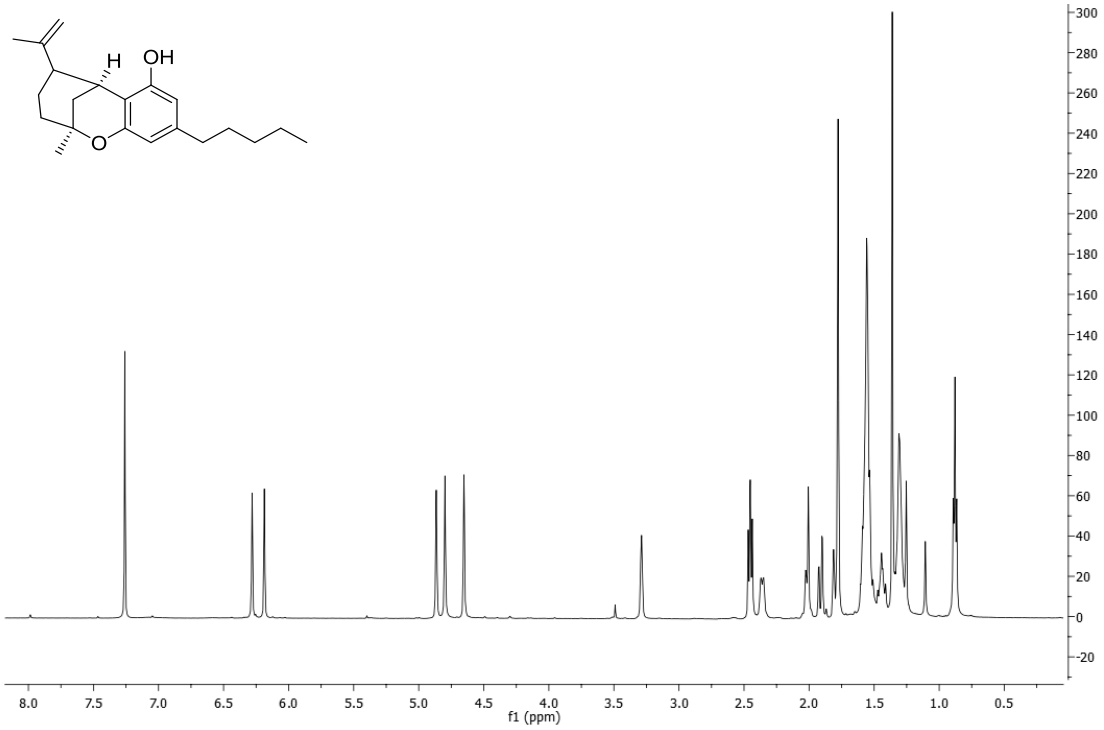

^{1}H NMR spectrum (700 MHz) of **27** (CD_3OD).

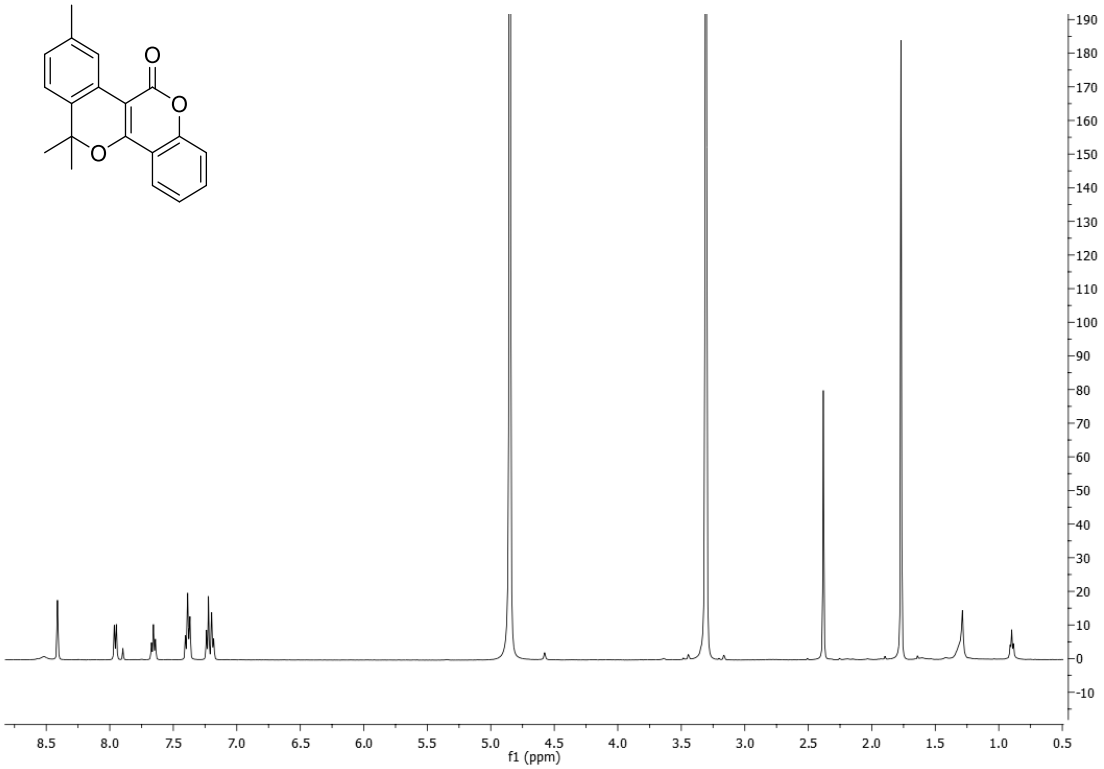

^{1}H NMR spectrum (700 MHz) of **28a** (CD_3OD).

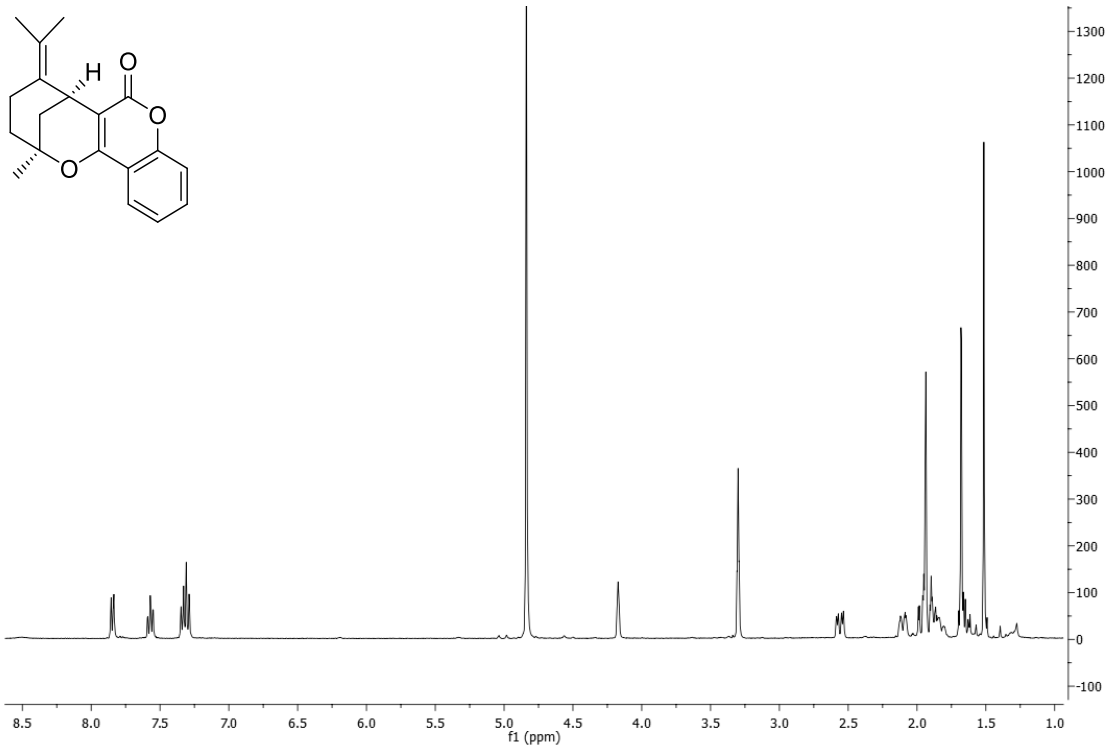

COSY spectrum (500 MHz) of **28a** (CD_3OD).

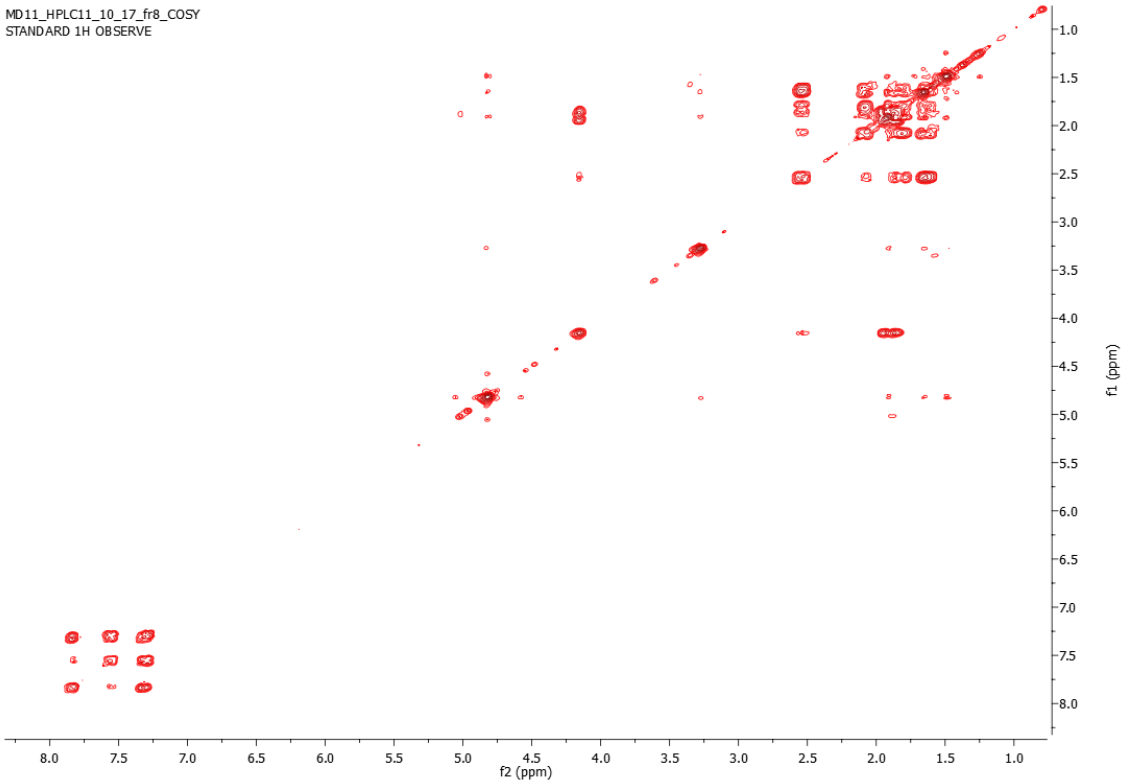

HMBC spectrum (500 MHz) of **28a** (CD_3OD).

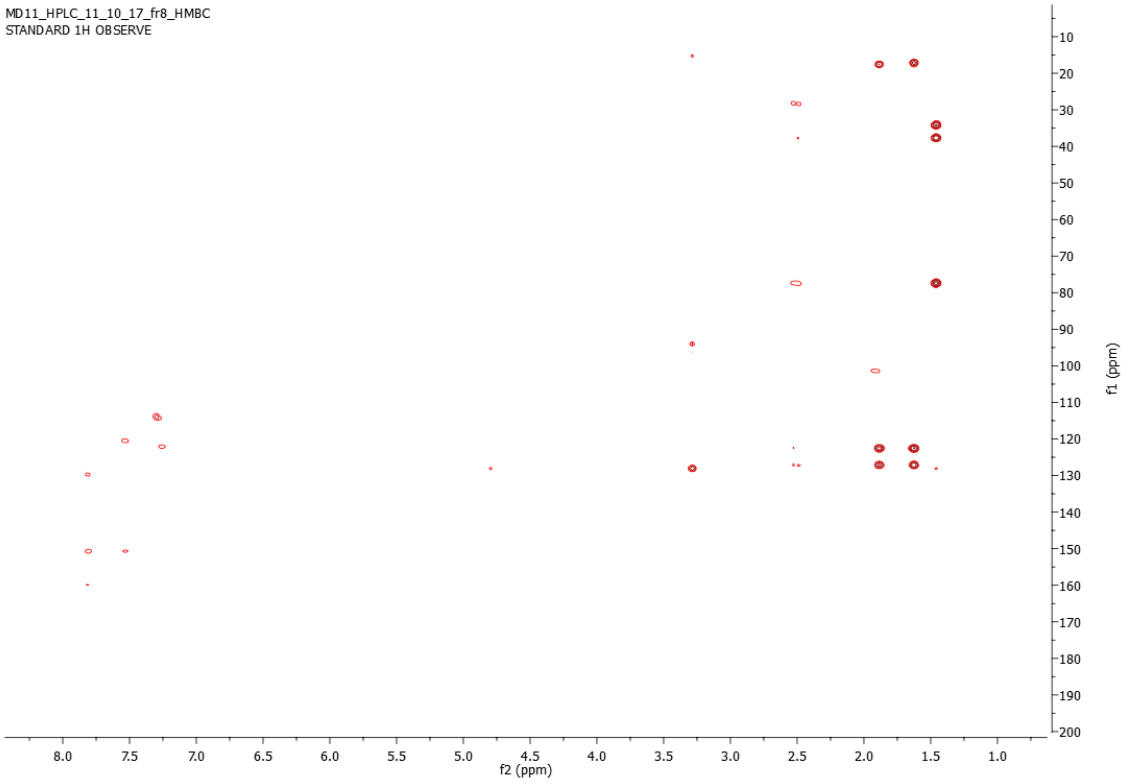

HSQC spectrum (500 MHz) of **28a** (CD_3OD).

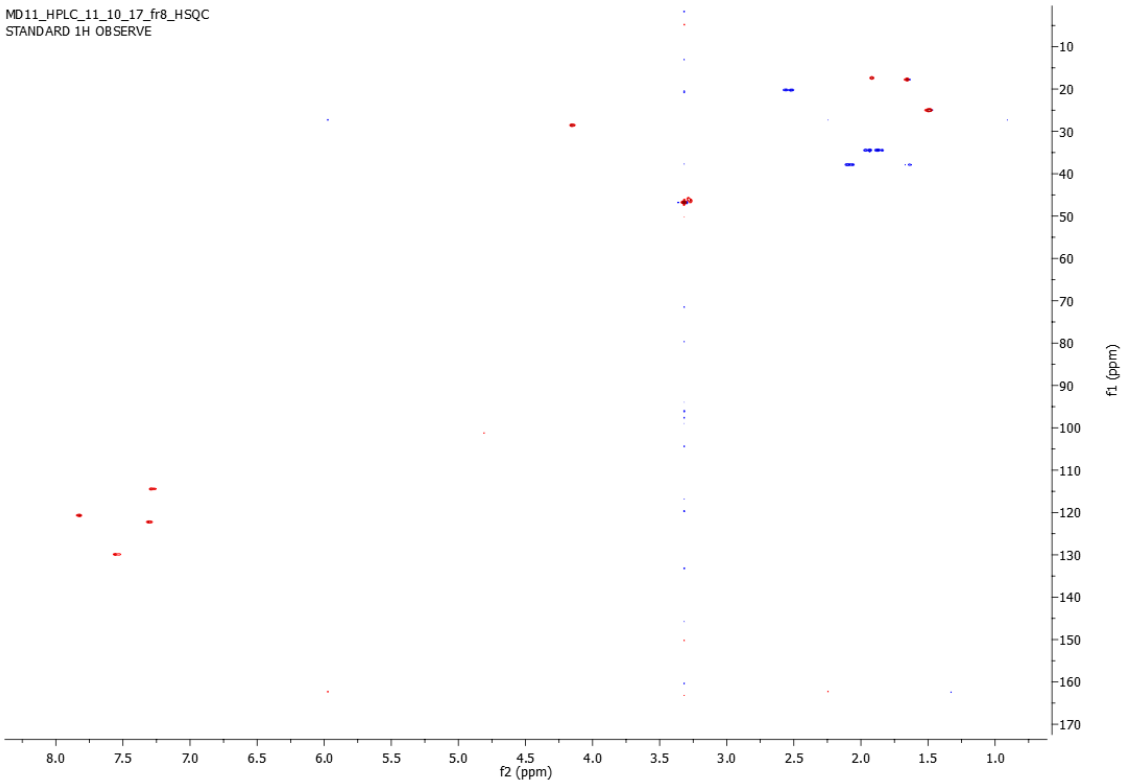

^1H NMR spectrum (700 MHz) of **28b** (CD_3OD).

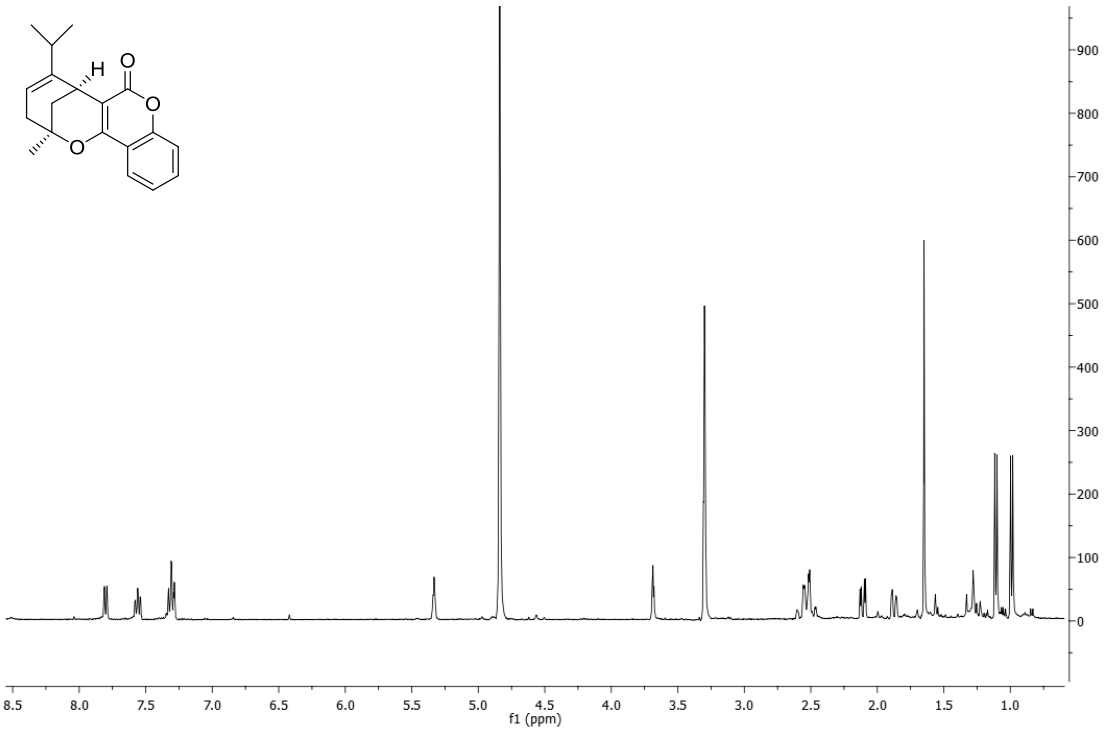

COSY spectrum (500 MHz) of **28b** (CD_3OD).

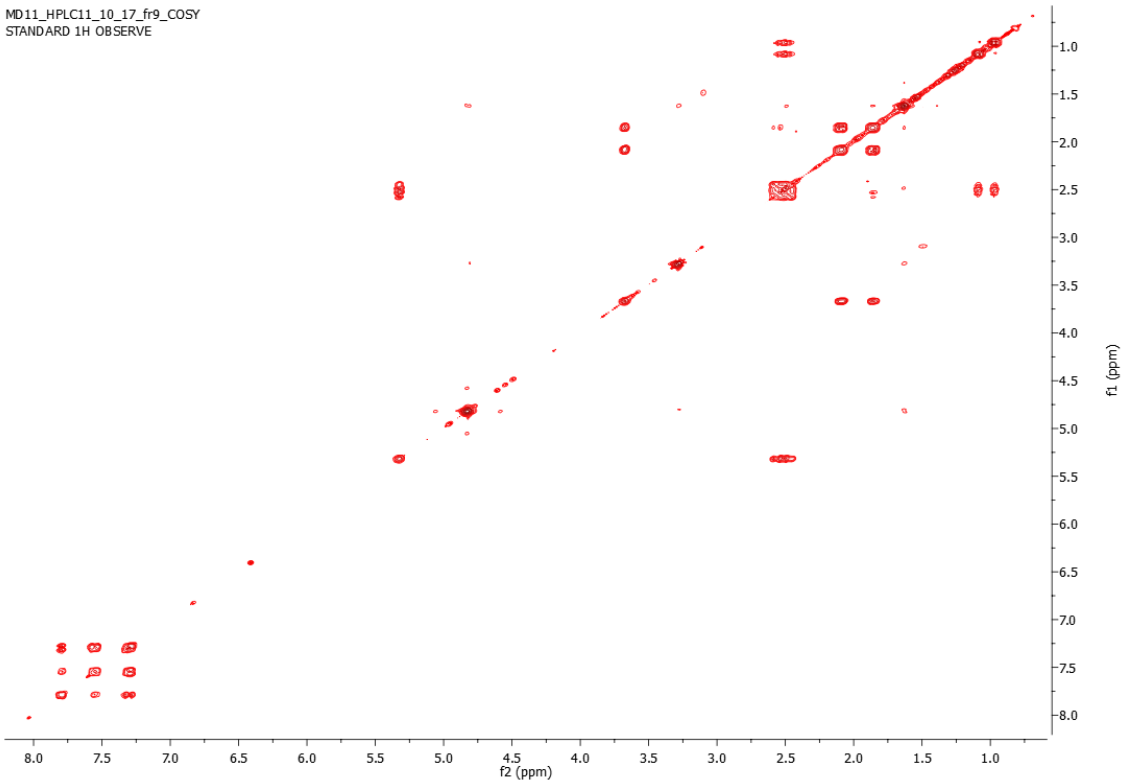

^{1}H NMR spectrum (400 MHz) of **38** (CD_3OD).

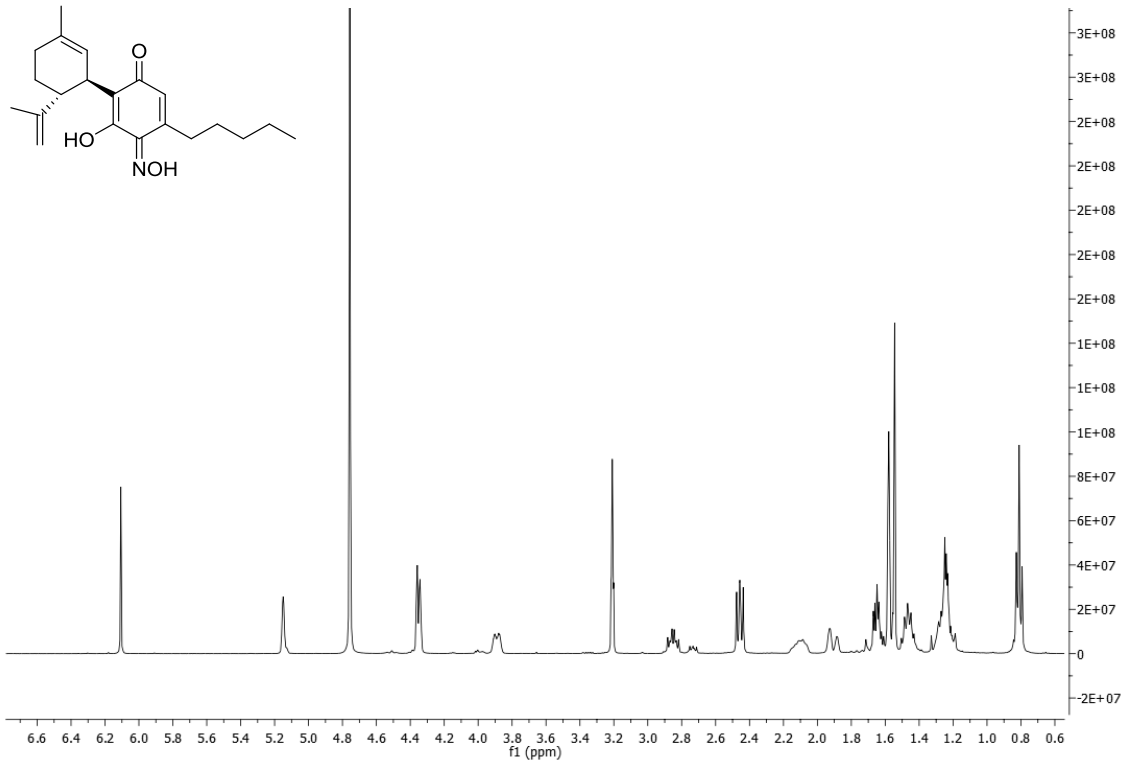

^{13}C NMR spectrum (400 MHz) of **38** (CD_3OD).

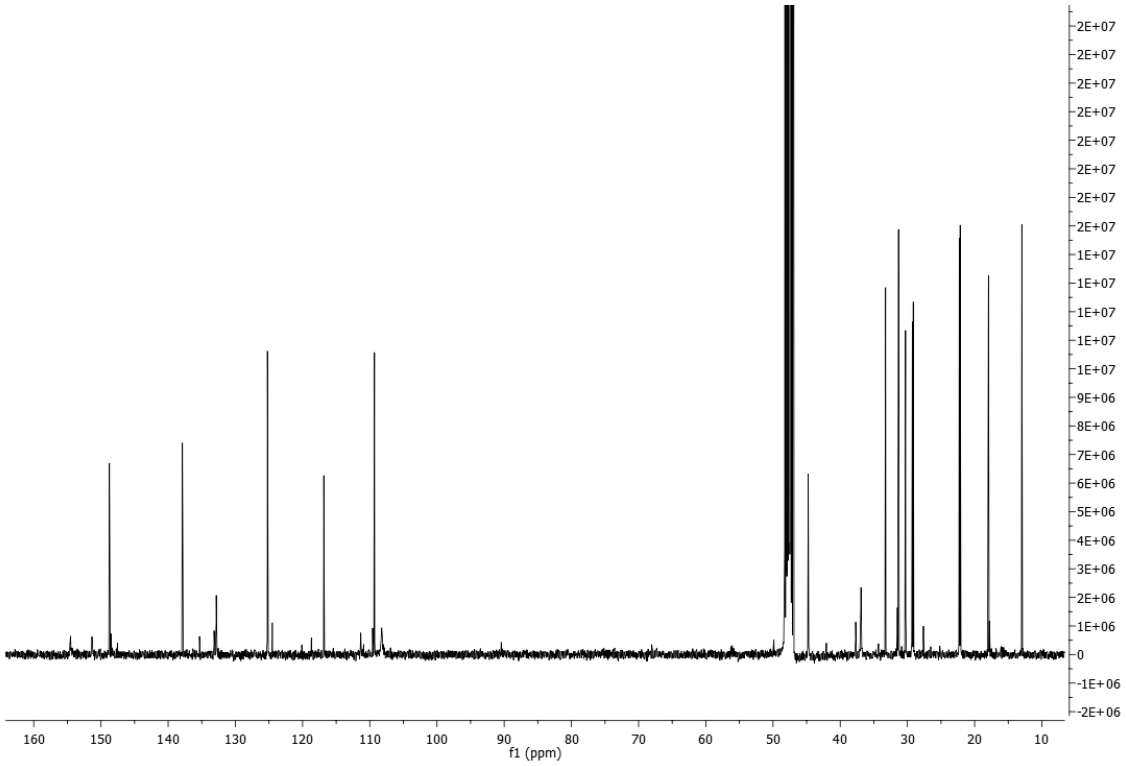

^{1}H NMR spectrum (400 MHz) of **39** CD_3OD).

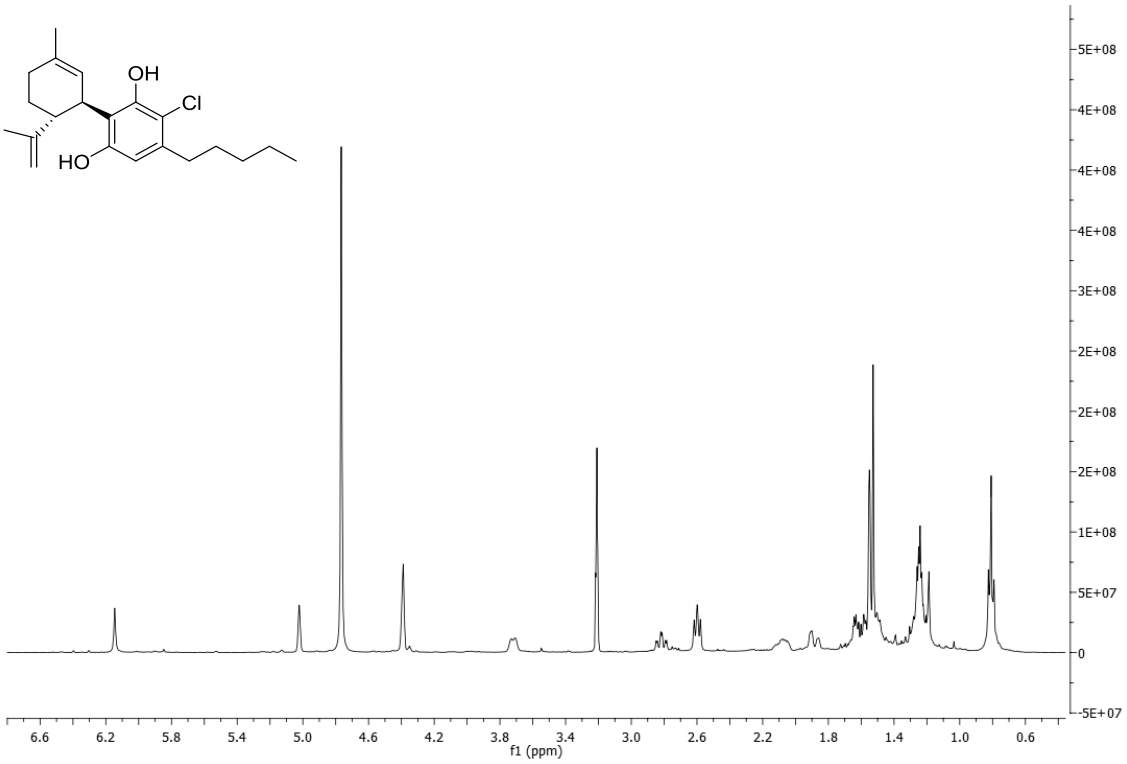

^{13}C NMR spectrum (400 MHz) of **39** (CD_3OD).

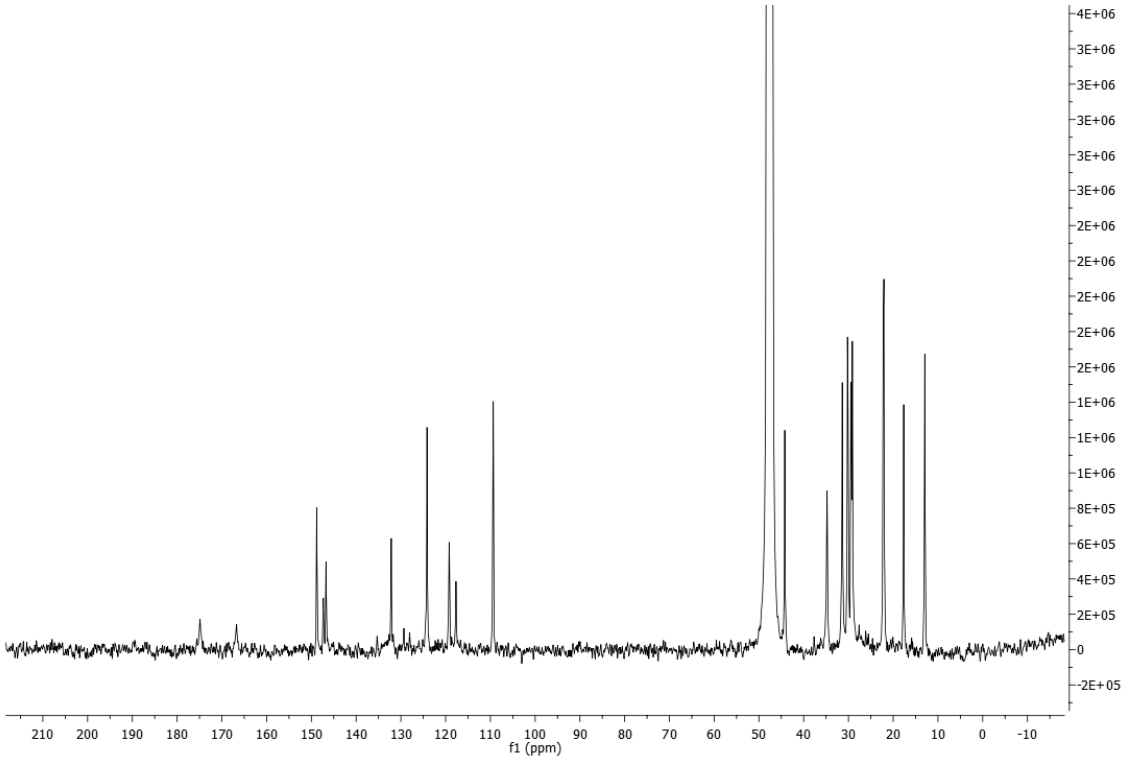

COSY spectrum (400 MHz) of **39** (CD_3OD).

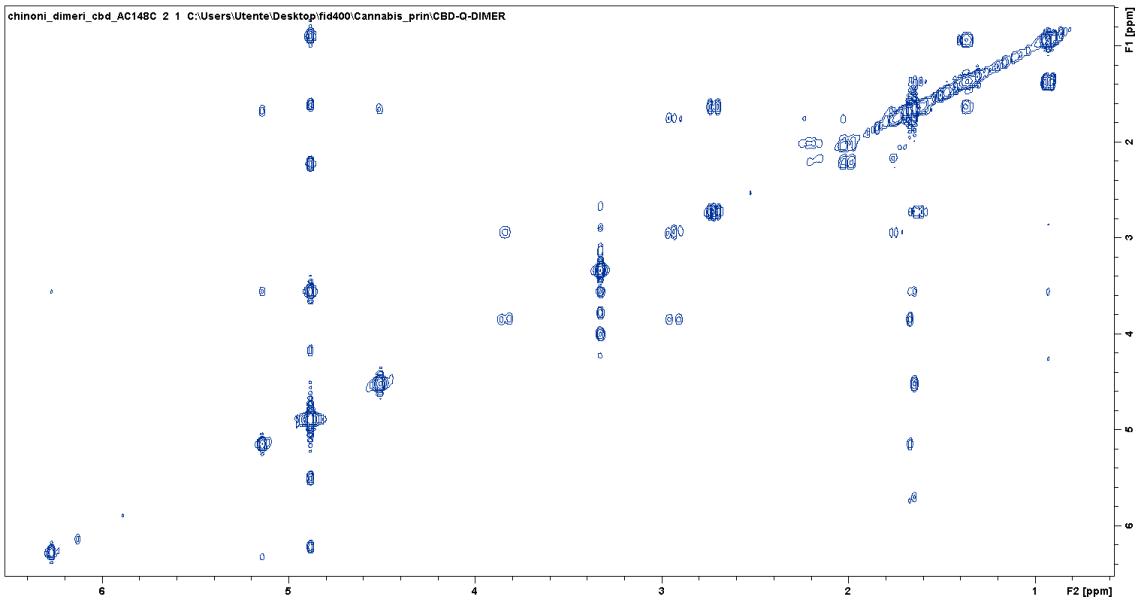

HMBC spectrum (400 MHz) of **39** (CD_3OD).

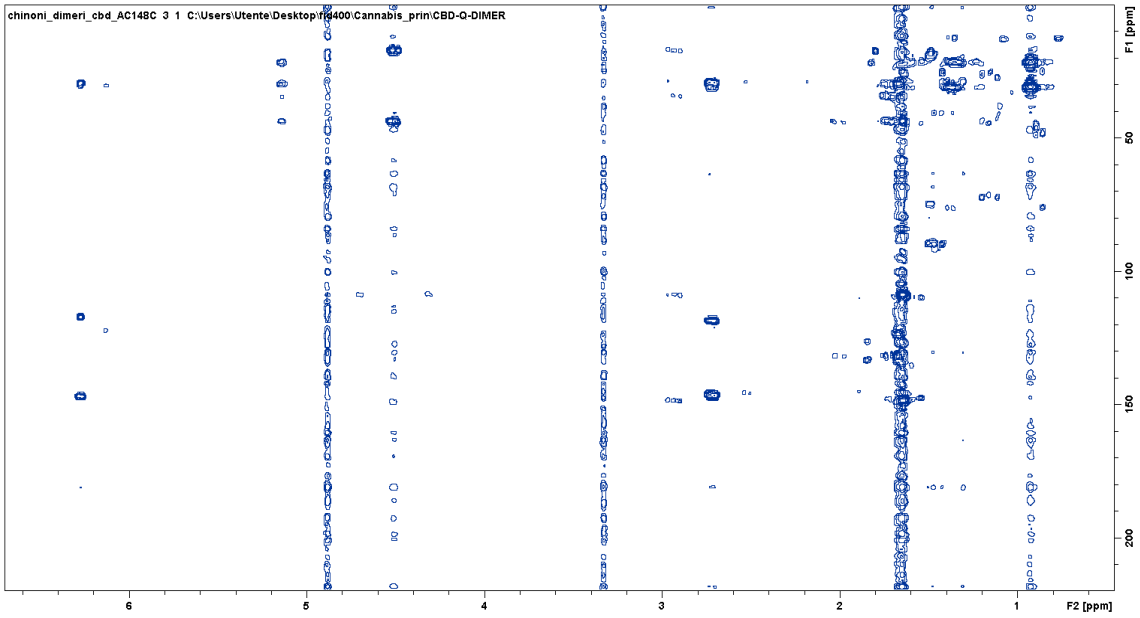

HSQC spectrum (400 MHz) of **39** (CD_3OD).

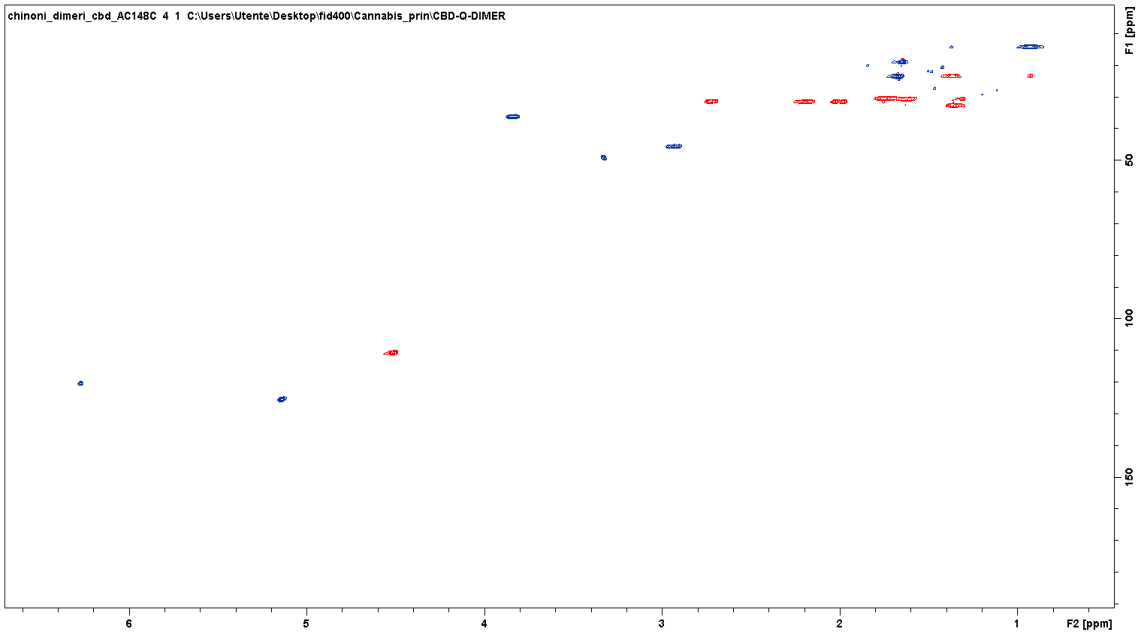

^{1}H NMR spectrum (400 MHz) of **45** ($CDCl_3$).

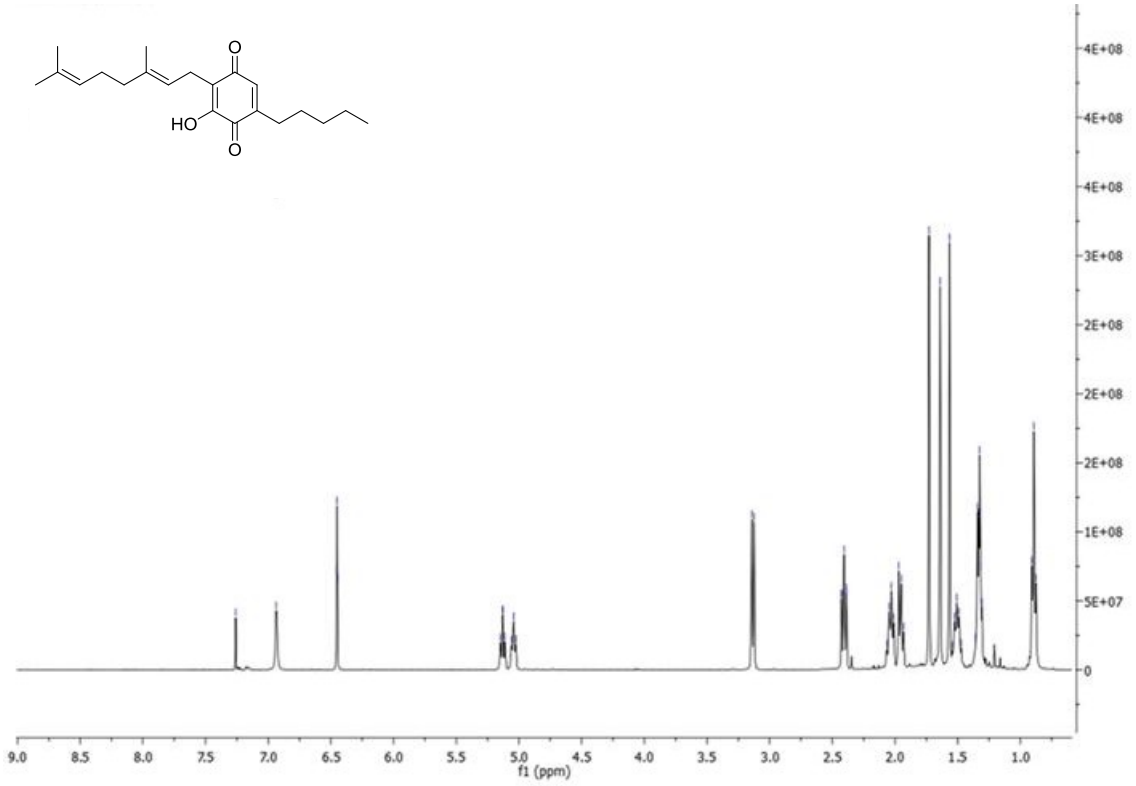

^{13}C NMR spectrum (400 MHz) of **45** ($CDCl_3$).

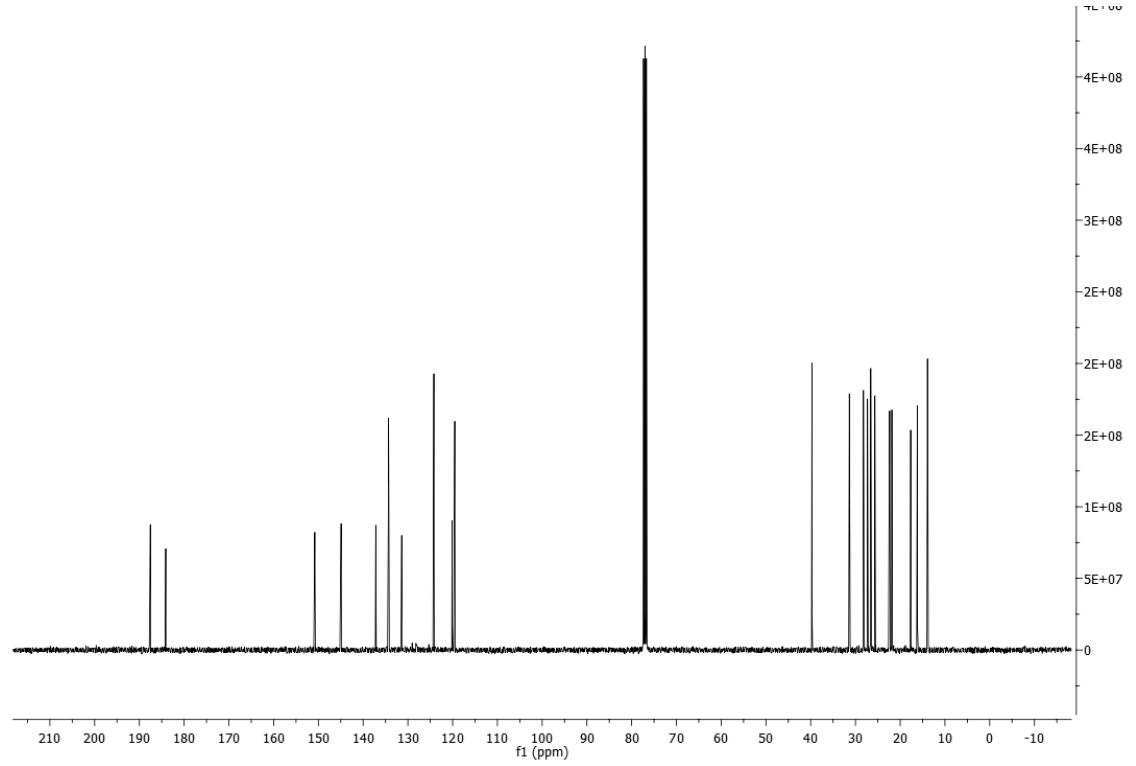

^{1}H NMR spectrum (400 MHz) of **46** ($CDCl_3$).

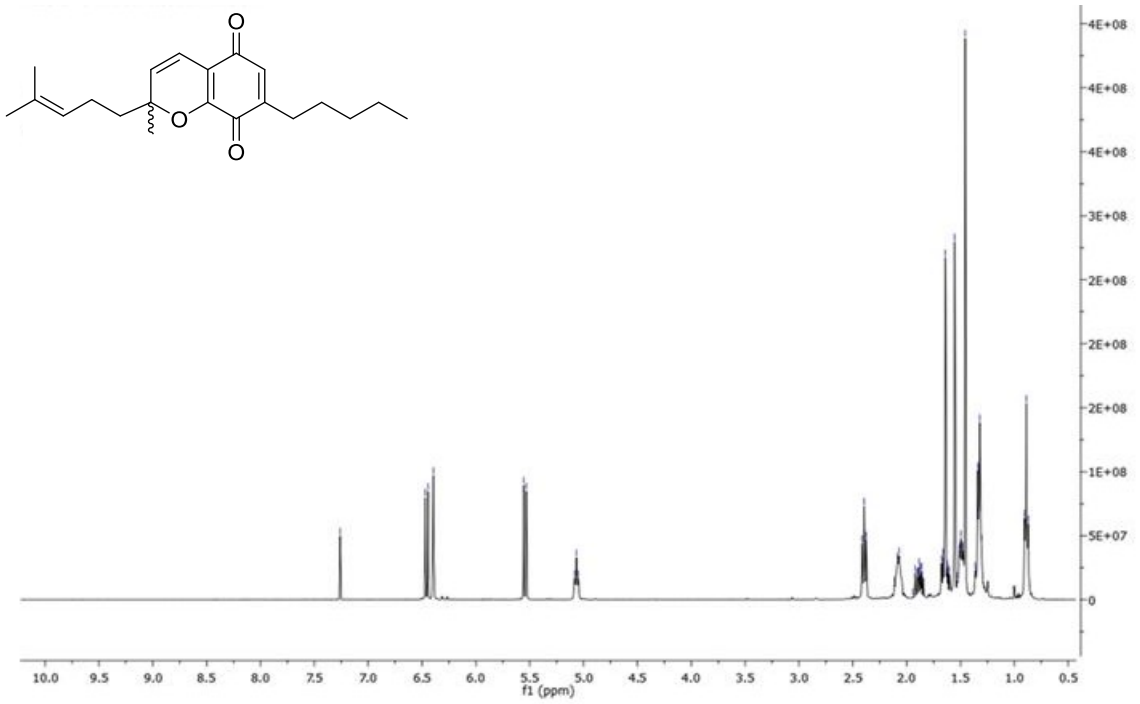

^{13}C NMR spectrum (400 MHz) of **46** ($CDCl_3$).

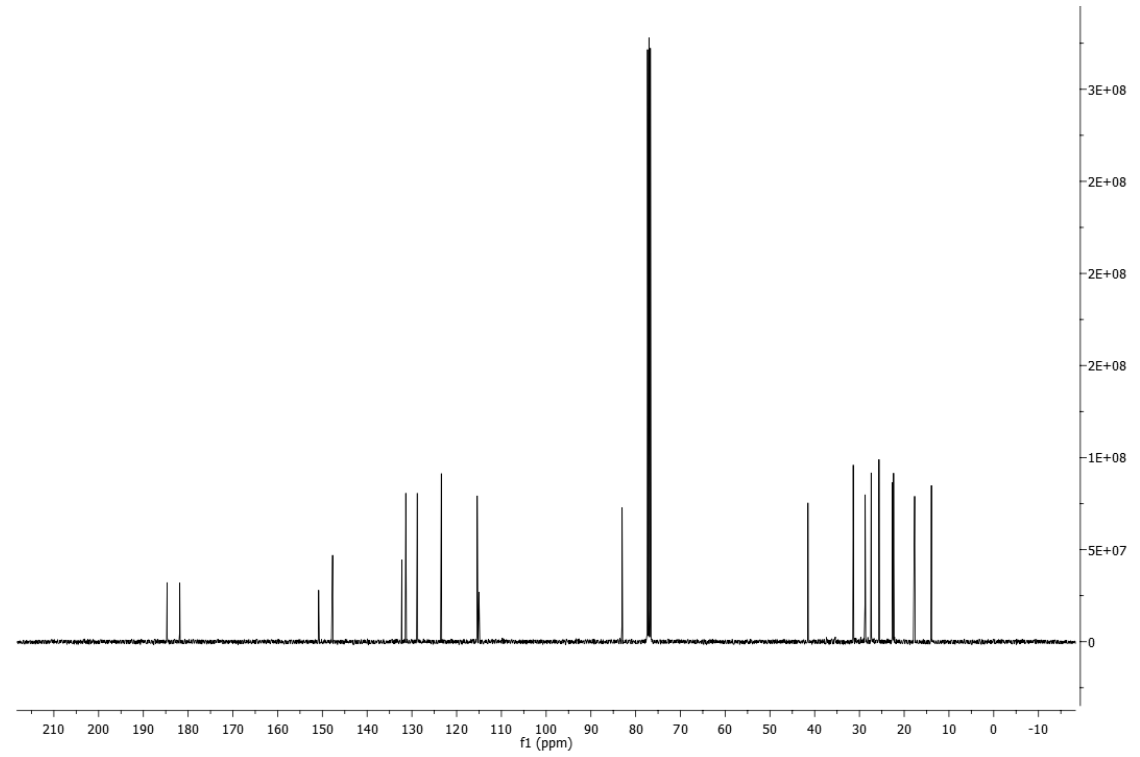

^{1}H NMR spectrum (400 MHz) of **47** ($CDCl_3$).

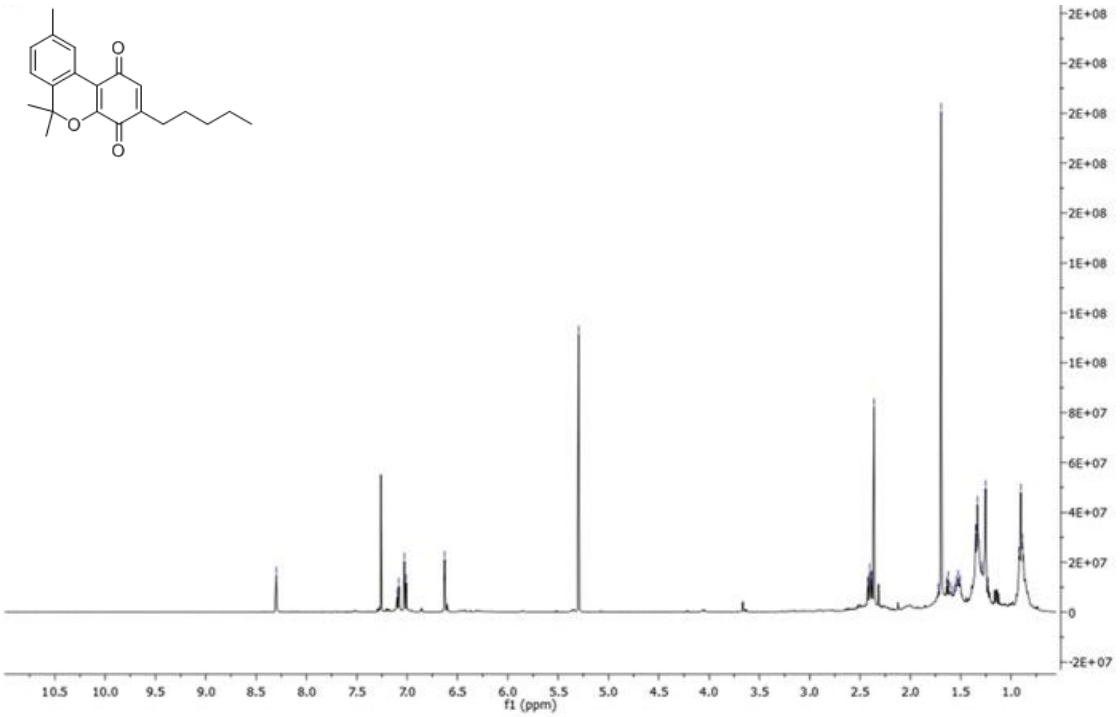

^{13}C NMR spectrum (400 MHz) of **47** ($CDCl_3$).